Improving the Accuracy of Camber Predictions for Precast Pretensioned Concrete Beams

BRIDGE ENGINEERING CENTER

Final Report
July 2015

IOWA STATE UNIVERSITY
Institute for Transportation

Sponsored by
Iowa Highway Research Board
(IHRB Project TR-625)
Iowa Department of Transportation
(InTrans Project 11-390)

About the Bridge Engineering Center

The mission of the Bridge Engineering Center (BEC) at Iowa State University is to conduct research on bridge technologies to help bridge designers/owners design, build, and maintain long-lasting bridges.

Disclaimer Notice

The contents of this report reflect the views of the authors, who are responsible for the facts and the accuracy of the information presented herein. The opinions, findings and conclusions expressed in this publication are those of the authors and not necessarily those of the sponsors.

The sponsors assume no liability for the contents or use of the information contained in this document. This report does not constitute a standard, specification, or regulation.

The sponsors do not endorse products or manufacturers. Trademarks or manufacturers' names appear in this report only because they are considered essential to the objective of the document.

Non-Discrimination Statement

Iowa State University does not discriminate on the basis of race, color, age, ethnicity, religion, national origin, pregnancy, sexual orientation, gender identity, genetic information, sex, marital status, disability, or status as a U.S. veteran. Inquiries regarding non-discrimination policies may be directed to Office of Equal Opportunity, Title IX/ADA Coordinator, and Affirmative Action Officer, 3350 Beardshear Hall, Ames, Iowa 50011, 515-294-7612, email eooffice@iastate.edu.

Iowa Department of Transportation Statements

Federal and state laws prohibit employment and/or public accommodation discrimination on the basis of age, color, creed, disability, gender identity, national origin, pregnancy, race, religion, sex, sexual orientation or veteran's status. If you believe you have been discriminated against, please contact the Iowa Civil Rights Commission at 800-457-4416 or Iowa Department of Transportation's affirmative action officer. If you need accommodations because of a disability to access the Iowa Department of Transportation's services, contact the agency's affirmative action officer at 800-262-0003.

The preparation of this report was financed in part through funds provided by the Iowa Department of Transportation through its "Second Revised Agreement for the Management of Research Conducted by Iowa State University for the Iowa Department of Transportation" and its amendments.

The opinions, findings, and conclusions expressed in this publication are those of the authors and not necessarily those of the Iowa Department of Transportation.

Technical Report Documentation Page

1. Report No.	2. Government Accession No.	3. Recipient's Catalog No.
IHRB Project TR-625		

4. Title and Subtitle	5. Report Date
Improving the Accuracy of Camber Predictions for Precast Pretensioned Concrete Beams	July 2015
	6. Performing Organization Code

7. Author(s)	8. Performing Organization Report No.
Ebadollah Honarvar, James Nervig, Wenjun He, Sri Sritharan, and Jon Matt Rouse	InTrans Project 11-390

9. Performing Organization Name and Address	10. Work Unit No. (TRAIS)
Bridge Engineering Center Iowa State University 2711 South Loop Drive, Suite 4700 Ames, IA 50010-8664	**11. Contract or Grant No.**

12. Sponsoring Organization Name and Address	13. Type of Report and Period Covered
Iowa Highway Research Board Iowa Department of Transportation 800 Lincoln Way Ames, IA 50010	Final Report Appendices
	14. Sponsoring Agency Code IHRB Project TR-625

15. Supplementary Notes

Visit www.intrans.iastate.edu for color pdfs of this and other research reports.

16. Abstract

The discrepancies between the designed and measured camber of precast pretensioned concrete beams (PPCBs) observed by the Iowa DOT have created challenges in the field during bridge construction, causing construction delays and additional costs. This study was undertaken to systematically identify the potential sources of discrepancies between the designed and measured camber from release to time of erection and improve the accuracy of camber estimations in order to minimize the associated problems in the field.

To successfully accomplish the project objectives, engineering properties, including creep and shrinkage, of three normal concrete and four high-performance concrete mix designs were characterized. In parallel, another task focused on identifying the instantaneous camber and the variables affecting the instantaneous camber and evaluated the corresponding impact of this factor using more than 100 PPCBs. Using a combination of finite element analyses and the time-step method, the long-term camber was estimated for 66 PPCBs, with due consideration given to creep and shrinkage of concrete, changes in support location and prestress force, and the thermal effects.

Utilizing the outcomes of the project, suitable long-term camber multipliers were developed that account for the time-dependent behavior, including the thermal effects. It is shown that by using the recommended practice for the camber measurements together with the proposed multipliers, the accuracy of camber prediction will be greatly improved. Consequently, it is expected that future bridge projects in Iowa can minimize construction challenges resulting from large discrepancies between the designed and actual camber of PPCBs during construction.

17. Key Words	18. Distribution Statement
creep—finite element analysis—instantaneous camber—long-term camber—modulus of elasticity—multipliers—precast pretensioned concrete beams—shrinkage—thermal effects—time-step method	No restrictions

19. Security Classification (of this report)	20. Security Classification (of this page)	21. No. of Pages	22. Price
Unclassified.	Unclassified.	265	NA

Form DOT F 1700.7 (8-72) **Reproduction of completed page authorized**

IMPROVING THE ACCURACY OF CAMBER PREDICTIONS FOR PRECAST PRETENSIONED CONCRETE BEAMS

Final Report
July 2015

Principal Investigator
Sri Sritharan, Wilson Engineering Professor
Civil, Construction, and Environmental Engineering, Iowa State University

Co-Principal Investigator
Jon Matt Rouse, Senior Lecturer
Civil, Construction, and Environmental Engineering, Iowa State University

Research Assistants
Ebadollah Honarvar, Wenjun He, and James Nervig

Authors
Ebadollah Honarvar, James Nervig, Wenjun He, Sri Sritharan, and Jon Matt Rouse

Sponsored by
the Iowa Department of Transportation and
the Iowa Highway Research Board
(IHRB Project TR-625)

Preparation of this report was financed in part
through funds provided by the Iowa Department of Transportation
through its Research Management Agreement with the
Institute for Transportation
(InTrans Project 11-390)

A report from
Bridge Engineering Center
Iowa State University
2711 South Loop Drive, Suite 4700
Ames, IA 50010-8664
Phone: 515-294-8103 / Fax: 515-294-0467
www.bec.iastate.edu

TABLE OF CONTENTS

LIST OF FIGURES

LIST OF TABLES

ACKNOWLEDGMENTS

The authors would like to thank the Iowa Highway Research Board (IHRB) and the Iowa Department of Transportation for sponsoring this research project. Also, the authors would like to acknowledge the three precast plants, Coreslab Structures in Omaha, Nebraska; Cretex Concrete Products in Iowa Falls, Iowa; and Andrews Prestressed Concrete in Clear Lake, Iowa, for their participation and cooperation in this project. Special thanks are due to Jeff Butler at Cretex Products, Teresa Nelson at Andrews Prestressed Concrete, and Todd Culp and Dennis Drews at Coreslab Structures, who graciously granted researchers access to their recorded past data and their facilities so that an independent set of instantaneous and long-term camber measurements on Iowa precast pretensioned concrete beams (PPCBs) could be taken.

Thanks are also due to all of the undergraduate and graduate students who assisted with camber measurements at the precast plants and at the bridge sites. The help and guidance provided by Doug Wood, structural engineering laboratories manager at Iowa State University, in performing material testing and preparing the instruments on a tight schedule is much appreciated.

The following individuals served on the technical advisory committee of this IHRB research project: Ahmad Abu-Hawash, Jeff Butler, Todd Culp, Dennis Drews, Jeff Devries, Norman McDonald, Stuart Nielsen, Michael Nop, Gary Novey, Daniel Redmond, and Wayne Sunday. Their guidance and feedback during the course of the project are also greatly appreciated.

EXECUTIVE SUMMARY

Camber is the net deflection caused by the upward deflection due to the applied prestress force and by the downward deflection resulting from the self-weight of a precast pretensioned concrete beam (PPCB), which typically occurs from the time the prestress is transferred to the beam. The instantaneous camber refers to the upward net deflection immediately after the transfer of prestress, which is often used as a basis to predict the long-term camber. Hence, the instantaneous camber not only indicates the camber at erection and other stages of the beam, but also affects the accuracy of the long-term camber. Currently, the design practice in Iowa is to carry out an elastic analysis (using CON/SPAN software) and Martin's multipliers (1977) to estimate the camber at release and erection, respectively. However, there are numerous factors that affect the at-erection camber, such as support locations, material properties, age of the PPCB erection, and vertical temperature gradients over the section depth, that are unknown at the time of design and not currently taken into account.

The method described above for predicting the camber of PPCBs used by the Iowa DOT has been observed to frequently overpredict the long-term camber of long bulb-tee PPCBs while underpredicting the long-term camber of the shorter PPCBs. Overpredicting or underpredicting the camber typically causes construction challenges in the field during bridge construction, causing delays in the construction schedule and an increase in the construction costs. Both overprediction and underprediction of the long-term camber requires additional unplanned haunch reinforcement, while underpredicting the long-term camber can also cause unexpected flexural cracking in the PPCB top flange and require changes to the bridge deck elevation.

The research presented in this report focuses on improving both short-term and long-term (at-erection) camber predictions. To achieve the project goal and minimize the influence of uncertainties, the research involved three precast plants that have regularly supplied PPCBs to bridge projects in Iowa. An evaluation of the current camber measurement methods adopted at the precast plants found discrepancies between the measured and predicted camber at release. Therefore, modifications to the camber measurement techniques were explored to help the techniques obtain consistent and accurate measurements of the instantaneous camber.

To reduce the error associated with the long-term camber prediction due to the variability of concrete time-dependent properties, the creep and shrinkage behavior of three normal concrete (NC) and four high-performance concrete (HPC) mix designs used by the three precast plants were evaluated through laboratory testing. The measured creep and shrinkage behavior indicated large discrepancies between the measured values and the values obtained from five different predictive models. Among these models, the AASHTO LRFD (2010) creep and shrinkage models gave the best estimates when compared to the measurements taken from the four HPC and three NC mixes over one year. Other models investigated were the ACI 209R-92 model, the ACI 209R model modified by Huo et al. (2001), the CEB-FIP 90 model, and the B3 model by Bazant (2000). While the AASHTO LRFD (2010) models gave better estimates than the other four models, large errors still existed between the measured and predicted values, with the models underpredicting both the creep coefficient and shrinkage strains. Hence, calculating the long-term camber by relying on these models was considered insufficient. Furthermore, creep

and shrinkage measurements taken from sealed specimens were found to represent the behavior of full-scale PPCBs more effectively than unsealed specimens. As a result, two equations were proposed to calculate the average creep coefficient and average shrinkage strain for four current HPC mixes used by the three precast plants; these calculations were then used to predict the long-term camber.

The challenges associated with instantaneous camber measurements were found to stem from bed deflections, inconsistent beam depth along the length, and friction between the PPCB and bed. The error in the camber measurement associated with each of these variables was quantified. Although the errors associated with measuring the instantaneous camber due to bed deflections, friction, and inconsistent top flange surfaces may be individually small, failing to account for each was shown to cause a large discrepancy between the measured and designed camber. Also, it was observed that reverse friction, if any exists between the PPCB and the bed when the PPCB is lifted and placed back, is small in magnitude and can be ignored. The contribution of vertical displacement due to friction was obtained by lifting and placing back the beam and then taking the camber measurement. Consequently, a measurement method was proposed to account for each of the aforementioned factors as accurately as possible and to quantify their impact on the instantaneous camber measurement.

For the long-term camber measurements, the effects of support locations and the thermal effects were investigated. An average overhang length was established by measuring the overhang length of 66 different PPCBs while they were stored at the precast plants. Moreover, examining the measured data revealed inconsistent trends in the long-term camber, such as high camber at early ages and a reduction or no increase in the camber over time. Therefore, 22 additional PPCBs were instrumented with thermocouples and string potentiometers to measure temperature and corresponding deflections over short time durations. The recorded data indicated that the long-term camber varied as much as 0.75 in. due to the temperature gradients over a 24 hour period.

The discrepancy between the measured and designed camber at release was caused by the difficulties in accurately modeling the concrete and prestressing steel properties and the procedures used to construct the PPCBs. Therefore, different parameters affecting instantaneous camber prediction were investigated analytically using the moment area method. The influence of the modulus of elasticity, prestress force, prestress losses, transfer length, sacrificial strands, and section properties on instantaneous camber prediction was quantified. The results indicated that using the AASHTO LRFD (2010) recommendation for estimating the modulus of elasticity with the specific unit weight and release strengths corresponding to specific PPCBs provided 98.2% ± 14.9% agreement with the measured instantaneous cambers. It was also observed that the release concrete strength was typically higher than the design strength, which increased the modulus of elasticity and subsequently reduced the actual camber. Ignoring sacrificial strands and transfer length in the camber prediction produced an average error of 2.6% and 1.5%, respectively. The designed prestress force value was observed to have an agreement of 100.9% ± 2.5% with the precasters' applied prestress force value when evaluating 41 PPCBs. A combination of instantaneous prestress losses contributed to an average reduction in prestress of 7.0%, which reduced the predicted camber by 11.3% on average. The transformed moment of

inertia along the length of the PPCB compared to the gross moment of inertia produced instantaneous cambers that differed by 2.9%.

Inspection of different simplified methods for predicting the long-term camber indicated that the Naaman method produced the best comparison, with an error of ±25%. In addition, a combination of the finite element analysis (FEA) approach and the time-step method was used to estimate the at-erection camber more accurately than other methods. Sophisticated analytical models were developed utilizing midas Civil software, in which all the parameters affecting the long-term camber, including support locations and thermal effects, were given consideration. The analytical results showed that the long-term camber can be predicted within a ±15% error for bulb-tee PPCBs, an improvement in camber prediction accuracy compared to the simplified analysis. Also, assuming a linear variation for the vertical temperature distribution, a sensitivity analysis of the temperature difference was undertaken. The results showed that the scatter in the measured data due to the thermal effects was best captured by a temperature difference of 15°F, with an error of -1.2% ± 10.7% and -14.7% ± 22.5% for the large- and small-camber PPCBs, respectively. The low values of the camber (i.e., less than 0.6 in.) obtained for the small-camber PPCBs caused relatively larger errors than the large-camber PPCBs with high camber values.

For design practice, different types of multipliers are recommended, including multiplier power functions, a set of average multipliers, and a single multiplier, to calculate the at-erection camber more accurately based on the predicted instantaneous camber. All these multipliers were developed with and without the effects of the overhang. However, by eliminating the contribution of the overhangs to the long-term camber, the accuracy of the multiplier methods was enhanced. In addition, a temperature multiplier, λ_T, was introduced to account for the additional deflection due to the thermal effects. In general, using the recommended multipliers and the temperature multiplier in combination with the adjusted data for the overhangs significantly improved the long-term camber estimation compared to the current Iowa DOT method.

CHAPTER 1: INTRODUCTION

1.1 Background

Prestressing has been defined as the "intentional creation of permanent stresses in a structure or assembly, for the purpose of improving its behavior under various service conditions" (Lin and Burns 1981). Prestressing is used in multiple structural members, including precast pretensioned concrete beams (PPCBs). PPCBs use prestressing reinforcement in an active state to develop high-compression stresses in the tension zone, thereby increasing their flexural tension resistance. Benefits associated with prestressing in PPCBs include effectively limiting deflection and avoiding flexural cracks while allowing a large span to depth ratio.

When prestressing steel is used with an eccentricity below the centroid of the beam section, as shown in Figure 1.1, a bending moment is produced that causes the PPCB to deflect upward, which is counteracted by the downward deflection due to the self-weight.

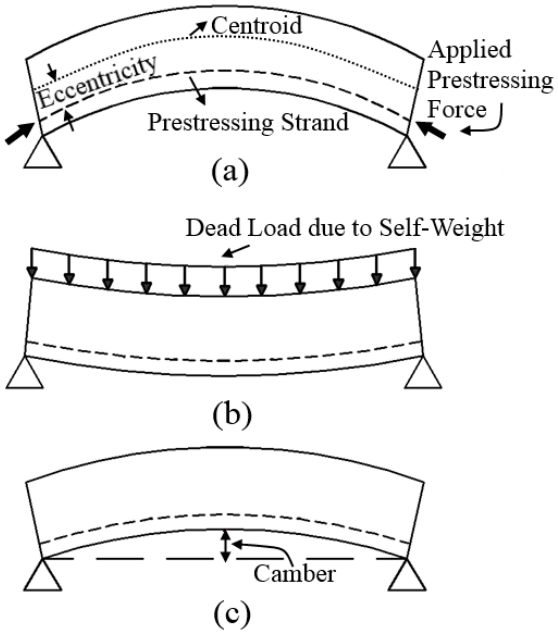

Figure 1.1. (a) Deflection due to prestressing force, (b) deflection due to self-weight, (c) camber

The upward deflection is dependent on the eccentricity and the amount of initial prestressing force. The self-weight deflection is dependent on the length of the member and the geometric and material properties. The camber of a PPCB is the net upward deflection resulting from the applied prestress force after subtracting the downward deflection due to the self-weight, as expressed by Equation 1-1; the camber exists from the time the prestress is transferred to PPCBs until the deflection due to the dead and live loads exceeds that due to the prestress.

$$\Delta_{Camber} = \left|\Delta_{Prestress(Upward\ Deflection)}\right| - \left|\Delta_{Self\text{-}Weight(Downward\ Deflection)}\right| \quad \textbf{(1-1)}$$

Camber changes with time, and thus it is stated at two common specific instants. They are the instantaneous value, which is defined immediately after the transfer of prestress, and the long-term value, which is defined at the time of erecting the PPCB in the field. The instantaneous camber is measured at the precast plant. The instantaneous camber is often used predictively to estimate the long-term camber and can indicate the accuracy of the camber at erection and other stages of the bridge's life.

1.2 Problem Statement

The Iowa Department of Transportation (DOT) currently uses the CON/SPAN program to estimate the instantaneous camber based on the elastic beam theory. The long-term camber is then estimated using Martin's multipliers (1977), and the estimated recommended multipliers are 1.80 for the upward deflection due to the effects of prestressing and 1.85 for the self-weight deflection. The long-term camber is then estimated by subtracting the long-term deflection due to the self-weight from the long-term deflection due to prestressing.

The current method of predicting the camber for PPCBs used by the Iowa DOT has been observed to frequently overpredict the long-term camber of some of the most frequently used long PPCBs in Iowa bridges while underestimating the long-term camber of shorter PPCBs. Long-term camber predictions are greatly influenced by the time of the bridge erection, which can generally cause overestimation or underestimation of the long-term camber for PPCBs. Furthermore, the camber of PPCBs cast on the same bed has been found to vary from one PPCB to another, although they were of the same type and had the same length. This inconsistency and the lack of accurate predictions of the long-term camber have led to increased construction costs and have raised quality control concerns. Overpredicting the camber typically changes the haunch design and leads to unplanned placement of reinforced concrete. Underpredicting the camber usually causes flexural cracking in the PPCB top flange due to tensile stresses from the prestressing that is present.

The camber of PPCBs is relatively complex because it is sensitive to fabrication practices such as the mix design, tolerances on prestressing forces and moisture control, bed configuration, curing process and handling, storage environment, and support location during storage. In addition, the aggregate type, cement, and admixtures used in the concrete play a significant role in the concrete's creep and shrinkage behavior, which in turn affect the long-term camber significantly. This report presents a systematic study to identify the most significant parameters, practices, and predictive analytical models in order to understand the challenges associated with estimating the camber accurately during design, thereby providing better camber control for standard PPCBs commonly used in Iowa.

1.3 Research Goals and Objectives

The goals of this research were to improve both the short-term and long-term camber predictions and to minimize the error between the expected and actual camber of PPCBs, especially at the time of erection. The project goals were achieved through systematically investigating the short-term and long-term material behavior, examining the camber measurement techniques, and quantifying the camber from the time of construction of PPCBs to the completion of bridges using these PPCBs. The following objectives were used to achieve the project goals:

1. Complete a thorough literature review with an emphasis on recently completed work on this research topic
2. Review the existing camber data recorded in the past by precasters at transfer and by contractors and the Iowa DOT at the time of erection
3. Quantify concrete properties such as compressive strength, modulus of elasticity, creep, and shrinkage for representative concrete mixes from three precasting plants
4. Obtain accurate camber measurements from a variety of Iowa DOT PPCBs at the time of transfer, during storage at the precast plants, at the time of erection, and before/after the casting of the deck
5. Investigate the potential sources of scatter in the measured data for both the instantaneous camber and the long-term camber and quantify the effects of different variables such as concrete material properties, camber measurement techniques, bed deflection, creep and shrinkage, support location (i.e., overhang length), and thermal effects
6. Propose a new measurement approach to accurately capture the instantaneous camber and recommend any modifications to the PPCB fabrication process to decrease variations in the camber of identical PPCBs
7. Improve the estimation of the instantaneous camber
8. In conjunction with the measured field data, develop analytical models using finite element analysis (FEA) and simplified analysis to compute a new set of long-term camber multipliers to predict the at-erection camber more accurately

1.4 Report Organization

This report is composed of eight chapters presenting the completed research. Chapter 1 reviews the background and purpose of the research.

In Chapter 2, an extensive literature review of previous research is presented that covers the following topics: material properties and long-term behavior of concrete, the instantaneous camber, and the long-term camber. Moreover, factors influencing the camber variability at release and erection are also presented in Chapter 2.

Chapter 3 describes the concrete material characterization completed through laboratory testing at the Iowa State University (ISU) structural engineering laboratories. Concrete cylinder samples were collected for seven mixes from three precasting plants to quantify the compressive strength and modulus of elasticity, as well as to monitor the creep and shrinkage behavior for more than one year.

Chapter 4 describes the collected instantaneous and long-term camber data from the different Iowa DOT PPCBs fabricated at the three precasting plants. Various errors caused by the current camber measurement practices at transfer are identified with a recommended procedure to minimize these errors in future camber measurements. Also, the effects of overhang length and temperature on long-term camber are discussed.

Chapter 5 presents the instantaneous camber prediction method using the moment area method.

Chapter 6 presents the long-term camber prediction methods using different simplified methods.

In Chapter 7, the results of the FEA using the midas Civil software are presented. Also, a set of long-term camber multipliers are recommended to estimate the at-erection camber more accurately with appropriate comparisons to the results presented in Chapter 6.

Finally, Chapter 8 summarizes the results and conclusions of this study and provides a set of recommendations for their use in practice.

The eight chapters are followed by 11 appendices, which are included in a separate companion pdf. The appendices provide additional information (mostly presented in figures and tables) about the material characterization and instantaneous and long-term camber measurements and analyses.

CHAPTER 2: LITERATURE REVIEW

2.1 Material Properties of Concrete

The material properties of concrete play an important role in the behavior of the short-term and long-term camber of PPCBs. In this section, an introduction on normal concrete (NC) and high-performance concrete (HPC) is presented, and the creep, shrinkage, and modulus of elasticity of concrete are also discussed. Creep and shrinkage of concrete have non-negligible effects on the long-term camber of bridge PPCBs. The modulus of elasticity of concrete affects the instantaneous and long-term camber of PPCBs.

2.1.1 Normal Concrete

Normal concrete is made essentially of Portland cement, water, and aggregates. NC has a relatively low compressive strength and a low resistance to freezing and thawing. Due to the relatively low and late strength of NC, it has a lower modulus of elasticity but a higher creep and shrinkage. Currently, NC is gradually being replaced by HPC.

2.1.2 High-Performance Concrete

High-performance concrete is defined by the American Concrete Institute (ACI) as concrete with a compressive strength greater than 6,000 psi (41 MPa). In HPC, chemical and mineral admixtures are typically added to improve the properties of concrete, and the size of aggregates is carefully selected. Typically, the water-to-cementitious materials (w/cm) ratio is between 0.20 and 0.45. HPC has a higher early strength than NC and a lower permeability. HPC is currently widely used in the construction of bridges, buildings, and other infrastructure.

2.1.3 Compressive Strength of Concrete

Compressive strength is the most common performance measure of concrete, which is calculated from the failure load divided by the cross-sectional area of a concrete specimen. The compressive strength of concrete is affected by factors including the w/cm ratio, mix proportion, and curing conditions. Typically, the compressive strength of concrete decreases with an increase in the w/c ratio. The compressive strength of concrete also depends on the strength of the aggregate itself and the relative ratio between the aggregate and cement paste. The higher the strength of the aggregate, the more aggregate in concrete, which would result in an increase in the strength of concrete. The cement type also plays an important role in the compressive strength of concrete. Because Type III cement hydrates more rapidly than Type I, Type III cement would yield a higher early strength of the concrete than Type I. In HPC, slag, fly ash, and other supplementary materials are frequently added, which typically leads to an increase of the early strength of the concrete.

2.1.4 Modulus of Elasticity of Concrete

The modulus of elasticity is an important property of hardened concrete. Concrete is a composite material that cinlcudes aggregates and cement paste. The modulus of elasticity of concrete greatly depends on the properties and proportions of the mixture materials. ASTM Standard C469 provides the method to measure the static modulus of elasticity of concrete in compression. The elastic modulus of concrete has a significant effect on the behavior of PPCBs, including the camber. In the following sections, factors affecting the modulus of elasticity of concrete and four prediction models are presented.

2.1.4.1 Factors Affecting Modulus of Elasticity of Concrete

The modulus of elasticity of concrete is greatly influenced by the material properties and mineral admixtures. The effect of other factors is not significant.

2.1.4.1.1 Material Properties

Concrete is a composite of aggregate and cement paste, and it is typically a soft composite material due to the higher modulus of elasticity of aggregate than cement paste. Neville (1970) cited two equations for the elastic moduli of the composite, shown below:

$E = (1-g)\,E_m + gE_p$ (composite hard material when $E_m > E_p$) **(2-1)**

$E = \left(\frac{1-g}{E_m} + \frac{g}{E_p}\right)^{-1}$ (composite soft material when $E_m < E_p$) **(2-2)**

where E is the modulus of elasticity of the composite material, E_m is the modulus of elasticity of the matrix phase, E_p is the modulus of elasticity of the particle phase, and g is the fractional volume of the particles.

Aggregates play an important role in the modulus of elasticity of concrete. Typically, higher aggregate content and higher modulus of elasticity of aggregate results in a higher elastic modulus of concrete. Those conclusions were confirmed by Hirsch (1962) and Hansen and Nielsen (1965), and empirical equations were also proposed.

The relations of stress and strain for the aggregate, cement paste, and concrete are shown in Figure 2.1 (Neville 1981).

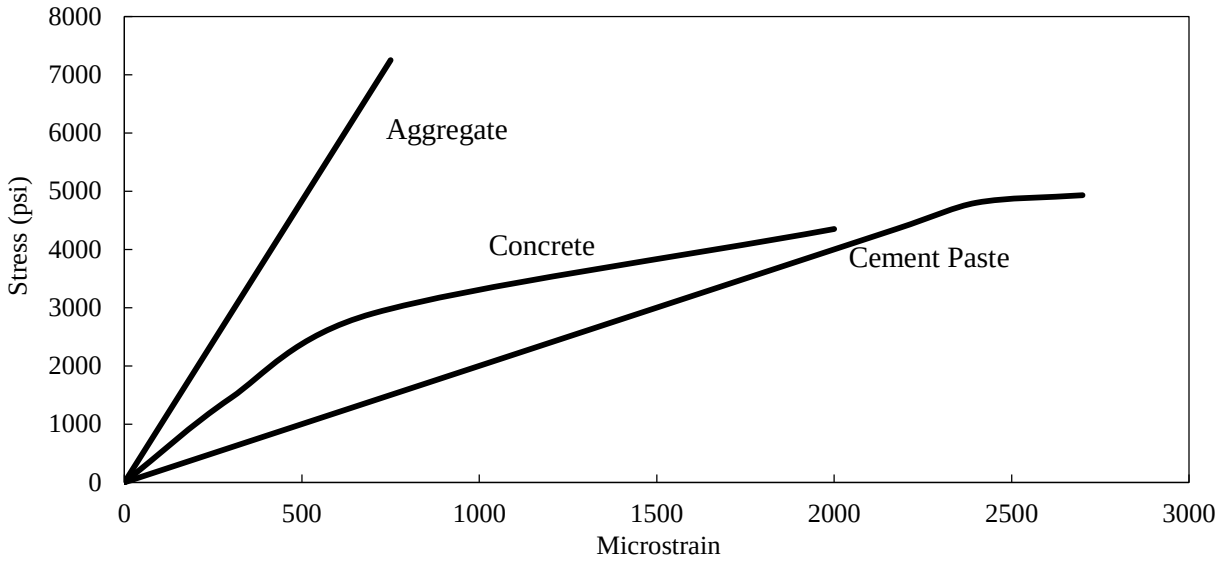

Figure 2.1. Stress-strain relations for aggregate cement paste and concrete

A reasonable explanation for the curved shape of concrete was given by Neville (1981). The rate of increase of the induced strain at the interface of the aggregate and cement paste was much higher than the rate of the applied stress development beyond a certain range. Further explanation of the effect of the bond between the aggregate and cement paste on the elastic modulus of concrete was also provided by Neville (1997). The difference in modulus of elasticity between the aggregate and cement paste plays an important role in the modulus of elasticity of concrete. In HPC, the difference in modulus of elasticity between the aggregate and the cement paste was smaller than that of normal concrete, which resulted in a better bond between the aggregate and cement and a higher modulus of elasticity of concrete. In HPC, the linear part in a stress and strain curve as high as 85% of the ultimate strength, or even higher, was observed.

2.1.4.1.2 Mineral Admixtures

Mineral admixtures are typically added to HPC as a partial replacement of Portland cement. The influence of slag on the modulus of elasticity of concrete is small (ACI 233R 2003). In a study by Brooks et al. (1992), the effect of 0%, 30%, 50%, and 70% slag replacement of Portland cement on the properties of concrete was investigated. No significant influence of the slag on the elastic modulus was observed. It was found that a dry-stored slag concrete had a higher elastic modulus at early ages, but a lower elastic modulus at later ages, compared to concrete without the slag. The opposite trend was found for water-stored concrete. Fly ash, including Class F fly ash (Lane and Best 1982) and Class C fly ash (Yildirim and Sengul 2011), also has a slight influence on the modulus of elasticity of concrete. The silica fume increases the elastic modulus of concrete up to a certain point. According to a study by Alfes (1992), it was found that a 10% silica fume replacement of Portland cement increased the elastic modulus of concrete by 12% at 28 days, but a 20% silica fume replacement increased it by 7% at 28 days, compared to concrete without the silica fume. In a study by Mazloom et al. (2004), the effect of four levels of

replacement of Portland cement with silica fume, including 0%, 6%, 10%, and 15%, on the modulus of elasticity of concrete was investigated. It was found that the elastic modulus increased by up to 10% at 7 days and 28 days with an increase of silica fume content.

2.1.4.2 Prediction of Modulus of Elasticity of Concrete

Typically, a relation between the modulus of elasticity of concrete and the corresponding compressive strength is assumed; this is not due to a direct relation between elastic modulus and compressive strength, but because of the convenience of the measurement of compressive strength. The following four models are commonly used for the prediction of the modulus of elasticity when the actual measurements are not available.

2.1.4.2.1 AASHTO LRFD (2010)

In the absence of measured data, the modulus of elasticity, E_c, for concretes with unit densities between 90 and 155 pcf and specified compressive strengths up to 15.0 ksi may be taken as follows:

$$E_c = 33\ K_1 w_c^{1.5} \sqrt{f_c'} \qquad \textbf{(2-3)}$$

where E_c is the elastic modulus of elasticity of concrete (psi); K_1 is the correction factor for a source of an aggregate to be taken as 1.0, unless determined by a physical test, and as approved by the authority of jurisdiction; w_c is the unit density for concrete (lb/ft^3); and f_c' is specified as the compressive strength of concrete (psi).

2.1.4.2.2 ACI 363R-92 (1992)

According to a study by Martinez et al. (1982), it was found that Equation 2-3 overestimated the modulus of elasticity for high-performance concretes with compressive strengths between 6,000 psi and 12,000 psi. A correlation between the modulus of elasticity, E_c, and the compressive strength, f_c', for normal weight concretes was reported as follows:

$$E_c = (40{,}000 \sqrt{f_c'} + 1.0 \times 10^6) \left(\frac{w_c}{145}\right)^{1.5} \quad (3{,}000 \text{ psi} < f'_c < 12{,}000 \text{ psi}) \qquad \textbf{(2-4)}$$

where f'_c is the specified compressive strength of concrete (psi) and w_c is the density of concrete (lb/ft^3).

2.1.4.2.3 CEB-FIP (1990)

The modulus of elasticity for normal weight concrete can be estimated from the specified characteristic strength by using the following:

$$E_{ci} = E_{co}\,[(f_{ck} + \Delta f)/f_{cmo}]^{1/3} \quad \textbf{(2-5)}$$

where E_{ci} is the modulus of elasticity (MPa) at a concrete age of 28 days, E_{co} is 2.15×10^4 MPa, f_{ck} is the characteristic strength (MPa) mentioned in Table 2.1.1 in CEB-FIP (1990), Δf is 8 MPa, and f_{cmo} is 10 MPa.

When the actual compressive strength of concrete at an age of 28 days f_{cm} is known, E_{ci} may be estimated from the following:

$$E_{ci} = E_{co}\,[f_{cm}\,/f_{cmo}]^{1/3} \quad \textbf{(2-6)}$$

When only an elastic analysis of a concrete structure is carried out, a reduced modulus of elasticity, E_c, can be calculated as follows in order to account for an initial plastic strain:

$$E_c = 0.85\,E_{ci} \quad \textbf{(2-7)}$$

2.1.4.2.4 Tadros et al. (2003)

The modulus of elasticity of high-performance concrete can be expressed as follows:

$$E_c = 33{,}000K_1K_2(0.140 + \frac{f'_c}{1000})^{1.5}\sqrt{f'_c} \quad (E_c \text{ is in ksi, and } f'_c \text{ is in ksi}) \quad \textbf{(2-8)}$$

where K_1 is the correction factor for local material variability, K_1 being 1.0 for the average of all data obtained by Tadros et al. (2003), and K_2 is the correction factor based on the 90th percentile upper-bound and the 10th percentile lower-bound for all data. For the average of all data, K_2 is 0.777 (10th percentile) and 1.224 (90th percentile).

2.1.5 Shrinkage of Concrete

Shrinkage is the decrease in volume of the hardened concrete with time. The shrinkage of hardened concrete is divided into the drying shrinkage, autogenous shrinkage, and carbonation shrinkage (ACI 209R-92 1992). The drying shrinkage is caused by moisture loss in the concrete. The autogenous shrinkage (basic shrinkage or chemical shrinkage) is due to the hydration of cement. Autogenous shrinkage typically is negligible in concrete with a relatively high w/cm ratio, but it becomes an issue for concrete with a relatively low w/c ratio, such as high-performance concrete (Nishiyama 2009). The carbonation shrinkage results from the carbonation of cement hydration products in the presence of carbon dioxide. Bazant (2000) found that in good concrete carbonation occurs only in the surface layer with a thickness of several millimeters, making the carbonation shrinkage negligible. This was confirmed by Persson (1998) and Malhotra et al. (2000). For high-performance concrete used for PPCBs, carbonation shrinkage is negligible compared to drying shrinkage and autogenous shrinkage.

2.1.5.1 Factors Affecting Shrinkage of Concrete

Shrinkage of concrete is influenced by intrinsic and extrinsic factors similar to creep. Intrinsic factors include the proportions and properties of mixtures. Extrinsic factors include size, age of exposure to the ambient condition, curing conditions, ambient temperature, and relative humidity after exposure.

2.1.5.1.1 Aggregate

Aggregate has a significant effect on the shrinkage of concrete and provides the restraining effect of shrinkage (Neville 1981). The more aggregate, the higher the restraining effect and the lower the shrinkage. Pickett (1956) proposed an equation to describe the effect of aggregate content on the shrinkage of concrete:

$$\text{Shrinkage ratio} = \frac{S_c}{S_p} = (1 - a)^n \quad \textbf{(2-9)}$$

where S_c is the shrinkage of concrete; S_p is the shrinkage of neat paste; a is the percent aggregate content by volume; and n is the experimental exponent, typically between 1.2 to 1.7 (L' Hermite and Mamillan 1986).

In the study by L' Hermite and Mamillan (1986), six levels of percent aggregate content by volume were used with a range from 0% to 62%. It was found that the shrinkage decreased with an increase in aggregate content, and the data fit the equation above when n was 1.7.

The effects of aggregate type on concrete shrinkage under drying conditions were investigated by Alexander (1996). In this study, two groups of concrete specimens with 23 different types of aggregates were prepared, including shrinkage-only specimens exposed to the air at 28 days and shrinkage specimens for creep testing exposed at the same age as the creep specimens (600 days for series 1 and 334 days for series 2). It was observed that shrinkage in the shrinkage-only test was in the range of 86 to 463 microstrain at 28 days and 247 to 841 microstrain at 6 months. It was also found that shrinkage for the creep test varied from 83 to 561 microstrain at 28 days, from 236 to 826 microstrain for series 1 at 325 days, and from 140 to 459 microstrain for series 2 at 140 days. It was additionally found that shrinkage for the creep test specimens had lower magnitudes than for the specimens in the shrinkage-only test, because the unloaded concretes for the creep test had a longer curing duration.

The modulus of elasticity of the aggregate also has a great effect on the shrinkage of concrete, and the higher the modulus of elasticity of the aggregate, the higher the restraining effect on the shrinkage and the lower the shrinkage (Neville 1981). Hobbs (1974) also proposed equations to illustrate the effect of aggregate properties, including aggregate content and the modulus of elasticity, on the ratio of the shrinkage of concrete and the shrinkage of cement paste. Other aggregate properties such as size and grading are indirect factors, and they affect shrinkage through the aggregate content (Neville 1981).

2.1.5.1.2 Cement

The cement type and fineness have some influence on the shrinkage of concrete (Neville 1981). According to a study by Swayze (1960), finer cement typically resulted in a higher shrinkage of cement pastes but did not necessarily cause a higher shrinkage of concrete. A similar conclusion was also made by Bennett and Loat (1970). Typically, rapid-hardening (Type III) Portland cement and other mineral admixtures, such as slag and fly ash, resulted in a higher autogenous shrinkage of concrete (Khayat and Mitchell 2009).

2.1.5.1.3 Water-to-Cementitious Materials Ratio

The w/cm ratio is another factor influencing both drying shrinkage and autogenous shrinkage. A higher w/c ratio typically causes a higher drying shrinkage, which is due to the reduction of the effective volume of the restraining aggregate caused by the higher water content (Neville 1981). In a study by Odman (1968), the effect of the w/c ratio on the shrinkage of concrete was investigated, and it was found that the shrinkage of concrete increased with an increase of the w/c ratio in a drying condition. Similar behaviors were observed by Soroka (1979).

The w/c ratio has the opposite effect on the autogenous shrinkage, and the autogenous shrinkage becomes a concern with lower w/c ratios, such as those used in HPC. According to a study by Tazawa and Miyazawa (1997), it was observed that the total shrinkage of cement paste almost stayed constant with a w/c ratio from 0.3 to 0.6, but increased significantly with a w/c ratio of 0.2 due to the great increase of the autogenous shrinkage. The autogenous shrinkage of cement paste was smaller than 100 microstrain when the w/c ratio was 0.5 or greater at 90 days, and it increased with a decrease of the w/c ratio from 0.5 to 0.2. The autogenous shrinkage of cement paste at 90 days was about half of the total shrinkage with a w/c ratio of 0.3, and it became about three-quarters with a w/c ratio of 0.2. These behaviors were consistent for observations by Tazawa and Miyazawa (1997) and Persson (1998). However, the extent of the effect of the autogenous shrinkage of cement paste on the autogenous shrinkage of concrete greatly depends on the properties of the aggregate. Typically, a higher autogenous shrinkage of cement paste means a higher autogenous shrinkage of concrete. The relation between the shrinkage of cement paste and shrinkage of concrete were proposed by Pickett (1956) and Hobbs (1974).

2.1.5.1.4 Chemical Admixtures

Chemical admixtures are widely used in HPC, and their effect on the shrinkage of concrete greatly depends on the chemical compositions and dosages. According to a study by Keene (1960), it was found that an air-entrainment agent had no effect on the shrinkage of concrete under drying conditions. This was confirmed by Kosmatka (2008). In a study by Brooks (1989), seven sets of data on the drying shrinkage of concrete were summarized, and it was found that plasticizers and superplasticiziers typically increased the drying shrinkage of concrete by 20%. However, some other investigators came to the opposite conclusion, and a decreased shrinkage of concrete was observed due to the use of high-range water reducing agents (Nagataki and Yonekura 1978).

2.1.5.1.5 Mineral Admixtures

Slag, fly ash, and silica fume are three types of partial replacement materials of Portland cement used in HPC. They also influence the behavior of the shrinkage of concrete. Slag has an effect on the shrinkage of concrete. In a study by Tazawa et al. (1989), there were three levels of replacement of Portland cement with slag: 0%, 35%, and 55%. It was observed that the slag decreased the shrinkage of concrete under drying conditions after 28 days of storage, and the higher the slag content, the lower the shrinkage of concrete. It was additionally found that the extent of the slag's effect on shrinkage under drying conditions also depended on the curing duration. The longer the curing time, the lower effect of the slag on the shrinkage of concrete. In another study, by Sakai et al. (1992), the effects of four levels of replacement of Portland cement with slag were investigated: 50%, 60%, 70%, and 80%. It was found that the shrinkage of concrete under drying conditions increased with an increase of the slag content from 50% to 60%, then decreased with an increase of the slag content from 70% to 80%. Similar behavior in the shrinkage of concrete with a high slag content was also observed by Brooks et al. (1992). According to a later study by Tazawa and Miyazawa (1997), the effects of slag content in the ranges of 0%, 25%, 50%, and 70% and the effects of three levels of slag particle fineness on autogenous shrinkage were investigated. It was found that the slag with the lowest fineness slightly decreased the autegenous shrinkage of cement paste with an increase of the slag content from 0% to 70%. For slags with a higher fineness, the autogenous shrinkage increased significantly with an increase of the slag content. It was found that the cement paste with 70% slag content and the highest fineness resulted in the highest autogenous shrinkage. It was additionally found that the cement paste and concrete showed a similar trend in the autogenous shrinkage in terms of the effect of the slag. Similar autogenous shrinkage behavior of slag concrete was observed by Lim and Wee (2000). In a study by Saric-Coric and Aitcin (2003), it was found that the autogenous shrinkage of cement paste increased with an increase of the slag content. Both studies by Lim and Wee (2000) and Saric-Coric and Aitcin (2003) confirmed Tazawa and Miyazawa's (1997) observations.

Generally, partial replacement of Portland cement with fly ash has no significant influence on the shrinkage of concrete under given drying conditions (ACI 232.2R 1996), but it affects the autogenous shrinkage. In a study by Naik et al. (2007), the effect of replacing Portland cement with 0% and 30% Class C fly ash on the shrinkage of concrete was investigated. It was observed that the fly ash decreased the early-age autogenous shrinkage of concrete, while it increased autogenous shrinkage at later ages. Fly ash concrete only had a 64% autogenous shrinkage at 7 days compared to concrete without fly ash, but 164% autogenous shrinkage at 56 days. The fly ash slightly increased the shrinkage of concrete under drying conditions. Class F fly ash used in HPC with a 20% replacement of Portland cement increased the autogenous shrinkage (Khayat and Mitchell 2009).

Silica fume is typically used in HPC. In a study by Mazloom et al. (2004), four levels of replacement of Portland cement with silica fume were used: 0%, 6%, 10%, and 15%. It was observed that the total shrinkage of HPC with a fixed w/c ratio of 0.35 under drying conditions decreased slightly with an increase in silica fume. The autogenous shrinkage of the HPC measured from the sealed specimens increased with an increase of the replacement level of the silica fume. It was found that the autogenous shrinkage of concrete increased from 37% to 58%

of the total shrinkage with an increase of the silica fume from 0% to 15% at the age of 587 days. The calculated drying shrinkage of concrete decreased with an increase of the silica fume content. Similar behaviors were also found previously by Roy and Larrard (1993) and Tazawa and Miyazawa (1993) with a silica fume content below 10%. When the replacement level is up to 20%, it has been found that the shrinkage of concrete increases slightly (ACI 234R 2006).

2.1.5.1.6 Size Effect

The size of a specimen has a significant effect on the shrinkage of concrete under drying conditions. In a study by Carlson (1937), the mass concrete was stored in the air with 50% relative humidity. It was observed that the drying thickness was about 3 in. from the surface after one month, about 9 in. after one year, and about 24 in. after ten years, which indicated the size effect on the drying process of concrete. Hansen and Mattock (1966) reported that the volume-to-surface (v/s) ratio was a reasonable indicator of the size effect on the drying shrinkage, and it was observed that a higher v/s ratio typically resulted in a lower drying shrinkage over 1,200 days. It was additionally found that the effect of the shape of concrete members on the drying shrinkage was small when specimens had similar v/s ratios. It was also found that concrete stored in water had a very small shrinkage compared to concrete stored in air at 50% relative humidity. This indicated that the size effect on the autogenous shrinkage of concrete was not significant. In a study by Bryant and Vadhanavikkit (1987), the thickness of a concrete member was used to account for the size effect on the shrinkage, and it was found that the shrinkage under drying conditions decreased with an increase of the thickness of the concrete members. It was also found that the shrinkage of sealed specimens was much smaller than for unsealed specimens, which confirmed the observations by Hansen and Mattock (1966).

2.1.5.1.7 Curing Conditions

The curing condition is an extrinsic factor affecting the shrinkage of concrete. Steam curing is widely used for the HPC of prestressed members. In a study by Townsend (2003), it was observed that steam-cured concrete had a 45% higher shrinkage than moist-cured concrete over one week of storage under drying conditions. After 14 weeks, this value became 11%. It was found that the steam curing increased the initial shrinkage of concrete significantly and decreased the rate of shrinkage at later ages. In a study by Haranki (2009), it was found that concretes with 14 days of moist-curing experienced smaller shrinkage under drying conditions compared to concretes with 7 days of moist-curing, due to the higher maturity of concrete after 14 days of moist curing.

2.1.5.1.8 Relative Humidity

The relative humidity of the storage has a great influence on the shrinkage under drying conditions. Concrete swells in the water or in air at 100% relative humidity and shrinks when the relative humidity is below 94% (Neville 1981). In a study by Troxell et al. (1958), concrete specimens were stored in three conditions of relative humidity: 50%, 70%, and 100% (requiring samples to be submerged in water). It was observed that the concrete in the water swelled with time with a relatively small strain. The shrinkage increased when relative humidity was

decreased to 50% and 70%. Concrete stored at 50% relative humidity had a 30% higher shrinkage at one year and a 45% higher shrinkage at 25 years compared to concrete stored at 70% relative humidity. A similar conclusion was made by Bissonnette et al. (1999).

2.1.5.2 Prediction of Shrinkage of Concrete

For the prediction of the shrinkage of concrete without actual measurements of local material mixtures, the following five models are typically used: AASHTO LRFD (2010), ACI 209R-92, ACI 209R modified by Huo et al. (2001), CEB-FIP 90, and Bazant B3.

2.1.5.2.1 AASHTO LRFD (2010)

The expression for the shrinkage strain is given as follows:

$$\varepsilon_{sh} = k_{vs} \cdot k_{hs} \cdot k_f \cdot k_{td} \, (0.48) \times 10^{-3} \quad \textbf{(2-10)}$$

In this equation, the ultimate shrinkage strain is taken as 0.00048 in./in.

k_{vs} can be found as follows:

$$k_{vs} = 1.45 - 0.13(V/S) \geq 1.0 \quad \textbf{(2-11)}$$

The detailed equation is as follows:

$$k_{vs} = \left[\frac{t}{\frac{26 \cdot e^{0.0142(\frac{V}{S})}}{} + t} \right] \left[\frac{1064 - 3.7(\frac{V}{S})}{923} \right] \quad \text{(maximum v/s is 6 in.)} \quad \textbf{(2-12)}$$

k_{hs} is the humidity factor for the shrinkage and can be found as follows:

$$k_{hs} = 2.00 - 0.014H \quad \textbf{(2-13)}$$

2.1.5.2.2 ACI 209R (1992)

The expression for the shrinkage strain at the standard condition is given as follows:

$(\varepsilon_{sh})_t = \frac{t}{35+t} (\varepsilon_{sh})_u$, shrinkage after seven days for moist-cured concrete **(2-14)**

$(\varepsilon_{sh})_t = \frac{t}{55+t} (\varepsilon_{sh})_u$, shrinkage after one to three days for steam-cured concrete **(2-15)**

where t is days after the end of the initial wet curing, $(\varepsilon_{sh})_t$ is shrinkage strain after t days, and $(\varepsilon_{sh})_u$ is the ultimate shrinkage strain. The suggested average value can be found as follows:

$$(\varepsilon_{sh})_u = 780\gamma_{sh} \times 10^{-3} \text{ in./in., } (\text{mm/mm})$$

γ_{sh} is the correction factors for conditions other than those of the standard concrete composition, which is defined as follows:

$$\gamma_{sh} = \gamma_\lambda \cdot \gamma_{vs} \cdot \gamma_s \cdot \gamma_\rho \cdot \gamma_c \cdot \gamma_\alpha \quad \textbf{(2-16)}$$

where γ_λ is the correction factor for the ambient relative humidity and can be determined as follows:

$\gamma_\lambda = 1.40 - 0.0102\lambda$, for $40 \leq \lambda \leq 80$, where λ is the relative humidity in percent **(2-17)**

$\gamma_\lambda = 3.00 - 0.030\lambda$, for $80 < \lambda \leq 100$, where λ is the relative humidity in percent **(2-18)**

γ_{vs} is the correction factor for the average thickness of a member or the volume-to-surface ratio. When the average thickness of a member is other than 6 in. (150 mm) or the volume-to-surface ratio is other than 1.5 in. (38 mm), two methods are offered.

2.1.5.2.3 Average Thickness Method

For the average thickness of members less than 6 in. (150 mm), the factors are given in Table 2.5.5.1 in ACI 209R-92. For the average thickness of members greater than 6 in. (150 mm) and up to 12 to 15 in. (300 to 380 mm), the following equations are given:

$\gamma_{vs} = 1.23 - 0.038h$, during the first year after loading **(2-19)**

$\gamma_{vs} = 1.17 - 0.029h$, for ultimate values **(2-20)**

where h is the average thickness of the member in inches.

2.1.5.2.4 Volume-Surface Ratio Method

For members with a volume-to-surface area other than 1.5 in. (38 mm), the following equations are given:

$$\gamma_{vs} = 1.2e^{-0.12(\frac{v}{s})} \quad \textbf{(2-21)}$$

where v/s is the volume-to-surface ratio in inches.

γ_s is the correction factor for slump and can be found as follows:

$$\gamma_s = 0.89 + 0.041s \quad \textbf{(2-22)}$$

where s is the observed slump in inches.

γ_ρ is the correction factor for the fine aggregate percentage, which is defined as follows:

$$\gamma_\rho = 0.30 + 0.014\rho, \text{ when } \rho \leq 50 \text{ percent} \quad \textbf{(2-23)}$$

$$\gamma_\rho = 0.90 + 0.002\rho, \text{ when } \rho > 50 \text{ percent} \quad \textbf{(2-24)}$$

where ρ is the ratio of the fine aggregate to the total aggregate by weight expressed as a percentage.

γ_c is the correction factor for the cement content, which is defined as follows:

$$\gamma_c = 0.75 + 0.00036c \quad \textbf{(2-25)}$$

where c is the cement content in lb/yd^3.

γ_α is the correction factor for the air content, which is defined as follows:

$$\gamma_\alpha = 0.95 + 0.008\alpha \quad \textbf{(2-26)}$$

where α is the air content in percent.

2.1.5.2.5 ACI 209R Modified by Huo et al. (2001)

$$\nu_t = \frac{t}{K_S + t} (\varepsilon_{sh})_u \quad (K_S = 45 - 2.5f'_c) \quad \textbf{(2-27)}$$

where $\gamma_{st,s}$ is the correction factor for the compressive strength of concrete and can be found as follows:

$$\gamma_{st,s} = 1.20 - 0.05f'c \quad \textbf{(2-28)}$$

where f'_c is the 28-day compressive strength in ksi.

2.1.5.2.6 CEB-FIP (1990)

The expression for the shrinkage strain in compression is given as follows:

$$\varepsilon_{cs}(t, t_s) = \varepsilon_{cso} \cdot \beta_s(t - t_s) \quad \textbf{(2-29)}$$

where ε_{cso} is the notional shrinkage coefficient, β_s is the coefficient to describe the development of shrinkage with time, t is the age of concrete (days), and t_s is the age of concrete (days) at the beginning of the shrinkage.

The notional shrinkage coefficient is given in the following equations:

$$\varepsilon_{cso} = \varepsilon s_{(}f_{cm}) \cdot \beta_{RH} \quad \textbf{(2-30)}$$

and

$$\varepsilon_s(f_{cm}) = [160 + 10 \cdot \beta_{sc}(9 - f_{cm}/f_{cmo})] \cdot 10^{-6} \quad \textbf{(2-31)}$$

where f_{cm} is the mean compressive strength of concrete at the age of 28 days (MPa); f_{cmo} is 10 MPa; β_{sc} is the coefficient, which depends on the type of cement: β_{sc} is 4 for slowly hardening cements SL, β_{sc} is 5 for normal or rapid hardening cements N and R, and β_{sc} is 8 for the rapid hardening high strength cements RS.

$$\beta_{RH} = -1.55 \cdot \beta_{sRH} \text{ for } 40\% \leq RH \leq 99\% \quad \textbf{(2-32)}$$

$$\beta_{RH} = +0.25 \text{ for } RH \geq 99\% \quad \textbf{(2-33)}$$

$$\text{where } \beta s_{RH} = 1 - \left(\frac{RH}{RH_0}\right)^3 \quad \textbf{(2-34)}$$

where RH is the relative humidity of the ambient atmosphere (%), and RH_0 is 100%.

The development of the shrinkage with time is given by the following:

$$\beta_s(t - t_s) = \left[\frac{(t - t_s)/t_1}{350 \cdot (h/h_0)^2 + (t - t_s)/t_1}\right]^{0.5} \quad \textbf{(2-35)}$$

where h is the notational size of member (mm) and the expression is $h = 2A_c/u$, where A_c is the area of cross-section and u is the perimeter of the member in constant with the atmosphere. Also, h_0 is100 mm, and t_1 is one day.

2.1.5.2.7 Bazant B3 Model (2000)

The shrinkage strain is expressed as follows:

$$\varepsilon_{sh}(t, t') = \varepsilon_{sh\infty} K_h S(t) \quad \textbf{(2-36)}$$

where $\varepsilon_{sh\infty}$ could be calculated by using Equation 2-78 and S(t) could be calculated by using Equation 2-80, and K_h can be calculated as follows:

$$K_h = \begin{cases} 1 - h^3 \text{ for } h < 0.98 \\ -0.2 \text{ for } h = 1 \\ \text{use linear interpolation for } 0.98 < h < 1 \end{cases}$$

2.1.6 Creep of Concrete

Creep is the time-dependent increase of the strain in the hardened concrete under sustained stress (ACI 209R-92 1992). Creep is generally obtained by subtracting the instantaneous strain after the load is applied and the shrinkage strain in the non-loaded specimen from the total measured strain with the change of time in a loaded specimen. Creep is classified into basic creep and drying creep. The basic creep occurs under conditions without moisture movement between the specimen and the environment. The drying creep is the additional creep due to the moisture movement between the specimen and the environment. Figure 2.2 shows the relation of the deformation of concrete after the loading application with time.

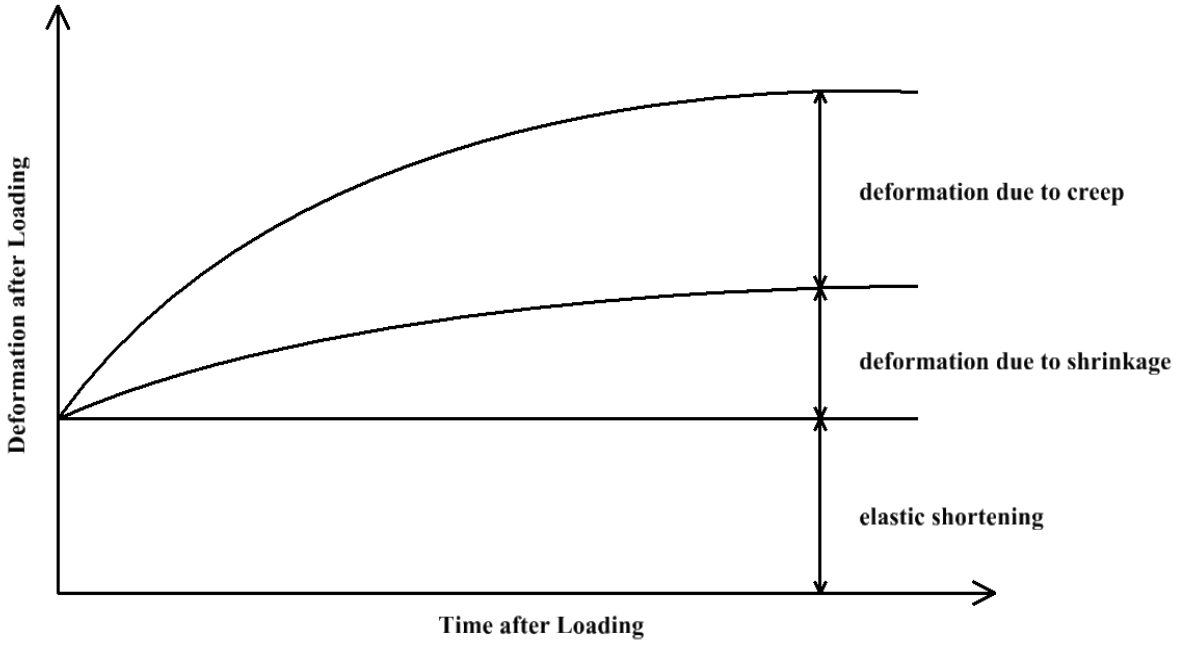

Figure 2.2. Relation of deformation after loading application versus time

Furthermore, the concrete creep strain is considered proportional to the initially applied stress. At any time t, the creep coefficient is defined as the ratio of creep strain to the instantaneous elastic strain. Also, at any time t, the ratio of the creep coefficient to the modulus of elasticity is defined as the specific creep. These parameters are discussed more in the proceeding sections.

2.1.6.1 Factors Affecting Creep of Concrete

The creep in the current study is focused on the creep behavior of the concrete under compressive stress. The creep of the concrete is influenced by many factors, which are classified as intrinsic and extrinsic. Intrinsic factors consist of the proportions and properties of materials in the concrete. Extrinsic factors include the size of the concrete member, the age of the loading application, the applied stress-strength ratio, the curing conditions, the ambient temperature, and the relative humidity surrounding concrete under the load.

2.1.6.1.1 Aggregate

Aggregates play an important role in the creep of the concrete. Aggregates provide a restraining effect on the creep (Neville 1970). Generally, a higher aggregate content results in a lower creep. Neville (1970) proposed equations to indicate the relation between the aggregate content and the creep, as follows:

$$\log\frac{c_p}{c} = \alpha \log\frac{1}{1-g} \quad \textbf{(2-37)}$$

$$\alpha = \frac{3(1-\mu)}{1+ \mu+2(1-2\mu_a)E/E_a} \quad \textbf{(2-38)}$$

where c_p is the creep of the neat cement paste, c is the creep of the concrete, g is the aggregate content, μ is Poisson's ratio of the concrete, $\mu_a$is Poisson's ratio of the aggregate, E is the modulus of elasticity of the concrete, and E_a is the modulus of elasticity of the aggregate.

According to a study by Neville (1970), for concrete specimens loaded at 14 days with a stress-strength ratio of 0.5 and stored in a 90% relative humidity condition, a linear relationship was obtained between $\log\frac{c_p}{c}$ and $\log\frac{1}{1-g}$ after 28 days of loading for the basic creep. The magnitude of α was based on the age of the initial loading and the change in the modulus of elasticity in the concrete with time after the loading application. Similar observations were made by Polivka et al. (1964) for both the basic creep and the drying creep of concrete.

Aggregate properties have a significant influence on creep, including the modulus of elasticity, porosity, the roughness of the surface, the shape, and the size. Neville (1970), citing a study by Morlie, investigated the creep of aggregates and divided aggregates into three types: elasto-brittle, visco-elastic, and visco-plastic. Elasto-brittle aggregates consisted of magmaic, non-altered gneiss. Hard limestone and quartzite fall into this category. This type of aggregate is typically used in concretes and generally has a small creep of 10% of the elastic shortening

deformation. Visco-elastic aggregates, such as calcareous minerals, shale, marl, porous limestone, and granular gypsum, have creep in the range of 12% to 40% of the elastic shortening deformation. The first two types of aggregates had a certain recoverable creep after the removal of the load. However, for visco-plastic aggregates such as chalk, no reversible creep was observed.

Concretes made with different types of aggregates generally have different creep behaviors. In a study by Davis and Davis (1931), six types of aggregates were used in the concrete, including limestone, quartz, granite, gravel, basalt, and sandstone. Concrete specimens were made with the same aggregate-cement ratio, water-cement ratio, and applied stress and were stored in the same conditions. It was found that the limestone concrete had the lowest creep, and the sandstone concrete had the highest creep. The sandstone concrete crept as much as 2.5 times more than the limestone concrete. Kordina (1960) investigated the effects of eight types of aggregates with creep, and it was observed that concretes with different aggregates had different creep behaviors, which confirmed the results reported by Davis and Davis (1931). According to a study by Alexander (1996), the influence of 23 different aggregates on the properties of concrete was investigated. The aggregates were divided into two series, including Series 1 with 13 types of aggregates and Series 2 with 10 types of aggregates. Series 1 and Series 2 concretes were stored in water before loading and stored in air (with 23°C temperature and 60% relative humidity) after loading. They were loaded approximately at the age of 600 days and 334 days, respectively, because the change in the mature concretes became minimal due to the hydration of the cement paste. It was found that the creep coefficient of the Series 1 concretes varied from 1.29 to 2.97 after 11 months of loading, whereas the Series 2 concretes were in the range of 0.78 to 1.85 after 140 days of loading.

An explanation of the effects of aggregate type on the creep of concrete provided by Neville (1970) was the modulus of elasticity of the aggregate. A higher modulus of elasticity of the aggregate generally provides a higher restraining effect on the cement paste, which causes a lower creep. Studies by Kordina (1960) and Alexander (1996) confirmed this explanation.

The porosity of an aggregate has an influence on the creep of concrete through the elastic modulus of the aggregate. In a study by Kordina (1960), the relation between the absorption of eight types of aggregates and the modulus of elasticity of the aggregates was investigated. It was found that a higher absorption caused a lower modulus of elasticity, which meant that a higher porosity resulted in a lower elastic modulus of the aggregates and a higher creep of the concrete.

The roughness of the aggregates' surfaces also affects the creep of the concrete. The rougher the surface of the aggregate, the stronger the interface between the aggregate and the cement paste, and the higher the restraining effect of the aggregate on the cement paste, which results in a lower creep.

The size of the aggregates also has an effect on the creep of the concrete through the aggregate content. Generally, larger sized aggregates result in a higher aggregate content, which leads to a lower creep. In a study by the U.S. Army Engineer Waterways Experiment Station (1958), sealed specimens were prepared using two aggregate sizes: 1.5 in. and 6 in. It was observed that

concrete with a 6 in. aggregate had a 20% to 25% lower creep than concrete with a 1.5 in. aggregate.

2.1.6.1.2 Cement

The cement paste is at the core of the creep phenomenon (Neville 1970), and thus it has a tremendous influence on the creep of the concrete. In a study by Neville (1970), it was observed that the creep was inversely proportional to the rate of the hardening of the cement. It is therefore logical that the higher the rate of the hardening of the cement, the more hydrated the cement and the more restraining the effect on the creep. Typically, concrete with a rapidly hardening Portland (Type III) cement results in a lower creep than concrete with a standard Portland (Type I) cement for the both dry-stored and wet-stored conditions (Glanville and Thomas 1939). This is due to the higher strength of the Type III Portland cement concrete at the age of the loading compared to the Type I cement concrete. Neville (1970) treated high-alumina cement as more special than other types of cement. According to observations by Hummel (1959), the rate of creep of concretes with Type I and Type III cement decreased with time, almost down to zero after three years. However, the creep of the concrete made with high-alumina cement had the most distinct behavior compared to the two types of cement concretes. After one year of loading application, the rate of creep of the high-alumina cement concrete increased sharply. It was also found by Hummel (1959) that the strength of the high-alumina cement concrete decreased considerably with time. For instance, concrete specimens at the age of three years only had 60% more strength than those at 90 days. This behavior was confirmed and explained by Neville (1958) and Neville (1963). The microstructure of the hydrated high-alumina cement pastes changed with time from a hexagonal to a cubic form, which resulted in an increase of porosity of the hydrated pastes. A considerable decrease of strength occurred, resulting in a considerable increase in creep.

2.1.6.1.3 Water-To-Cementitious Materials Ratio

Typically, creep increases with an increase of the w/cm ratio (Neville 1970). Lorman (1940) suggested that the creep was approximately proportional to the square of the w/c ratio. This phenomenon was confirmed by Wagner and Hummel, whose results were cited by Neville (1970). In the study by Wagner, the effect of the w/c ratio on creep was investigated, and specimens were prepared with a constant cement paste content of 20% by weight with a w/c ratio ranging from 0.35 to 0.9. It was found that the higher the w/c ratio, the higher the ultimate specific creep. In the study by Hummel, all concretes had an aggregate-cement ratio of 5.4, and a similar trend was found. The ultimate specific creep with a w/c ratio of 0.4 was approximately 10% higher than that with a w/c ratio of 0.3.

2.1.6.1.4 Chemical Admixtures

Chemical admixtures such as plasticizers and superplasticizers are commonly used in HPC. The effects of chemical admixtures depend greatly on their chemical compositions and dosages. According to a study by Brooks (1989), admixtures added to the HPC typically increased the creep and drying shrinkage of concrete. In the study, two types of plasticizers and three types of

superplasticizers were investigated. It was found that generally the plasticizers and superplasticizers increased the creep of the concrete compared to concrete without any admixtures. The mean increase of the concrete creep due to admixtures was about 20%.

2.1.6.1.5 Mineral Admixtures

Mineral admixtures, including ground, granulated blast furnace slag (GGBFS); fly ash; and silica fume, are widely used as a partial replacement of Portland cement in HPC. GGBFS is a glassy material with a cementitious property formed when molten blast furnace slag is rapidly cooled by immersion in water, and the slag mainly consists of silicates and aluminosilicates of calcium (ACI 233R 2003). The fly ash is a by-product of coal combustion, with both pozzolanic and cementitious properties (ACI 232.2R 1996). Fly ash primarily consists of silicon dioxide, aluminum oxide, and iron oxide. Silica fume is a by-product of the ferrosilicon industry and consists of very fine particles (4 to 8 x 10^{-6} in.) with a high pozzolanic content (ACI 234R 2006). Silica fume consists primarily of non-crystalline silicon dioxide.

Neville (1975) investigated the effects of slag on the properties of concrete. Concrete specimens, with three levels of replacement of Portland cement with slag (0%, 30%, and 50%) were loaded with the same stress after 28 days of moist curing. It was found that the slag decreased the basic creep, and the higher level of the slag replacement led to a lower basic creep. It was also observed that the slag resulted in a slightly higher total creep under drying conditions compared to concrete without the slag. These behaviors of slag concrete were confirmed by Chern and Chan (1989). The effect of slag on creep highly depends on the age and strength of the concrete at loading (Swamy 1986). If the slag concrete was loaded with the same stress at the early ages, such as one to three days, a higher creep was observed under both dry and wet conditions. A plausible explanation for this observation was that the slag concrete developed strength more slowly compared to the concrete without the slag. This resulted in a higher stress-strength ratio at an early age of loading and a higher creep.

Fly ash is another type of mineral admixture commonly used in HPC. Fly ash is classified into Class F and Class C. Class F fly ash has pozzolanic properties but little or no cementitious properties, while Class C fly ash has pozzolanic properties and some autogenous cementitious properties. Ghosh and Timusk (1981) and Lane and Best (1982) showed that, when concrete with Class F fly ash and concrete without fly ash had a similar strength at loading and a similar applied stress, lower creep was observed for the fly ash concrete due to its higher rate of strength gain after the loading application. Yuan and Cook (1983) investigated the effect of Class C fly ash on the creep of concrete. There were four levels of replacement for the Portland cement with fly ash, including 0%, 20%, 30%, and 50%. It was found that the 20% fly ash concrete had the lowest creep during the first eight months of loading and had a comparable creep with 0% fly ash concrete after that, until one year of loading. For the 20%, 30%, and 50% fly ash concretes, the creep increased with the level of the replacement.

In HPC, silica fume is also used to partially replace Portland cement. The silica fume, within a certain percentage, decreases the creep of the concrete. In a study by Khatri et al. (1995), a significant decrease in the creep was observed in concrete with a 10% silica fume compared to

concrete without silica fume. This behavior was due to the great increase in the strength of the concrete with 10% silica fume at its early days. According to studies by Saucier (1984) and Buil and Acker (1985), it was found that concrete with both 15% and 33% silica fume had a comparable creep to concrete without silica fume.

2.1.6.1.6 Stress-Strength Ratio at Loading

According to a wide range of investigations (Neville 1970), creep is proportional to the applied stress and inversely proportional to the strength at the time of the loading application. Although other researchers have indicated a higher upper limit of the stress-strength ratio of 0.75 or 0.80, generally the upper limit was approximately 0.60, as in a study conducted by Jones and Richart (1936). In this study, the measured creep of the concrete specimens was proportional to the stress-strength ratio up to 0.6. Beyond this limit, the creep increased more quickly than the increase of the applied stress. A similar behavior was observed by Gvozdev (1966) for concrete specimens with different stress-strength ratios and different initial applications of load. According to a study by L'Hermite and Mamilla (1968), a linear relation was obtained for concrete stored initially in water and loaded at 7 days, 35 days, 70 days, 1 year, and 5.5 years. In a study by Haranki (2009), the linear limit was 0.5 for HPC after a loading of 91 days. The linear limit for the creep in compression is 40% of the concrete compressive strength in ASTM C512 (2002).

2.1.6.1.7 Age at Loading

The same concrete loaded at different ages undergoes a different growth in strength, so for the constant applied stress, the creep depends on the age at loading. The strength of the younger concrete is lower, but its creep is higher, with the opposite characteristics for older concretes. In a study by Yashin (1959), it was found that when the strength gain of concrete was smaller, the creep was higher. Another study by Poivka et al. (1964) also confirmed this behavior, and for the same concrete, 18% higher creep was obtained at the age of 28 days for concrete loaded at one day versus three days. The effect of loading age on creep (i.e., the earlier loading, the higher creep) was also observed by Bryant and Vadhanavikkit (1987) for both unsealed and sealed specimens. In a study by Khan et al. (1997), the effect of the age of loading on creep for normal concrete, medium-strength concrete, and high-strength concrete was investigated. It was found that the creep of the high-strength concrete was more sensitive to the early age of loading than that of the normal and medium-strength concretes.

The extent of the effect of loading age of concrete strength also depends on the storage condition. In a study by Davis et al. (1934), sustained stress was applied to all specimens for 80 days, and it was found that water-stored concrete specimens loaded at 7 days, 28 days, and 3 months had a ratio of creep deformations of 3:2:1. For the dry-stored concrete specimens, the effect of the age of the loading was considerably smaller, and the creep of concrete that was loaded at 28 days was only 10% to 20% higher than that of concrete that was loaded at 3 months. A possible explanation for this observation was that after 28 days of drying, the strength gain of the concrete was very small. Davis et al. (1934) also found that the concrete that was loaded at early ages had a higher rate of creep than the older concrete. Glanville (1933) found a similar

behavior and found that the rate of creep after one month was independent of the age at the time of loading.

2.1.6.1.8 Size Effect

The shape and size of specimens is important for translating the results obtained in the laboratory to actual full-size concrete members under drying conditions. Neville (1970) summarized several investigations and found that the measured creep decreased with an increase in the size of the concrete specimens, but when the specimen thickness was greater than 3 ft (90 cm), the size effect became negligible. Generally, the influence of the size on creep under drying conditions is great during the initial period (i.e., over the first several weeks) after the application of load. But after that the rate of creep is comparable for all specimens with different sizes. In a study by Weil cited by Neville (1970), the size effect of specimens with different diameters ranging from 3.9 in. (10 cm) to 23.6 in. (60 cm) on the creep of the concrete under drying conditions was investigated. It was found that during the first two months after the initial load application a larger specimen size resulted in a lower creep and a lower rate of creep, but after two months all specimens had similar rates of creep up to three years. L'Hermite and Mamillan (1968) observed similar behavior. In this study, specimens of 7 cm and 20 cm thickness were loaded at the age of seven days; it was found that after three months all specimens had similar rates of creep up to three years. The size effect on the creep of concrete under drying conditions was also observed by Bryant and Vadhanavikkit (1987), and it was found that an increase of the effective thickness of a concrete member resulted in a decrease in the creep of concrete.

The loss of water from specimens to the ambient environment is an explanation for the effect of the size on creep. This explanation is correct for unsealed specimens but not applicable for sealed specimens without moisture movement. According to a study by Hansen and Mattock (1966), the size effect was absent for sealed specimens, which indicated that the basic creep was independent of the size and shape—a conclusion that has been confirmed by ACI Committee 209.2R-08 (2008).

2.1.6.1.9 Curing Conditions

Curing condition has a great effect on the creep of concrete. Low-pressure steam curing is frequently used in the construction of PPCBs due to considerations of efficiency and economy. Generally, low-pressure steam curing results in a lower creep of concrete than moist curing, which is due to the accelerated hydration of cement causing a higher strength of concrete at the age of loading (Neville 1970). In a study by ACI Committee 517 (1963), the effect of two curing conditions was investigated, including steam curing at 150 °F (66 °F) for 13 hours and moist curing at 75°F (24 °F) for five or six days. It was observed that steam-cured concrete had a lower specific creep by 30% to 50% compared to moist-cured concrete loaded at the same stress-strength level. This behavior was confirmed by Hanson (1964), who also indicated that using Type III Portland cement resulted in a lower creep of concrete at the same steam curing conditions than Type I Portland cement. In a study by Townsend (2003), the effect of 1-day steam curing and 7-day moist curing on creep and shrinkage of HPC stored in an environmentally controlled chamber with 50% relative humidity was investigated. HPC

contained 40% slag replacement of Portland cement with a 0.3 w/c ratio. It was found that the steam-cured concrete had 5% lower creep strain during storage for a period of 1 week than moist-cured concrete, which ended up with 19% higher creep strain in storage after 14 weeks. It was found that steam curing decreased the initial creep strain of HPC but increased it afterward. It was additionally found that steam-cured concrete had similar creep coefficients to moist-cured concrete during the first week but a higher creep coefficient afterward, ultimately producing up to about 30% higher creep coefficients when stored for 14 weeks.

2.1.6.1.10 Relative Humidity

Relative humidity is an important extrinsic factor affecting the creep of concrete. Typically, a higher relative humidity during the loading application results in a lower creep due to the decrease of the drying effect of concrete (Neville 1981). In a study by Troxell et al. (1958), 4 in. by 14 in. cylindrical specimens were prepared and were loaded after 28 days of moist-curing at relative humidities of 50%, 70%, and 100%. It was observed that the creep values of the concrete specimens loaded at 50% relative humidity were two to three times higher than those of concretes loaded at a relative humidity of 100% after 25 years. Concrete loaded at 70% relative humidity had a moderate creep. Concrete loaded at 50% relative humidity had the highest rate of creep during the first two years, and the rate of creep decreased with an increase in the relative humidity. However, after two years the concretes loaded at the three levels of relative humidity had a comparable rate of creep. L'Hermite and Mamillan (1968) found a similar behavior of concrete specimens at relative humidities of 50%, 75%, and 100%. The effects on creep of changing the relative humidity decreased with an increase in the size of the concrete specimens, which was recognized by Troxell et al. (1958) and confirmed by Keeton (1960).

Actual structures usually are loaded under varying humidities, which has an influence on the creep of concrete. In a study by L'Hermite and Mamillan (1968), the difference in the deformations of concrete specimens between the laboratory and open air was observed. Concrete specimens with dimensions of 8 in. x 8 in. x 24 in. were prepared, and constant stress was applied. Half of the specimens were placed in the laboratory with a constant 50% relative humidity, and the rest were located in the open air with the humidity ranging from 60% to 90%. During the 600 days of loading, it was found that specimens in the laboratory had a lower total deformation under load but a higher deformation without load than the specimens in the open air. When the additive theory was used to calculate the creep by subtracting the unloaded deformation from total deformation, it was found that the creep of the specimens in the laboratory was lower than the creep of those specimens stored in the open air. In a study by Muller and Pristl (1993), slightly lower total strain was observed for concretes stored at a 65% relative humidity compared with concretes stored at a relative humidity ranging from 40% to 90%. Glucklich (1968) gave a possible explanation for the increase in creep due to the sudden wetting and drying. Sudden wetting induced cracking on the surface of the solid specimens with the absorption of water, and the cracks resulted in a reduced surface tension of the solid specimens. This reduction led to the re-propagation of stable cracks, which further increased the creep. Sudden drying induced not only the cracks, due to the moisture gradient, but also the reduction of the effective cross-section of the concrete, which resulted in a higher creep.

2.1.6.1.11 Temperature under Load

The temperature under load is another extrinsic factor affecting creep. Generally, a higher temperature results in a higher creep over a certain temperature range (Neville 1981). This behavior was confirmed by Hannant (1967). In this study, it was observed that the specific creep of sealed specimens had a linear relationship with temperatures in the range of 81°F to 176°F (27°C to 80°C) over a duration of loading of 733 days. Nasser and Neville (1965) conducted another study to investigate the influence of temperature on the creep of concrete. All specimens were submerged in water for the duration of the test, and they were loaded at the age of 14 days. After 15 months under load, a linear behavior was observed between the creep and temperature at the stress-strength ratio of 0.35 for temperatures in the range of 115°F to 205°F (46°C to 96°C). According to a study by Brooks et al. (1991), the effect of the change of temperature within a certain range on the basic creep of normal concrete and of slag concrete was insignificant. Concrete specimens with three levels of replacement of Portland cement with slag were prepared, including 0%, 50%, and 70%. After comparing the specimens stored at a constant temperature (40°C) and at an increasing and decreasing temperature within a certain range (40°C–65°C for normal concrete, 40°C–61°C for 50% slag concrete, and 40°C–53°C for 70% slag concrete), it was found that the effect of the temperature change on the basic creep of the concrete in compression was negligible.

2.1.6.2 Prediction of Creep of Concrete

For the prediction of the creep of concrete without actual measurements of local material mixtures, the following five models are commonly used: AASHTO LRFD (2010), ACI 209R-92, ACI 209R modified by Huo et al. (2001), CEB-FIP 90, and Bazant B3 (2000). CEB-FIP 90 also provides the relation between the temperature and maturity of the concrete. Therefore, if the concrete is steam-cured, the maturity of the concrete after steam-curing could be calculated, and the adjusted age of concrete could be used in the creep and other concrete models.

2.1.6.2.1 AASHTO LRFD (2010)

Equations provided by AASHTO LRFD (2010) are applicable for a concrete strength of up to 15.0 ksi. The expression for the creep coefficient is given as follows:

$$\Phi(t,t_i) = 1.9 \cdot k_{vs} \cdot k_{hc} \cdot k_f \cdot k_{td} \cdot t_i^{-0.118} \quad \textbf{(2-39)}$$

where t is the maturity of the concrete (in days), defined as the age of the concrete between the time of loading for the creep calculations, or the end of curing for shrinkage calculations, and the time being considered for the analysis of the creep or shrinkage effect. The age of the concrete is t_i when the load is initially applied (in days); the factor for the effect of the volume-to-surface ratio of the component is k_{vs} and can be found as follows:

$$k_{vs} = 1.45 - 0.13(V/S) \geq 1.0 \quad \textbf{(2-40)}$$

The detailed equation is as follows:

$$k_{vs} = \left[\frac{\frac{t}{26e^{0.0142(V/S)+t}}}{\frac{t}{45+t}}\right]\left[\frac{1.80+1.77e^{-0.0213(V/S)}}{2.587}\right] \quad \textbf{(2-41)}$$

V/S is the volume-to-surface ratio, and the maximum is 6 inches.

k_{hc} is the humidity factor for the creep and can be found as follows:

$$k_{hc} = 1.56 - 0.008H \quad \textbf{(2-42)}$$

where H is the relative humidity of the ambient condition in percent.

k_f is the factor for the effect of the concrete strength and can be found as follows:

$$k_f = \frac{35}{7+f'_{ci}} \quad \textbf{(2-43)}$$

where f'_{ci} is the specified compressive strength of the concrete at the time of prestressing for pretensioned members and at the time of the initial loading for nonprestressed members.

k_{td} is the time development factor and can be found as follows:

$$k_{td} = \frac{t}{61-0.58f'_{ci}+t} \quad \textbf{(2-44)}$$

2.1.6.2.2 ACI 209R-92 (1992)

The expression for the creep coefficient at standard conditions is given as follows:

$$\nu_t = \frac{t^{0.60}}{10+t^{0.60}}\,\nu_u \quad \textbf{(2-45)}$$

This equation is applicable at both one to three days for steam-cured concrete and seven days for moist-cured concrete.

In the equation, t is the days after loading; ν_t is the creep coefficient after t days of loading and ν_u is the ultimate creep coefficient. The average value suggested for ν_u is 2.35 γ_c, where γ_c is the correction factors for conditions other than those of the standard concrete composition. The γ_c parameter is defined as follows:

$$\gamma_c = \gamma_{la}\cdot\gamma_\lambda\cdot\gamma_{vs}\cdot\gamma_s\cdot\gamma_\rho\cdot\gamma_\alpha \quad \textbf{(2-46)}$$

where γ_{la} is the correction factor for the loading age, which is defined as follows:

$\gamma_{la} = 1.25t^{-0.118}$ for loading ages later than seven days for moist cured concrete **(2-47)**

$\gamma_{la} = 1.13t^{-0.094}$ for loading ages later than one to three days for steam cured concrete **(2-48)**

γ_{λ} is the correction factor for the ambient relative humidity, which is defined as follows:

$\gamma_{\lambda} = 1.27 - 0.0067\lambda$, for $\lambda > 40$ **(2-49)**

where λ is the relative humidity in percent.

γ_{vs} is the correction factor for the average thickness of a member or the volume-to-surface ratio. When the average thickness of member is other than 6 in. (150 mm) or the volume-to-surface ratio is other 1.5 in. (38 mm), two methods are offered.

2.1.6.2.3 Average Thickness Method

For the average thickness of a member less than 6 in. (150 mm), the factors are given in Table 2.5.5.1 in ACI 209R-92. For the average thickness of members greater than 6 in. (150 mm) and up to about 12 to 15 in. (300 to 380 mm), the equations are as follows:

$\gamma_{vs} = 1.14 - 0.023h$, during the first year after loading **(2-50)**

$\gamma_{vs} = 1.10 - 0.017h$, for ultimate values **(2-51)**

where h is the average thickness of the member in inches.

2.1.6.2.4 Volume-Surface Ratio Method

For members with a volume-to-surface ratio other than 1.5 in. (38 mm), the equations are given:

$\gamma_{vs} = \frac{2}{3}[1+1.13e^{-0.54(\frac{v}{s})}]$ **(2-52)**

where v/s is the volume-to-surface ratio in inches.

γ_s is the correction factor for slump, and the equations are given as follows:

$\gamma s = 0.82 + 0.067s$ **(2-53)**

where s is the observed slump in inches.

γ_ρ is the correction factor for the fine aggregate percentage, which is defined as follows:

$$\gamma_\rho = 0.88 + 0.0024\rho \quad \textbf{(2-54)}$$

where ρ is the ratio of the fine aggregate to total aggregate by weight expressed as a percentage.

γ_α is the correction factor for the air content, which is defined as follows:

$$\gamma_\alpha = 0.46 + 0.09\alpha \geq 1.0 \quad \textbf{(2-55)}$$

where α is the air content in percent.

2.1.6.2.5 ACI 209R Modified by Huo et al. (2001)

This model is the same as for ACI 209-90, and additional modification factors for the compressive strength are taken into account:

$$\nu_t = \frac{t^{0.60}}{K_C + t^{0.60}} \nu_u \quad (K_C = 12 - 0.50f'_c) \quad \textbf{(2-56)}$$

$\gamma_{st,c}$ is the correction factor for the compressive strength of concrete and can be found as follows:

$$\gamma_{st,c} = 1.18 - 0.045f'_c \quad \textbf{(2-57)}$$

where f'_c is the 28-day compressive strength in ksi.

2.1.6.2.6 CEB-FIP (1990)

The expression for creep coefficient is given as follows:

$$\varphi(t, t_0) = \varphi_0 \cdot \beta_c(t - t_0) \quad \textbf{(2-58)}$$

where t is the age of concrete (in days) at the moment considered, t_0 is the age of concrete at the loading (in days), φ_0 is the notional creep coefficient, and β_c is the coefficient describing the development of the creep with time after loading.

The expression for the notional creep coefficient is given as follows:

$$\varphi_0 = \varphi_{RH} \cdot \beta(f_{cm}) \cdot \beta(t_0) \quad \textbf{(2-59)}$$

where φ_{RH} is the coefficient for the relative humidity and the dimension of member. The expression is given as follows:

$$\varphi_{RH} = 1 + \frac{1 - RH/RH_0}{0.46 \cdot (h/h_0)^{1/3}} \quad \textbf{(2-60)}$$

where RH is the relative humidity of the ambient environment in percent (%), RH_0 being 100%, and h is the notational size of the member (mm). The expression for h is $h = 2A_c/u$, where A_c is the area of a cross-section, and u is the perimeter of the member in constant contact with the atmosphere; h_0 is 100 mm.

$$\beta(f_{cm}) = \frac{5.3}{(f_{cm}/f_{cmo})^{0.5}} \quad \textbf{(2-61)}$$

where f_{cm} is the mean compressive strength of the concrete at the age of 28 days (MPa); f_{cmo} is 10 MPa.

$$\beta(t_0) = \frac{1}{0.1 + (t_0/t_1)^{0.2}} \quad \textbf{(2-62)}$$

where t_1 is 1 day.

The expression for the development of the creep with time is given as follows:

$$\beta_c(t - t_0) = \left[\frac{(t - t_0)/t_1}{\beta_H + (t - t_0)/t_1}\right]^{0.3} \quad \textbf{(2-63)}$$

where

$$\beta_H = 150 \cdot \{1 + 1.2(\frac{RH}{RH_0})^{18}\} \cdot \frac{h}{h_0} + 250 \leq 1500 \quad \textbf{(2-64)}$$

where t_1 is 1 day, RH_0 is 100%, and h_0 is 100 mm.

If concrete undergoes elevated or reduced temperature, the maturity of the concrete could be calculated by using the following equation:

$$t_T = \sum_{i=1}^{n} \Delta t_i \exp\left[13.65 - \frac{4000}{273 + T(\Delta t_i)/T_0}\right] \quad \textbf{(2-65)}$$

where t_T is the maturity of the concrete, which can be used in the creep and shrinkage models; Δt_i is the number of days where a temperature T prevails; $T(\Delta t_i)$ is the temperature (°C) during the time period Δt_i; and T_0 is 1°C.

2.1.6.2.7 Bazant B3 (2000)

The compliance function for loaded specimens is expressed as follows:

$$J(t, t') = q_1 + C_0(t, t') + C_d(t, t', t_0) \quad \textbf{(2-66)}$$

where q_1 is the instantaneous strain due to the unit stress and can be found as follows:

$$q_1 = 10^6/E_{ci} \text{ or } (0.6 \times 10^6)/E_{c28} \quad \textbf{(2-67)}$$

with

$$E_{ci} = 57000\sqrt{f'_{ci}} \text{ } (f'_{ci} \text{ is the compressive strength at the age of loading, in psi}) \quad \textbf{(2-68)}$$

$$E_{c28} = 57000\sqrt{f'_{c28}} \text{ } (f'_{c28} \text{ is the 28-day compressive strength, in psi}) \quad \textbf{(2-69)}$$

$C_0(t, t')$ is the compliance function for the basic creep (in./in./psi) and can be found as follows:

$$C_0(t, t') = q_2 Q(t, t') + q_3 \ln[1 + (t - t')^n] + q_4 \ln(t / t') \quad \textbf{(2-70)}$$

where t is the age of the concrete after casting (in days); t' is the age of the concrete at loading (in days); and t_0 is the age of the concrete at the beginning of the shrinkage (in days).

$$q_2 = 451.4c^{0.5}(f'_{c28})^{-0.9} \text{ (c is the cement content in pcf)} \quad \textbf{(2-71)}$$

$$Q(t, t') = Q_f(t')\left[1 + \left(\frac{Q_f(t')}{Z(t,t')}\right)^{\Upsilon(t')}\right]^{1/\Upsilon(t')} \quad \textbf{(2-72)}$$

$$Q_f(t') = [0.086(t')^{2/9} + 1.21(t')^{4/9}]^{-1} \quad \textbf{(2-73)}$$

$$Z(t, t') = (t')^{-m} \ln(1 + (t - t')^n) \quad (m=0.5, n=0.1) \quad \textbf{(2-74)}$$

$$\Upsilon(t') = 1.7(t')^{0.12} + 8 \quad \textbf{(2-75)}$$

$C_d(t, t', t_0)$ is the additional compliance function due to the simultaneous drying (in./in./psi) and can be found as follows:

$$C_d(t, t', t_0) = q_5[\exp\{-8H(t)\} - \exp\{-8H(t')\}]^{1/2} \quad \textbf{(2-76)}$$

$$q_5 = 7.57 \times 10^5 (f'_{c28})^{-1} \text{ABS}(\varepsilon_{sh\infty})^{-0.6} \quad \textbf{(2-77)}$$

$\varepsilon_{sh\infty} = \alpha_1\alpha_2\,[26\omega^{2.1}(f'_{c28})^{-0.28} + 270]$ (ω is the water content in pcf) **(2-78)**

$$\alpha_1 = \begin{cases} 1.0 \text{ for type I cement} \\ 0.85 \text{ for type II cement} \\ 1.1 \text{ for type III cement} \end{cases}$$

and

$$\alpha_2 = \begin{cases} 0.75 \text{ for steam} - \text{curing} \\ 1.2 \text{ for sealed or normal curing in air with inital protection against drying} \\ 1.0 \text{ for curing in water or at 100\% relative humidity} \end{cases}$$

$H(t) = 1 - (1- h)S(t)$ **(2-79)**

where h is the relative humidity.

$S(t) = \tanh[(t - t_0)/\tau_{sh}]^{1/2}$ **(2-80)**

$\tau_{sh} = K_t(K_sD)^2$ **(2-81)**

$D = 2v/s$ **(2-82)**

$K_t = 190.8(t_0)^{-0.08}\,(f'_{c28})^{-0.25}$ **(2-83)**

K_s = 1.00 for infinite slab

= 1.15 for infinite cylinder

= 1.25 for infinite square prism

= 1.30 for sphere

= 1.55 for cube

= 1.00 for undefined member

$H(t') = 1 - (1- h)S(t')$ **(2-84)**

where h is the relative humidity.

$S(t') = \tanh[(t' - t_0)/\tau_{sh}]^{1/2}$ **(2-85)**

The creep strain should be calculated as follows:

$$\varepsilon_{cr} = [C_0(t, t') + C_d(t, t', t_0)]\sigma \quad \textbf{(2-86)}$$

where σ is the applied stress in psi.

The creep coefficient should be expressed as follows:

$$\varphi(t, t') = \frac{\varepsilon_{cr}}{q_1\sigma} \quad \textbf{(2-87)}$$

The total strain may be expressed as follows:

$$\varepsilon_{total} = J(t, t')\,\sigma + \varepsilon_{sh} \quad \textbf{(2-88)}$$

where $\varepsilon_{sh}$is the shrinkage strain from Section 2.1.5.2.7.

2.1.6.2.8 Comparison of the Five Models

The parameters considered in each model and their corresponding ranges are shown in Table 2.1.

Table 2.1. Comparison of five models for prediction of creep of concrete

Considered Parameters	AASHTO LRFD (2010)	ACI 209R-92	ACI 209R-Modified by Huo et al. (2001)	CEB-FIP 90	Bazant B3
f_{cm28}, psi	up to 15,000	-	up to 12360	2,900 to 13,000	2,500 to 10,000
Aggregate to cement ratio, a/c	-	-	-	-	2.5 to 13.5
Water to cementitous materials ratio, w/c	-	-	-	-	0.35 to 0.85
Cement content, pound per cubic yard	-	Considered	Considered	-	270 to 1215
Relative humidity, %	35 to 100	40 to 100	40 to 100	40 to 100	40 to 100
Type of cement	I, II, III	I or III	I, II, III	I, II, III	I, II, III
Age of steam curing before loading	1 to 3 days	1 to 3 days	1 to 3 days	-	-
Age of moist curing before loading	≥ 1 day	≥ 1 day	≥ 1 day	≤ 14 days	≥ 1 day
Age of loading	≥ 1 day	≥ 1 day	≥ 1 day	≥ 1 day	≥ 1 day
Fine aggregate content in total aggregate, %	-	Considered	Considered	-	-
Air content	-	Considered	Considered	-	-
Slump	-	Considered	Considered	-	-
Size effect	Considered	Considered	Considered	Considered	Considered

2.2 Instantaneous Camber

2.2.1 Introduction

This section provides some background for the factors that affect the camber, such as material properties, camber measurement techniques, and methods of estimating instantaneous camber, and how they have been accounted for in the past. The challenges of predicting the instantaneous camber are shared by designers and precasters. A current challenge that exists for designers is improving the accuracy of the variables used for design and the prediction techniques, while precasters face difficulties with the current measurement methods and fabrication procedures adopted for PPCBs. These challenges result in camber measurements that may vary by as much as 50% (Tadros et al. 2011). To improve and understand the instantaneous camber prediction for PPCBs, an investigation of past studies was undertaken and is discussed in this section.

Factors that affect the camber, such as variables used in the design, can complicate the ability of designers to accurately predict the camber. Variables that are used to calculate the instantaneous camber and that affect prediction accuracy include the modulus of elasticity of the concrete, the prestress force, and the estimated prestress losses. Predicting the modulus of elasticity of the concrete has presented problems due to the variability associated with concrete properties. Each

concrete mix is composed of disproportionate materials and is subjected to different curing conditions, which can complicate the prediction of this variable. Additionally, the prestress force applied to the PPCB can lack accuracy due to the tensioning procedure and the prediction of prestress losses. For the long-term camber, further challenges arise because concrete and prestressing properties continuously change with time. The rearrangement and reduction in concrete materials, as a result of creep, shrinkage, and the relaxation of the prestressing strands, will result in a reduction of the prestress force. The creep, shrinkage, and loss of prestress force will affect the long-term camber and present further challenges with camber prediction.

Difficulties with measuring the camber occur at the transfer of prestress and throughout the life of the PPCBs. Many measurement techniques have been recommended, and some are frequently used more than others for measuring the camber. The methods employed differ among precasters and regions, and these methods are certainly different from those used by other researchers for accurately measuring the camber. A common goal is finding a method to measure the camber accurately without extensive amounts of time. The different methods of taking the camber measurements will be outlined and discussed in Section 2.3, along with the potential errors that each method can present.

The camber prediction methods have been investigated in past research as well. Methods include simplified methods as well as methods such as those based on advanced finite element models (FEMs). The accuracy of simplified hand calculations and finite element models are dependent on the accuracy of the material properties of concrete and steel and the assumptions used for each method. Reviewing previous research, as summarized in Sections 2.2.2 to 2.2.5, helped determine the assumptions used in both simplified and advanced models that cause discrepancies between the analytical and measured camber.

2.2.2 Factors Influencing Instantaneous Camber

In addition to errors associated with the measurement technique and the camber prediction technique, variables such as the prestress force, prestress losses, and modulus of elasticity affect the accuracy of the instantaneous camber prediction. A review of past research on the factors that influence camber predictions is presented in this section.

2.2.2.1 Prestress Losses

Prestress losses describe the loss of tension in the prestressing steel. Prestress losses are subtracted from the tensioning prestress force to determine the effective prestress force that is present in a PPCB. Underestimation of prestress losses will result in a reduction of the camber, while overestimation of prestress losses can result in an excessive camber. Prestress losses can be divided into the time periods of instantaneous and long-term losses. Instantaneous prestress losses primarily include elastic shortening, seating, and relaxation after the initial tensioning to the time of bonding to the concrete. Both seating and relaxation are sometimes ignored when calculating instantaneous prestress losses because they are typically small in magnitude. Long-term losses include the instantaneous losses as well as losses due to the creep and shrinkage of the concrete.

Various models used to predict prestress losses differ from each other in their ability to incorporate material properties, time increments, and prestress losses. According to Gilbertson and Ahlborn (2004), the parameters that have the greatest impact on prestress losses are the initial strand stress, initial concrete strength at release, relative humidity, and strand eccentricity. Methods of predicting prestress losses have different levels of computational involvement, time, and accuracy. Three common methods listed in order of assumed accuracy, according to Jayaseelan and Russell (2007), are the time-step method, refined methods, and lump sum loss method. The time-step method requires dividing the time into intervals as the concrete ages (Jayaseelan and Russell 2007). Iterating the stress in the strands for each time step allows for the calculation of the prestress values at a specific time. This is the most involved method because multiple iterations are usually required. Refined methods use prestress losses from the elastic shortening and the time-dependent losses that are calculated separately. The total loss is the sum of the individual losses that are calculated. The lump sum loss method utilizes parametric studies for PPCBs based on average conditions. Trends obtained from parametric studies have resulted in the lump sum method (Jayaseelan and Russell 2007). Naaman (2004) states that although the three procedures vary in the method used to determine the long-term prestress losses, they all use primarily the same method of calculating instantaneous losses. Sections 2.2.2.1.1 to 2.2.2.1.3 focus on the agreement between the designed and measured instantaneous losses.

2.2.2.1.1 Elastic Shortening

When the prestress is transferred to a PPCB, the prestressing strands exert a prestress force that acts along the length of the PPCB. This force will cause the PPCB to shorten from its original length by a small amount (see Figure 2.3). Due to the bonding between the prestressing strands and the concrete, the prestressing strands shorten as well. As a result, there is a reduction in the amount of the initial prestress strain in each strand, and thus the overall prestress force of the PPCB is reduced. Conversely, if a PPCB cambers upward, the self-weight of the PPCB causes an increase in the strain of the prestressing strands that are located below the neutral axis. The sum of the three components is referred to as the elastic shortening.

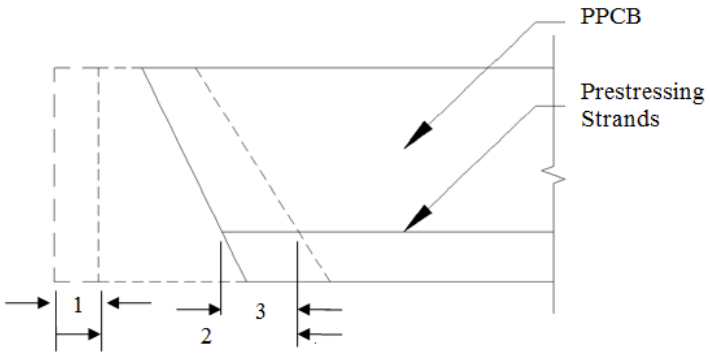

where: 1= PPCB shortening due to the applied prestress force.
2= PPCB shortening due to the application of prestress at the centroid of the prestressing strands.
3= Increase in PPCB length due to the self-weight.

Figure 2.3. PPCB length after the transfer of prestress

Throughout the different code changes, calculating the elastic shortening by determining the average compressive stress in the concrete at the center of gravity of the tendons has remained constant. Differences have occurred with how the average compressive stress in the concrete at the center of gravity of the tendons is calculated.

Comparing different methods of calculating the elastic shortening to the measured elastic shortening values has allowed researchers to see which method agrees best. Tadros et al. (2003) found that the proposed detailed method of calculating prestress losses agreed with the measured value. This method warrants neglecting the calculation of elastic shortening losses when using the transformed section properties. The results in Table 2.2 show seven PPCBs from different locations and the agreement between the measured and estimated elastic shortening values.

Table 2.2. Measured versus estimated prestress losses (Tadros et al. 2003)

PPCB	Elastic Shortening		
	Measured (kip)	Estimated (kip)	Percent Error
Nebraska G1	17.02	19.67	15.6
Nebraska G2	16.50	19.67	19.2
New Hampshire G3	25.17	17.94	28.7
New Hampshire G4	24.42	17.94	26.5
Texas G7	12.88	14.71	14.2
Washington G18	27.62	20.87	24.4
Washington G 19	25.49	20.87	18.1

Five prestress loss methods, including the proposed detailed method whose results are shown in Table 2.2, were compared in National Cooperative Highway Research Program Report 496 (NCHRP 496) (Tadros et al. 2003). The five different methods, which can be seen in Table 2.3, included an AASHTO LRFD lump-sum method, the AASHTO LRFD (2010) refined method, the proposed approximate method using gross section properties, the proposed approximate method using transformed section properties, and the proposed detailed method.

The results in Table 2.3 show that there are slight differences among the calculated elastic shortening losses. For the purposes of a comparison between the methods when using the transformed section properties, elastic losses were neglected, and the total elastic shortening losses due to the combination of the prestress transfer and the PPCB self-weight were estimated.

Table 2.3. Comparison of prestress losses and concrete bottom fiber stress (Tadros et al. 2003)

Loading stage	Loading	Prestress loss method* (ksi)					Concrete bottom fiber stress (ksi)				
		1	2	3	4	5	1	2	3	4	5
Prestress transfer	P_i	26.13	29.50	29.50	26.13	29.50	4.16	4.69	4.69	4.16	4.69
PPCB self-weight	M_g	-6.01	-6.80	-6.80	-6.01	-6.80	-1.08	-1.20	-1.20	-1.08	-1.20
	Elastic loss		-2.95	-2.95		-2.95		-0.47	-0.47		-0.47
Subtotal		20.12	19.75	19.75	20.12	19.75	3.08	3.02	3.02	3.08	3.02

*Method 1: Proposed approximate method with transformed section properties.
Method 2: Proposed approximate method with gross section properties.
Method 3: AASHTO LRFD Lump-Sum method with gross section properties.
Method 4: Proposed detailed method with transformed section properties.
Method 5: AASHTO-LRFD Refined method with gross section properties.

Ahlborn et al. (2000) instrumented two PPCBs and compared the measured prestress losses to the predicted values using the following methods: time-step methods, PCI Committee on Prestress Losses (1975), PCI Handbook (1992), and AASHTO LRFD (2010). The results in Table 2.4 are in terms of the percentage of the strand stress at the time of the initial tensioning. Evaluating the percent loss with respect to the initial tensioning value includes relaxation losses; however, this value is affected by the ambient temperature for PPCB I and PPCB II.

Table 2.4. Measured losses and predicted design losses

	Measured[1]		Time-Step Nominal Design Case[2]	Time-Step HSC Nominal Case[3]	PCI Committee on Prestress Losses (1975)	PCI Handbook (1992)	AASHTO (1996)
	PPCB I[*]	PPCB II[*]					
Initial	15.5 %	18.6%	11.2%	13.8%	10.6%	9.9%	10.2%

[1] Lower bound measured losses from vibrating wire gages embedded in each PPCB.
[2] Predictions using nominal design values with normal strength concrete relationships.
[3] Predictions using nominal design values with high strength concrete relationships.
[*] Concrete stress before transfer is assumed to be zero.

The results in Table 2.4 indicate that the Time-Step High-Strength Concrete (HSC) Nominal Case shows greater initial prestress losses than the Time-Step Nominal Design Case. The elastic modulus that correlates with the measured HSC model is lower than that of the normal strength model, which results in the higher elastic shortening loss seen in Table 2.4 (Alhborn et al. 2000). Additionally, methods such as the PCI Committee on Prestress Losses (1975), PCI Handbook (1992), and AASHTO LRFD (2010) use the normal-strength concrete properties to obtain the prestress losses as well. The method that agreed best with the measured prestress losses from the two PPCBs that were instrumented is the Time-Step HSC Nominal Case. This is because high-strength concrete was used in PPCBs I and II and was also used in the prediction method.

2.2.2.1.2 Seating

Seating is the movement of the prestressing steel when it is allowed to rest in the anchorage. After the prestress is applied, the anchoring devices (chucks) are placed around the prestressing strands to hold the prestress force, while workers fabricate the PPCB and place the concrete in the forms. The chucks are known to slip small distances when the strands are initially tensioned. The slip or seating will result in a loss of the prestress force. Seating losses are typically small, and if a long prestressing bed is used, then they are ignored (Zia et al. 1979). However, the PCI Committee on Prestress Losses (1975) suggests that the seating losses should be taken into account, regardless of the length of the prestressing bed, when determining the effective prestress force.

2.2.2.1.3 Relaxation

Relaxation occurs due to the loss in the tension in a prestressing strand with respect to time when it is held at a constant length. The loss of tension in a stressed prestressing strand reduces the prestressing force. Relaxation occurs from the time the prestressing strands are tensioned to the end of the service life of the member. The methods used to predict relaxation typically neglect relaxation from the time of tensioning to the time of the transfer of the prestress. However, ACI Committee 343R-95 (1995) suggests including the relaxation loss from the time before the transfer of the prestress.

2.2.2.2 Modulus of Elasticity

The factors that influence the modulus of elasticity as well as its prediction methods were discussed earlier in Section 2.1.4. The modulus of elasticity is an important variable in the prestressed concrete that affects the instantaneous camber. The AASHTO LRFD (2010) method of computing the modulus of elasticity accounts for the time-dependent effects by using the compressive strength, which was discussed in Section 2.1.3. If the PPCB is steam cured, the strength of the test cylinders loosely reflects the maturity of the concrete by indicating the strength that is achieved. Therefore, time-dependent effects on the modulus of elasticity can be accounted for by using the release strength following the AASHTO LRFD (2010) recommendation for finding E_c. Hence, the specified modulus of elasticity is dependent on the release compressive strengths when using the AASHTO LRFD (2010) method.

The measured release strengths are required to be greater than the designed strength in order to transfer the prestress to the PPCB. The increase in the compressive strength will give a larger modulus of elasticity, which will decrease the camber. Adjusting the compressive strength so that it is representative of the strength of the PPCB is important for accurately predicting the camber. O'Neill and French (2012) suggest that the release strength data collected from 2006–2010 on average is 15.5% higher than the $f'_{ci,design}$, with some cases reaching as high as 35%. Rizkalla et al. (2011) found that the release strengths were underpredicted by 24% on average, with the maximum ratio of the measured-to-designed release strength of 110%. The 24% underprediction of the release strength affected the modulus of elasticity by 15%. To solve this problem, Rizkalla et al. (2011) suggest a multiplier of 1.25 to be used to account for the

underpredicted release strengths. Table 2.5 shows the results of past studies where the release strengths were obtained and measured.

Table 2.5. Multipliers for compressive strengths

Reference	Multiplier for Instantaneous Release Strength	Multiplier for Long-Term Release Strength
O'Neill and French (2012)	1.15	-
Rizkalla et al. (2011)	1.25	1.45
Rosa et al. (2007)	1.10	1.25

Based on the average ratio of the measured-to-designed release strengths, multipliers were developed by O'Neill and French (2012), Rizkalla et al. (2011), and Rosa et al. (2007) to accurately predict the modulus of elasticity, as seen in Equation 2-89.

$$f'_c = f'_{ci} \times \text{multiplier} \quad \textbf{(2-89)}$$

where f'_{ci} is the specified concrete strength.

A study determining the effect that the release strength has on the modulus of elasticity and ultimately the camber was conducted by O'Neill and French (2012), the results of which are presented in Table 2.6.

Table 2.6. Impact of high-strength concrete release strengths on camber (O'Neill and French 2012)

Percent Increase in Concrete Strength	Percent of Reduction in Release Camber (ACI 363)
5%	1.6%
10%	3%
15%	4.5%
20%	7.6%
25%	7.1%
30%	8.3%
35%	9.4%

Due to the modulus of elasticity being a function of the square root of the concrete strength, the increase in the compressive strength does not correlate to the same decrease in the camber. In this study, the modulus of elasticity was determined by using the ACI 363R-92 method. The results revealed that the AASHTO LRFD (2010) equation for the modulus of elasticity should replace the ACI 363 equation that was currently used by the Minnesota Department of Transportation (MnDOT) in the camber calculations due to the AASHTO equation's ability to account for the stiffer concrete that was being produced at the precast plant (O'Neill and French 2012). Therefore, the decrease in the design release camber due to the increase in the concrete strength was replicated in Chapter 5 of this report using the AASHTO LRFD (2010) method for determining the modulus of elasticity.

2.2.3 Camber Measurement Technique

Over the past several decades, research efforts have attempted to resolve the camber measurement problems at the transfer of the prestress. Many methods have been recommended, and some are currently being used for measuring the camber at the precast plant. Methods include measuring the camber with the stretched-wire system, surveying equipment from the top or bottom flange, tape measuring from the bottom flange, and photogrammetry.

Inaccurate camber measurement techniques can fail to represent the correct camber that is actually present in a PPCB. Unexpected camber growth will ensue when techniques are based on the inaccurately measured camber. When evaluating whether analytical prediction methods are accurate based on their agreement with the measured camber, the accuracy of the measurement technique is equally important. Eliminating potential errors due to the measurement technique will allow researchers to determine the magnitude of errors relating to the analytical camber. The errors associated with measuring the camber can be related to the accuracy of the instrument that is used, the location from which the measurements are taken, the time when the camber is measured, and additional measurement factors such as friction between the precasting bed and PPCB, bed deflections, and the roughness of the surface where the camber is measured. Evaluating the measurement technique based on these factors can provide a guide to developing accurate measurement techniques. The following section investigates the methods used to measure the camber from past research.

2.2.3.1 Stretched-Wire Method

A system that has been used by precasters and multiple researchers is the stretched-wire method. This method uses a wire that is stretched along the length of the PPCB. The distance between the string and the top flange at the midspan is measured to obtain the camber.

The method used for measuring the camber with the stretched-wire method involves attaching the string at each end of the PPCB at the same elevation. The string is pulled tight or calibrated to a certain tension. A measurement of the distance between the string and the top of the PPCB at midspan is taken. Because the midspan measurement is taken with respect to the elevation of the ends of the PPCB, the distance between the string and the top flange at the midspan is a representation of the camber. Precasters and past research that have used the stretched-wire system have used variations regarding the anchorage of the string to the ends of the PPCB, the materials used, the location from where the measurement is taken, and the procedure for measuring the camber. All of these variations influence the accuracy of the instantaneous camber.

Anchoring the string at each end of the PPCB has been done multiple ways. The most common way to attach the string to the PPCB end is by an anchor bolt that is attached to the PPCB. Anchor bolts can be embedded or drilled into the concrete surface. Figure 2.4 shows the string being connected to the end of a PPCB using an anchor bolt.

Figure 2.4. Anchored end with a pulley of wire used for the stretched-wire system (O'Neill and French 2012)

In Figure 2.4, the pulley that is shown was also used to position the string at the correct height at the anchored end. Another alternative to using anchor bolts to connect the string to the ends of the PPCB is embedding pieces of rebar. Rizkalla et al. (2011) attached the string to the end of the PPCB by embedding a piece of rebar on each end with a notched surface (Figure 2.5).

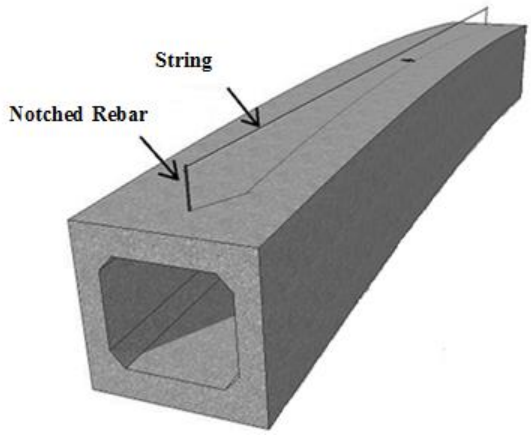

Figure 2.5. PPCB with rebar and string in place for camber measurements (Rizkalla et al. 2011)

The notched surface is a specified distance above the end of the top flange to ensure that end elevations are equal. If unequal end elevations are present, the measured camber does not represent the camber accurately.

A sag in the string due to the self-weight may be present when using the stretched-wire system. The accuracy may depend on the type of wire, the tension put on the wire, and the ambient

temperature. Variations, from the piano wire used by Kelly et al. (1987) to the 80 pound fishing wire used by O'Neill and French (2012), have been used in the past. Additionally, calibrating the wire before the camber measurements are taken so that the discrepancy caused by temperature and relaxation in the wire is reduced is important to the accuracy of the stretched-wire system. Various methods of calibration have been used in the past. A method to calibrate the tension in the wire involves attaching a mirror and a ruler at midspan (Figure 2.6).

Figure 2.6. Ruler and mirror located at the midspan (O'Neill and French 2012)

In this method, the mirror is used to eliminate the effects of the parallax, while the ruler reading is recorded and serves as a reference point to the initial position of the string at the midspan. Subsequent measurements are then compared to the baseline reading. Calibration can occur by increasing the tension with mechanical means or by hanging a weight at the end of the string, as seen in Figure 2.7.

Figure 2.7. Free end of the stretched-wire system with the weight and pulley (O'Neill and French 2012)

Another method is to hang a 35 pound trolley from the midspan, as seen in Figure 2.8.

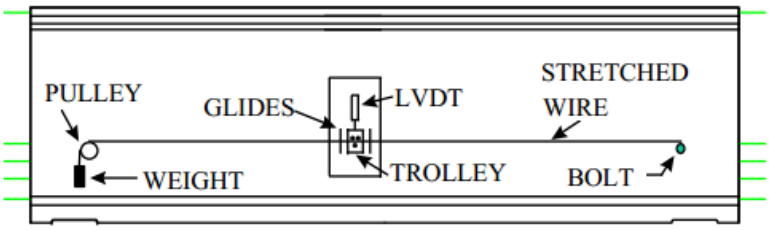

Figure 2.8. Stretched-wire system with a weighted trolley at midspan (Barr et al. 2000)

In this figure, the green lines represent that the prestressing force is adjustable if required. Hanging the trolley minimizes the vibration in the wire at the midspan that can misrepresent the camber. The method involving a trolley at the midspan would also require an adjustment to the tension in the wire due to relaxation and thermal effects.

The location of the camber measurement using the stretched-wire system has been observed to be different from study to study. Kelly et al. (1987) measured the camber using the stretched-wire system from the bottom flange. Complications with the measurements from the bottom flange were present due to the inconsistent PPCB depths. Using the stretched-wire method, Rizkalla et al. (2011) measured the camber from the top flange using rebar that extended above the top flange surface. This is beneficial because the same reference point from the top flange is used by contractors at the bridge site to set the haunch heights.

Results from using the stretched-wire method may differ depending on the time the camber measurements are taken. A camber measurement was taken before the transfer of prestress by O'Neill and French (2012) to establish a datum. Additional measurements were taken immediately after the transfer of prestress and periodically throughout the lifespan of the PPCB. Taking the original datum ensured that the camber measurements could be compared using a similar reference point and that any inconsistencies would be accounted for in the PPCB depth.

Multiple errors can be eliminated with the stretched-wire system method by eliminating the influence of the bed deflections, friction between the PPCB ends and the precasting bed if the measurement is taken after the PPCB has been lifted, and inconsistent top flange surfaces. Variations regarding the anchorage of the string to the ends of the PPCB, the materials used to take measurements, the measurement location, and the procedure for measuring the camber can influence the accuracy in the camber as well.

2.2.3.2 Tape Measure

Using a tape measure to determine the camber is one of the simplest ways to measure the camber. Precasters typically measure the camber of PPCBs while they rest on the precasting bed or while they are suspended by a travel crane. In this method, instantaneous camber measurements are taken by reading the midspan elevation relative to the precasting bed with a tape measure (Figure 2.9).

Figure 2.9. Camber measurement with a tape measure at midspan of a PPCB (Iowa DOT 2013b)

This measurement method has inaccuracies due to not accounting for the bed deflections, the friction between the precasting bed and PPCB if the PPCB is not lifted, and the inconsistent PPCB depths along the length of the PPCB. In a study conducted by Rosa et al. (2007), it was observed that precasters took the camber measurements from the bottom flange while the PPCB was suspended by travel cranes. The camber is calculated from this method by subtracting the

midspan measurement from the average of the two end measurements. Difficulties in this technique that will result in inaccurate measurements include the travel cranes not being able to hold the PPCB at a consistent elevation, the effect of wind acting on the PPCB, and an increase in the camber due to the location of lifting the PPCB.

2.2.3.3 Survey Equipment

Survey equipment such as transits, total stations, and laser levels have been used to measure the camber. The survey equipment is used to take the elevation readings of the PPCB to determine the relative displacement of the midspan with respect to the ends. Subtracting the average elevation readings of both ends from the midspan elevation reading gives the camber at the midspan. Variations of this method depend on the location of the measurements, the time the measurement was taken, and the equipment used.

The location of the camber measurement when taken with survey equipment has differed across past studies. Rosa et al. (2007) took the camber measurements from the web of the PPCB using a wooden template to reduce errors. A template was made and fitted to the web with a ruler attached (Figure 2.10).

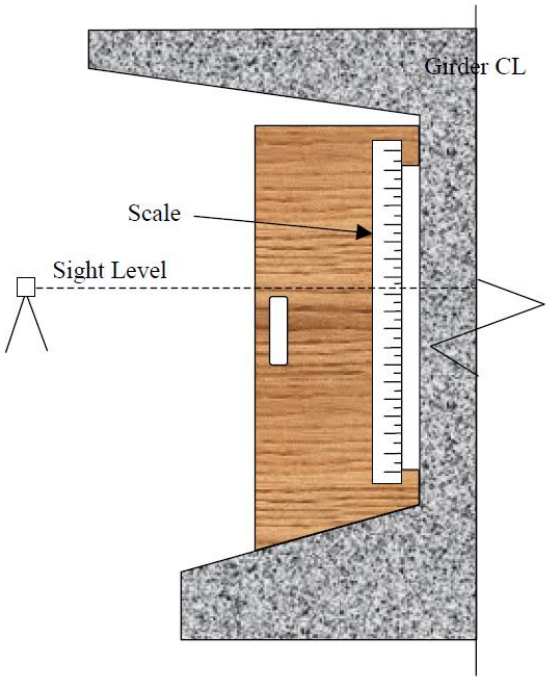

Figure 2.10. Camber measuring template (Rosa et al. 2007)

Survey readings of the ruler were taken at the ends and at the midspan of the PPCB to determine the camber. The discrepancy between the web and the bottom flange of the PPCB due to inconsistencies in the PPCB depth were observed to be within the range of ±0.25 in., which

resulted in a 7.1% difference. Hinkle (2006) measured the camber from the bottom flange using a laser level. A template was made that fit onto the top of the bottom flange (Figure 2.11).

Figure 2.11. Taking readings with a laser level surveying system (Hinkle 2006)

This ensured that the measurement consistently occurred from the same location on the bottom flange. Similarly, Woolf and French (1998) measured the camber using a grade rod that was fabricated to have a 90 degree angle that extended below the bottom flange to obtain the camber.

Measurements from the top flange were taken by Johnson (2012). In this study, bolts were embedded into the surface so that the elevation measurements were taken from the same location at various times throughout the PPCBs life (Figure 2.12).

Figure 2.12. Camber measurement marker (Johnson 2012)

The time at which the camber measurement is taken affects the accuracy. Woolf and French (1998) noticed that during the transfer of the prestress the friction between the precasting bed

and PPCB inhibited the camber from reaching its full potential. Due to the PPCB shortening after the transfer of the prestress, the ends will attempt to overcome the friction and slide toward each other. When the PPCB ends overcome the friction of the precasting bed, the camber increases at the midspan. The procedure for quantifying the increase in the camber due to friction was determined by taking the average of the camber measurements before and after the PPCB was lifted and placed down on the precasting bed after the transfer of the prestress. Taking the average of the camber readings before and after the PPCB was lifted was believed by O'Neill and French (2012) to be a close approximation of the reverse friction, or the decrease in midspan elevation due to the reverse of the friction forces. In a similar study, Rosa et al. (2007) found the influence of friction to be 0.15 in. The studies conducted by Woolf and French (1998) and O'Neill and French (2012) signify the importance of taking the camber measurements before and after lifting the PPCB to determine the magnitude of the friction. In addition to the friction, the creep of concrete will begin immediately after the transfer of the prestress. The constant prestress force that is applied to a PPCB will allow creep to occur, thus increasing the camber with respect to time. Failure to take the camber measurements where the friction and creep of concrete are misrepresented will inhibit the accuracy of the camber. The topics of friction and creep are discussed in Chapter 4 in more detail.

2.2.3.4 Photogrammetry

In addition to the methods listed above, camber measurements have been recorded by using photogrammetry. Photogrammetry involves taking two-dimensional photographs and relating them to three-dimensional measurements of an object. The process involves taking pictures of an object with targets on it and control points around it before and after an event. The difference between the two pictures allows researchers to determine the change in the deflection of a PPCB. Typically, this measurement technique is not used by precasters due to its high cost, large time commitments, and limited use.

A specific experiment conducted by Jáuregui et al. (2003) investigated noncontact photogrammetric measurements on two bridges and in one laboratory test on a PPCB. The test compared the method of photogrammetry to dial gauge readings, a total station reading, survey level and rod readings, and also a finite element model. The results in Table 2.7 show that a close agreement between the different methods and photogrammetry is possible. Errors introduced between the methods could have resulted from uneven surface conditions along with inaccuracies in the types of equipment that are being compared to the photogrammetry.

Table 2.7. Experiments and results from noncontact photogrammetric measurement of vertical bridge deflections (Jáuregui et al. 2003)

Test and Specimen	Experiment	Methods Compared with Noncontact Photogrammetry	Results
Laboratory Experiment-W21X62 Steel PPCB	1. Loaded with steel plates to compare deflection.	Dial Gauge Readings	0.02-0.05 in. difference in measurements which represent 2-10% accuracy.
Field Test 1-Prestressed Concrete Bridge PPCB	1. Initial PPCB camber compared with level and rod.	Level and Rod	Agreement of 1-10% of the maximum measured PPCB camber.
	2. PPCB deflection caused by concrete deck and traffic barriers.	Total Station	Agreement of 0.13 in. with total station before and after concrete deck and traffic barriers were cast.
Field Test 2-Noncomposite Steel PPCB	1. Live load PPCB deflections with two dump trucks (56 kips each)	Level Rod and Finite Element Models	0.02-0.06 agreement between level rod readings, and conjugate PPCB method.

Of the measurement methods used in the past by researchers and precasters, errors can be introduced by bed deflections, friction between the precasting bed and PPCB, inconsistent top flange surfaces that affect the camber, or even an operator error. Some methods, although convenient, are not practical from a researcher's standpoint because they can lack accuracy. Contrarily, labor-intensive methods of taking the camber measurements are inefficient for the tight schedule precasters are often faced with.

2.2.4 Prediction of Instantaneous Losses

The current methods for predicting the instantaneous losses, including elastic shortening, seating, and relaxation, are presented in Sections 2.2.4.1 to 2.2.4.3.

2.2.4.1 Elastic Shortening

Elastic shortening occurs when there is a reduction in strain in the prestressing strands at the transfer of prestress due to the concrete member shortening. The three components listed in Section 2.2.2.1.1 contribute to the total elastic shortening loss. The change in stress of the prestressing strands due to elastic shortening is represented in different ways and is further discussed in subsequent sections.

2.2.4.1.1 AASHTO LRFD (2010)

The AASHTO LRFD (2010) method for predicting the elastic shortening is listed in Equation 2-90. This method involves calculating the concrete stress at the center of gravity of the prestressing strands and multiplying it by the ratio of the modulus of elasticity of the steel to that of the concrete.

$$\Delta f_{pES} = \left(\frac{E_p}{E_{ci}} f_{cgp}\right) \quad \textbf{(2-90)}$$

where E_p is the modulus of elasticity of the prestressing steel (ksi), E_{ci} is the modulus of elasticity of the concrete at the transfer or time of the load application (ksi), and f_{cgp} is the concrete stress at the center of gravity of the prestressing tendons due to the prestressing force immediately after the transfer and the self-weight of the member at the section of the maximum moment (ksi).

Determining the concrete stress at the center of gravity of the prestressing tendons has been done in multiple ways. Typically, iterations are required to determine the stress in the strands after elastic shortening losses occur. The variables that are required to determine the concrete stress at the center of gravity include the initial jacking force of the prestressing tendons, the moment of inertia, the area of the section, the eccentricity between the center of gravity of the section and the prestressing strands, and the moment caused by the PPCB self-weight. Differences in the variables used to calculate the elastic shortening losses occur with the cross-section properties and the initial jacking force that is used.

When determining the initial jacking force prior to the transfer of prestress (P_o), calculations by different departments of transportation have been observed to be different. The Iowa PPCB standard (Iowa DOT 2011b) suggests that the initial jacking force be taken at 72.6% of the nominal prestressing force, while in AASHTO LRFD (2010) and ACI 318-11 (2011) the initial jacking force is taken at 75% of the nominal strength multiplied by the area of the strand. A reduced percentage of the nominal prestressing force, such as 72.6%, is used to eliminate the inaccuracies with the tensioning prestressing strands due to losses associated with the cold weather stressing. When reducing the prestress force from 75% to 72.6% of the nominal prestressing force, additional strands may need to be added to account for the reduction in prestress. However, the standard remains constant at 75% for most applications unless specified differently.

It is stated in AASHTO LRFD (2010) that if gross section properties are used, the prestress force may be assumed to be 90% of the initial prestress force before transfer. Through the iteration of f_{cgp}, the prestress loss due to elastic shortening will converge. The concrete stress at the center of gravity can be calculated using Equation 2-91 when gross section properties are used.

$$f_{cgp} = \left(\frac{P_i}{A_g} + \frac{P_i e^2}{I_g}\right) - \frac{M_g e}{I_g} \quad \textbf{(2-91)}$$

where P_i is the total prestressing force immediately after transfer (initially assumed to be 90 percent of jacking force); e is the eccentricity of the centroid of the prestressing strands at the midspan with respect to the centroid of the PPCB; A_g is the area of the gross cross-section of the PPCB; I_g is the moment of inertia of the gross cross-section of the PPCB; and M_g is the moment at the midspan due to the PPCB self-weight, assuming simply supported conditions = $\frac{W_g L^2}{8}$

where w_g is the uniformly distributed load due to the PPCB self-weight and L is the PPCB length.

If transformed section properties are used to calculate the stress at the center of gravity, it is assumed that the PPCB behaves as a composite section, where the steel and concrete are equally strained. AASHTO LRFD (2010) states that if transformed section properties are used, the effect of losses and gains due to elastic shortening deformations are implicitly accounted for, and Δf_{pES} should not be included in the prestressing force applied to the transformed section at the transfer. In other words, instead of using 90% of the initial prestressing force, use of the initial or jacking prestressing force is sufficient.

$$f_{cgp} = \frac{P_o}{A_{tr}} + \frac{P_o e_{tr}^2}{I_{tr}} + \frac{M_g e_{tr}}{I_{tr}} \quad \textbf{(2-92)}$$

where P_o is the initial prestressing force prior to the transfer.

There have been discussions about whether it is appropriate to use the gross or transformed section properties when calculating elastic shortening. Namman (2004) states that transformed section properties will result in greater accuracy, but gross section properties can be used as a first approximation. Tadros et al. (2003) shows in NCHRP Report 496 that, when using transformed section properties, the elastic shortening can be represented by Equation 2-92. It is also suggested that the elastic shortening loss of the prestress is automatically accounted for if transformed properties are used in the analysis. For the AASHTO LRFD Bridge Design Specifications, Swartz et al. (2012) confirms the NCHRP 496 results by saying that using transformed section properties will provide a direct solution by applying the prestressing force before the transfer (not calculating any elastic shortening losses explicitly) to the transformed section properties.

Additionally, the loss due to the elastic shortening in pretensioned members may be determined by Equation 2-93.

$$\Delta f_{pES} = \frac{A_{ps} f_{pbt} (I_g + e_m^2 A_g) - e_m M_g A_g}{A_{ps}(I_g + e_m^2 A_g) + \frac{E_{ci} I_g A_g}{E_p}} \quad \textbf{(2-93)}$$

where A_{ps} is the area of the prestressing steel (in.^{2}), A_g is the gross area of the section (in.^{2}), E_{ci} is the modulus of elasticity of the concrete at the transfer (ksi), E_p is the modulus of elasticity of the prestressing tendons (ksi), e_m is the average prestressing steel ececntiricy at the midspan (in.), f_{pbt} is the stress in the prestressing steel immediately prior to the transfer (ksi), I_g is the moment of inertia of the gross concrete section (in.^{4}), and M_g is the midspan moment due to the member self-weight (kip-in.).

Equation 2-93 is a general equation used to summarize the elastic shortening of an entire PPCB. When a more detailed elastic shortening analysis is desired, the elastic shortening should be calculated from Equation 2-90. Equation 2-90 has the ability for variables to be adjusted for the different properties of the PPCB at specific locations.

Rosa et al. (2007) used the AASHTO LRFD (2006) guidelines to calculate the prestress losses due to the elastic shortening. When using this method, complications arose due to the calculation of losses of the permanent and temporary prestressing strands. Temporary prestressing strands are external reinforcements used to minimize damage to the PPCB during its storage and shipping. Both groups of strands were accounted for by calculating different levels of stress separately. Using equilibrium and strain compatibility conditions, Rosa et al. (2007) was able to determine the prestress force after the transfer of prestress.

$$P_i = \frac{P_j + M_{sw} e_p A_p n}{1 + np(1 + e_p^2 \frac{A_c}{I_g})} \quad \textbf{(2-94)}$$

where n is the modular ratio equal to $\frac{E_p}{E_c}$ and P is the reinforcement ratio equal to $\frac{A_{ps}}{A_c}$.

2.2.4.1.2 PCI Method (PCI 2010)

The PCI method of calculating prestress losses follows the AASHTO LRFD (2010) method found in Equations 2-90 through 2-92. The jacking force is multiplied by 90%, which is assumed to be the reduction in prestress due to the elastic shortening; however, the procedure is not iterated. The initial jacking force is taken as 75% of the nominal strength multiplied by the strand area.

2.2.4.2 Seating Loss

As stated in Section 2.2.2.1.2, the seating loss is caused by the movement of the prestressing strand before the chucks can anchor and hold the prestressing force. According to AASHTO LRFD (2010), the seating loss causes most of the difference between the jacking stress and the stress at the transfer. Ultimately, the seating settlement of the prestressing strands depends on the tensioning system and anchors that are used. Power seating is recommended (AASHTO LRFD 2010) for short tendons because the prestress loss tends to be significant. However, the power seating is not necessary for long tendons because the loss of prestress is minimal. For wedge-type strand anchors, the seating may vary between 0.125 and 0.375 in., but 0.25 in. is the value that is recommended in the AASHTO LRFD specifications (2010).

Although the AASHTO LRFD (2010) does not give the equation for seating losses, using Hooke's law in Equation 2-95 will relate the stress and strain to give an accurate seating value. Rearranging the values will result in Equation 2-96, which is used to calculate the loss in prestress due to the seating.

$$\Delta_s = \frac{\Delta P_{pS} L}{AE} \quad \textbf{(2-95)}$$

$$\Delta P_{pS} = \frac{\Delta_s AE}{L} \quad \textbf{(2-96)}$$

where Δ_{PpS} is the prestress loss due to the seating (kips); Δ_s is the seating distance (in.); L is the length of the prestressing strand (in.); A is the cross-sectional area of the prestressing strand (in.^{2}); and E is the modulus of elasticity of the prestressing strand (ksi), which is taken as 28,500 ksi.

An example of a PPCB is explained to clarify the impact that seating can have on the prestress force and ultimately the camber. An Iowa DOT BTE 145 PPCB has 42 straight bottom prestressing strands and 10 harped strands. If the prestressing strand length is 440 ft and the seating distance is assumed to be 0.25 in., there will be a 0.29 kip reduction in the prestress per strand. Although this seems insignificant, multiplying the loss per strand by the total number of strands results in a 15.22 kip or 0.7% reduction in the prestress.

2.2.4.3 Relaxation

Relaxation, as stated in Section 2.2.2.1.3, is the loss in the tension in a prestressing strand with respect to time when it is held at a constant length. Relaxation is dependent on the properties of steel, the applied tension, and the temperature that the prestressing strands are subjected to. In design, relaxation is accounted for after the transfer of the prestress. ACI Committee 343R-95 (1995) accounted for the loss in prestress due to relaxation at the time between the tensioning and the transfer. Rizkalla et al. (2011) agreed with the results from ACI Committee 343R-95 (1995) and used Equation 2-97 for calculating the relaxation, where time is divided into two periods, before and after the transfer of the prestress.

$$\Delta f_{pR1} = \frac{\log(24.0t)}{40.0}\left[\frac{f_{pi}}{f_{py}} - 0.55\right] f_{pi} \qquad \textbf{(2-97)}$$

where t is the time between the initial jacking and transfer (days), f_{pi} is the strand stress after the jacking (ksi), and f_{py} is the yield strength of the strand (ksi).

An example of how relaxation losses can affect the prestress force is described below. An Iowa DOT BTE 145 PPCB that is tensioned on a Friday and concrete is placed on a Monday morning will have more than two full days of relaxation losses before the concrete is bonded to the prestressing tendons. Assuming that the initial jacking force (f_{pi}) is 196 ksi after the seating losses, with a yield strength of the prestressing steel of 243 ksi, the loss in the prestress when using Equation 2-97 is 2.11 ksi, or 0.46 kips per prestressing strand. Multiplying the loss per strand by the total number of strands results in a 23.85 kip or 1.08% reduction in the prestress.

2.2.5 Method of Predicting Instantaneous Camber

To predict the camber, several methods have been used by designers. Designers generally use computer programs to predict the instantaneous and long-term camber on the prestressed concrete PPCBs. Examples of some of these programs include PG Super (Bridgesight 2008–2010), CON/SPAN (CONTECH Construction Products Inc. 2002–2010), and CSI Bridge (Computers and Structures, Inc. 1978–2011). Along with predicting the camber using computer

models, designers can also use simplified hand calculation methods to verify results. Verifying the moment area method, Ahlborn et al. (2000) found that the instantaneous camber prediction results were nearly identical for the nominal design case when compared to the finite element model. Additionally, variables such as the prestress losses and the modulus of elasticity also affect the accuracy of the instantaneous camber predictions. An investigation into the methods used to predict the instantaneous camber along with variables important to the camber calculations are discussed in the following sections.

2.2.5.1 Moment Area Method

After calculating the instantaneous losses according to Sections 2.2.4.1 though 2.2.4.3, the effective prestress force can be determined for subsequent estimation of the camber at release using the moment area method. Also, the concrete modulus of elasticity can be predicted using the equations discussed in Section 2.1.4.2.

The moment area method uses the linear elastic analysis to predict the upward deflection of PPCBs. Assumptions when using the moment area method for a PPCB include that the prestress force is constant along the PPCB length, the member is not undergoing plastic deformation, and the cross-section is uniform and uncracked. When these assumptions are used, the moment area method captures the behavior of a PPCB at release and can be considered adequate for predicting the instantaneous camber. Using simple elastic beam formulas, the downward deflection due to the self-weight of the PPCB can also be determined. Adding the upward and downward components gives the total instantaneous camber. The expression of the camber at point j relative to point i is shown in the following:

$$\Delta_{j/i} = \int_{x_i}^{x_j} x\left(\frac{M}{EI}\right)dx \qquad \textbf{(2-98)}$$

For PPCBs, it is convenient to choose the midspan as point i and the end span as point j. Figure 2.13 shows the typical strand layout of a PPCB, the curvature diagram, and the deflected shape of a PPCB.

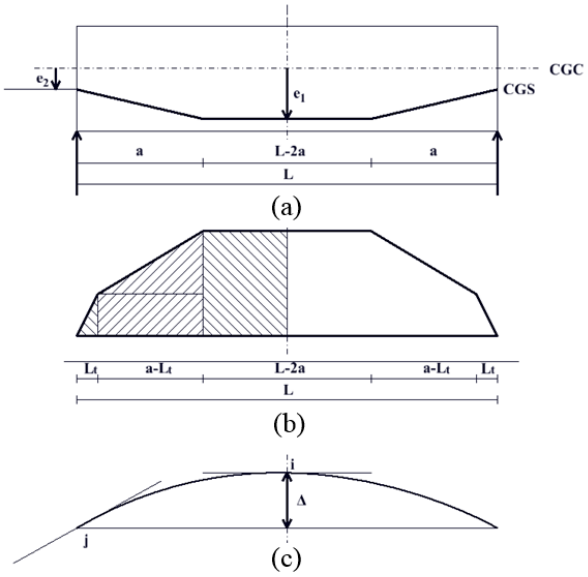

Figure 2.13. Moment area method for a PPCB: (a) Typical strand layout, (b) Curvature diagram, (c) Deflected shape of a PPCB

Also, L_t is the transfer length for a PPCB and can be determined using the equation in AASHTO LRFD (2010) 5.11.4.1 as follows:

$$L_t = 60\, d_b \qquad \textbf{(2-99)}$$

where d_b is the diameter of the strand.

The moment area method uses the moment created by the prestressing strands to relate to the PPCBs elastic deflection curve (Hinkle 2006). The first step in using the moment area method is to determine the moment diagram due to the prestress force. Multiplying the effective prestress force by the eccentricity of the prestressing strands from the centroid of the cross-section will provide the moment diagram at a specific location of the PPCB. Because the profile of prestressing strands is usually composed of straight and harped layouts, the moment for each set of strands is determined independently. The sets of strands include the straight bottom strands, the harped strands, and the sacrificial top strands (Figure 2.14).

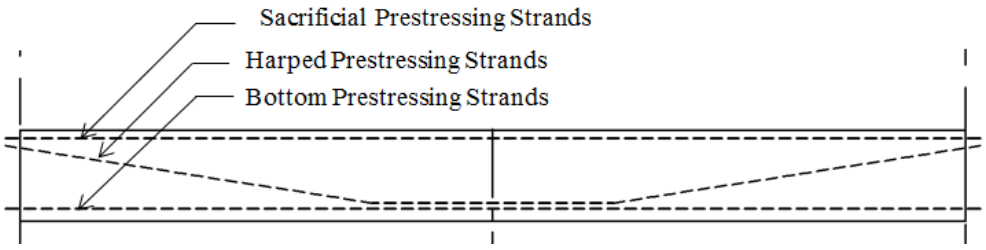

Figure 2.14. PPCB with sacrificial, harped, and bottom prestressing strands

The sacrificial top strands are typically stressed from 3–5 kips and are sometimes ignored due to their low prestress force. These sacrificial top strands are usually used to facilitate the placement of the PPCB shear reinforcement. However, accurately accounting for the sacrificial prestressing strands will result in increased accuracy. Taking the sum of the moments caused by the straight and harped strands will give the total moment due to prestressing at certain locations of the PPCB.

Once the moment diagram is established, it is integrated. This integrated area is multiplied by the distance from the end of the PPCB to the centroid of the section of interest. In order to simplify calculations, various sections of the moment diagram can be broken into different areas, as seen in the shaded areas of Figure 2.13. Taking the product of the area and the distance to the centroid of the section on the moment diagram will give the moment (M) of the PPCB. Dividing the moment (M) by the product of the modulus of elasticity (E) and the moment of inertia (I) will give the upward deflection due to the prestressing.

Determining the downward deflection due to the self-weight of the PPCB is determined using an elastic beam formula. PPCBs are simply supported until composite action is achieved when the piers and PPCBs are bonded together through a diaphragm. The elastic equation for a simply supported PPCB at the midspan is $\Delta_{sw} = \frac{5WL^4}{384EI}$. The moment of inertia can vary along the length of the PPCB depending on the profile of the prestressing strands. The value of I is based on transformed section properties. Adjusting the moment of inertia so that it is representative of the behavior that the PPCB is experiencing is important for accurate results. The final camber can be determined by adding the deflection from the upward deflection due to prestressing and the downward deflection due to the self-weight.

Naaman (2004) presents pre-derived formulas for calculating the prestressing and deflection based on multiple prestressing and loading cases. The pre-derived formulas shown are obtained by the moment area method but can be verified by other linear elastic methods. The moment area method was used for this study; Naaman's method of using the pre-derived formulas was not used for calculating the instantaneous camber due to its inability to account for the transfer length and material properties that vary.

2.2.6 Summary

A review of past literature shows that multiple studies have been conducted on the topic of predicting the camber in PPCBs. Of these studies, the primary focus has been on the long-term camber prediction and the long-term prestress losses. While the long-term camber is important, the instantaneous camber can be an indicator of the magnitude of the long-term camber. For this reason, an emphasis was placed on the instantaneous camber in this section and in Chapter 5. From research that has been conducted on the instantaneous camber, topics such as prestress losses, material properties, measurement techniques, and prediction methods have been investigated.

When predicting the camber, Naaman (2004) states that, although the procedures vary in the method used to determine the long-term prestress losses, they all use primarily the same method of calculating the instantaneous losses. Differences that exist with the calculation of the instantaneous losses occur due to the different variable properties used for the concrete and prestressing steel. Tadros et al. (2003) and Ahlborn et al. (2000) found that the AASHTO LRFD (2010) instantaneous prestress losses agree closely with the behavior of PPCBs. However, the AASHTO LRFD (2010) neglects the losses due to the relaxation from the time the tendon is tensioned to the time it is released. Accounting for the relaxation prestress losses along with the proper estimation of the elastic shortening and seating losses will improve the prediction of the amount of prestress applied to a PPCB, thus improving the camber. Additional factors that are found to contribute to the accuracy of the camber prediction are the modulus of elasticity and the concrete release strength. It was found that the concrete release strengths are higher than designed, which causes an increase in the modulus of elasticity and a decrease in the camber. Using concrete material properties that model the behavior of concrete is suggested and was done in the following chapters.

In evaluating the past measurement techniques, it was found that methods such as the stretched-wire method and the use of survey equipment are the most common. Inaccuracies occur with each method depending on the equipment that is used or the procedures that are followed. Due to the misrepresentation of the measured camber, a new method of camber measurement was used to gather data, and a simplified method is proposed for future measurements in Chapter 4.

The camber prediction method for the instantaneous camber can be conducted by advanced finite element modeling or by simplified hand calculations. Of the different hand calculation methods, similarities were found due to the initial assumptions that the linear elastic behavior was present in the PPCB. Due to similarities in the instantaneous camber prediction methods, the moment area method was chosen because of its simplicity and ability to account for the transfer length and the varying material properties (see Chapter 5).

2.3 Long-Term Camber of PPCBs

At any time, t, the total upward deflection (camber), can be divided into two parts: (1) the instantaneous short-term part, (2) the time-dependent part. The first part is referred to as the instantaneous camber and was discussed in Section 0. The time-dependent part at the end of the service life is defined as the additional long-term camber and is of interest for designers. The additional long-term camber, or the camber growth, is caused by concrete creep and shrinkage. Figure 2.15 shows the two components of the PPCB deflection over time.

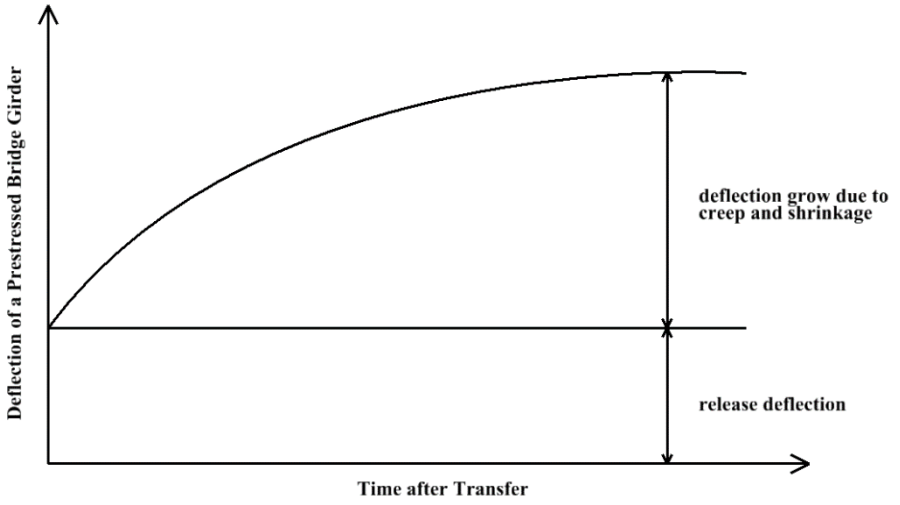

Figure 2.15. Camber of a PPCB versus time after transfer

2.3.1 Previous Long-term Camber Research

Three previous studies on the prediction of the long-term camber of PPCBs were reviewed and are summarized in the following sections: the Washington study (Rosa et al. 2007), the North Carolina study (Rizkalla et al. 2011), and the Minnesota study (O'Neill and French 2012).

2.3.1.1 Washington Study (Rosa et al. 2007)

Rosa et al. (2007) found that, in order to improve the accuracy of the long-term camber prediction for PPCBs, the properties of the concrete produced from local materials should be taken into account; these are used to calibrate the camber. The time effect should be also taken into account to calculate the camber by using the time-step method. A computer program was developed to calculate the long-term camber, in which the time-step method was used to calculate the time-dependent camber with consideration of the time-dependent material properties, including those of the concrete and prestressing steel. Two adjustment factors were used to calibrate the calculated camber, including 1.15 for the elastic modulus of the AASHTO LRFD model and 1.4 for the creep coefficient of the AASHTO LRFD model. A refined method for calculating the prestress loss based on AASHTO LRFD (2006) was recommended for predicting the long-term camber of PPCBs. Creep and shrinkage tests were performed using concrete produced from local materials, but the unexpected elongation of some shrinkage specimens was observed, which could result in errors in the calculation of the creep strain and the camber of the PPCB.

2.3.1.2 North Carolina Study (Rizkalla et al. 2011)

In Rizkalla et al. (2011), in order to improve the accuracy of the long-term camber prediction for PPCBs, adjustment factors for the concrete properties were recommended, including 1.25 for the design compressive strength at release, 1.45 for the design compressive strength at 28 days, and

0.85 for the elastic modulus of the AASHTO LRFD model. In addition, approximate and refined methods for camber prediction were proposed. Simple multipliers from the PCI method were used to create the approximate method, and the refined method for calculating the prestress losses from AASHTO LRFD (2010) was used to calculate the camber at 28 days and one year and thus create the refined method for calculating the camber. The effect of temperature gradient on the measurement of the PPCBs was recognized, and it was recommended that the measurement of the PPCB be taken before dawn. It was also found that the transfer length of the PPCB had an effect on the camber of the PPCB. Creep and shrinkage tests on concretes produced from local materials were not taken, and the AASHTO LRFD (2010) creep and shrinkage model was used.

2.3.1.3 Minnesota Study (O'Neill and French 2012)

In order to improve the accuracy of the long-term camber prediction for PPCBs, O'Neill and French (2012) suggested adjustments to the concrete properties, including 1.15 for the design compressive strength at release and the change of elastic modulus prediction method from that used by ACI 363 to that used by the AASHTO LRFD model. Additional prestress losses due to the relaxation and thermal effects were considered in the calculation of the camber. Creep and shrinkage tests on concretes produced from local materials were not performed, and the ACI 209R-92 (1992) creep and shrinkage model was selected for the calculation of prestress losses and the camber. The effect of relative humidity and temperature on the creep and shrinkage were taken into account to calculate the time-dependent camber. A computer program was used to predict the time-dependent camber with due consideration given to the aforementioned factors. Also, simple multipliers were proposed to predict the long-term camber.

2.3.1.4 Comparison of the Three Studies

According to the three studies, it was found that the inaccurate predictions of the concrete properties, including the compressive strength, the elastic modulus, and the creep and shrinkage, were an important cause of errors in the long-term camber of PPCBs. In the three studies, compressive strength and elastic modulus tests were performed, and adjustment factors for the material properties were provided. The three studies also provided prediction methods for the time-dependent camber of the PPCB by using computer programs or time-dependent equations. In two of the studies, simple multipliers were also proposed for the prediction of the camber. The three studies indicated that the AASHTO LRFD (2010) refined method for prestress losses provided a good prediction of the camber of PPCBs. Creep and shrinkage tests were only taken in the study by Rosa et al. (2007).

2.3.2 Factors Affecting Long-Term Camber

The long-term camber of a PPCB is affected by prestress forces and losses, creep, cross-section properties, support locations, and environmental conditions (temperature). In the following sections, each factor is discussed.

2.3.2.1 Prestress Losses

Pretress losses, which occur before the deck is placed, consist of short-term losses and long-term losses. Short-term losses and their prediction methods were discussed in Sections 2.2.2.1 and 2.2.4, respectively. Long-term losses result from the creep, shrinkage, and relaxation after the transfer. Prestress losses result in a decrease in the camber of a PPCB. For a pretensioned concrete member, the total prestress losses, Δf_{pT}, can be defined as follows:

$$\Delta f_{pT} = \Delta f_{pST} + \Delta f_{pLT} \quad \textbf{(2-100)}$$

where Δf_{pST} is the total short-term losses (see Section 2.2.4) and Δf_{pLT} is the total long-term losses.

Total long-term losses, Δf_{pLT}, can be calculated based on the AASHTO LRFD (2010) method for obtaining the refined estimates of the time-dependent losses, as follows:

$$\Delta f_{pLT} = \Delta f_{pR1} + \Delta f_{pCR} + \Delta f_{pSR} \quad (2\text{-}101)$$

where Δf_{pR1} is the prestress loss due to the relaxation of the prestressing strands between the time of transfer and the deck placement, Δf_{pCR} is the prestress loss due to the creep of the PPCB between the transfer and deck placement, and Δf_{pSR} is the prestress loss due to the shrinkage of the PPCB between the transfer and deck placement.

2.3.2.1.1 Prestress Loss due to Relaxation

When a strand is stressed, the magnitude of stress decreases with time, which is the relaxation loss. The relaxation loss occurs not only between the jacking and transfer (see Section2.2.4.3), but also between the transfer and deck placement. Based on AASHTO LRFD (2010), Δf_{pR1} can be determined as follows:

$$\Delta f_{pR1} = \frac{f_{pt}}{K_L}\left(\frac{f_{pt}}{f_{py}} - 0.55\right) \quad (2\text{-}102)$$

where f_{pt} is the stress in the prestressing strands immediately after the transfer; K_L is a factor accounting for the type of steel, which is 30 for the low-relaxation strands and 7 for the other prestressing steel; and f_{py} is the yield strength of the prestressing steel.

Also, Δf_{pR1} may be assumed to be equal to 1.2 ksi for low-relaxation strands according to AASHTO LRFD (2010). Moreover, according to a study by Tadros et al. (2003), the relaxation loss after the transfer is between 1.8 to 3.0 ksi and is a relatively small part of the total prestressing losses.

2.3.2.1.2 Prestress Loss Due to Creep

Based on AASHTO LRFD (2010), the prestress loss due to creep between the transfer and deck placement can be determined as follows:

$$\Delta f_{pCR} = \Delta f_{pES} \Phi_{bid} K_{id} \quad \textbf{(2-103)}$$

where

$$K_{id} = \frac{1}{1+\frac{E_p A_{ps}}{E_{ci} A}\left(1+\frac{Ae_{pg}^2}{I}\right)[1+0.7\Phi_{bif}]} \quad \textbf{(2-104)}$$

where Φ_{bid} is the specified creep coefficient of the concrete, Φ_{bif} is the ultimate creep coefficient of the concrete, A_{ps} is the total area of the prestressing strands (in.^{2}), A is the area of the cross-section (in.^{2}), I is the moment of inertia of the cross-section (in.^{4}), and e_{pg} is the eccentricity of the strand with respect to the centroid of the PPCB (in.).

2.3.2.1.3 Prestress Loss Due to Shrinkage

Based on AASHTO LRFD (2010), the prestress loss due to shrinkage between the transfer and deck placement can be determined as follows:

$$\Delta f_{pSH} = E_p \, \varepsilon_{bid} \, K_{id} \quad (2\text{-}105)$$

where ε_{bid} is the specified shrinkage strain (10^{-6} in./in.).

2.3.2.2 Camber Due to Creep

After the transfer, the prestressing force and self-weight result in different stresses along the cross-section of the concrete of a PPCB, and the applied stress increases the upward camber. This additional camber is due to the creep of the concrete.

2.3.2.3 Cross-Section Properties

The cross-section of a PPCB has two types of properties: the gross section properties and the transformed section properties. It is easier to calculate the gross section properties. The transformed section properties are dependent on the ratio of the modulus of elasticity of the strands and the concrete, strand locations, and strand quantities. The transformed section properties are widely used for reinforced concrete. The short-term and long-term cambers calculated using the gross section and transformed section properties are compared in Chapter 6.

2.3.2.4 Support Locations

When all the pretensioned tendons are released, the PPCBs are transported from the precasting bed to the precasting yard for storage, where they rest on temporary supports. The supports are usually concrete blocks or timber placed underneath the PPCB. The locations of the two end supports from each other can vary from PPCB to PPCB by a few feet, unless there is a guideline dictating certain overhang lengths for each PPCB. However, any overhang length will induce a certain amount of camber growth during the storage time. The additional camber due to overhang consists of two components: (1) the elastic deflection and (2) the time-dependent deflection. The elastic deflection is caused by the weight of cantilever, while the time-dependent deflection is the result of the overhang creep over time. Significant camber variability can result if the PPCBs are stored differently, which can lead to an undesirable amount of the camber at the time of bridge erection. Moreover, Tadros et al. (2011) investigated the effect of the storage conditions and suggested that it be considered in predicting the at-erection camber.

The increase in camber due to the shifting of the supports can be quantified by three components. One component is the added moment at the support from the overhanging end of the PPCB (Figure 2.16).

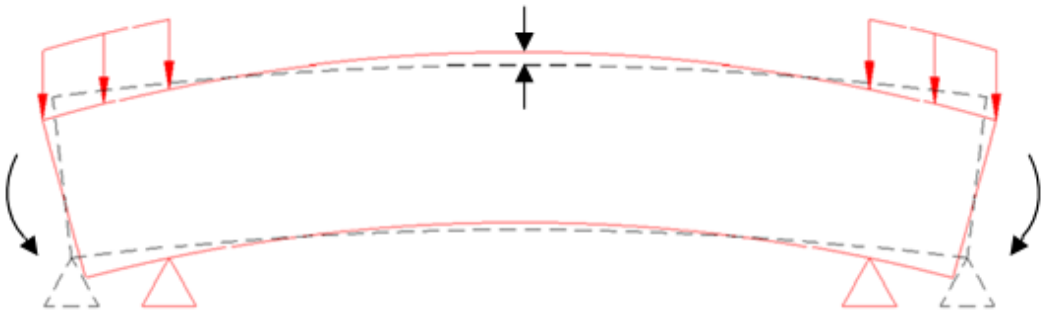

Figure 2.16. PPCB with increased midspan deflection caused by the moment from the overhang

This moment acts to increase the camber at the midspan. The second component is the reduced clear span length (Figure 2.17).

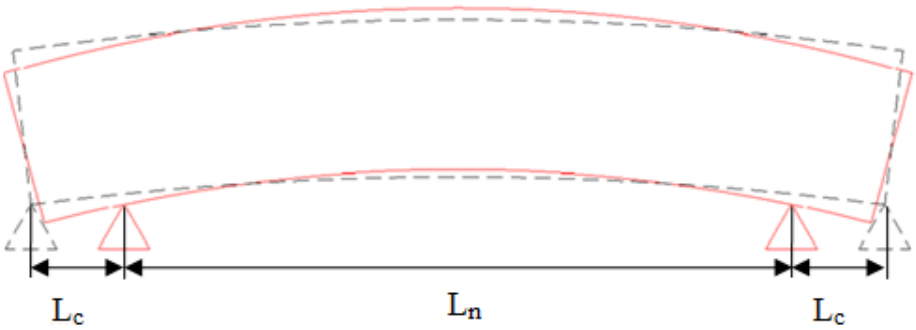

Figure 2.17. PPCB with increased midspan deflection due to self-weight caused by the reduced clear span

While the PPCB is resting on the precasting bed, the clear span length is assumed to be the length of the PPCB. When supports are placed in from the ends, the clear span is reduced. A smaller clear span length will result in smaller self-weight deflections at the midspan. In simple elastic beam formulas, the clear span length is typically multiplied to the fourth power, which changes the final deflection. The third component is the deflection at the end relative to the support from the cantilever section (Figure 2.18). Although this deflection is typically small, it should be recognized for research purposes.

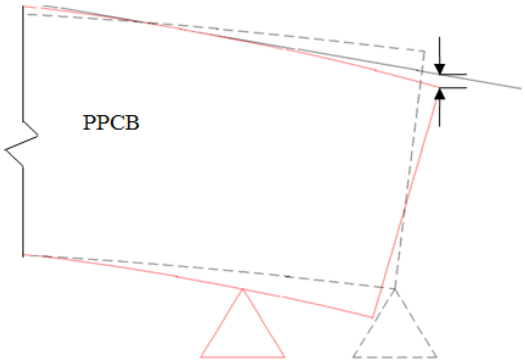

Figure 2.18. Increased deflection of a PPCB relative to the support from the overhang

An elevation survey that determines the haunch thicknesses is taken at the time of erection of the PPCB. The supports at erection are typically 6–10 in. in from the end of the PPCB. Because this is the most critical time for the prediction of the camber and the supports are near the end of the PPCB, all the other camber measurements should be compared to a PPCB with zero overhang to maintain accuracy.

The elastic deformation that occurs when the supports are shifted closer to the center of the PPCB will misrepresent the contribution of the friction, and thus the amount of camber present, if it is not revised. In order to determine the contribution of the elastic deformation, the camber must be measured at the ends of the PPCB when the PPCB is resting on temporary supports, and the distance from the ends of the PPCB to the supports must also be measured.

Equation 2-106 is used to calculate the deflection due to the self-weight of a PPCB when the supports are placed at the ends of the PPCB. This equation represents the support locations that the PPCB is exposed to while resting on the precast bed immediately after the transfer of prestress.

$$\Delta_{sw} = \frac{5w_{sw}L^4}{384E_{ce}I} \quad \textbf{(2-106)}$$

where w_{sw} is the self-weight per unit length, L is the length of a PPCB, and I is the moment of inertia of the cross-section.

If there is an overhang, the camber at the midspan with respect to the end of the PPCB due to the self-weight can be calculated as follows:

$$\Delta_{sw} = \Delta_{overhang} + \Delta_{midspan} \quad \textbf{(2-107)}$$

$$\Delta_{overhang} = \frac{\omega_{sw}L_c}{24E_{ce}I}\left[3L_c^2\left(L_c + 2L_n\right) - L_n^3\right] \quad \textbf{(2-108)}$$

$$\Delta_{midspan} = \frac{\omega_{sw}L_n^2}{384E_{ce}I}\left[5L_n^2 - 24L_c^2\right] \quad \textbf{(2-109)}$$

where $\Delta_{overhang}$ is the deflection of the end of the overhang relative to the support, $\Delta_{midspan}$ is the camber at the midspan relative to the support, L_c is the length of the overhang, and L_n is the distance between the two supports.

2.3.2.5 Thermal Effects

PPCBs are affected by daily and seasonal temperature changes during storage at the precast yard. As a result, vertical temperature gradients develop down the PPCB depth due to uneven heating and cooling. Solar radiation provides heat energy most directly to the top flange of the PPCBs. Convection to or from the surrounding atmosphere can contribute to additional heat gain or loss. Different factors such as wind speed, ambient temperature, relative humidity, weather conditions (clear or cloudy), surface characteristics, time of day, and time of year affect the changes in the temperature. A maximum temperature difference can be expected when solar radiation is high and wind speed is low. Conditions such as these would most likely occur in the summer, when solar radiation is most intense.

PPCB depth mainly governs the shape of the vertical temperature gradients. For shallow sections with depths smaller than one foot, the temperature distribution is nearly linear, while the temperature distribution tends to be more nonlinear for depths greater than one foot. The simple support conditions for PPCBs induce no axial or bending stresses due to thermal effects in the section. Consequently, self-equilibrating stresses are assumed to develop in the PPCB due to the strains induced in the member that countered the distortion from the nonlinear thermal strain

profile in the section. A constant curvature along the PPCB length can be assumed based on the resultant strain profile and can be used to calculate the theoretical camber resulting from a temperature gradient.

O'Neill and French (2012) recommended that all of the camber measurements be performed before mid-afternoon, when possible, to obtain consistent measurements and to eliminate the effect of solar radiation. Barr et al. (2005) monitored strain and temperature for one PPCB intermittently over the span of three years outside the Structural Engineering Research Laboratory at the University of Washington. They found that solar radiation can induce a thermal deflection as high as 15 mm (0.6 in.). Moreover, a 10% increase in camber due to solar radiation during the course of a day was reported by Woolf and French (1998). Thus, the temperature effect can produce inconsistent trends in the collected data, such as high cambers at early ages and the reduction of or no significant increase in the camber over time, which contradicts the theory.

2.3.3 Long-Term Camber Prediction Methods

For a PPCB, the creep increases the camber, the prestress losses decrease the camber, and the combination of these two typically results in an increase of the camber. Tadros' method, Naaman's method, and the incremental method are discussed in the following sections. These three methods are used in this study to calculate the long-term camber of PPCBs. It should be noted that Naaman's method and the incremental method are based on the moment area theorem, which was discussed in Section 2.2.5.1.

2.3.3.1 Tadros' Method

Tadros et al. (2011) provided a simplified method to calculate the long-term camber of PPCBs before the placement of the deck. The method is expressed as follows:

$$\Delta_{long\text{-}term} = (1 + \Phi_{bid})\,\Delta_{release} - (1 + 0.7\Phi_{bid})\,\Delta_{loss} \quad \textbf{(2-110)}$$

where $\Delta_{long\text{-}term}$ is the long-term camber of a PPCB before the placement of a deck (in.); $\Delta_{release}$ is the release camber of a PPCB (in.); and Δ_{loss} is the camber loss due to prestress losses resulting from the creep, shrinkage, and relaxation between the time of transfer to the time of placement of the deck (in.). The Δ_{loss} can be determined as follows:

$$\Delta_{loss} = \frac{\Delta f}{f}\,\Delta_{ip} \quad \textbf{(2-111)}$$

where Δf is the long-term prestress losses due to the creep, shrinkage, and relaxation (ksi); f is the prestress stress after the transfer (ksi); Δ_{ip} is the upward deflection due to prestress; and Φ_{bid} is the specified creep coefficient of the concrete.

In Equation 2-110, 0.7 is an aging coefficient used to calculate the camber loss due to prestress losses, which is based on considerations of the v/s ratio, relative humidity, and loading age.

2.3.3.2 Naaman's Method

Naaman (2004) proposed another simplified method based on the moment area theorem to calculate the long-term camber of PPCBs. An equivalent modulus is used for the calculation of the camber as follows:

$$E_{ce}(t, t_A) = \frac{E_c(t)}{1+C_C(\tau)} \quad \textbf{(2-112)}$$

where $E_c(t)$ is the time-dependent modulus of the elasticity of the concrete equal to $\sqrt{\frac{t}{b+ct}}\,E_c(28)$, with the following:

Moist-curing: $b = \begin{cases} 4.0 \text{ for Type I cement} \\ 2.3 \text{ for Type III cement} \end{cases}$ and $c = \begin{cases} 0.85 \text{ for Type I cement} \\ 0.92 \text{ for Type III cement} \end{cases}$

Steam-curing: $b = \begin{cases} 1.0 \text{ for Type I cement} \\ 0.7 \text{ for Type III cement} \end{cases}$ and $c = \begin{cases} 0.95 \text{ for Type I cement} \\ 0.98 \text{ for Type III cement} \end{cases}$

$C_C(\tau)$ is specified as the creep coefficient of the concrete, t is the age of concrete (days), and t_A is the age of concrete at the transfer (days).

The long-term camber of a PPCB, shown in Figure 2.13, can be calculated by using the following equations:

$$\Delta_{\text{long-term}} = \frac{FL^2}{8\,Ece\,(t,t_A)\,I}\left[e_1 + (e_2 - e_1)\frac{4a^2}{3L^2}\right] \quad \textbf{(2-113)}$$

where F is the prestressing force in strands; and I is the moment of inertia of a cross-section.

The long-term camber may be also determined as follows:

$$\Delta_{\text{long-term}} = (\phi_1 - \phi_2)\frac{a^2}{6} - \phi_1\frac{L^2}{8} \quad (2\text{-}114)$$

where ϕ_1 is the curvature at the midspan of the PPCB due to the prestressing force and self-weight and can be determined as follows:

$$\phi_1 = \frac{M_{ps1} + M_{sw1}}{Ece\,(t,t_A)\,I} \quad \textbf{(2-115)}$$

where M_{ps1} is the moment due to the prestressing force at the midspan of a PPCB and M_{sw1} is the moment due to the self-weight at the midspan.

ϕ_2 is the curvature at the end of the PPCB due the prestressing force and the self-weight and can be determined as follows:

$$\phi_2 = \frac{M_{ps2} + M_{sw2}}{Ece\ (t,t_A)\ I} \quad \textbf{(2-116)}$$

where M_{ps2} is the moment due to the prestressing force at the end of a PPCB and M_{sw2} is the moment due to the self-weight at the end (for a simply supported PPCB, this value equals zero).

2.3.3.3 Incremental Method

For the incremental method, a PPCB is divided into 1 in. sections, and the properties of each section are analyzed, including the cross-section properties and applied moments and stresses. The curvature of each section is calculated by using the time-dependent equivalent modulus, and the camber of the PPCB is obtained by integrating the curvature along the half-span of the PPCB:

$$\Delta_{long\text{-}term} = \int_0^{L/2} \frac{M_i}{E_{ce}\ (t,t_A)\ I_i}\, dx \quad \textbf{(2-117)}$$

where i is the number of 1 in. sections in a half-span of a PPCB; M_i is the applied moment on section i due to the prestress force and self-weight of a PPCB, in which time-dependent prestress losses are calculated section by section using the time-dependent cross-section properties; $E_{ce}(t, t_A)$ is the equivalent modulus of concrete, which can be calculated using Equation 2-112; and I_i is the moment of inertia on section i.

CHAPTER 3: MATERIAL CHARACTERIZATION

3.1 Introduction

This chapter describes the material characterization completed as a part of this study. Each testing procedure used in this study was performed according to the appropriate ASTM specification. Materials and concrete specimens are discussed in Section 3.2. The compressive strength, creep, and shrinkage tests are presented in Sections 3.3, 3.4, and 3.5, respectively. The results of a shrinkage test performed on a 4 ft PPCB section are described in Section 3.6, along with measurements. The results of materials tests are described in Section 3.7. An analysis and discussion of material properties are presented in Section 3.8. Conclusions and recommendations regarding material properties are presented in Section 3.9.

3.2 Preparation of Test Specimens

A total of seven different concrete mix designs, representing mixes from three precast plants, were investigated for time-dependent behavior. Four of the seven mixes were HPCs and are currently used for casting PPCBs. The rest were NCs used in PPCBs in the recent past. In the HPCs, slag and fly ash were added as partial replacement materials for Portland cement. The NCs did not contain these materials. Cylindrical concrete specimens 4 in. in diameter by 8 in. in height were used in this study, and all were cast by the quality control staffs at the respective precast plants. The HPC specimens were made and stored in the mold along with steam-cured PPCBs. The NC specimens were cast and stored in the mold in the quality control room at the precast plants. Plastic molds were used to prevent water loss during transportation, which would have a significant influence on the initial creep and shrinkage of the concrete. HPC 1 and NC 1 were prepared by Plant A; HPC 2, HPC 4, and NC 2 were cast by Plant B; and HPC 3 and NC 3 were provided by Plant C.

Typically, the PPCBs were released after one day of steam curing, and thus both the HPC and NC specimens at the age of one day were transported from the precast plants to the laboratory on campus during the early morning of the day of the PPCB release. Sometimes the PPCBs were kept on the fabrication bed over the weekend, and those PPCBs were released at the age of two to four days. However, the concrete specimens were transported at the age of one day.

In total, 14 cylindrical specimens for each mix design were brought to the laboratory. Three specimens were used for 1-day compressive strength tests, three were used for 28-day compressive strength tests, four were subjected to creep tests, and the remaining four were used to monitor shrinkage strains. For the creep and shrinkage tests, half of the specimens were sealed using a coating material (Sikagard 62), and the rest were unsealed. All specimens were sulfur-capped, according to ASTM C617 (2009), prior to perfoming the compressive strength, creep, and shrinkage tests. Photos of the sealed and unsealed specimens are shown in Figure 3.1.

Figure 3.1. Sulfur-capped and sealed (left) and unsealed (right) specimens

3.3 Compressive Strength Tests

Except for those cylinders tested at the age of one day, all test specimens, including those prepared for the creep and shrinkage tests, were stored in an environmental chamber, where the temperature and humidity were maintained at 73.4°F ± 2.0°F (23.0°C ± 1.1°C) and 50% ± 4%, respectively. Compressive strength tests were performed according to ASTM C39 (2004). Photos of the compressive strength test are shown in Figure 3.2.

Figure 3.2. Compressive strength test of a cylindrical specimen

3.4 Creep Tests

3.4.1 Introduction

Creep tests under compression load were performed according to ASTM C 512 (2002). Details of the creep frame, the loading of the creep test specimens, the storage of the specimens, and the methods of measurement are presented in the following sections.

3.4.2 Creep Frame

The creep frame was designed and assembled in accordance with ASTM C512 (2002). Figure 3.3 shows the details of a creep frame.

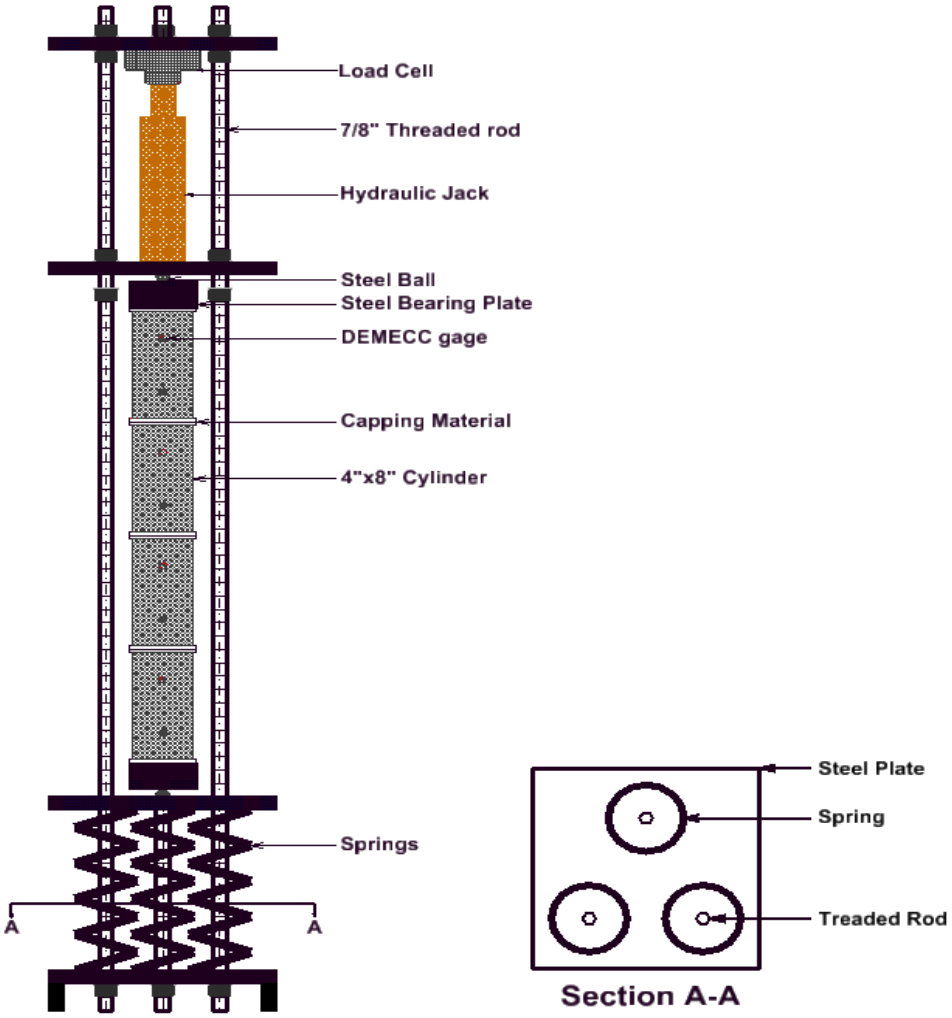

Figure 3.3. Details of a creep frame

For each steel plate in the creep frame, the locations of three holes for threaded rods and the geometric center of the triangle made by the three holes were carefully determined. Steel nuts were also carefully selected in order to minimize the relaxation of the frame after the application of the load.

3.4.3 Loading of Creep Specimens

Each creep frame, as shown Figure 3.3, used four 4 in. by 8 in. cylindrical specimens stacked on top of each other. A load cell and a hydraulic jack were used to apply the load in the creep frame, and these were removed after the load was applied to reach a target stress of 2,125 psi. To ensure that the load would be applied at the same location each time, a circle that fit the bottom shape of the hydraulic jack was drawn. The load was reapplied every time before measurements were taken due to the relaxation of the creep frame after the loading application. The tolerance of load variation was 2%, in accordance with ASTM C512 (2002).

3.4.4 Storage Condition of Specimens

The creep test, shrinkage test, and 28-day compressive strength test specimens were stored in an environmentally controlled chamber, in which a temperature of 73.4°F ± 2.0 °F (23.0°C ± 1.1 °C) and a relative humidity of 50% ± 4% were maintained. This chamber was large enough to accommodate all of the creep frames. The shrinkage specimens were stored horizontally in open wooden shelves. Photos of the creep frames with loaded specimens and shrinkage specimens are shown in Figure 3.4 and Figure 3.5, respectively.

Figure 3.4. Loaded specimens for the creep tests in the environmentally controlled chamber

Figure 3.5. Unloaded specimens for the shrinkage tests in the environmentally controlled chamber

3.4.5 Method of Measurements

A demountable mechanical (DEMEC) strain gage was used to measure the change of length between two vertical gage points attached to the concrete cylinders, with a gauge length of 4 in. The DEMEC gage had a precision of 0.00005 in. On each specimen, three sides of the vertical gage points were attached. For each measurement, three instantaneous readings were obtained from each side, and the average was used as the reading of this side. If the difference among those three readings was greater than 0.00010 in., three additional measurements were taken, and the average of the six total readings was used as the reading of the two gage points. Photos of the DEMEC gage and the measurement procedure are shown in Figure 3.6.

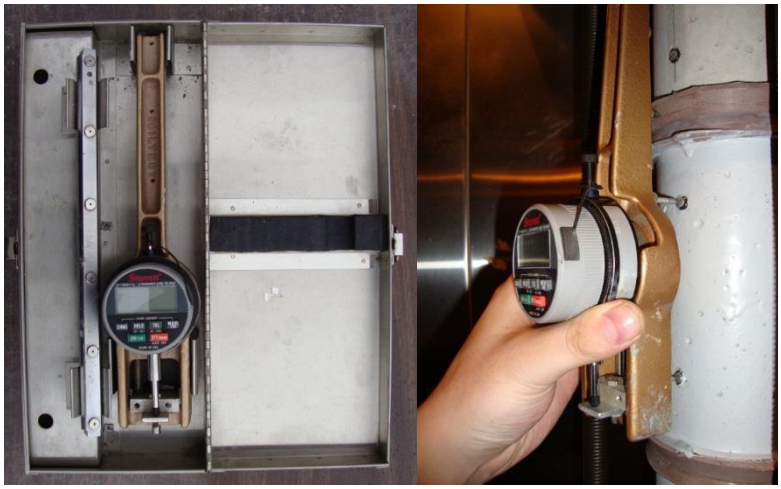

Figure 3.6. DEMEC gage device (left) and measurement of strain (right)

The strain was the quotient of the change of length and the initial length between two gage points. The strain measured in the loaded specimens in the creep frame was the total strain due to creep and shrinkage, and the strain measured in the unloaded specimens was only due to shrinkage. Sealed and unsealed creep strains could be calculated by subtracting the sealed and unsealed shrinkage strain from the total sealed and unsealed strain as the values changed over time. The creep coefficient was the ratio of the creep strain to instantaneous strain after the load application.

3.5 Shrinkage Measurements

The shrinkage specimens were unloaded specimens stored in the same chamber as the loaded specimens. The shrinkage strain was measured in the unloaded specimens at the same time as the total strain measured in the loaded specimens.

3.6 Shrinkage Behavior of a Four-foot PPCB Section

In order to correlate the shrinkage behavior of actual PPCBs and specimens in the laboratory, a BTB PPCB section with a length of 4 ft was cast and stored in the yard of a precast plant. Strands in the PPCB section were debonded by using plastics and grease. The DEMEC gauge and gage points were used to measure the strain on this short PPCB. Each group of two gage points was glued to the surface of the middle part of the PPCB section horizontally, and there were six groups of gage points along one side and seven groups along the other side. Four temperature sensing thermistor probes attached by wires were placed on the PPCB section when the PPCB section was cast. Three probes were laid at the bottom flange, web, and top flange along the center of the cross-section at the center of the PPCB section, and the rest were placed near the end of the top flange. A handheld thermistor thermometer was used to obtain the reading from the thermistor probes. A photo of this PPCB section is shown in Figure 3.7.

Figure 3.7. Debonded 4 ft BTB PPCB section stored at precast plant A

Four 4 in. by 8 in. cylindrical specimens were also cast along with the PPCB section, and these specimens were transported to the laboratory for shrinkage tests on the same day as the release of the PPCB section. Two cylindrical specimens were sealed and the other two were unsealed.

3.7 Results of Materials Tests

This section discusses the measurements taken and the results of the tests. The compressive strength and modulus of elasticity results are presented in Section 3.7.1 and Section 3.7.2, respecitively. Measurements from the creep and shrinkage tests are shown in Section 0.

3.7.1 Compressive Strength

For each mix, 1-day and 28-day compressive strengths were measured, and the results shown below are the average magnitude, standard deviation, and maximum difference in percent of three measurements. Table 3.1 shows the results of the 1-day compressive strength test, and Table 3.2 summarizes the results of the 28-day compressive strength test.

Table 3.1. Results of the 1-day compressive strength test

Mix ID	HPC 1	HPC 2	HPC 3	HPC 4	NC 1	NC 2	NC 3
Average 1-Day Strength (psi)	6,784	6,247	5,417	6,640	8,902	6,547	9,750
Standard Deviation (psi)	182	116	132	91	89	55	123
Maximum Difference of Three Specimens	9%	8%	11%	6%	4%	4%	5%

Table 3.2. Results of the 28-day compressive strength test

Mix ID	HPC 1	HPC 2	HPC 3	HPC 4	NC 1	NC 2	NC 3
Average 28-Day Strength (psi)	8,750	7,938	6,884	8,212	10,215	7,545	11,020
Standard Deviation (psi)	86	35	161	106	58	132	227
Maximum Difference of Three Specimens	4%	2%	10%	6%	5%	7%	9%

The maximum difference of the three specimens ranges from 4% to 11% for the 1-day compressive strength test and from 2% to 10% for the 28-day compressive strength test. These values are less than the limit value of 14% according to ASTM C39 (2004), confirming that the results of the compressive strength tests are acceptable.

3.7.2 Modulus of Elasticity

The modulus of elasticity is the quotient of the applied stress and elastic shortening measured in the creep test immediately before and after the load application at one day. The average magnitude and standard deviation for each mix are summarized in Table 3.3 for sealed specimens and Table 3.4 for unsealed specimens.

Table 3.3. Results of the modulus of elasticity test for the sealed specimens

Mix ID	HPC 1	HPC 2	HPC 3	HPC 4	NC 1	NC 2	NC 3
Modulus of Elasticity (ksi)	4,870	5,596	5,226	5,629	5,425	4,399	4,671
Standard Deviation (ksi)	306	593	517	389	369	202	442

Table 3.4. Results of the modulus of elasticity test for the unsealed specimens

Mix ID	HPC 1	HPC 2	HPC 3	HPC 4	NC 1	NC 2	NC 3
Modulus of Elasticity (ksi)	3,216	3,105	4,080	5,129	5,602	5,027	4,297
Standard Deviation (ksi)	91	233	324	413	543	480	302

3.7.3 Creep and Shrinkage

Table 3.5 summarizes the stress-strength ratios resulting from the creep tests.

Table 3.5. Stress-strength ratio of creep tests

Mix ID	HPC 1	HPC 2	HPC 3	HPC 4	NC 1	NC 2	NC 3
Average 1-Day Strength (psi)	6,784	6,247	5,417	6,640	8,902	6,547	9,750
Applied Stress (psi)	2,125	2,125	2,125	2,125	2,125	2,125	2,125
Stress-strength Ratio	0.31	0.34	0.39	0.32	0.24	0.32	0.22

It was found that the stress-strength ratio ranges from 0.31 to 0.39 for the four HPC mixes and from 0.22 to 0.32 for the three NC mixes. The stress-strength ratios are less than 0.40, which is the limit of the linear theory provided by ASTM C512 (2002), as mentioned previously.

Table 3.6 to Table 3.8 present the results of the creep and shrinkage tests, including the three-month, six-month and one-year tests.

Table 3.6. Results of the creep and shrinkage tests for seven mixes at three months

Mix ID	Unsealed Total Strain (10^{-6} in./in.)	Sealed Total Strain (10^{-6} in./in.)	Unsealed Shrinkage Strain (10^{-6} in./in.)	Sealed Shrinkage Strain (10^{-6} in./in.)	Unsealed Creep Coefficient	Sealed Creep Coefficient
HPC 1	1,596	1,292	353	171	0.63	0.84
HPC 2	1,587	1,054	254	185	0.89	1.03
HPC 3	1,151	1,088	404	344	0.38	0.74
HPC 4	1,650	1,086	306	229	0.78	0.82
NC 1	1,196	1,076	287	246	0.59	0.55
NC 2	1,254	979	315	157	0.48	0.58
NC 3	1,126	1,005	278	204	0.34	0.53

Table 3.7. Results of the creep and shrinkage tests for seven mixes at six months

Mix ID	Unsealed Total Strain (10^{-6} in./in.)	Sealed Total Strain (10^{-6} in./in.)	Unsealed Shrinkage Strain (10^{-6} in./in.)	Sealed Shrinkage Strain (10^{-6} in./in.)	Unsealed Creep Coefficient	Sealed Creep Coefficient
HPC 1	1,698	1,370	414	188	0.68	0.94
HPC 2	1,756	1,149	344	260	1.00	1.08
HPC 3	1,212	1,152	465	373	0.38	0.82
HPC 4	1,716	1,145	330	251	0.84	0.89
NC 1	1,422	1,178	391	333	0.81	0.58
NC 2	1,345	1,068	358	172	0.56	0.71
NC 3	1,260	1,190	375	277	0.40	0.73

Table 3.8. Results of the creep and shrinkage tests for seven mixes at one year

Mix ID	Unsealed Total Strain (10^{-6} in./in.)	Sealed Total Strain (10^{-6} in./in.)	Unsealed Shrinkage Strain (10^{-6} in./in.)	Sealed Shrinkage Strain (10^{-6} in./in.)	Unsealed Creep Coefficient	Sealed Creep Coefficient
HPC 1	1,942	1,448	576	214	0.79	1.03
HPC 2	2,027	1,245	429	324	1.26	1.16
HPC 3	1,345	1,234	533	410	0.50	0.92
HPC 4	1,820	1,249	353	263	0.93	1.07
NC 1	1,506	1,217	443	344	0.86	0.63
NC 2	1,507	1,353	425	360	0.73	0.88
NC 3	1,358	1,360	375	285	0.54	1.01

From the data, the following observations were made:

- The unsealed total strain for each mix was higher than the sealed total strain. The differences ranged from 6% to 52% at three months, from 5% to 53% at six months, and from 0% to 63% at one year.
- The unsealed shrinkage strain for each mix was higher than the sealed shrinkage strain, ranging from 17% to 106%, from 17% to 120%, and from 18% to 169% at three months, six months, and one year, respectively.
- The unsealed total strain of the HPC 4 mix was higher than that of the other six mixes, ranging from 3% to 43% at three months, and the unsealed total strain of HPC 2 was higher than that of the other six mixes, ranging from 2% to 45% at six months and ranging from 4% to 51% at one year. The HPC 3 mix had the lowest unsealed total strain at three months, six months, and one year.
- The sealed total strain of the HPC 1 mix was higher than that of the other six mixes, ranging from 19% to 29% at three months, from 19% to 28% at six months, and from 6% to 19% at one year. The NC 2 mix had the lowest sealed total strain at three months and six months, and the NC 1 mix had the lowest sealed total strain at one year.

- The unsealed shrinkage strain of the HPC 3 mix was higher than that of of the other six mixes, ranging from 14% to 59% at three months and from 12% to 41% at six months, and the unsealed shrinkage strain of HPC 1 was higher than that of the other six mixes, ranging from 8% to 63% at one year. The HPC 2 mix had the lowest unsealed shrinkage strain at three months, and the HPC 4 mix had the lowest unsealed shrinkage strain at six months and at one year.
- The sealed shrinkage strain of the HPC 3 mix was higher than that of the other six mixes, ranging from 40% to 101% at three months, from 12% to 117% at six months, and from 27% to 92% at one year. The NC 2 mix had the lowest sealed shrinkage strain at three months and six months, and the HPC 1 mix had the lowest sealed shrinkage strain at one year.
- The HPC 2 mix had the highest unsealed and sealed creep coefficient at one year. The HPC 2 mix had a higher unsealed creep coefficient, ranging from 13% to 163%, and a higher sealed creep coefficient, ranging from 23% to 96%, than those of the other six mixes at three months. The HPC 2 mix had a higher unsealed creep coefficient, ranging from 20% to 165%, and a higher sealed creep coefficient, ranging from 15% to 87%, than those of the other six mixes at six months. The HPC 2 mix had a higher unsealed creep coefficient, ranging from 35% to 154%, and a higher sealed creep coefficient, ranging from 9% to 84%, than those of the other six mixes at one year.
- The unsealed creep coefficient of NC 3 was the lowest of all seven mixes at three months, and the unsealed creep coefficient of HPC 3 was the lowest of all seven mixes at six months and one year.
- The sealed creep coefficient of NC 3 was lower than that of the other six mixes at three months, and the unsealed creep coefficient of NC 1 was the lowest of all seven mixes at six months and one year.

Detailed results of the creep and shrinkage tests for seven mixes are shown in Table 3.9 to Table 3.15.

Table 3.9. Results of the creep and shrinkage test for HPC 1

Time after Loading (days)	Unsealed Total Strain (10^{-6} in./in.)	Sta. Dev. (10^{-6} in./in.)	Sealed Total Strain (10^{-6} in./in.)	Sta. Dev. (10^{-6} in./in.)	Unsealed Shrinkage (10^{-6} in./in.)	Sta. Dev. (10^{-6} in./in.)	Sealed Shrinkage (10^{-6} in./in.)	Sta. Dev. (10^{-6} in./in.)	Unsealed Creep Coefficient	Sealed Creep Coefficient
0	0	0	0	0	0	0	0	0	0.00	0.00
0	764	66	609	46	0	0	0	0	0.00	0.00
1	898	53	744	51	98	8	31	23	0.05	0.17
2	1,002	64	794	55	163	9	62	25	0.10	0.20
3	1,031	50	824	68	166	7	59	21	0.13	0.26
7	1,145	59	916	64	219	13	74	18	0.21	0.38
14	1,268	95	1,005	65	276	13	101	16	0.30	0.48
21	1,323	97	1,041	65	285	16	115	19	0.36	0.52
28	1,379	101	1,077	66	295	19	129	18	0.42	0.56
60	1,543	117	1,227	73	319	25	151	21	0.60	0.77
90	1,596	117	1,292	89	353	27	171	22	0.63	0.84
120	1,631	119	1,330	96	373	28	180	25	0.65	0.89
150	1,663	120	1,359	97	392	29	187	22	0.66	0.92
180	1,698	122	1,370	92	414	29	188	23	0.68	0.94
210	1,737	126	1,382	93	433	29	192	24	0.71	0.95
240	1,760	128	1,388	93	443	34	197	24	0.72	0.96
270	1,786	129	1,395	94	453	29	205	23	0.74	0.95
300	1,867	129	1,420	93	500	30	213	25	0.79	0.98
330	1,905	130	1,434	94	538	38	214	26	0.79	1.00
360	1,942	132	1,448	95	576	42	214	32	0.79	1.03
	Average	**103**	**Average**	**78**	**Average**	**22**	**Average**	**21**		

Table 3.10. Results of the creep and shrinkage test for HPC 2

Time after Loading (days)	Unsealed Total Strain (10^{-6} in./in.)	Sta. Dev. (10^{-6} in./in.)	Sealed Total Strain (10^{-6} in./in.)	Sta. Dev. (10^{-6} in./in.)	Unsealed Shrinkage (10^{-6} in./in.)	Sta. Dev. (10^{-6} in./in.)	Sealed Shrinkage (10^{-6} in./in.)	Sta. Dev. (10^{-6} in./in.)	Unsealed Creep Coefficient	Sealed Creep Coefficient
0	0	0	0	0	0	0	0	0	0.00	0.00
0	706	47	427	52	0	0	0	0	0.00	0.00
1	831	66	535	62	51	7	20	2	0.11	0.21
2	880	70	573	70	76	11	30	3	0.14	0.27
3	976	66	657	73	125	13	46	10	0.21	0.43
7	1,092	68	712	72	132	17	50	8	0.36	0.55
14	1,254	88	789	71	142	23	54	9	0.58	0.72
21	1,365	108	842	71	150	29	61	10	0.72	0.83
28	1,429	119	874	71	157	33	68	11	0.80	0.89
60	1,530	123	985	82	216	38	131	10	0.86	1.00
90	1,587	136	1,054	76	254	37	185	10	0.89	1.03
120	1,650	144	1,092	74	287	37	216	12	0.93	1.05
150	1,707	143	1,127	69	319	39	245	12	0.97	1.07
180	1,756	138	1,149	65	344	40	260	13	1.00	1.08
210	1,805	133	1,166	65	366	40	269	13	1.04	1.10
240	1,851	126	1,186	66	383	40	279	14	1.08	1.12
270	1,884	123	1,203	65	396	40	290	14	1.11	1.14
300	1,938	139	1,213	69	404	45	302	25	1.17	1.13
330	1,979	137	1,231	70	418	45	313	26	1.21	1.15
360	2,027	145	1,245	72	429	48	324	36	1.26	1.16
	Average	**111**	**Average**	**69**	**Average**	**31**	**Average**	**13**		

Table 3.11. Results of the creep and shrinkage test for HPC 3

Time after Loading (days)	Unsealed Total Strain (10^{-6} in./in.)	Sta. Dev. (10^{-6} in./in.)	Sealed Total Strain (10^{-6} in./in.)	Sta. Dev. (10^{-6} in./in.)	Unsealed Shrinkage (10^{-6} in./in.)	Sta. Dev. (10^{-6} in./in.)	Sealed Shrinkage (10^{-6} in./in.)	Sta. Dev. (10^{-6} in./in.)	Unsealed Creep Coefficient	Sealed Creep Coefficient
0	0	0	0	0	0	0	0	0	0.00	0.00
0	542	44	429	38	0	0	0	0	0.00	0.00
1	687	60	533	36	105	9	36	6	0.07	0.16
2	852	82	657	38	147	7	73	12	0.30	0.36
3	873	79	685	38	164	11	90	16	0.31	0.39
7	997	62	856	47	265	10	195	15	0.35	0.54
14	1,009	55	885	46	277	10	214	13	0.35	0.56
21	1,026	50	925	44	295	10	242	12	0.35	0.59
28	1,048	54	977	41	317	10	277	14	0.35	0.63
60	1,088	63	1,033	45	351	16	311	13	0.36	0.68
90	1,151	85	1,088	62	404	16	344	13	0.38	0.74
120	1,165	83	1,103	61	418	16	352	14	0.38	0.75
150	1,192	80	1,129	59	445	17	365	15	0.38	0.78
180	1,212	80	1,152	55	465	19	373	16	0.38	0.82
210	1,226	79	1,170	52	478	21	381	19	0.38	0.84
240	1,247	78	1,179	50	486	23	389	16	0.41	0.84
270	1,274	87	1,196	60	500	21	392	15	0.43	0.87
300	1,296	90	1,207	62	509	24	399	18	0.45	0.88
330	1,321	102	1,221	71	522	29	404	20	0.47	0.91
360	1,345	112	1,234	77	533	26	410	22	0.50	0.92
	Average	**75**	**Average**	**52**	**Average**	**16**	**Average**	**14**		

Table 3.12. Results of the creep and shrinkage test for HPC 4

Time after Loading (days)	Unsealed Total Strain (10^{-6} in./in.)	Sta. Dev. (10^{-6} in./in.)	Sealed Total Strain (10^{-6} in./in.)	Sta. Dev. (10^{-6} in./in.)	Unsealed Shrinkage (10^{-6} in./in.)	Sta. Dev. (10^{-6} in./in.)	Sealed Shrinkage (10^{-6} in./in.)	Sta. Dev. (10^{-6} in./in.)	Unsealed Creep Coefficient	Sealed Creep Coefficient
0	0	0	0	0	0	0	0	0	0.00	0.00
0	814	53	525	32	0	0	0	0	0.00	0.00
1	870	55	540	27	22	9	17	5	0.20	0.21
2	919	57	579	29	33	11	26	7	0.22	0.24
3	959	60	604	34	51	12	40	9	0.25	0.26
7	1,145	77	719	60	133	14	103	14	0.38	0.36
14	1,334	99	874	60	229	16	160	15	0.49	0.55
21	1,459	108	959	67	286	35	212	19	0.57	0.61
28	1,493	107	983	63	293	38	220	24	0.61	0.64
60	1,581	109	1,044	51	296	42	225	28	0.71	0.75
90	1,650	120	1,086	52	306	40	229	33	0.78	0.82
120	1,683	128	1,113	51	312	38	235	27	0.82	0.86
150	1,701	131	1,133	65	319	36	244	23	0.83	0.88
180	1,716	143	1,145	73	330	48	251	29	0.84	0.89
210	1,732	151	1,155	81	341	46	259	36	0.84	0.89
240	1,750	158	1,174	86	344	49	260	38	0.86	0.93
270	1,768	162	1,197	97	342	57	257	43	0.89	0.98
300	1,785	164	1,214	104	345	59	259	46	0.90	1.01
330	1,802	167	1,230	109	351	61	262	48	0.92	1.03
360	1,820	172	1,249	114	353	63	263	45	0.93	1.07
	Average	**117**	**Average**	**66**	**Average**	**33**	**Average**	**25**		

Table 3.13. Results of the creep and shrinkage test for NC 1

Time after Loading (days)	Unsealed Total Strain (10^{-6} in./in.)	Sta. Dev. (10^{-6} in./in.)	Sealed Total Strain (10^{-6} in./in.)	Sta. Dev. (10^{-6} in./in.)	Unsealed Shrinkage (10^{-6} in./in.)	Sta. Dev. (10^{-6} in./in.)	Sealed Shrinkage (10^{-6} in./in.)	Sta. Dev. (10^{-6} in./in.)	Unsealed Creep Coefficient	Sealed Creep Coefficient
0	0	0	0	0	0	0	0	0	0.00	0.00
0	570	91	515	68	0	0	0	0	0.00	0.00
1	604	92	538	69	25	7	19	6	0.06	0.04
2	665	113	596	109	40	9	30	8	0.10	0.09
3	714	126	654	117	68	11	59	13	0.13	0.14
7	845	137	797	123	150	18	130	15	0.22	0.27
14	901	189	869	142	185	23	161	16	0.26	0.34
21	928	212	890	153	193	27	167	18	0.29	0.36
28	944	206	903	162	199	31	171	24	0.31	0.38
60	1,105	217	1,025	172	253	39	216	27	0.50	0.52
90	1,196	231	1,076	182	287	37	246	28	0.59	0.55
120	1,295	230	1,114	200	328	38	278	29	0.70	0.56
150	1,379	225	1,150	193	369	41	312	32	0.77	0.57
180	1,422	227	1,178	197	391	42	333	37	0.81	0.58
210	1,442	226	1,190	189	397	49	338	39	0.83	0.59
240	1,455	228	1,195	210	406	50	339	34	0.84	0.60
270	1,464	254	1,197	208	417	59	338	36	0.84	0.60
300	1,478	267	1,204	194	426	69	340	43	0.85	0.61
330	1,493	284	1,212	186	434	69	343	48	0.86	0.62
360	1,506	289	1,217	203	443	67	344	47	0.86	0.63
	Average	**202**	**Average**	**162**	**Average**	**36**	**Average**	**26**		

Table 3.14. Results of the creep and shrinkage test for NC 2

Time after Loading (days)	Unsealed Total Strain (10^{-6} in./in.)	Sta. Dev. (10^{-6} in./in.)	Sealed Total Strain (10^{-6} in./in.)	Sta. Dev. (10^{-6} in./in.)	Unsealed Shrinkage (10^{-6} in./in.)	Sta. Dev. (10^{-6} in./in.)	Sealed Shrinkage (10^{-6} in./in.)	Sta. Dev. (10^{-6} in./in.)	Unsealed Creep Coefficient	Sealed Creep Coefficient
0	0	0	0	0	0	0	0	0	0.00	0.00
0	666	75	489	36	0	0	0	0	0.00	0.00
1	791	83	564	46	130	14	70	8	-0.01	0.01
2	841	94	604	49	161	16	73	11	0.02	0.07
3	940	110	685	53	225	20	77	14	0.09	0.21
7	984	117	727	56	236	22	91	17	0.15	0.26
14	1,069	118	802	55	259	27	122	25	0.25	0.34
21	1,108	124	835	66	271	28	139	30	0.30	0.36
28	1,138	129	862	83	279	30	141	33	0.34	0.41
60	1,214	131	936	89	299	34	150	40	0.44	0.52
90	1,254	135	979	95	315	39	157	47	0.48	0.58
120	1,280	135	1,008	98	330	40	161	46	0.50	0.63
150	1,321	119	1,053	91	352	45	165	44	0.53	0.70
180	1,345	123	1,068	103	358	55	172	46	0.56	0.71
210	1,381	129	1,136	115	373	59	218	45	0.60	0.75
240	1,411	135	1,203	107	387	60	265	49	0.63	0.79
270	1,437	149	1,236	119	396	69	286	53	0.66	0.81
300	1,465	152	1,292	122	408	69	325	56	0.69	0.84
330	1,492	158	1,337	136	419	68	354	52	0.71	0.87
360	1,507	164	1,353	144	425	77	360	59	0.73	0.88
	Average	**125**	**Average**	**88**	**Average**	**40**	**Average**	**35**		

Table 3.15. Results of the creep and shrinkage test for NC 3

Time after Loading (days)	Unsealed Total Strain (10^{-6} in./in.)	Sta. Dev. (10^{-6} in./in.)	Sealed Total Strain (10^{-6} in./in.)	Sta. Dev. (10^{-6} in./in.)	Unsealed Shrinkage (10^{-6} in./in.)	Sta. Dev. (10^{-6} in./in.)	Sealed Shrinkage (10^{-6} in./in.)	Sta. Dev. (10^{-6} in./in.)	Unsealed Creep Coefficient	Sealed Creep Coefficient
0	0	0	0	0	0	0	0	0	0.00	0.00
0	655	75	499	28	0	0	0	0	0.00	0.00
1	677	77	545	32	14	9	9	5	0.01	0.07
2	694	84	578	39	28	11	18	8	0.02	0.11
3	711	91	610	43	42	14	27	11	0.02	0.15
7	753	98	667	46	67	19	48	15	0.05	0.21
14	839	108	753	55	104	25	88	21	0.14	0.29
21	876	117	777	69	126	24	99	22	0.17	0.31
28	1,012	109	864	73	204	24	140	27	0.27	0.40
60	1,084	123	946	79	252	28	180	37	0.31	0.47
90	1,126	127	1,005	84	278	29	204	41	0.34	0.53
120	1,179	139	1,074	89	315	32	233	43	0.37	0.60
150	1,230	127	1,145	96	353	34	261	47	0.39	0.68
180	1,260	149	1,190	99	375	29	277	43	0.40	0.73
210	1,270	143	1,203	117	383	31	281	42	0.41	0.74
240	1,298	155	1,252	103	387	38	282	45	0.45	0.83
270	1,313	167	1,283	114	383	34	280	48	0.48	0.88
300	1,331	156	1,311	135	391	49	283	51	0.50	0.93
330	1,347	162	1,341	149	392	52	283	46	0.53	0.98
360	1,358	178	1,360	157	395	61	285	53	0.54	1.01
	Average	**126**	**Average**	**85**	**Average**	**27**	**Average**	**30**		

3.8 Analysis and Discussion of Material Properties

3.8.1 Introduction

The analysis and discussion of the concrete compressive strength and modulus of elasticity test results are presented in Sections 3.8.2 and 3.8.3. Section 3.8.4.4 compares the measured creep and shrinkage strains with those predicted by five different models. Prediction models to estimate creep coefficient and shrinkage based on the data from the sealed specimens are proposed in Section 3.8.4.6.

3.8.2 Compressive Strength

The average compressive strength of the four HPC mixes was 6,272 psi at one day and 7,946 psi at 28 days, whereas the average compressive strength of the three NC mixes was 8,400 psi at one day and 9,593 psi at 28 days. Accordingly, the average compressive strength of the three NC mixes was 34% higher at one day and 21% higher at 28 days than those obtained for the four HPC mixes. The values of the strength gain in percent from 1 to 28 days for the HPC and NC mixes are shown in Table 3.16.

Table 3.16. Strength gain from 1 day to 28 days for HPC and NC

Mix ID	HPC 1	HPC 2	HPC 3	HPC 4	NC 1	NC 2	NC 3
Average 1-Day Strength (psi)	6,784	6,247	5,417	6,640	8,902	6,547	9,750
Average 28-Day Strength (psi)	8,750	7,938	6,884	8,212	10,215	7,545	11,020
Strength Gain from 1-Day to 28-Day	29%	27%	27%	24%	15%	15%	13%
Average Strength Gain from 1-Day to 28-Day	**27%**				**14%**		

These values confirm that the HPC mixes had a higher rate of strength gain over this time than the NC mixes. This observation is believed to be due to the effect of the slag and fly ash in the HPC mixes and is consistent with the outcomes of previous studies, including Brooks et al. (1992), Baalbaki et al. (1992) and Wainwright and Rey (2000).

3.8.3 Modulus of Elasticity

A comparison of the modulus of elasticity of concrete at loading is given in Table 3.17 for the measured values and the values obtained from four suggested models.

Table 3.17. Comparison of the measured concrete modulus of elasticity with values obtained from four recommended models (in ksi)

Mix ID	Sealed	Unsealed	AASHTO	ACI 363R-92	CEB-FIP 90	Tadros
HPC 1	4,870	3,216	5,114	4,628	5,215	4,834
HPC 2	5,596	3,105	4,422	4,041	5,074	4,613
HPC 3	5,226	4,080	4,334	4,030	4,838	4,259
HPC 4	5,629	5,129	4,733	4,293	5,178	4,775
NC 1	5,425	5,602	5,653	4,964	5,709	5,657
NC 2	4,399	5,027	4,867	4,423	5,154	4,737
NC 3	4,671	4,297	5,882	5,118	5,885	5,971

Table 3.18 and Table 3.19 summarize the percentage difference in the modulus of elasticity between the measured values and expected values from the four models for the sealed and unsealed specimens, respectively.

Table 3.18. Difference in the percentage of the concrete modulus of elasticity between measured values and four models for sealed specimens

Mix ID	Sealed Samples	AASHTO	ACI 363R-92	CEB-FIP 90	Tadros
HPC 1	0	5	-5	7	-1
HPC 2	0	-21	-28	-9	-18
HPC 3	0	-17	-23	-7	-19
HPC 4	0	-16	-24	-8	-15
NC 1	0	4	-8	5	4
NC 2	0	11	1	17	8
NC 3	0	26	10	26	28
Average	**0**	**-1**	**-11**	**4**	**-2**

Table 3.19. Difference in the percentage of the concrete modulus of elasticity between measured values and four models for unsealed specimens

Mix ID	Unsealed Samples	AASHTO	ACI 363R-92	CEB-FIP 90	Tadros
HPC 1	0	59	44	62	50
HPC 2	0	42	30	63	49
HPC 3	0	6	-1	19	4
HPC 4	0	-8	-16	1	-7
NC 1	0	1	-11	2	1
NC 2	0	-3	-12	3	-6
NC 3	0	37	19	37	39
Average	**0**	**19**	**7**	**27**	**19**

The measured values of the modulus of elasticity versus the compressive strength of the HPC specimens from this project, along with values reported by four others (Haranki 2009, Schindler et al. 2007, Townsend 2003, and Wang et al. 2013), are summarized in Figure 3.8

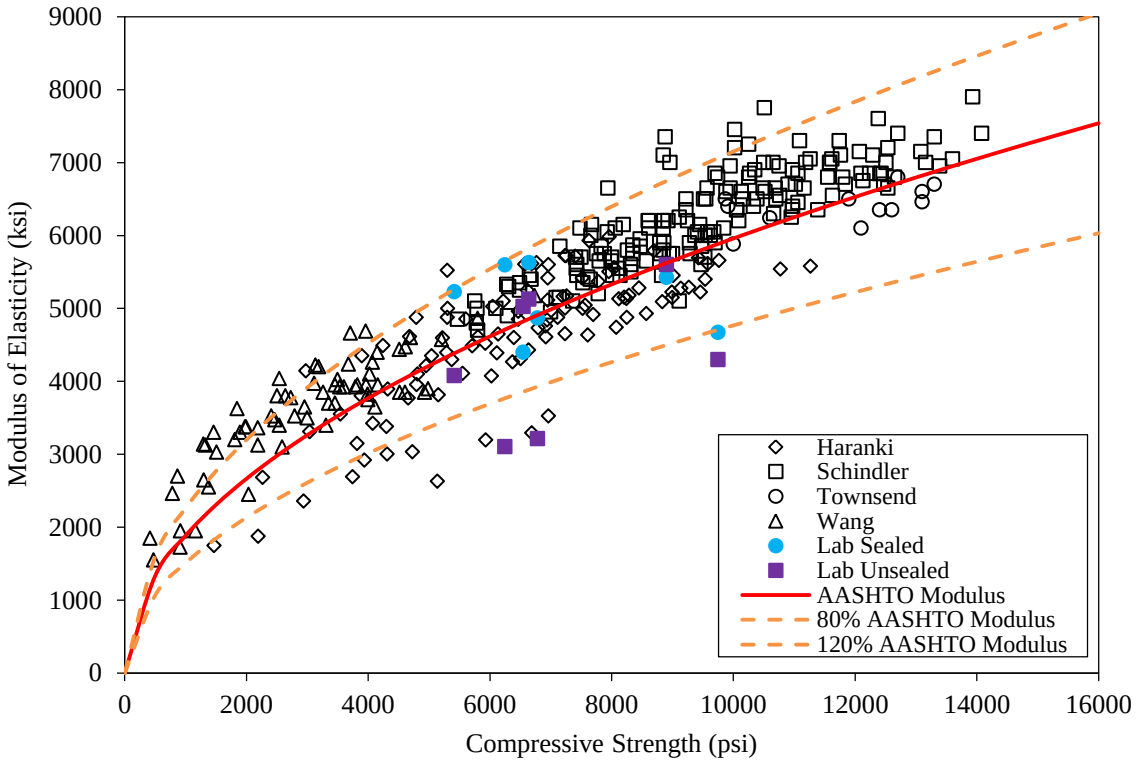

Figure 3.8. Comparison of the modulus of elasticity between the AASHTO LRFD model and measured values from five studies

For the sealed specimens, it was found that the AASHTO LRFD (2010) and Tadros et al. (2003) models produced better agreement with the measured values, and the ACI 363R-92 model showed the largest difference from the measured values. It was found that for the unsealed specimens the ACI 363R-92 model gave a better prediction, and the CEB-FIP 90 model showed the largest difference from the measured data.

As discussed previously, sealed specimens represent the behavior of large concrete members, such as PPCBs, better than unsealed specimens. The AASHTO LRFD model is preferred for estimating the elastic modulus of concrete used for PPCBs. Tadros' model can also be used when it is in good agreement with the AASHTO LRFD model for compressive strengths from 5,000 psi to 11,000 psi, which is the range of observed release strengths for different types of PPCBs.

In Figure 3.8, the average density of all concrete mixes was used for the AASHTO LRFD model. It was observed that most data points fall within ±20% margins of the AASHTO LRFD model, which means that the AASHTO LRFD model provides a good prediction of the concrete modulus of elasticity as a function of the compressive strength. Therefore, the AASHTO LRFD

model is primarily used for the modulus of elasticity when calculating the camber of PPCBs in the remainder of this study.

3.8.4 Summary of the Creep and Shrinkage Tests

Three subsections are presented below that provide a summary of seven mixes, relations between the creep and shrinkage and material properties, and a comparison of the creep and shrinkage behavior between the HPC and NC mixes.

3.8.4.1 Summary of the Seven Mixes

Key details of the seven concrete mixes are summarized in Table 3.20 in terms of weight, which includes w/c ratio, coarse aggregate content, aggregate to cementitious materials (a/c) ratio, and slag and fly ash replacement percentages.

Table 3.20. Summary of the seven concrete mixes

Mix ID	w/c Ratio	Coarse Aggregate Content	a/c Ratio	Slag Replacement	Fly Ash Replacement
HPC 1	0.335	41%	4.0	20%	0%
HPC 2	0.380	34%	4.1	25%	10%
HPC 3	0.300	33%	3.9	30%	0%
HPC 4	0.370	40%	3.5	25%	10%
NC 1	0.334	41%	3.9	0%	0%
NC 2	0.380	29%	4.0	0%	0%
NC 3	0.360	41%	4.0	0%	0%

The w/c ratio of the seven mixes ranged from 0.300 to 0.380, the a/c ratio ranged from 3.5 to 4.1, the slag replacement varied from 0% to 25%, and the fly ash replacement ranged from 0% to 10%.

3.8.4.2 Relations between the Results of the Creep and Shrinkage Tests and Material Properties

Relations between the shrinkage strain and creep coefficient over a period of one year and the material properties are shown from Figure 3.9 to Figure 3.18.

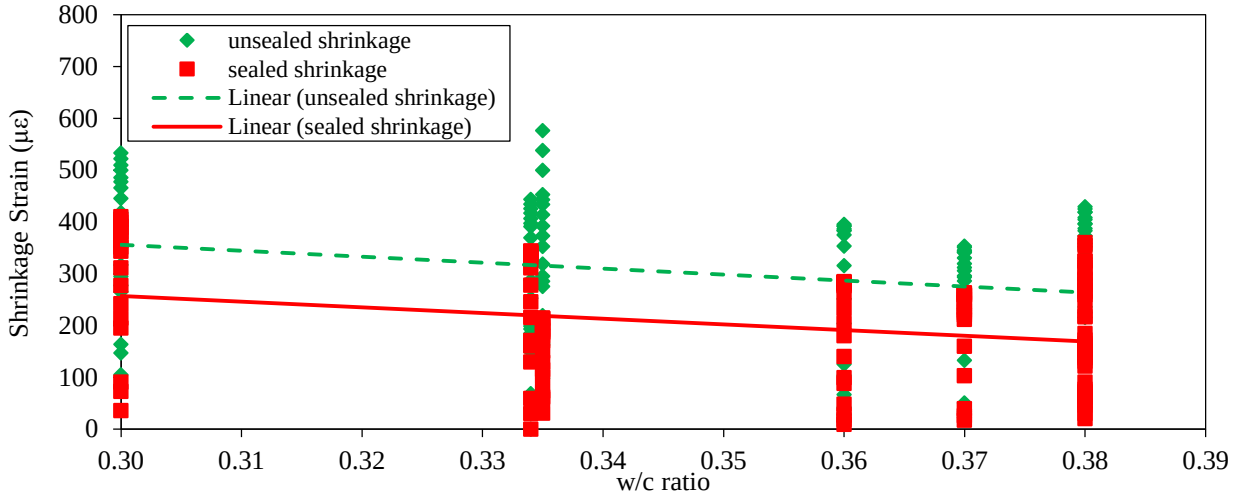

Figure 3.9. Relation between shrinkage and w/c ratio

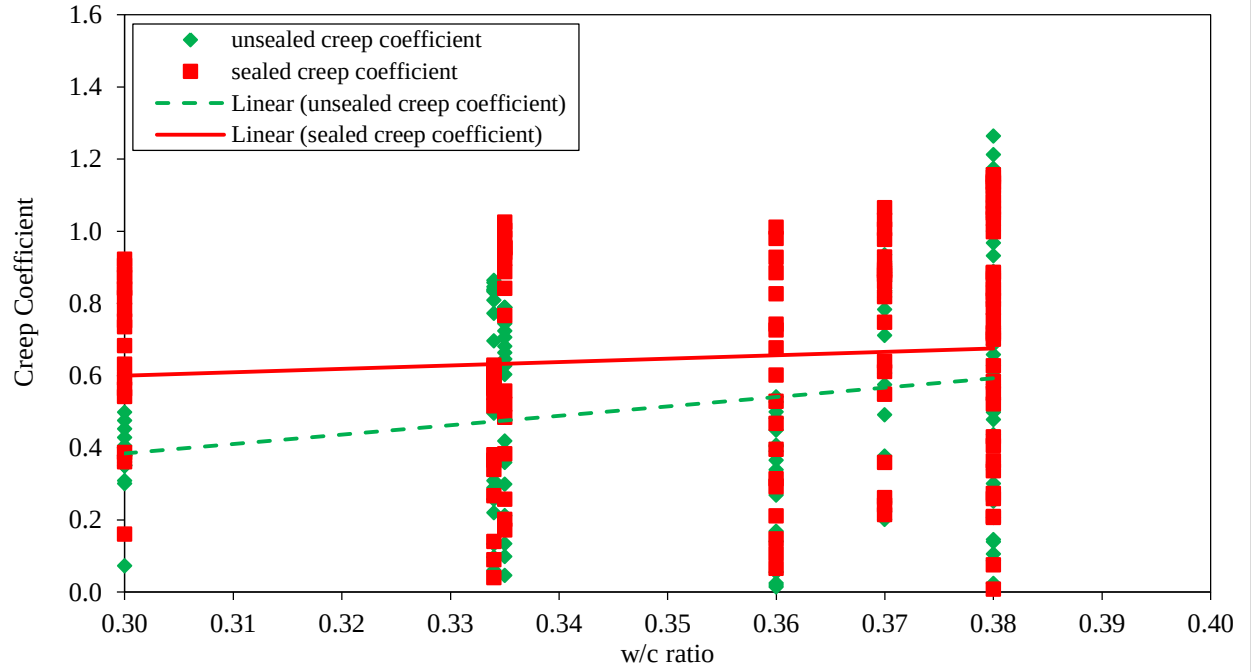

Figure 3.10. Relation between creep coefficient and w/c ratio

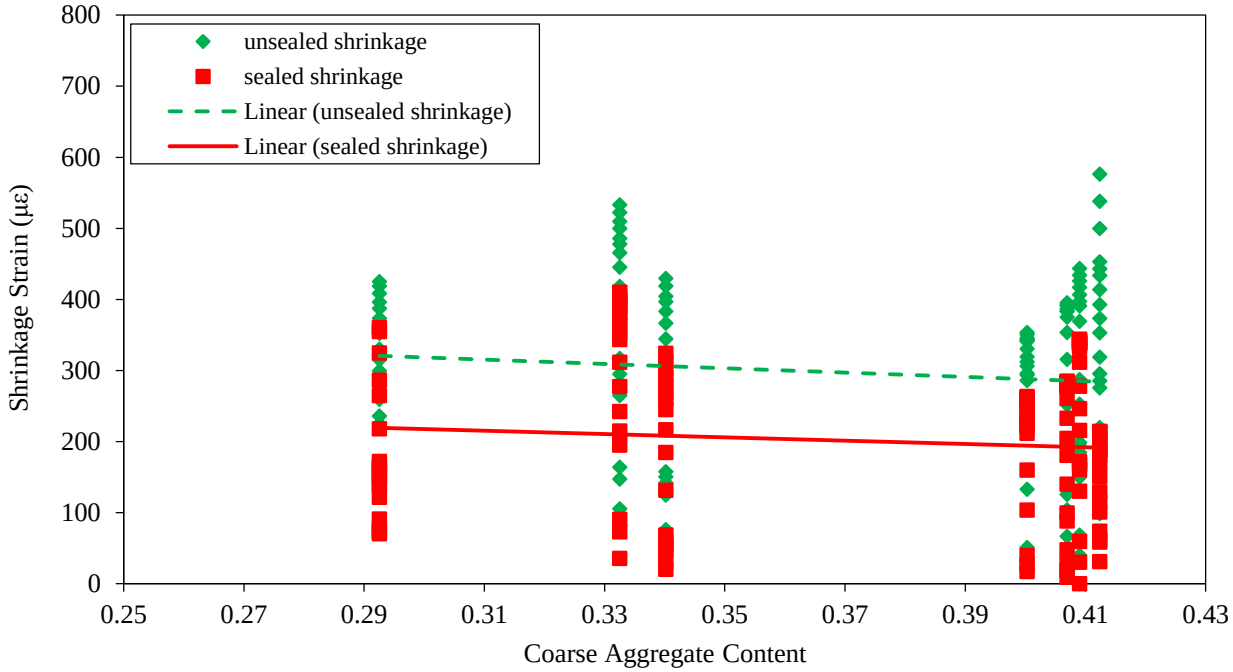

Figure 3.11. Relation between shrinkage strain and coarse aggregate content

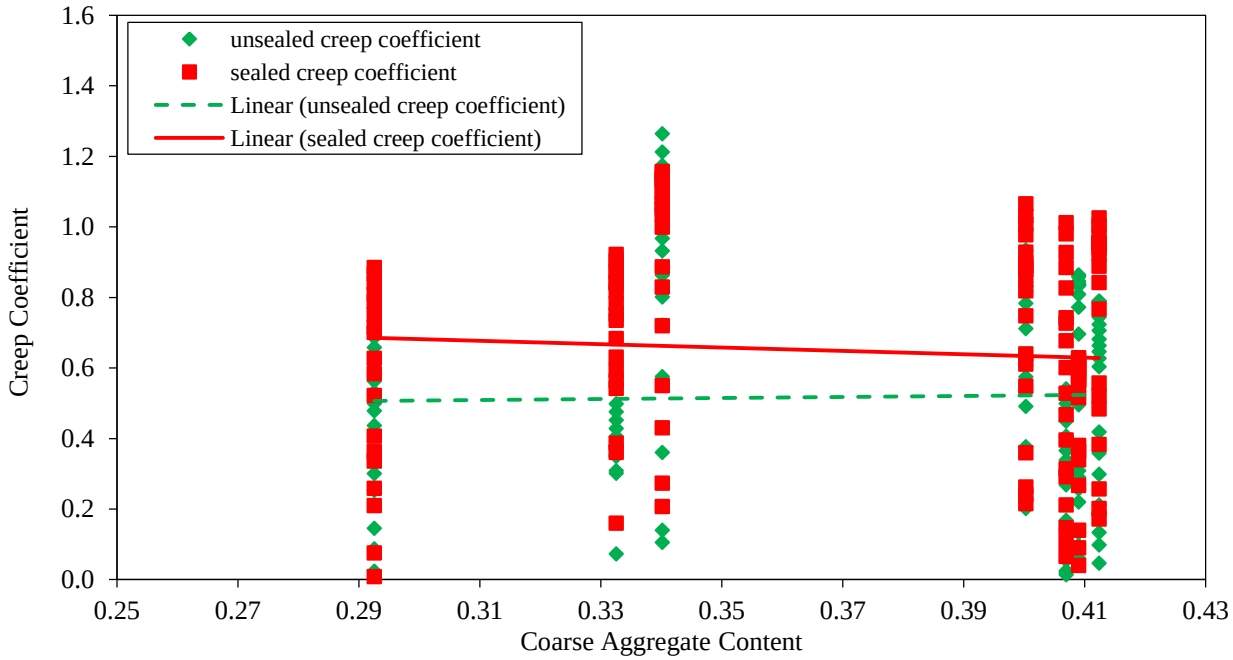

Figure 3.12. Relation between creep coefficient and coarse aggregate content

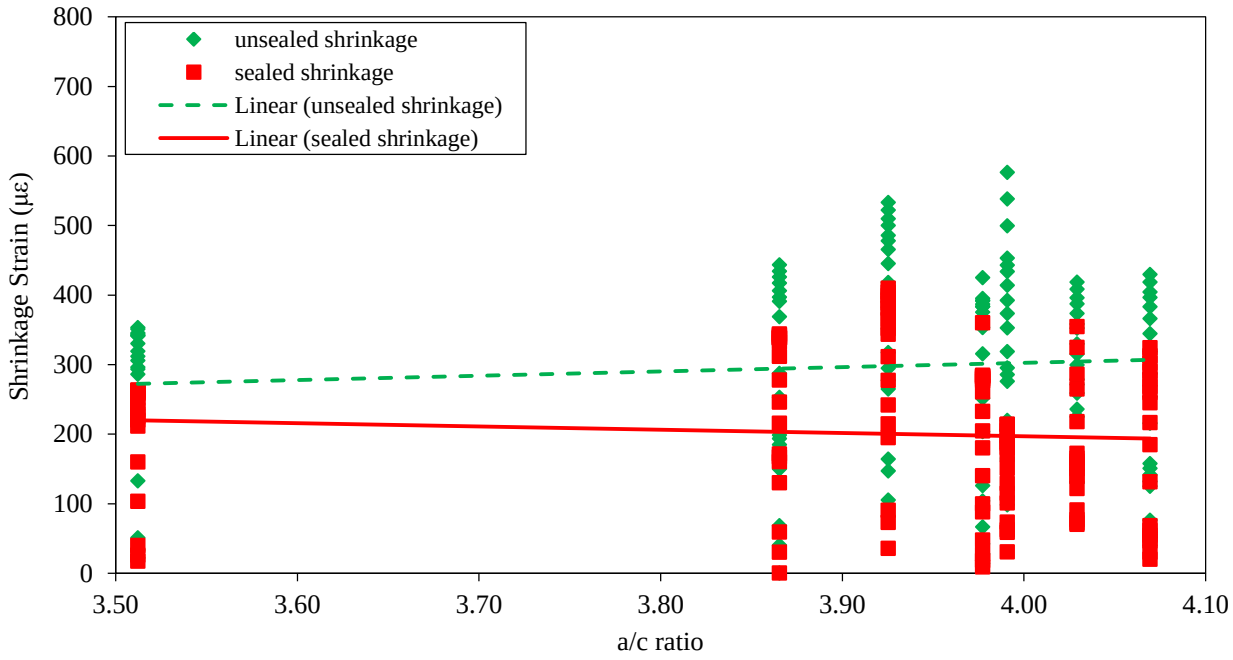

Figure 3.13. Relation between shrinkage strain and a/c ratio

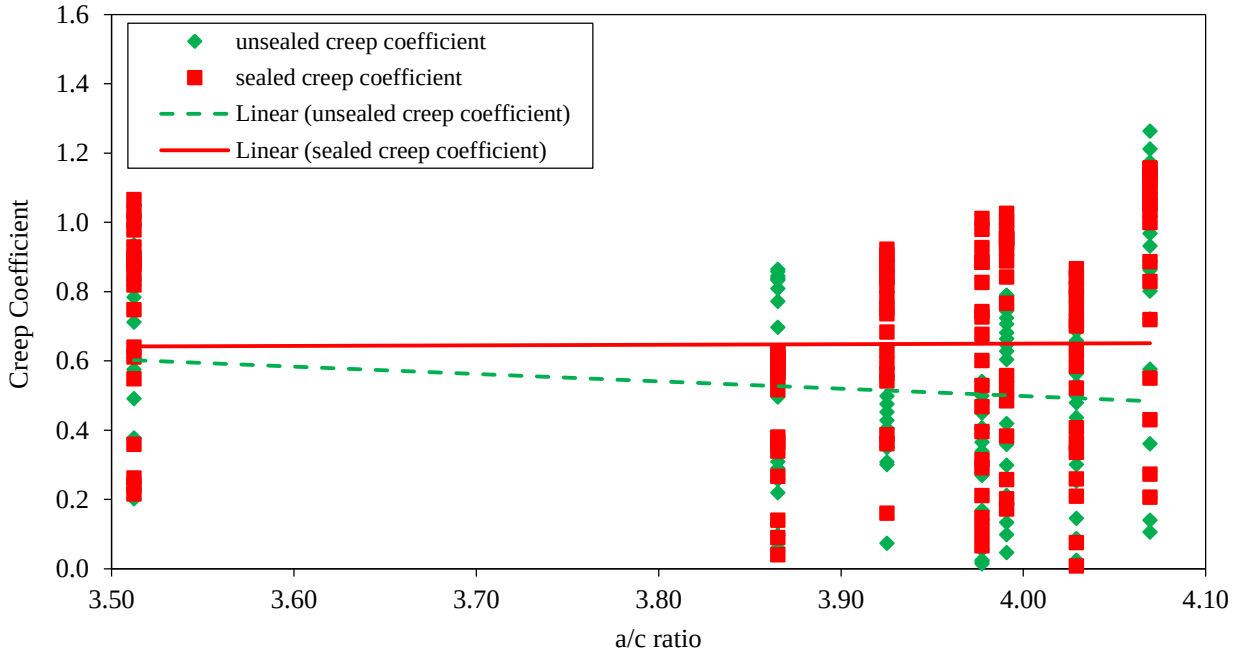

Figure 3.14. Relation between creep coefficient and a/c ratio

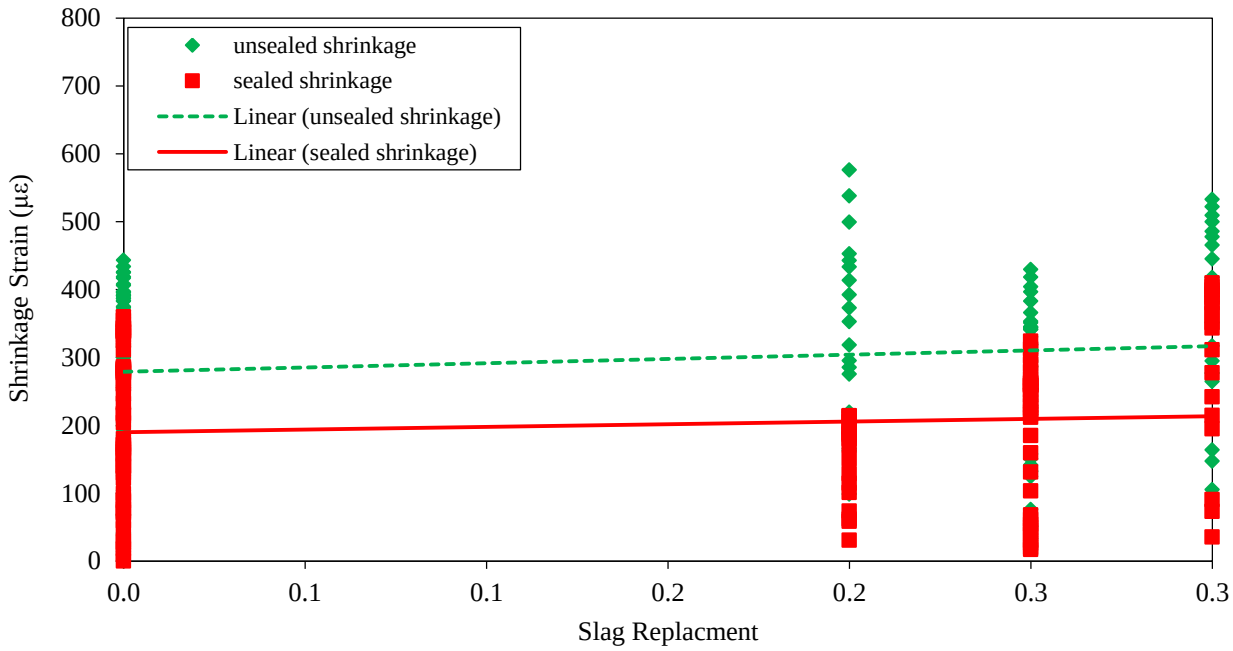

Figure 3.15. Relation between shrinkage strain and slag replacement percentage

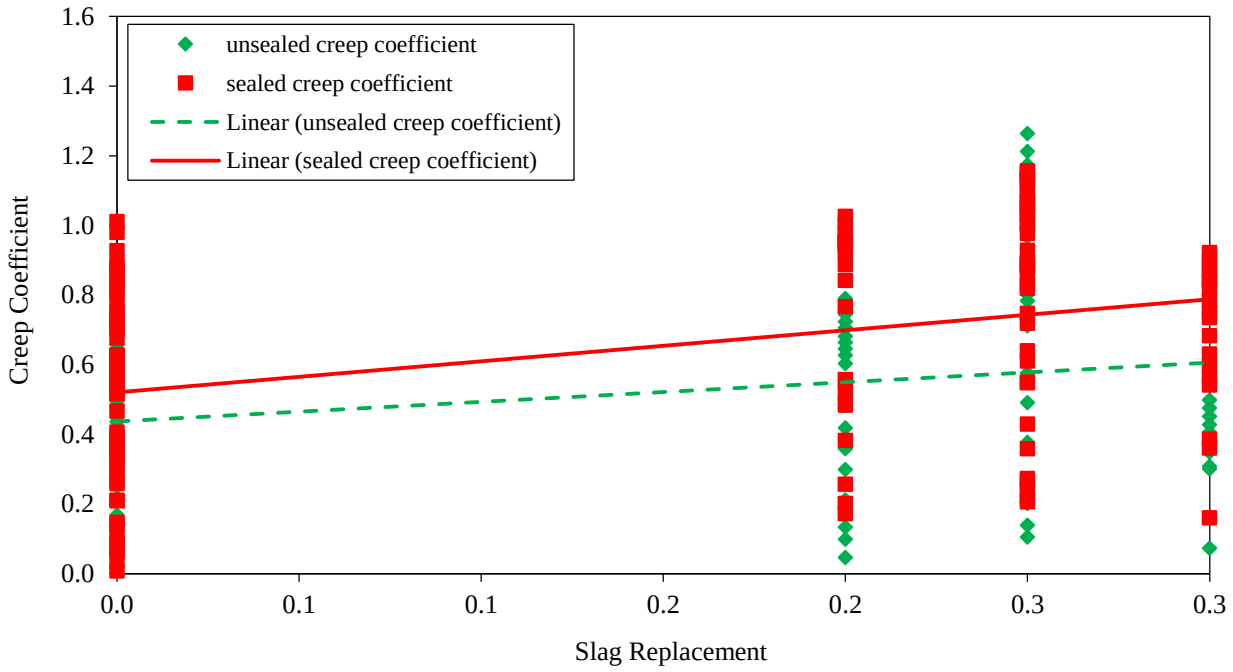

Figure 3.16. Relation between creep coefficient and slag replacement percentage

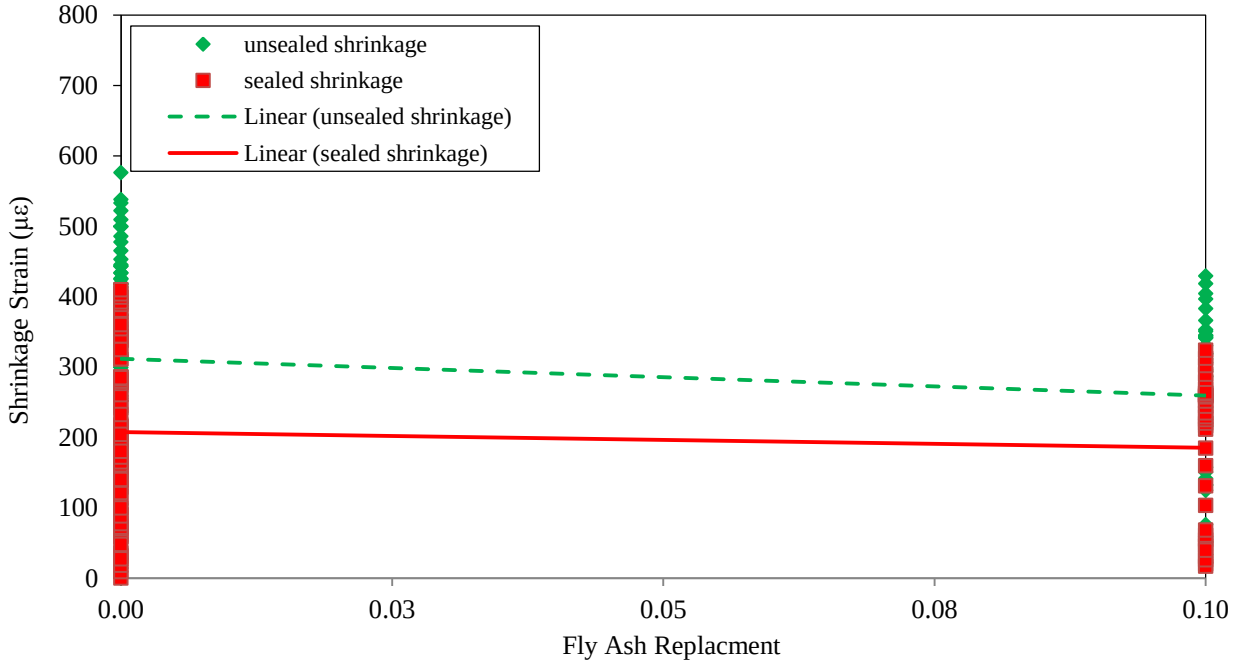

Figure 3.17. Relation between shrinkage strain and fly ash replacement percentage

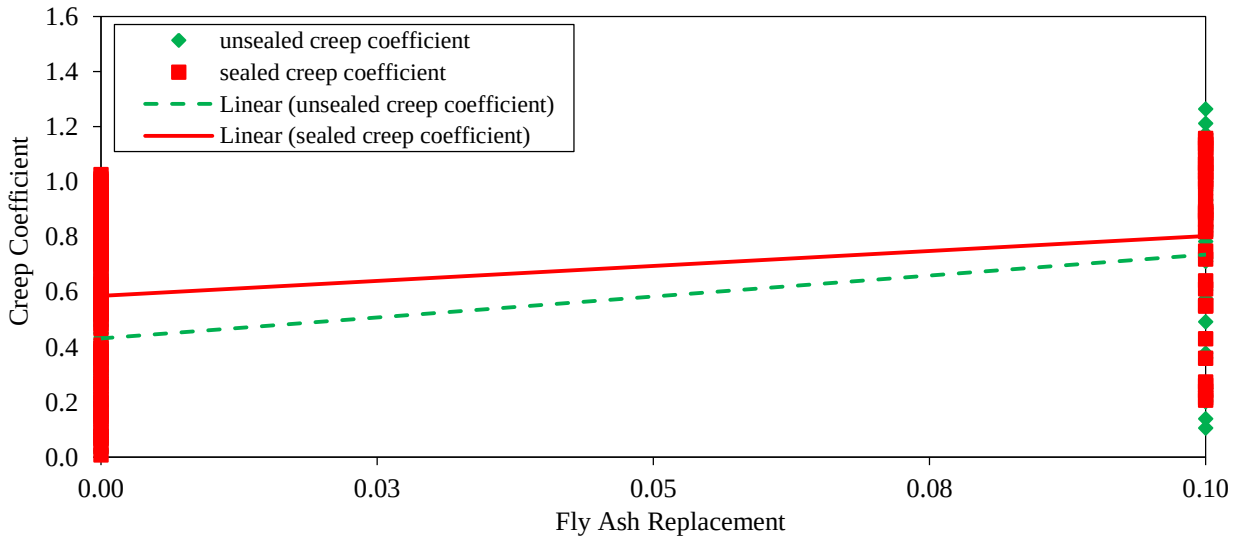

Figure 3.18. Relation between creep coefficient and fly ash replacement percentage

It was observed that the results of the sealed creep coefficient and the sealed shrinkage agree well with the results published in previous research, as summarized in Chapter 2, except for the influence of w/c ratio. However, the unsealed creep coefficient and the unsealed shrinkage showed trends opposite to those reported by other researchers. More detailed observations are presented below:

- The shrinkage strain for both the unsealed and sealed specimens decreased with an increase in the w/c ratio, which is the opposite of the trend reported in previous research, as

summarized in Section 2.1.5.1.3. The possible reason is that the range of the w/c ratio for the seven mixes is narrow. Other factors could have also contributed to this opposite trend, including the coarse aggregate content, the a/c ratio, and the slag and fly ash replacement percentages.

- The creep coefficient for both the unsealed and sealed specimens increased with an increase in the w/c ratio, which is the same trend as reported in Section 2.1.6.1.3.
- Both the unsealed and sealed shrinkage strains decreased with an increase in the coarse aggregate content, which is consistent with previous studies (see Section 2.1.5.1.1).
- The unsealed creep coefficient was not affected significantly by the coarse aggregate content, and it increased slightly with an increase in the coarse aggregate content, which was not consistent with the previous observations summarized in Section 2.1.6.1.1. The unsealed creep coefficient is also affected by factors such as the w/c ratio, the a/c ratio, and the slag and fly ash replacement percentages. The sealed creep coefficient decreased with an increase in the coarse aggregate content, which is consistent with previously reported findings.
- The unsealed shrinkage strains increased with an increase in the a/c ratio, which is the opposite of the trend noted in Section 2.1.5.1.1. The possible reason for this discrepancy is that other factors could have also influenced the unsealed shrinkage, including the w/c ratio and the slag and fly ash replacement percentages. The sealed shrinkage decreased with an increase in the a/c ratio, and this observation is consistent with previous investigations.
- The unsealed creep coefficient decreased with an increase in the a/c ratio, which is consistent with the previous studies discussed in Section 2.1.6.1.1. The influence of the a/c ratio on the sealed creep coefficient was small, which was possibly influenced by the w/c ratio and the slag and fly ash replacement percentages.
- Both the unsealed and sealed shrinkage strains increased with an increase of the slag replacement percentage from 0% to 30%, and the effect of the slag replacement percentage was similar for both unsealed and sealed specimens. A similar trend was observed by other researchers, as summarized in Section 2.1.5.1.5 for the early age loaded slag concrete.
- Both the unsealed and sealed creep coefficients increased with an increase in the slag replacement percentage from 0% to 30%, and the extent of the effect of the slag replacement percentage for sealed specimens was higher than that for the unsealed specimens. These observations are consistent with those reported in previous studies using an early age loaded slag concrete.
- Class C fly ash decreased the shrinkage for both the unsealed and sealed specimens, and the extent of the decrease for the unsealed specimens was slightly higher than that for the sealed specimens, which is consistent with previous findings.
- Class C fly ash increased both the unsealed and sealed creep coefficients, and the extent of the effect for the unsealed specimens was slightly higher than that for the sealed specimens. These observations are also consistent with previous findings.

3.8.4.3 Comparison between HPC and NC Specimens

Comparisons of the average unsealed and sealed creep coefficients and shrinkage strains for the HPC and NC specimens over a one-year duration are shown from Figure 3.19 to Figure 3.22.

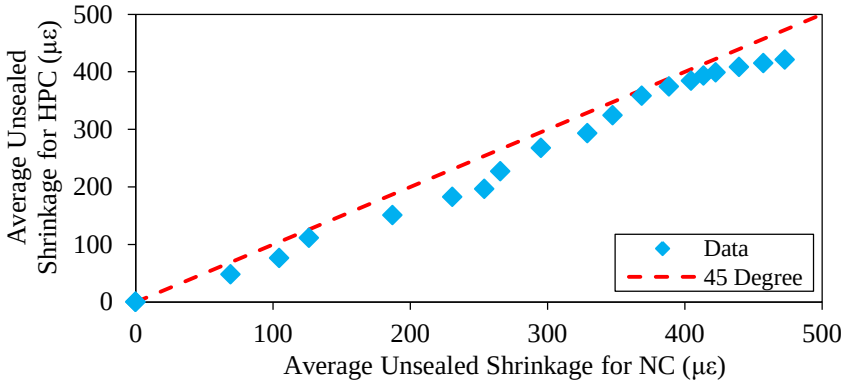

Figure 3.19. Comparison of the average unsealed shrinkage strains obtained for the HPC and NC specimens over 12 months

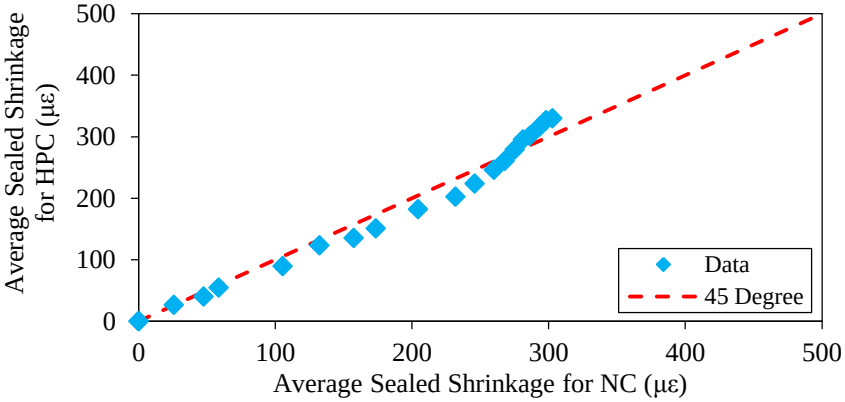

Figure 3.20. Comparison of the average sealed shrinkage strains for the HPC and NC specimens over 12 months

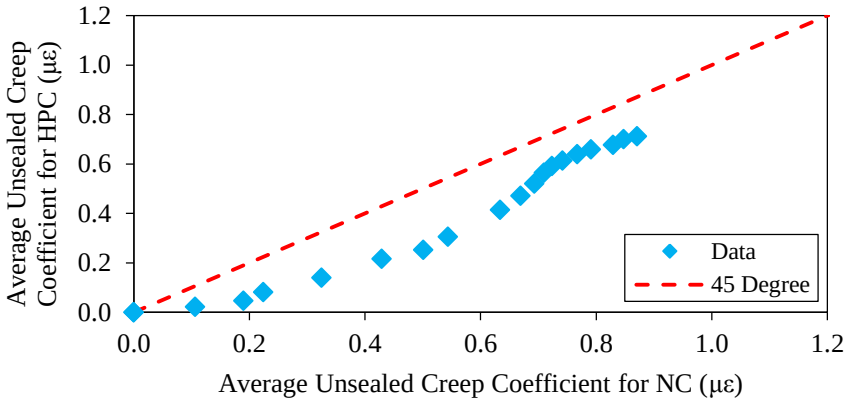

Figure 3.21. Comparison of the average unsealed creep coefficients for the HPC and NC specimens

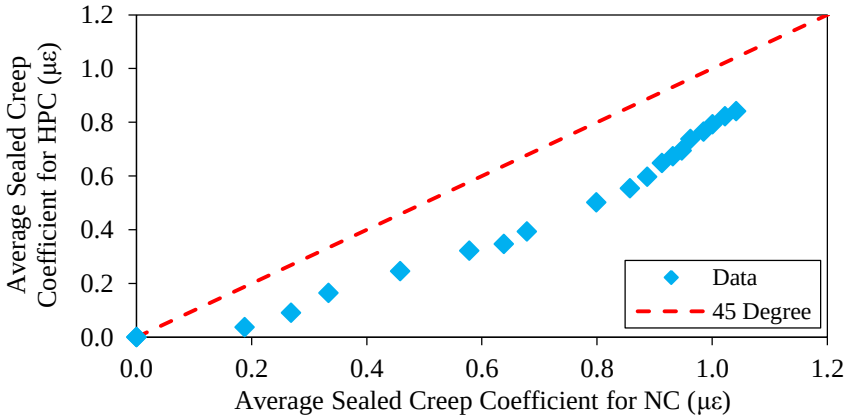

Figure 3.22. Comparison of the average sealed creep coefficients for the HPC and NC specimens

The differences between the HPC and NC specimens are also summarized in Table 3.21 in terms of percentage (i.e., difference in percent = $\frac{\text{HPC value}-\text{NC value}}{\text{NC value}}$ *100%).

Table 3.21. Comparison of the HPC shrinkage strains and creep coefficients with respect to the NC in terms of percentage

Time after Loading (days)	Unsealed Shrinkage (%)	Sealed Shrinkage (%)	Unsealed Creep Coefficient (%)	Sealed Creep Coefficient (%)
0	0	0	0	0
0	0	0	0	0
1	44	-2	381	398
2	37	19	308	197
3	13	8	175	102
7	24	18	133	87
14	26	7	98	79
21	29	16	98	84
28	17	15	78	72
60	10	12	53	59
90	12	15	42	55
120	7	10	33	49
150	3	6	26	41
180	4	3	22	38
210	5	-1	21	36
240	5	-5	20	30
270	6	-5	20	29
300	8	-7	23	26
330	10	-9	21	24
360	12	-8	22	24
Average	**15**	**5**	**88**	**79**

From these comparisons, the following observations have been made:

- The average unsealed shrinkage strains for the HPC specimens were 15% higher than those obtained for the NC specimens. The difference in the average unsealed shrinkage strains for the HPC and the NC specimens reduced with time.
- The average sealed shrinkage strains for the HPC specimens were higher than those of the NC specimens for the first six months and were lower than those obtained for the NC specimens over the next six months, with the average difference over the 12 months being 5%.
- The average unsealed creep coefficients of the HPC specimens were higher than those of the NC specimens, with the average difference being 88%. The difference decreased with time from 381% at the age of one day to 22% at one year.
- The average sealed creep coefficients for the HPC specimens were higher than those obtained for the NC specimens, and the average difference over 12 months was 79%. The difference decreased with time from 398% at one day to 24% at one year.

From the observations summarized above, it can be concluded that the HPC specimens had higher shrinkage strains and creep coefficients than the NC specimens for both the unsealed and sealed specimens. The differences were smaller for shrinkage strains and larger for creep coefficients. At the early age after loading, especially during the first month, significantly higher creep was observed, which reduced with time.

3.8.4.4 A Comparison of the Measured Creep and Shrinkage with Predicted Values

Comparisons of the measured creep and shrinkage values with those obtained from five different models over a one-year period are shown in Table 3.22 and Table 3.23, where the unsealed creep coefficient, the sealed creep coefficient, the unsealed shrinkage, and the sealed shrinkage are presented in terms of a percentage difference (i.e., difference in percentage = $\frac{\text{Model value} - \text{Measured value}}{\text{measured value}} \times 100\%$).

Table 3.22. Average difference in percent between the creep coefficient and shrinkage of four HPC mixes and five models in one year

Models	Unsealed Creep Coefficient	Sealed Creep Coefficient	Unsealed Shrinkage	Sealed Shrinkage	Average Difference in Percent	Rank
AASHTO LRFD (2010)	95	-32	-1	-44	4	1
ACI 209R-92	233	-30	-23	-	60	3
ACI 209R-Modified by Huo et al. (2001)	203	-37	-21	-	48	2
CEB-FIP 90	264	-14	47	-	99	4
Bazant B3	335	94	57	-62	106	5

Table 3.23. Average difference in percent between the creep coefficient and shrinkage of three NC mixes and five models in one year

Models	Unsealed Creep Coefficient	Sealed Creep Coefficient	Unsealed Shrinkage	Sealed Shrinkage	Average Difference in Percent	Rank
AASHTO LRFD (2010)	119	-6	0	-49	16	1
ACI 209R-92	292	31	-1	-	107	3
ACI 209R-Modified by Huo et al. (2001)	396	21	0	-	139	4
CEB-FIP 90	128	95	31	-	85	2
Bazant B3	291	322	91	-60	161	5

Of the different models, it was found that the AASHTO LRFD (2010) model gave the best predictions for both the HPC and NC specimens. It was also found that the B3 model has the largest errors for both the HPC and NC specimens. Comparisons of the measured and predicted data for both the creep and shrinkage are given in Appendix A.

3.8.4.5 Comparison of the Shrinkage Behavior between a Four-foot PPCB Section and Laboratory Specimens

Figure 3.23 compares the shrinkage strains obtained from a 4 ft full-scale PPCB section with those measured from unsealed and sealed specimens that were stored in the environmentally controlled chamber.

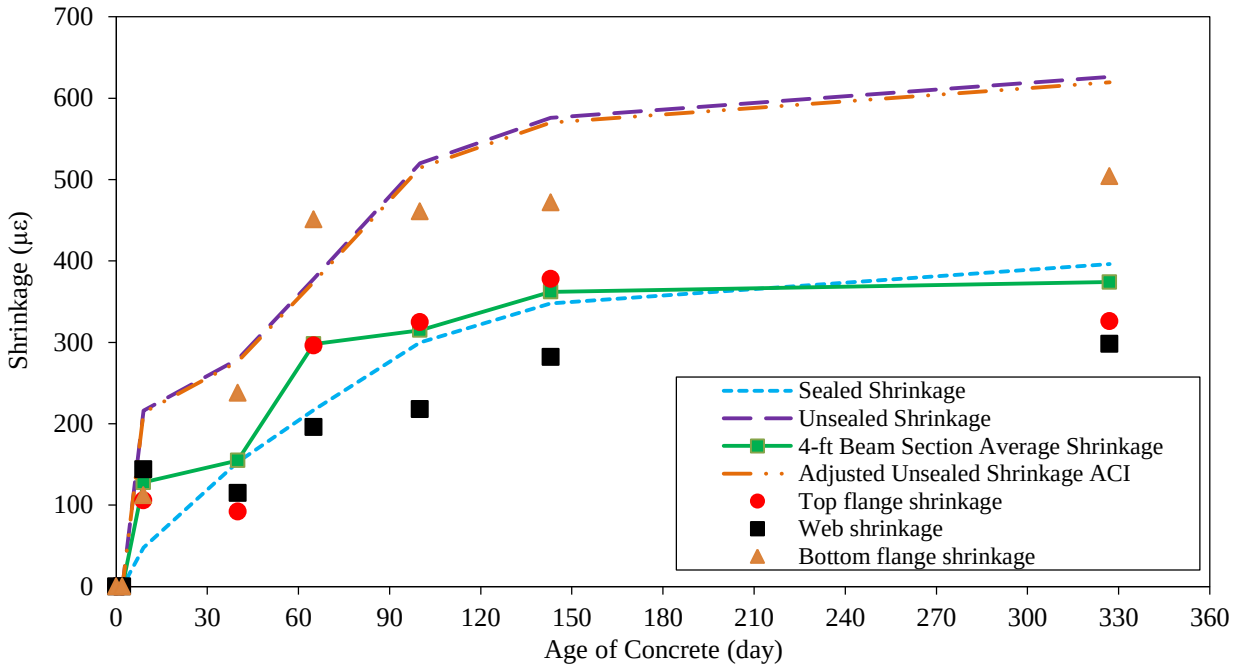

Figure 3.23. Comparison of shrinkage strains measured from a 4 ft full-scale PPCB section and standard cylindrical specimens

The PPCB section was left at the precast plant in an outdoor environment. It was found that the 4 ft PPCB section had a shrinkage behavior comparable to that observed for the sealed specimens, which means that the sealed specimens could represent the shrinkage behavior of the PPCBs better than the unsealed specimens. This observation was consistent with previous studies, such as Hansen and Nielsen (1966) and Bryant and Vadhanavikkit (1987).

Also included in Figure 3.23 is the shrinkage of the unsealed specimen after adjusting for the v/s ratio according to Equation 2-21 (ACI 209R 1990). It was observed that the average shrinkage of the PPCB section was similar to that of the sealed specimens. It was also found that the bottom flange of the PPCB had a higher shrinkage strain than the top flange and web, which could have been due the strands in the bottom PPCB not fully debonding and the PPCB section being subjected to a temperature gradient during sunny days. The extent of the debonding between strands, the concrete, and the temperature gradient would have had some effects on the web of the PPCB section. It is also observed that the shrinkage of the web was lower than that observed in the sealed specimens.

3.8.4.6 Proposed Equations for Predicting the Creep and Shrinkage of HPC

Based on the findings reported above, the measured average creep coefficients and shrinkage strains from the sealed specimens of the four HPC mixes were used to establish appropriate methods for accurately calculating the long-term camber of PPCBs.

Table 3.24 and Table 3.25 summarize the measured sealed creep coefficients and shrinkage strains and the corresponding average values for the four HPC mixes using the test specimens stored in the environmental chamber. All data were collected over a period of one year, and thus for times beyond one year the data should be applied with caution.

Table 3.24. Measured sealed creep coefficients and average values for the four HPC mixes

Time after Loading (days)	HPC 1	HPC 2	HPC 3	HPC 4	Average	Sta. Dev.
0	0.00	0.00	0.00	0.00	0.00	0.00
0	0.00	0.00	0.00	0.00	0.00	0.00
1	0.17	0.21	0.16	0.21	0.19	0.01
2	0.20	0.27	0.36	0.24	0.27	0.03
3	0.26	0.43	0.39	0.26	0.33	0.04
7	0.38	0.55	0.54	0.36	0.46	0.04
14	0.48	0.72	0.56	0.55	0.58	0.04
21	0.52	0.83	0.59	0.61	0.64	0.06
28	0.56	0.89	0.63	0.64	0.68	0.06
60	0.77	1.00	0.68	0.75	0.80	0.06
90	0.84	1.03	0.74	0.82	0.86	0.05
120	0.89	1.05	0.75	0.86	0.89	0.05
150	0.92	1.07	0.78	0.88	0.91	0.05
180	0.94	1.08	0.82	0.89	0.93	0.05
210	0.95	1.10	0.84	0.89	0.95	0.05
240	0.96	1.12	0.84	0.93	0.96	0.05
270	0.95	1.14	0.87	0.98	0.99	0.05
300	0.98	1.13	0.88	1.01	1.00	0.04
330	1.00	1.15	0.91	1.03	1.02	0.04
360	1.03	1.16	0.92	1.07	1.04	0.04

Table 3.25. Measured sealed shrinkage strains and average values for the four HPC mixes (10^{-6} in./in.)

Time after Loading (days)	HPC 1	HPC 2	HPC 3	HPC 4	Average	Sta. Dev.
0	0	0	0	0	0	0
0	0	0	0	0	0	0
1	31	20	36	17	26	4
2	62	30	73	26	48	10
3	59	46	90	40	59	10
7	74	50	195	103	105	28
14	101	54	214	160	132	30
21	115	61	242	212	157	36
28	129	68	277	220	174	40
60	151	131	311	225	205	35
90	171	185	344	229	232	34
120	180	216	352	235	246	32
150	187	245	365	244	260	32
180	188	260	373	251	268	33
210	192	269	381	259	275	34
240	197	279	389	260	281	35
270	205	290	392	257	286	34
300	213	302	399	259	293	34
330	214	313	404	262	298	35
360	214	324	410	263	303	37

To establish suitable predictive equations, the format of the AASHTO LRFD (2010) creep and shrinkage models was used, and the least squares method was adopted to obtain the appropriate coefficients. The resulting equation to obtain the average creep coefficients for the HPC used by the three precast plants is given in Equation 3-1.

$$\phi(t) = \frac{1.9t^{0.48}}{8+ t^{0.54}} \quad \textbf{(3-1)}$$

where t is the duration after loading for the creep in number of days.

The corresponding equation to estimate the average shrinkage strains is given by Equation 3-2.

$$\varepsilon(t) = \frac{480t^{0.60}}{12+ t^{0.62}} \quad \textbf{(3-2)}$$

where t is the duration in days after the concrete is exposed to the air.

Figure 3.24 and Figure 3.25 show the comparison of the predicted values from the proposed equations, the average measured values, and the standard deviations.

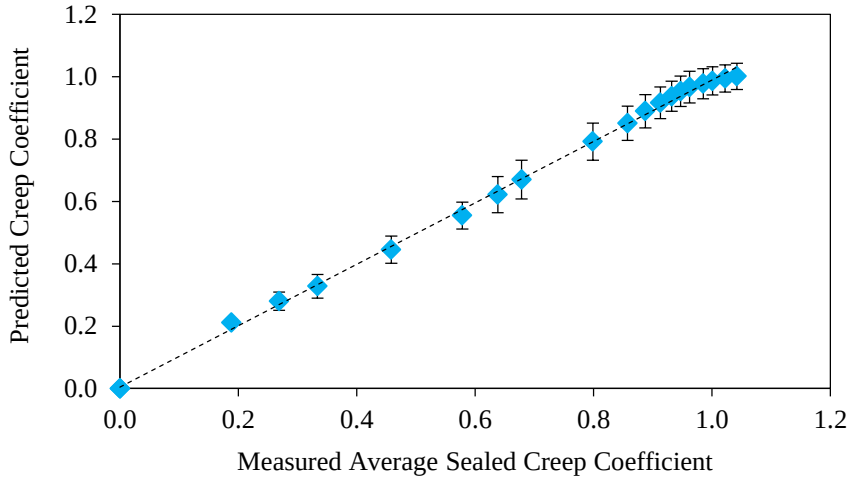

Figure 3.24. Comparison of the predicted sealed creep coefficients and the measured average values for the HPC specimens

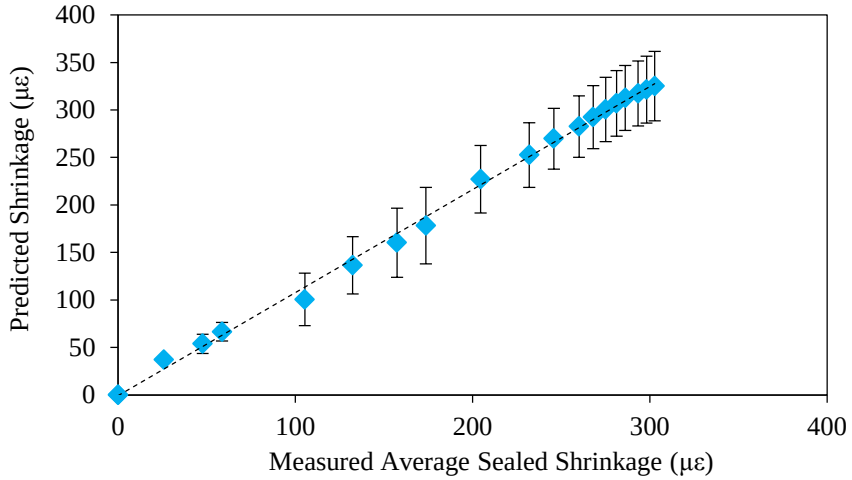

Figure 3.25. Comparison of the predicted sealed shrinkage strains and the measured average values for the HPC specimens

The vertical bars in these figures represent the standard deviations of the measured values for the four HPC mixes. The standard deviation between the predicted sealed creep coefficients and the measured values at one year was 0.00342. The standard deviation between the predicted sealed shrinkage strains and the measured values was 4.03 microstrains. According to Equation 3-1, the ultimate sealed creep coefficient at the age of one year was 1.06.

3.9 Conclusions

Based on the materials presented in this chapter, the following conclusions can be drawn:

- The modulus of elasticity of concrete can be predicted within ±20% of the actual values using the AASHTO LRFD model.
- The sealed specimens represented the creep and shrinkage behavior of the full-scale PPCBs much better than the unsealed specimens.
- The AASHTO LRFD (2010) creep and shrinkage models were found to give the best estimates when compared to the measurements taken from the four HPC and three NC mixes over one year. Other models investigated were the ACI 209R-92 model, the ACI 209R model modified by Huo et al. (2001), the CEB-FIP 90 model, and the B3 model by Bazant (2000). Although the AASHTO LRFD (2010) model was found to be better than the other four models, large errors still existed between the measured and predicted values using the AASHTO LRFD model, which underpredicted the creep coefficient and shrinkage strains on average by 32% and 44%, respectively.
- For the four HPC mixes, the results of the creep and shrinkage tests for the sealed specimens had smaller standard deviations than the results for the unsealed specimens, which means that the errors in the creep and shrinkage of the sealed specimens are smaller than those of the unsealed specimens.

CHAPTER 4: CAMBER MEASUREMENTS

4.1 Instantaneous Camber Measurements

4.1.1 Introduction

Problems with predicting the camber are typically evident at the bridge site after the PPCBs have been set on the piers. Although the camber prediction problems are evident at the bridge site, they originate from inaccurate predictions during the design of the PPCB, at the precast plant during fabrication, or during the transfer of the prestress. The inaccurate instantaneous camber measurements were investigated by examining past camber measurements as well as by measuring the camber at three precast plants. A combination of the measurement techniques used by precasters and researchers and new methods was explored to determine a consistent, accurate way to measure the instantaneous camber. While some previous measuring methods neglect measurement errors caused by bed deflections, inconsistent PPCB depths, and friction between the PPCB and the bed, the measurement method used to gather data on over 100 PPCBs, as described in Section 4.1.6, accounts for each of these sources of error.

Although errors relating to bed deflections, top flange inconsistencies, and the friction between the precasting bed and the PPCB vary in magnitude, they have been observed to be consistently present at three different precast plants. The magnitude of the errors depends on a combination of fabrication procedures, the method used for the transfer of the prestress, the type of precasting bed, and concrete material properties. While the behavior of the PPCB is dependent on the precaster's procedures and the material properties of the PPCB, the resulting camber can be accurately captured by using the correct measurement technique. The following sections will describe the methods used to measure the instantaneous camber in this research project. Although it is noted in Section 4.1.2 that the current industry practice fails to account for the common sources of error, it should be recognized that researchers are able to capture and quantify bed deflections and inconsistent top flange friction between the PPCB and the bed.

4.1.2 Industry Practice Camber Data

A database of over 1,300 instantaneous cambers was available. It consisted of measurements and recorded data by the precast plant foremen and Iowa DOT inspectors at three precast plants that produce bridge PPCBs for the Iowa DOT. The method that was used to measure the camber was dictated by the Iowa DOT and is listed below.

4.1.2.1 Iowa DOT Camber Measurement Procedure

The Iowa DOT camber measurement procedure, according to the Iowa DOT's Precast and Prestressed Concrete Bridge Units instructional memorandum (Iowa DOT 2013a), is as follows:

- The camber due to prestress shall be measured while the PPCB is on the bed by checking the PPCB profile immediately (within three hours) after the detensioning and separation of the

PPCB.

- The camber shall be measured from the pallet to the bottom of the PPCB at mid-point, utilizing a conventional tape measure. The camber shall be measured and recorded to the nearest 1/8 inch.
- The PPCB shall be resting free on the pallet at the time of the camber measurement. The camber acceptance shall be achieved prior to shipping.
- The noncompliant camber of any PPCB shall be verified at a later date. PPCBs cannot be accepted without a compliant camber and without the specific approval of the engineer.

The Iowa DOT standard for measuring camber is applicable for the instantaneous and long-term camber and is followed throughout all the precast plants that make bridge PPCBs for the State of Iowa. However, small changes in the technique have been observed to differ between the three plants that produce PPCBs. The common discrepancies between precast plants are as follows:

- The location along the PPCB where the camber measurement is taken
- The accuracy of the value that is read from the tape measure
- The time the camber measurement is taken

A detailed discussion of each of these issues is given in Sections 4.1.2.1.1 through 4.1.2.1.3.

4.1.2.1.1 Location of Camber Measurement

It has been observed that the foreman, quality control manager, or construction engineer is the person who measures the camber from the bottom flange at the midspan of the PPCB at the transfer of the prestress. It was typically found that the center of the PPCB, as indicated by a centerline mark made on the precasting bed or by estimating the midspan, is relative to the cylindrical holes used for the interior diaphragms of the PPCB. The cylindrical holes used to attach the interior diaphragms were typically located in the web of the PPCB, and the placement was determined by the designer (see Figure 4.1).

Figure 4.1. PPCB with two cylindrical holes for the interior diaphragm

The project team observed that the diaphragm placement was typically anywhere from 1 1/2 ft to 20 ft from the centerline of the PPCB. Approximating where the midspan is located on a PPCB based on the diaphragm holes may cause the precast personnel to measure the camber at an incorrect location on the PPCB.

4.1.2.1.2 Accuracy of the Camber Measurement

The camber measurements are taken by a tape measure while the PPCB is resting on the precasting bed before the PPCB is lifted. Although most workers read the tape measure to the nearest 1/16 in., the camber is recorded to the nearest 1/8 in. or 1/4 in. The camber tape measure reading is taken from the top of the precasting bed to the bottom flange of the PPCB. Problems with the accuracy were evident at two precast plants due to a permanent metal chamfer that was attached to the precasting bed (Figure 4.2).

Figure 4.2. Precasting bed with metal chamfer

In this case, a tape measure reading was taken from the top of the metal chamfer to the top of where the chamfer was when the PPCB was cast. This produced uncertainty due to the consistency of the concrete on the edge where the chamfer was resting when the PPCB was cast. One plant used a removable rubber strip to create the chamfer at the bottom flange of the PPCB (Figure 4.3).

Figure 4.3. Precasting bed with removable rubber chamfer

The rubber chamfer can be removed, and a tape measure reading can be taken from the precasting bed to the smooth bottom surface of the PPCB (Figure 4.3), which results in a higher accuracy when the camber is measured from the bottom flange. However, the camber is measured from the top flange when the PPCBs are erected, which may result in a discrepancy from the instantaneous camber that is measured from the bottom flange.

4.1.2.1.3 Time of Camber Measurement

The time when the measurements are taken depends on the precast plant's release process and the availability of the foreman, quality control manager, or construction engineer. The process of releasing a PPCB is different among the three plants because of the equipment and methods used. It should be noted that due to the friction between the precasting bed and PPCB, along with the creep, the camber at the midspan continually grows after the transfer of the prestress. Due to the increase in the camber after the transfer of the prestress, the time at which the camber measurements are taken can impact the recorded camber. Below is a summary of procedure at the precasting plants, which includes when the camber was observed to be measured.

> The top sacrificial prestressing strands and harped strands, if present, were released by using an acetylene torch. If there were any harped hold-down points, they were released next by using a wrench. Depending on the precasting plant, an acetylene torch or hydraulic jack was used to detension the bottom prestressing strands. If the bottom prestressing strands were released by the hydraulic jack, workers then cut the strands that were present between the adjacent PPCBs. After the last reinforcement strands were released, but before the PPCB was lifted from the precasting bed, a tape measure reading was recorded. The recorded tape measure reading most frequently occurred immediately after the last prestressing strand had been released. However, there were times when the camber was recorded before the prestressing strands were completely free or other times 1 1/2 hours after release.

Organizing and evaluating past data obtained from the precasters and the Iowa DOT inspectors from three separate precast plants provided valuable insight into the quality of the data and the problems that the precast plants and contractors face on a regular basis. An examination of the data from three different precast plants showed similar trends, which may be due to comparable procedures adopted for the camber measurements, similar concrete properties due to the plants' close geographic proximity, and similar methods for fabricating and constructing the PPCBs.

Figure 4.4 shows the absolute difference in the measured and the predicted camber of bulb-tee PPCBs arranged in order by increasing PPCB length. Due to the large scatter that was present, the data shown in Figure 4.4 were regrouped. Figure 4.5 shows trends that were found by calculating the difference between the designed and the measured camber and dividing the difference by the length of the PPCB (Equation 4-1). The data were then arranged by increasing PPCB length.

$$\text{Error of Camber With Respect to Length} = \frac{(\text{Measured Camber} - \text{Designed Camber})}{\text{Length}} \quad \textbf{(4-1)}$$

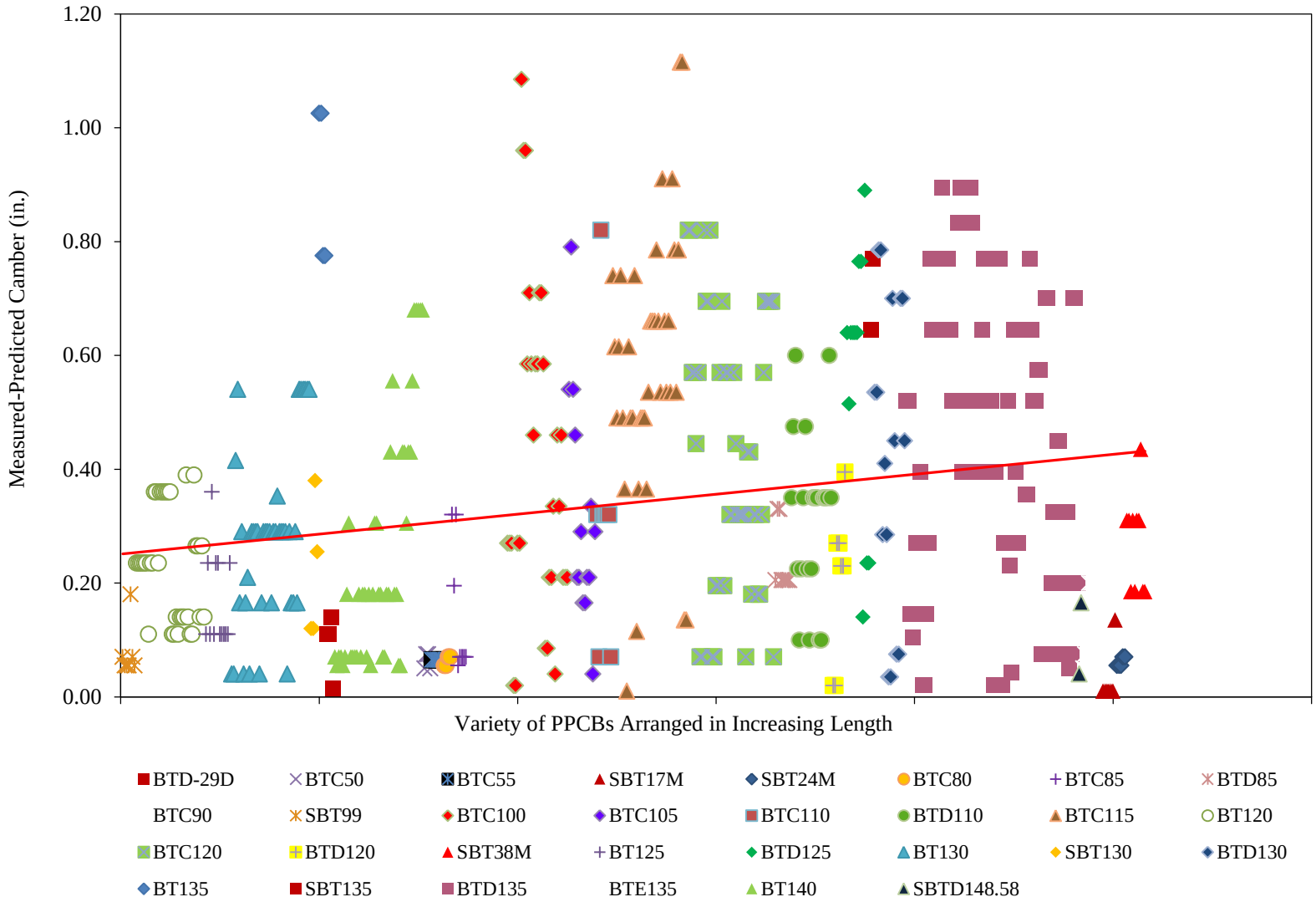

Figure 4.4. Difference in the measured and predicted industry practice camber data versus the length of the PPCB

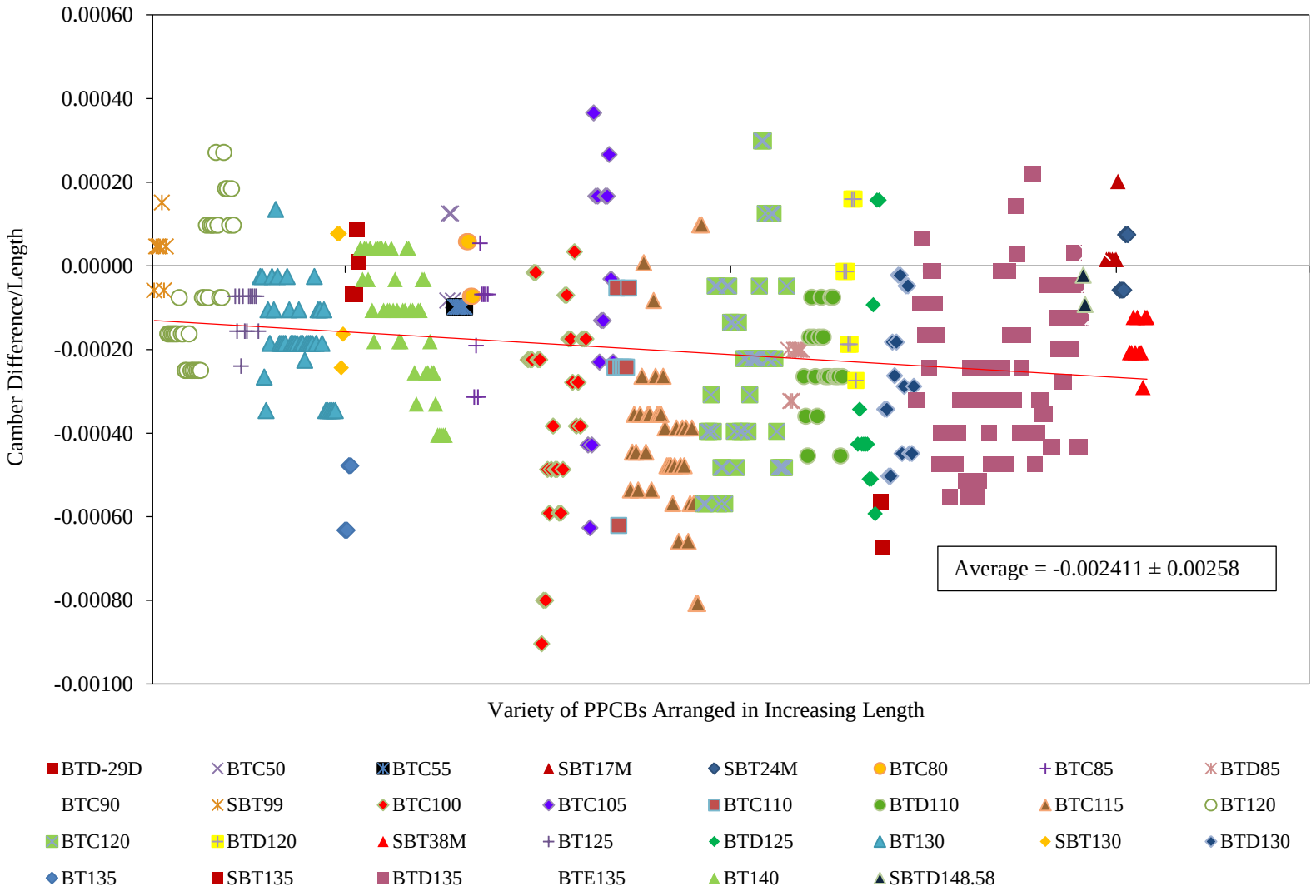

Figure 4.5. Difference in the camber/length of industry practice data arranged by increasing PPCB length

Dividing the difference between the measured and the designed camber by length normalizes error and eliminates the variable of length.

Arranging the PPCBs by increasing length, starting with the shortest, showed the following trends:

- For each PPCB type, the error between the measured and predicted camber is not consistent.
- On average, as the PPCB length increases, the error between the predicted and measured camber also increases.

Arranging the industry practice camber data revealed that the measured cambers of the PPCBs are in disagreement with the predicted cambers. The trends discovered from Figure 4.5 show that the camber is overpredicted 75% of the time. However, for certain PPCB types, the agreement between the measured and predicted camber is underpredicted. This indicates that the differences in the camber are most likely due to unique conditions in fabrication, measurement, and materials. Additionally, as the PPCB length increases, the error between the predicted and measured camber increases, as is also shown in Figure 4.5. This is caused by inaccuracies in the industry practice camber measurement technique, which fail to account for the bed deflections, the inconsistent top flange surfaces along the length of the PPCB and across the top flange, and the friction between the precasting bed and the PPCB. As the PPCBs increase in length, the weight of the PPCB typically increases. The increase in weight causes more bed deflection and more friction to be present. Failing to account for these factors results in inaccurate instantaneous camber measurements that differ from the camber that is actually present. Inaccurate instantaneous camber measurements reduce the accuracy of the camber prediction technique and the estimation of the long-term camber.

Due to the inaccurate camber measurements, an investigation of the method used to measure the camber at the transfer of the prestress was undertaken. As part of this research, a combination of the measurement techniques used by precasters and past research studies along with new methods were explored to determine a consistent, accurate way to measure the instantaneous camber. Some previous measuring methods neglect bed deflections, inconsistent PPCB depths and surfaces, and the friction between the PPCB and the bed. The method used in this research accounts for each of these issues as accurately as possible and quantifies their impact on the instantaneous camber measurement.

The focus was placed on measuring the camber of over 100 PPCBs from three different precast plants. Three different methods were used to measure the camber: a tape measure reading taken from the bottom flange at the midspan, a rotary laser level, and string potentiometers. The current errors in the camber measurement, along with the procedures for measuring the camber with the three different methods, are described in the following sections.

4.1.3 String Potentiometers

String potentiometers have been used to instrument PPCBs at several different locations to verify the camber measurements and verify the vertical movement of the precasting bed during the release. String potentiometers are composed of a string that is wrapped around a spring-loaded coil. One end of the coil is connected to an external hook that can be pulled from the string potentiometer to record the displacement. When an object moves with a string potentiometer attached, the string unravels from the internal portion of the string potentiometer. The string potentiometers are connected to a data recording device that measures the displacement of each string potentiometer once every second. This allows the displacement versus time graph to be obtained for multiple string potentiometers at different locations along the PPCB and precasting bed. Recording significant events during the transfer of the prestress and relating them to the time versus displacement graphs gives clear evidence about the behavior of the PPCB and the precasting bed during the release.

String potentiometers were attached to the PPCBs by clamping the instrument at the top flange of the PPCB at the midspan. A string was connected from the string potentiometer to a weight on the ground beside the precasting bed (Figure 4.6).

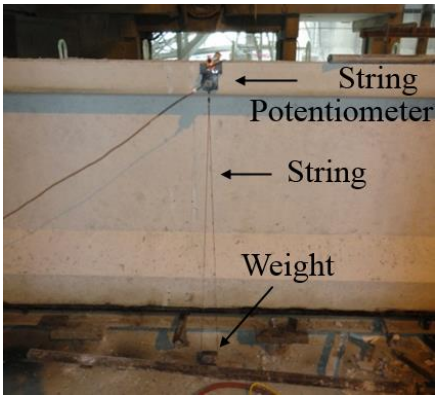

Figure 4.6. String potentiometer attached to the midspan of a PPCB

The weight was placed on the ground and did not move during the process of the release. The instruments were connected to the PPCB before the transfer of the prestress, and monitoring the instruments during the release gave valuable information about displacements at critical points.

When monitoring the precasting bed for deflections, a different method was used to attach and instrument the string potentiometers. String potentiometers were attached to a wood block that was anchored to the ground by weights. A magnet was attached to the precasting bed with a rod that extended out (Figure 4.7).

Figure 4.7. String potentiometer attached to the precasting bed at the end of a PPCB

A small chain was connected from the rod to the string potentiometer resting on the ground. This method gave valuable information about the upward and downward precasting bed displacements that were present at the midspan and ends of the PPCB, respectively, during the transfer of the prestress.

String potentiometers were instrumented on the precasting bed and multiple PPCBs before, during, and after the transfer of the prestress. Recording the displacement with respect to time made it possible to continuously monitor a progressive change in the camber of the PPCBs and the corresponding impact to the precasting bed. The results from two PPCBs that were each instrumented with three string potentiometers are shown in Figure 4.8 and Figure 4.9.

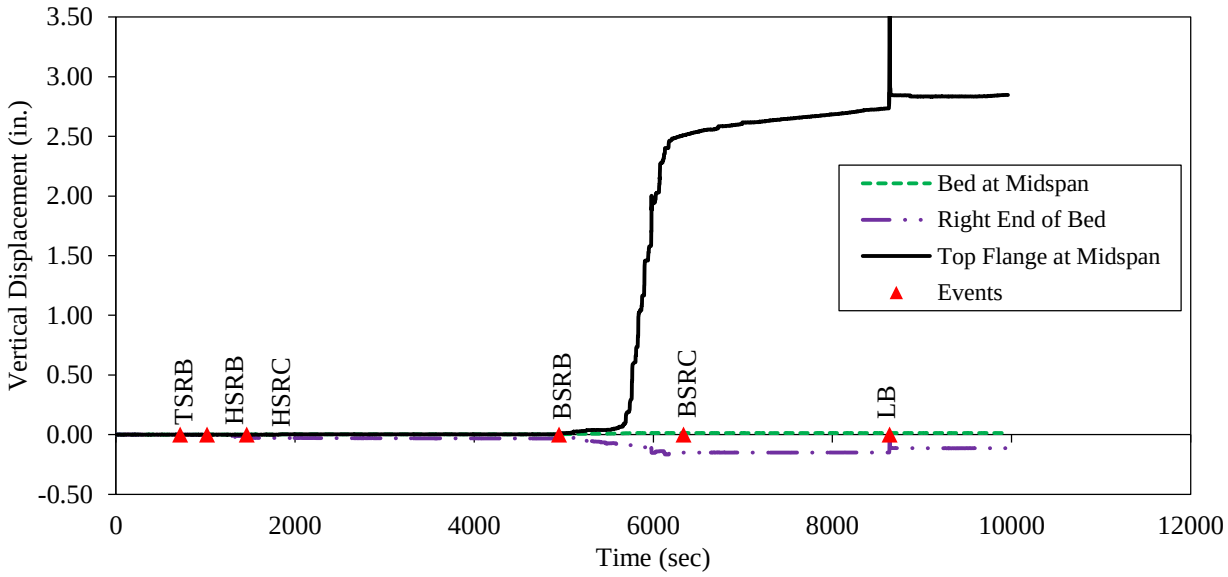

BSRB = bottom strands, release began; BSRC = bottom strands, release completed; HSRB = harped strands, release began; HSRC = harped strands, release completed; LB = lifted PPCB; TSRB = top strands, release began; TSRC = top strands, release completed

Figure 4.8. Time versus vertical displacement of a BTB 100 PPCB

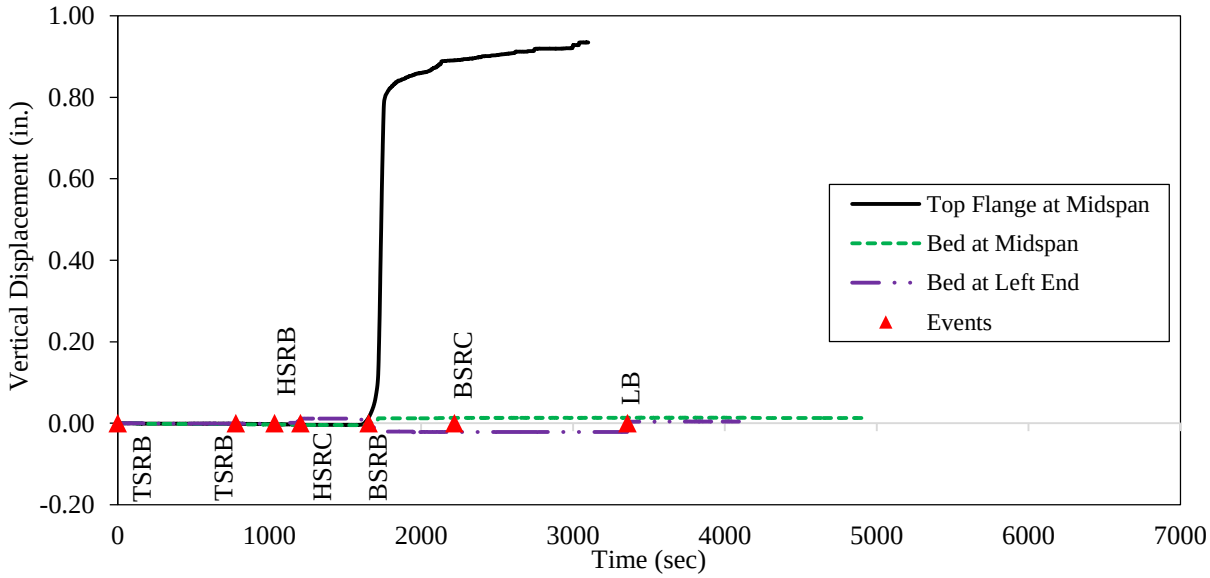

BSRB = bottom strands, release began; BSRC = bottom strands, release completed; HSRB = harped strands, release began; HSRC = harped strands, release completed; LB = lifted PPCB; TSRB = top strands, release began; TSRC = top strands, release completed

Figure 4.9. Time versus vertical displacement of a BTE 110 PPCB

Both PPCBs, which were cast for Iowa DOT bridge projects, were similar in length (100 ft versus 110 ft). However, they were cast and released at separate precasting plants; had different cross-sections, amounts of prestress, and concrete mixes; and went through different prestress

releasing procedures. Despite the differences that were present between the two PPCBs, similarities in the behavior of the string potentiometers' vertical displacements were present.

The string potentiometers in Figure 4.8 and Figure 4.9 were instrumented at the midspan on the PPCB and on the precast bed at the end of the PPCB and at the midspan. Before the release of the strands, the data collection was started. As time progressed, workers cut the top sacrificial prestressing strands. A low prestress force caused small changes in vertical displacement, which are noted in Figure 4.8 and Figure 4.9. The next event in the recorded data was the release of the harped prestressing strands, which also caused a small vertical uplift. The magnitude of the vertical displacement is controlled by the amount of the harped reinforcement present and the eccentricity. The string potentiometer at the end of the PPCB on the precasting bed in Figure 4.8 was observed to undergo a downward vertical displacement after the prestressing strands were released. This is because the PPCB weight shifted from being applied along the length of the PPCB to the location of the string potentiometer. Figure 4.9 shows a small positive displacement after the harped reinforcement was released from the string potentiometer located at the PPCB end. The small positive displacement was due to the positive moment produced by the harped prestressing strands that outweighed the PPCB self-weight. During the release of the bottom strands, the negative moment applied by the transfer of prestress shifted the weight of the PPCB toward the ends of the PPCB. The result was downward deflections for the string potentiometers at the ends of the PPCB and an upward deflection for the string potentiometers at the midspan of the precasting bed. Additionally, the prestress force caused the PPCB to start to camber upward. The points where the bottom strands were completely free represent the time when the full prestress was applied to the PPCB while the PPCB was resting on the precasting bed.

There was still a small increase in the camber as a function of time due to the PPCB overcoming the friction between the precasting bed and the PPCB. Figure 4.9 shows small discontinuities in the increase in the vertical displacement after the bottom strands were released. This can be attributed to the precaster's lifting adjacent PPCBs off the precasting bed. Figure 4.8 shows the point when precasters were able to lift the PPCB and place it down on the precasting bed after the last prestressing strands were released. At the time the PPCB was lifted, there was a large vertical increase, as shown in Figure 4.8. The lift released the remaining friction that was present and allowed the PPCB to reach its full instantaneous camber. After the PPCB was set down, there was a slight decrease in the camber. This could be due to the PPCB readjusting on the precasting bed or to the effects of reverse friction. The precasters of the PPCB in Figure 4.9 were unable to lift/set the PPCB because of the manufacturing time constraints and the potential for damaging the newly cast PPCB. There is believed to be an additional upward displacement that would take place at the ending time due to the release of friction. The data recording was consequently terminated before the precaster transported the PPCB to the storage yard. By instrumenting the PPCBs with string potentiometers and taking laser-level readings, the behavior of the PPCBs was verified, and the magnitude of the bed deflections, inconsistent top flange surfaces along the length and due to local effects, and friction were quantified.

4.1.4 Errors in the Current Camber Measurement Practice

The industry measurement practices were evaluated in Section 4.1.2. Conducting independent measurements on PPCBs confirmed errors in the current industry practice measurement techniques. This section presents detailed sources of errors that have been observed to contribute to the instantaneous camber measurement. Error sources include bed deflections, friction between the precasting bed and the end of the PPCB, the inconsistent top flange surface along the length of the PPCB, and the inconsistent top flange surface due to local effects. All of these issues are discussed in detail.

4.1.4.1 Bed Deflections

A PPCB that has not been released exerts a uniformly distributed load along the length of the bed due to its self-weight (Figure 4.10).

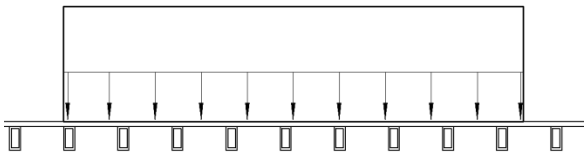

Figure 4.10. PPCB before the transfer of the prestress, generating a uniform load on the bed

When the prestressing strands are released, the prestress force that is applied to the PPCB may cause the PPCB to camber upward. When the camber is present, the weight of the PPCB shifts from being a uniformly distributed load along the length of the bed to two point loads at the PPCB ends (Figure 4.11).

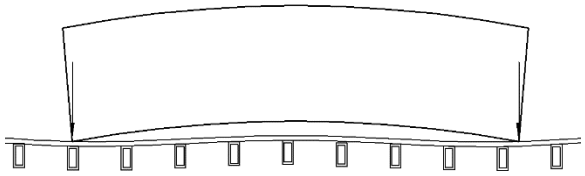

Figure 4.11. PPCB after the transfer of the prestress, with the PPCB self-weight acting only at two points on the bed

Shifting of the PPCB's weight to the ends produces downward bed deflections at the ends of the PPCB and an upward rebound of the bed at the midspan, which causes a discrepancy between the measured and the actual camber. The magnitude of the bed deflection depends on where the PPCB ends are situated in relation to the precasting bed supports.

There are numerous factors that influence the magnitude of the bed deflections, including the material properties of the precasting bed, the design of the precasting bed members, the foundation of the precasting bed, and the distance between the precasting bed supports.

Figure 4.12 displays the bed deflections taken by a rotary laser level. The graph is composed of the differences in individual points on the precasting bed before and after the transfer of the prestress. The graph also shows the average of the bed deflections from the individual bed elevation readings. The average of the bed elevation readings was the most accurate value because it was taken with respect to the midspan rather than the local deflection at the end of the PPCB. The bed deflections are represented in Figure 4.12 by triangles and are arranged on the x-axis in order of increasing length.

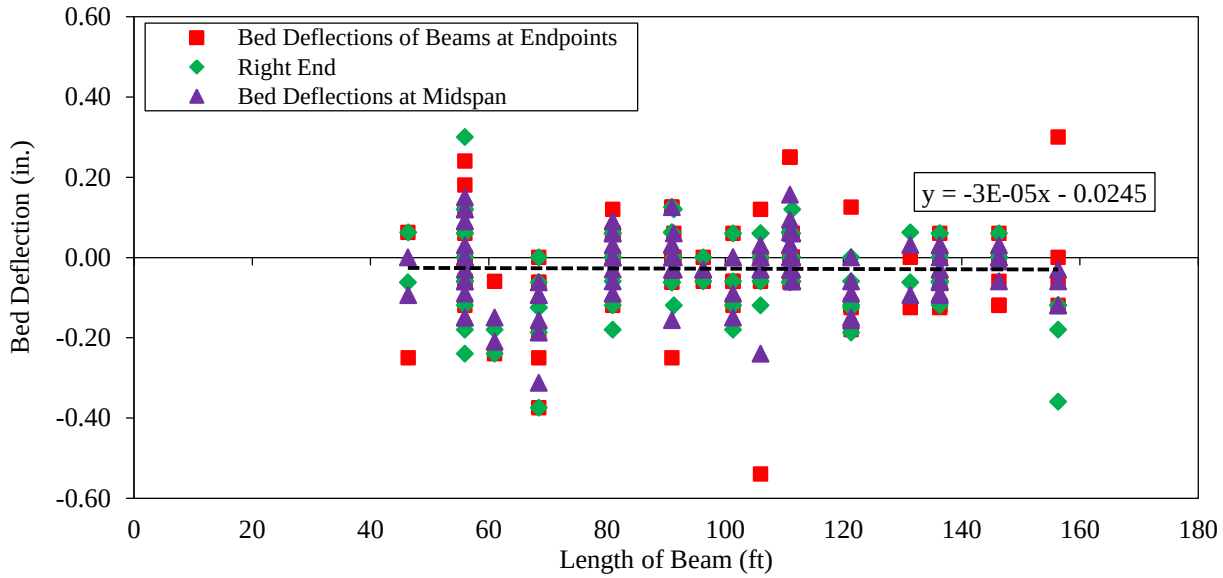

Figure 4.12. Bed deflection versus the length of multiple PPCBs

The trends from Figure 4.12 show the following:

- The average of the final camber with respect to the ends was below the zero line, which suggested that there was a negative bed deflection with the average of all the measured PPCBs. This was in agreement with the theory that, as the weight of the PPCB shifts to the ends, the bed elevation will produce a downward displacement.
- As the PPCBs increased in length, the bed deflections increased as well. The weight of the PPCB was affected by the size of the cross-section, the unit weight of the concrete, and the length of the PPCB. The PPCBs had similar cross-sections and unit weights of concrete. As the length of the PPCB increases, the weight of the PPCB also increases, thus causing an increase in the bed deflection at the end of the PPCB.

Figure 4.12 has a large scatter due to different precasting beds among the three precasting plants and the sensitivity of the measurements to the measurement locations. Bed deflection measurements were taken from three precasting beds that had similar designs. However, the

location of the PPCBs relative to the precasting bed supports influenced the magnitude of the bed deflections. Figure 4.13 shows the ends of two PPCBs as they rested on the precasting bed.

Figure 4.13. Two PPCB ends in relation to the supports on a precasting bed

When the ends of the PPCBs were placed directly over the bed's supports, the net bed deflection was reduced compared to the alternative of placing the PPCB ends between the precasting bed supports. In addition, measurements taken after the transfer of the prestress are prone to the PPCB shifting along the length of the prestressing bed due to the uneven release of the prestress. The shifting of the PPCB inhibited the ability for the researchers to measure the bed elevation after the release at the exact position where the bed elevation was measured before the transfer of the prestress.

The results from over 100 PPCBs measured by the researchers indicate that neglecting bed deflections reduces the camber by 2.8% (±8.2%). The average bed deflection was -0.0297 in., with the maximum value being 0.3125 in. The results from the bed deflection measurements with respect to the midspan are listed in Table 4.1.

Table 4.1. Summary of the bed deflections

Average (in.)	Standard Deviation (in.)	Maximum (in.)	Minimum (in.)
-0.0297	0.0615	0.1563	-0.3125

4.1.4.1.1 Positive Bed Deflection

When recording bed measurements with the rotary laser level, there were cases that suggest that upward bed deflections occur at the ends of the PPCBs. This is contrary to the expectation that, after the transfer of the prestress, the weight shifts to the ends of the PPCB, causing a downward deflection. Due to adjacent PPCBs and the placement of supports, it is possible for a positive bed deflection to occur. A scenario when a PPCB end can have a positive bed deflection is outlined in the following steps:

1. Two separate PPCBs were placed adjacent to each other at a close distance.
2. One PPCB end was placed between two precast bed supports, while the adjacent PPCB end was closer to the support.
3. The cantilever action of the first PPCB forced the adjacent PPCB to have an upward bed displacement.
4. Because the PPCB may slide during the release process, the original measurement location was used in order to eliminate the effects of inconsistencies on the precasting bed surfaces. The resulting measurement distance away from the PPCB can result in a positive deflection after the transfer of the prestress (Figure 4.14).

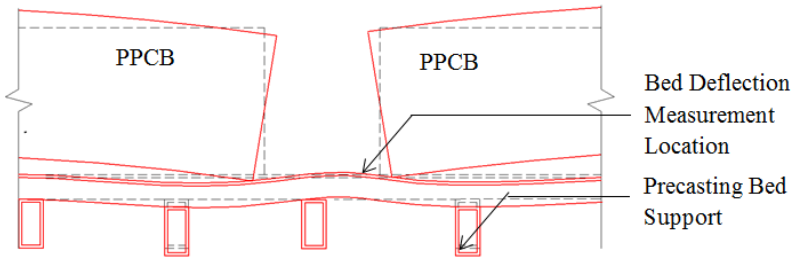

Figure 4.14. Two PPCBs and a placement scenario that results in a positive bed deflection

4.1.4.2 Inconsistent PPCB Depth

The elevation of the top flange has been observed to vary across the length and width of the PPCB. This results in inconsistent elevations before the transfer of prestress, which can give the illusion of more or less camber than is present. The inconsistent elevation has been observed to vary along both the length and width of the PPCB. The causes of the inconsistent top flange on PPCBs were found to be due to the way the forms were set as well as the type and consistency of the finish that was used. Although the instantaneous camber is not typically measured with respect to the top surface, all field camber measurements are taken from the top surface, ultimately causing discrepancies between the measured and expected camber and casting doubt on the initial camber produced for the PPCB.

4.1.4.2.1 Inconsistent Surface Finish due to Local Inconsistencies

Workers finishing the top flange of a PPCB intentionally roughen the surface, which leads to problems with measuring the camber from the top flange (see Figure 4.15).

Figure 4.15. Inconsistent top flange surfaces of PPCBs

Several measurements across the top flange were taken to determine the local deficiencies present. The results show that the average difference across the top flange length is 0.113 in., while a maximum value has been observed to be 0.90 inches. Failure to account for the inconsistent top flange due to local imperfections misrepresents the camber by -4.4% (±12.8%).

The results of the local inconsistency measurements reveal that the roughness of the top flange surface is not dependent on the PPCB length. The roughness of the PPCB is intended to be similar for all PPCBs so that the surface of the deck will bond easily to the top flange. However, there was an observable trend in the relationship between the level of roughness and the precasting plant that produced the PPCB. The roughness of the top flange surface was uniform between different PPCBs produced at the same plant due to the same finishing practices, but the roughness differed from plant to plant.

4.1.4.2.2 Inconsistent Finished Surface along the Length of the PPCB

The finish that is applied to the PPCB by the workers can contribute to the inconsistent depth of the PPCB along the length (see Figure 4.16).

Figure 4.16. Inconsistent troweled surface along the length of the PPCB

After the concrete is placed in the form, workers tend to evenly distribute the concrete so that the top flange surface maintains a constant thickness. The ability for workers to uniformly finish the PPCB is often impeded by the stirrups that protrude from the top flange. Finishing the concrete around the stirrups along the length of the PPCB can cause rises and falls in the surface. Consistently keeping a uniform thickness along the length is directly related to the finishing practices.

Measuring the elevation of the top flange of the PPCB before the transfer of the prestress made it possible to see if the midspan of the PPCB was higher or lower than the average of the two ends. From these results, it was possible to determine if the PPCB had an upward or downward elevation at the midspan before applying the prestress. The results showed that the greatest difference along the top flange length was 0.787 in., while an average value was 0.099 in. Failure to account for the inconsistent top flange along the length of the PPCB misrepresents the camber on average by 94.8% ± 24. 5%. Trends in the top flange inconsistencies along the length of the PPCB reveal that, as the PPCB length increased, the magnitude of the out-of-planeness increased. This was due to the adjustments between the multiple forms that are needed to meet the length requirements of the PPCB. Additionally, it was observed that, on average, Plant A had the largest inconsistencies in the camber along the length of the PPCB. Plant B and C had similar average values for the inconsistent top flange along the PPCB length, 0.145 in. and 0.155 in., respectively. Reasons for why Plant A had larger values for the top flange inconsistencies along

the length may include the quality of the uniform depth of the formwork or the survey of the forms before casting.

4.1.4.2.3 Method of Setting Forms

The precasters' methods of setting forms will affect the uniformity of the elevation of the PPCB before the transfer of the prestress in the PPCBs. The ability for a precaster to produce a uniform PPCB relies heavily on the trueness of the forms and the way they are assembled around the precasting bed. The three precast plants use free-standing forms. Free-standing forms rest on supports that are connected to the precasting bed. The process for setting the forms is described for each of the plants below.

In one plant, free-standing forms are put into place by a crane. The forms are placed on movable metal supports that lie every 10–20 ft. A string is strung along the length of the top flange of the PPCB. Bends from adjacent forms are adjusted based on the distance from the form to the string. After the bends are taken out of the forms, workers take measurements from the top of the precasting bed to the top of the form. This is typically done every 10–20 ft. If adjustments need to be made to the height of the form, workers can shim the forms up or down to meet the correct elevations. Workers will then place intermediate supports along the length of the PPCB, similar to the setup shown in Figure 4.17, and secure the forms.

Figure 4.17. Temporary support used for supporting a PPCB form

In the second plant, free-standing forms on rollers are utilized. This setup consists of having a form that is typically moved six inches to and from the precasting bed. The other side of the form can be rolled from the precasting bed. When placing the forms, the back form is rolled into place before the prestressed reinforcement is tensioned. When the remaining reinforcement is placed and tied, the other form is rolled into place. It is assumed that the forms are within the correct

tolerance along the length of the PPCB. The forms are secured together at a specified distance from each other along the top and bottom flange.

The third plant uses free-standing forms that are placed by a travel lift crane on the bed supports (see Figure 4.18).

Figure 4.18. Forms on a PPCB

The longitudinal length of the precasting bed requires multiple sets of forms to be placed along the length of the bed. The multiple sets of forms can have slight bends along the length of the precasting bed. Similarly to the first plant, a string is tightly strung between the lift-up hooks on the PPCB. This string lies in the center of the top flange of the PPCB. Workers can measure the distance between the string and the top of the form to make sure the distances are uniform along the length of the PPCB. If the distances between the top of the form and the string are different along length of the PPCB, workers use a small hand jack to raise the bottom of the form on the opposing side so the top of the form rotates into place. Once the forms are slightly adjusted, they can be secured into place by tightening the clamps at the bottom of the form.

4.1.4.3 Friction between the PPCB Ends and the Precasting Bed

After the transfer of the prestress, friction occurs between the PPCB ends and the precasting bed. This friction has been observed to inhibit the PPCB from reaching its full instantaneous camber immediately after the release. The force of the friction that limits the increase in the camber is found in Equation 4-2 and is dependent on the normal force and the coefficient of the friction. The normal force is the force acting perpendicular to the plane of contact and is from the weight of the PPCB. Because the friction is acting when the PPCB has cambered, only half of the PPCB's weight is at the point of contact. Selected PPCBs were cast with metal sole plates in the ends. The purpose of the sole plate was to prevent damage to the bottom flange of the PPCB. Due to the smooth precast surface and the similar trends shown in Figure 4.19 for PPCBs with

and without sole plates, the coefficient of friction was assumed to be 0.35 based on the AISC coefficient of friction for surfaces that are unpainted, clean mill steel.

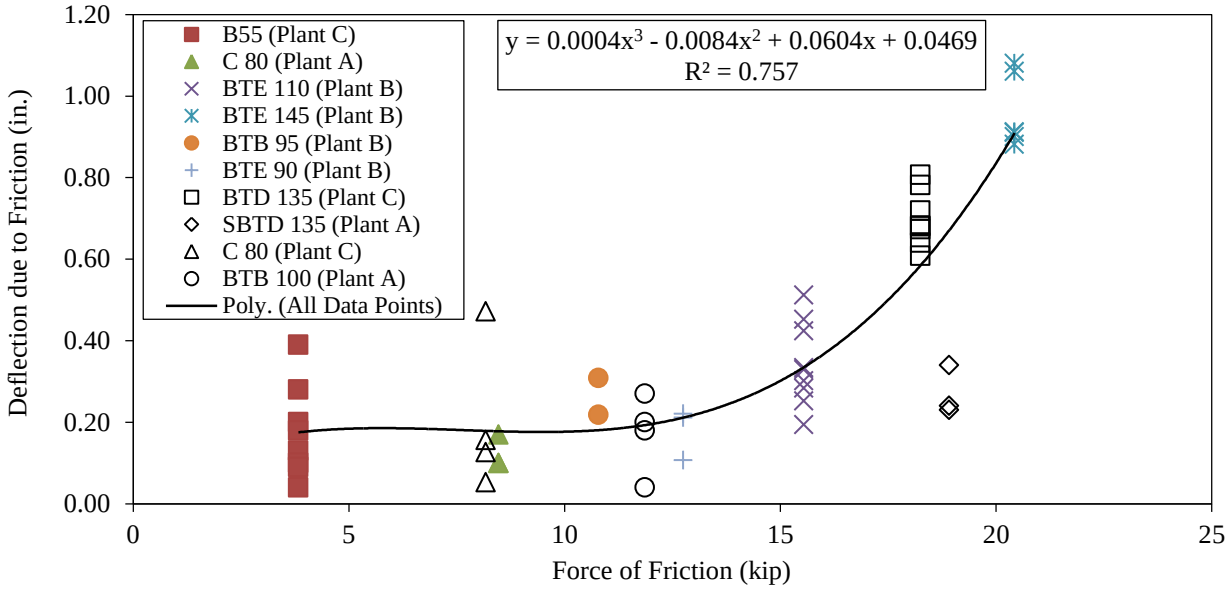

Figure 4.19. Force of the friction versus deflection due to the friction for multiple PPCBs

The force of the friction that limits the increase in the camber is found in Equation 4-2 and is dependent on the normal force of the PPCB and the coefficient of friction. The normal force is the force acting perpendicular to the plane of contact and is dependent on the weight of the PPCB. Because friction was acting when the PPCB cambered, only half of the PPCB's weight was at the point of contact. Selected PPCBs were cast with metal sole plates in the ends. The purpose of the sole plate was to prevent damage to the bottom flange of the PPCB. Due to the smooth precast surface and the similar trends shown in Figure 4.19 for PPCBs with and without sole plates, the coefficient of friction was assumed to be 0.35.

$$F_f = F_n \times \mu \qquad \textbf{(4-2)}$$

where F_f is the force of the friction, F_n is the normal force, and μ is the coefficient of friction.

Figure 4.19 displays the force of the friction obtained from Equation 4-2 versus the measured deflection due to the friction. The results show scatter throughout all values of the force of the friction, which is due to the wide variety of PPCBs produced at the three different plants. While plants have similar bed dimensions and procedures, it should be noted that small discrepancies may be present due to the coefficient of friction and the precasting bed geometry specific to each plant.

Taking rotary laser level measurements before and after the PPCB was lifted made it possible to quantify the contribution of the friction on the PPCBs (Figure 4.20).

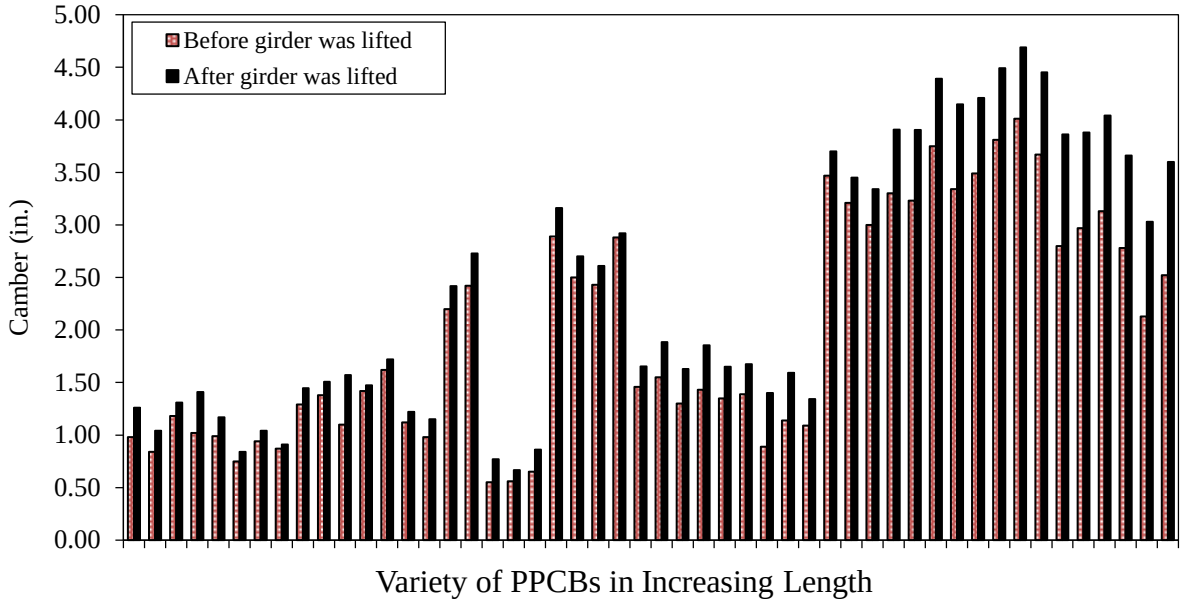

Figure 4.20. Effect of friction on the camber measurements for different types and lengths of PPCBs

The lengths of the PPCBs on which the friction was measured varied from 56 ft to 146.33 ft and consisted of A-D and bulb-tee PPCBs. As Figure 4.20 shows, lifting the PPCB immediately after detensioning can produce up to a 1.08 in. increase in the measured camber. For the 50 PPCBs that were studied for friction, there was an average of a 17% difference between the camber measured before lifting the PPCBs and after lifting the PPCBs.

4.1.4.3.1 Evaluating Friction with String Potentiometers

Instrumenting PPCBs at the midspan with string potentiometers made it possible to isolate the contribution of the friction to the camber with respect to time. After the last prestressing strand is cut during the transfer of the prestress, there are no outside forces acting on the PPCB. The increase in the vertical displacement that is observed beyond this point is a result of the PPCB ends overcoming friction and sliding toward each other.

The contribution of the friction is shown in Figure 4.21 and can be divided into two components.

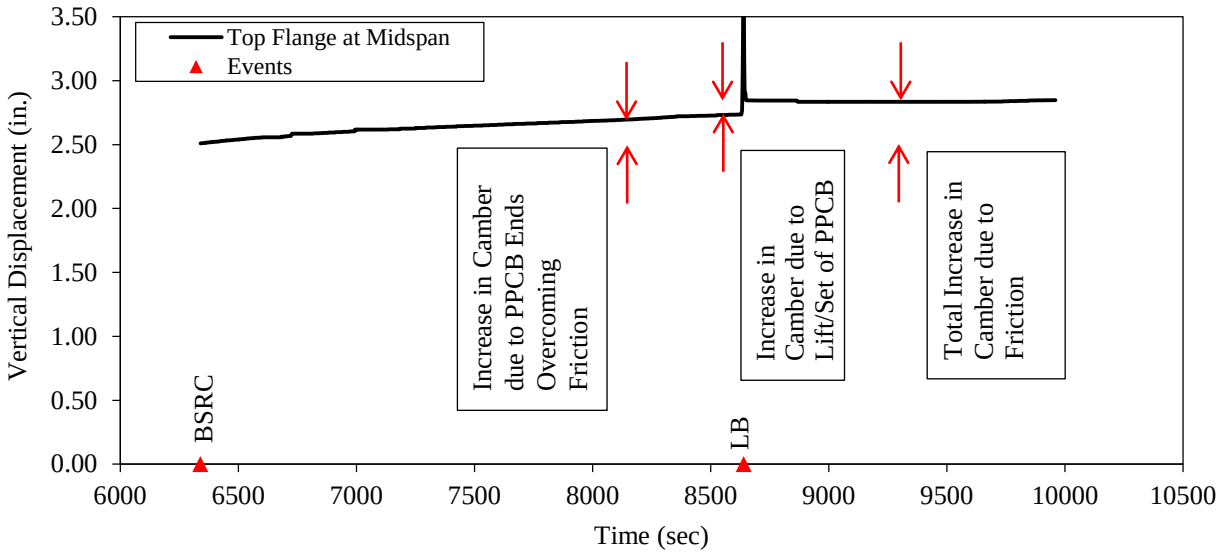

BSRC = bottom strands, release completed; LB = lifted PPCB

Figure 4.21. Time versus displacement after the transfer of the prestress on a BTB 100 PPCB

The first component is the gradual increase in the camber after the last prestressing strand was detensioned. The second part is the additional camber that was gained when the PPCB was lifted from the precasting bed and placed back down. Once the PPCB had been lifted and was no longer in contact with the bed, the friction forces were released, and there was an increase in the camber. It should be noted that if the gradual increase in the camber due to overcoming the force of the friction is extrapolated over an extended time, the final camber value appears to reach the same value that was obtained from lifting the PPCB. However, an error that could be introduced if PPCBs were allowed to sit for an extended period of time would be the gain in vertical displacement due to the creep of the concrete.

4.1.4.3.2 Effect of Friction with Different PPCB End Constraints

An additional exercise was conducted to investigate the effects on the camber when eliminating the friction on PPCBs. In this experiment, three PPCBs were instrumented with string potentiometers at the midspan. The process of releasing the prestressing strands was conducted under normal conditions. After the last prestressing strands were released, the time versus displacement for three different end restraints on three different PPCBs was observed (Figure 4.22).

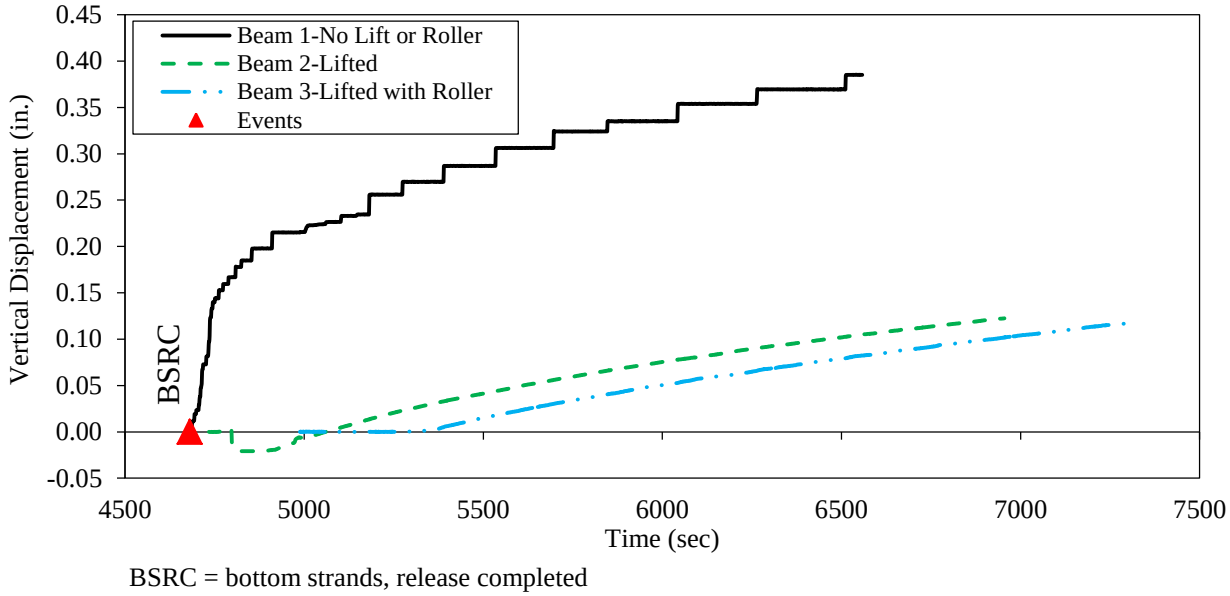

BSRC = bottom strands, release completed

Figure 4.22. Increase in camber due to friction for three PPCBs

The string potentiometers were left on each PPCB after the transfer of the prestress for an extended period of time to compare the effects of the friction. The graph starts after the last prestressing strand was cut, and all PPCBs were resting on the precasting bed freely.

PPCB 1 was not lifted, and the friction and creep contributed to the growth of the camber. Because PPCB 1 was undisturbed, a portion of friction would still be present at the last recorded time. Lifting the PPCB and setting it back down would increase the amount of the camber due to releasing the remaining friction. The large amount of growth in PPCB 1 in the early stages after the release can be explained by the PPCB initially overcoming the friction. As time increases, the rate of growth due to the friction decreases.

PPCB 2 released the friction forces by lifting the PPCB and setting it immediately back down on the precasting bed. Because the friction was immediately released, the camber growth was smaller than that of PPCB 1, which was expected and observed. Immediately after the PPCB was lifted and placed back down, there was a small decrease in the vertical displacement. In that time, from 4,767 through 4,988 seconds (when the downward displacement is noticeable), PPCB 3 was lifted from the precasting bed. PPCBs 2 and 3 were placed adjacent to each other, and the shift in weight from PPCB 3 influenced the camber in PPCB 2. After this downward deflection, there was a slight growth in the camber. The camber growth of 0.12 in. at time 7,300 seconds can be attributed to the creep because there were no other forces acting on the PPCB at that time.

In PPCB 3, the friction was eliminated by lifting the PPCB immediately after the transfer of the prestress and placing it down on a roller support resting on the precasting bed (Figure 4.23 and Figure 4.24).

Figure 4.23. D90 PPCB with a roller support

Figure 4.24. Roller support under a PPCB

Because one end of the PPCB is resting on a frictionless roller support, the PPCB had the ability to camber to its full potential. Like PPCB 2, there was a slight increase in the camber after the PPCB had been placed on the roller support. The resulting increase in the camber can be attributed to creep because the PPCB had the ability to move longitudinally in and out from the midspan with relatively little effort to overcome the friction of the roller support.

4.1.4.3.3 Reverse Friction

Reverse friction occurs when the PPCB end is set on the bed and the friction acts in the opposite direction to resist the weight of the PPCB pushing the PPCB end back outward (O'Neill and French 2012). This effect is believed to be present in prestressed PPCBs after lifting and setting

the PPCBs down after the transfer of the prestress. Ahlborn et al. (2000) suggest that reverse friction should be accounted for in the recorded camber by taking the average of the camber measurements before and after the lift/set of the PPCB. The average of the two measurements is used because researchers believe that, before lifting the PPCB, the friction is inhibiting the upward growth. After the PPCB is lifted and placed back down on the precasting bed, the friction is inhibiting the downward sagging of the camber. A correct representation of the camber, according to O'Neill and French (2012), would be the average of two measurements. This is incorrect according to Figure 4.22, which shows that, after PPCB 3 had been lifted and placed back down, there was no downward decrease in the camber. If reverse friction were present, a downward displacement would be shown in PPCB 3.

The results from the three instrumented PPCBs have definite trends that are summarized as follows:

- PPCB 1 had a significantly greater increase in camber than PPCB 3. This can be attributed to the friction that was still present.
- The increase due to friction was eliminated after the PPCBs were lifted and set down on the precasting bed. Because PPCB 3 had a roller present, it was allowed to move in and out freely without the effect of the friction. The similar rates of growth in PPCB 2 and PPCB 3 prove that the friction was no longer present in PPCB 2.
- The additional increase in the camber after the friction was no longer present for PPCBs 2 and 3 can be attributed to creep, which was 4.5% of the total camber.
- The downward deflection in PPCB 2 occured when PPCB 3 was lifted from the precasting bed.
- The reverse friction, if present, was small in magnitude and can be ignored.

4.1.5 Tape Measure

A tape measure reading at the midspan of the PPCBs at the transfer of the prestress was one method that was used to determine the camber. This was done by first taking a tape measure reading across the entire length of the PPCB and determining where the midspan of the PPCB was located. After all prestressing strands were detensioned, a tape measure was used to measure the distance from the bottom flange of the PPCB to the surface of the bed (see Figure 4.25).

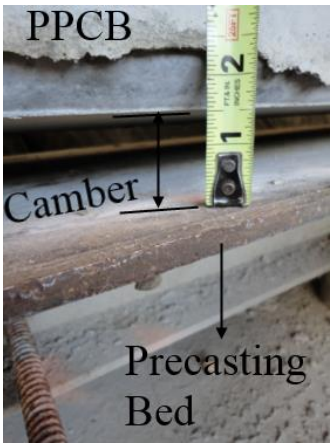

Figure 4.25. Typical tape measure reading at the midspan of a PPCB taken at a precast plant

The tape measure readings were recorded at a maximum of 30 minutes after the last prestressing strand was released. Although measuring the camber with a tape measure is efficient for the precasters with respect to time and schedule, it fails to account for inconsistent PPCB depths, bed deflections, and potential friction if the PPCB is not lifted.

4.1.6 Rotary Laser Level

A rotary laser level was also used to take the camber measurements on PPCBs. The rotary laser level operates by projecting a horizontal laser that can be detected by a receiver (see Figure 4.26).

Figure 4.26. Rotary laser level

The receiver is mounted on a grade rod that can be read to determine elevations with respect to the laser level. Because the laser level is stationary during the whole process, any differences in measurements can be attributed to deflections of the PPCBs or the precasting bed. The manufacturer's reported precision for the rotary laser level device used in the study was ±1/16 of an inch at 100 ft.

4.1.6.1 Measuring the Camber with a Rotary Laser Level

The process of measuring the camber with a rotary laser level included a number of measurements and procedures to account for bed deflections, inconsistent PPCB depths, and friction between the PPCB and the precasting bed. To limit the error associated with the inconsistent top flange surface, a marker was used to trace the cross-section of the grade rod when it was placed for the first measurement. The remaining measurements throughout the transfer of the prestress were taken by placing the grade rod at the location of the marker outline, where the first measurement was taken. This would ensure that the error associated with the inconsistent top flange surface was eliminated. When using the receiver and grade rod for taking the camber measurements, a level that is built into the receiver was used to ensure that the grade rod was held perpendicular to the top flange surface.

Before the transfer of the prestress, measurements were taken on the precasting bed at the ends of the PPCB and on the top flange at the midspan, as seen in Figure 4.27.

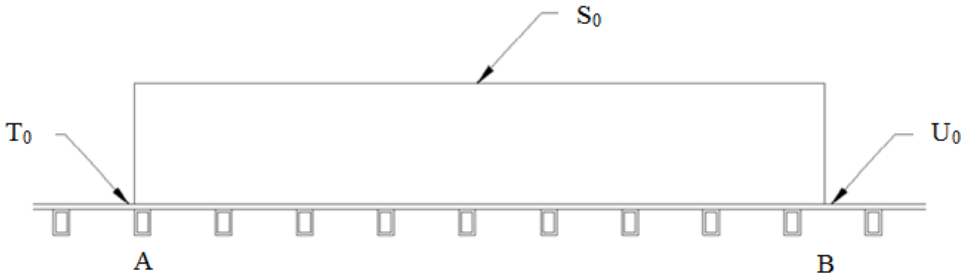

Figure 4.27. PPCB before the transfer of the prestress

After the transfer of the prestress, but while the PPCB was resting on the precasting bed, measurements were taken on the precasting bed at the PPCB ends and along the top flange at the ends and at the midspan. The measurement locations can be seen in Figure 4.28.

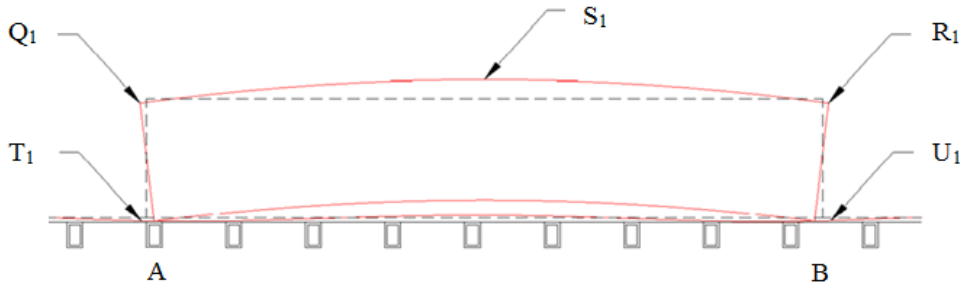

Figure 4.28. PPCB after the transfer of the prestress but before the PPCB is lifted

Once the PPCB was lifted, the friction forces dissipated and another reading was taken along the top flange at the ends and at the midspan. Figure 4.29 represents the PPCB after the PPCB has been lifted.

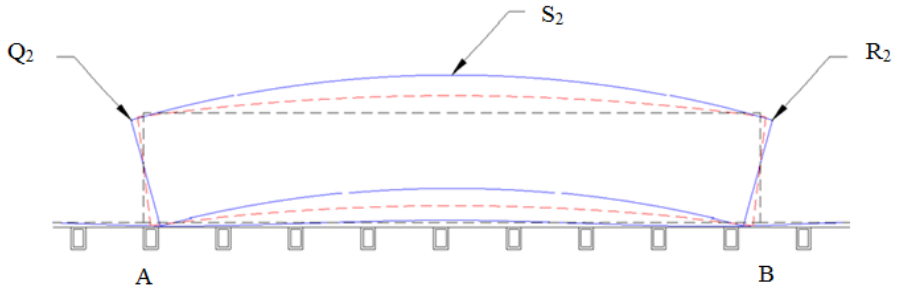

Figure 4.29. PPCB after the transfer of the prestress and after the PPCB was lifted and placed back on the bed

The following is the procedure used for calculating the camber using the measurements that were taken. This method accounts for inconsistencies in the top flange surface, the bed deflections, and the friction between the bed and the PPCB.

Bed deflections were accounted for by taking laser level measurements of the bed elevation before and after the transfer of the prestress. By determining the differential bed elevations at the end of the PPCB from before to after the transfer of the prestress, the magnitude of the bed deflection was obtained.

Bed deflections at points A and B $= T_0$-T_1 and, respectively U_0-U_1 **(4-3)**

Equation 4-3 gives a bed deflection at each end of the PPCB. To determine the total effect of the bed deflections on the camber, the average elevation of the bed at each end is computed to obtain the bed deflection with respect to the PPCB.

The bed deflection with respect to the PPCB at the midspan $= \frac{(T_0-T_1)+(U_0-U_1)}{2}$ **(4-4)**

Inconsistent PPCB depths were found to misrepresent the camber if the midspan of the PPCB does not have a cross-section identical to that of the ends. Equation 4-5 was used to determine the differential change in the deflection at the midspan. By taking an elevation measurement at the same location before and after the transfer of the prestress, the inconsistent top flange surface was accounted for.

The change in the deflection at the midspan,
accounting for the inconsistent top flange surface = $S_0 - S_1$ **(4-5)**

The issue of friction was present in determining the camber at the transfer of the prestress. Friction develops at the transfer of the prestress as a result of the PPCB and bed being in contact with each other. The friction can inhibit the full deflection from being detected. Lifting the PPCB and placing it down on the precasting bed dissipates the friction between the PPCB and bed. However, the process of lifting and setting the PPCB may cause it to be displaced from its original position. To solve this problem, top flange measurements were taken at the midspan and at the ends of the PPCB before and after the PPCB was lifted. Subtracting the upward deflection before the PPCB was lifted from the upward deflection after the PPCB was lifted gives the increase in the camber due to the dissipation of friction, as expressed in Equation 4-6.

$$\text{The deflection due to the dissipation of friction } = \left(\frac{(Q_2+R_2)}{2} - S_2\right) - \left(\frac{(Q_1+R_1)}{2} - S_1\right) \quad \textbf{(4-6)}$$

In the absence of PPCB overhangs after the lift/set of the PPCBs, it is possible to determine the total camber from Equations 4-3 through 4-6.

$$\text{Camber} = \left(\frac{(T_0-T_1)+(U_0-U_1)}{2}\right) + S_0 - S_1 + \left(\frac{(Q_2+R_2)}{2} - S_2\right) - \left(\frac{(Q_1+R_1)}{2} - S_1\right) \quad \textbf{(4-7)}$$

Problems are introduced if precasters are not able to lift and set the PPCBs on the precasting bed to dissipate the force of the friction in the PPCBs. It has been observed that precasters tend not to lift and set down the PPCBs on the precast bed to eliminate the friction. This is due to the risk of damaging the newly cast PPCB and the precasting bed, along with the scheduling and economic issues related to lifting a precast PPCB multiple times. Instead, precasters prefer to lift the PPCBs from the precasting bed and place them on temporary supports in a storage yard until they can be shipped to the job site. The supports are placed anywhere from the edge of the PPCB to several feet in from the end of the PPCB (see Figure 4.30). When PPCBs have the supports placed in from the ends, the measured camber will be greater due to elastic deformation.

Figure 4.30. End of a PPCB on a temporary wooden support

In cases where the PPCB was lifted and placed on temporary supports, the contributions of friction to the camber were determined by subtracting the value of the friction that was obtained from Equation 4-6 from the difference in deflection due to the self-weight from the movement of the supports. The result of the contribution of friction to the camber when accounting for elastic deformation due to temporary supports is shown in Equation 4-8.

$$\text{Adjusted deflection due to the dissipation of friction} = \Delta_{\text{DEFLECTION DUE TO DISSIPATION OF FRICTION}} - \text{The Difference in Deflection due to the Self-Weight from the Movement of Supports} \quad \textbf{(4-8)}$$

The final camber, when adjusting for the temporary supports, is defined by Equation 4-9.

$$\text{Camber} = \left(\frac{(T_0 - T_1) + (U_0 - U_1)}{2}\right) + S_0 - S_1 + \left(\frac{(Q_2 + R_2)}{2} - S_2\right) - \left(\frac{(Q_1 + R_1)}{2} - S_1\right) - \frac{5\omega_{sw}L^4}{384EI} - \frac{\omega_{sw}L_c}{24E_{ce}I}[3L_c^{\,2}(L_c + 2L_n) - L_n^{\,3}] + \frac{\omega_{sw}L_n^2}{384E_{ce}I}[5L_n^{\,2} - 24L_c^{\,2}] \quad \textbf{(4-9)}$$

4.1.7 Agreement of Adjusted Camber Values

The process and procedures for taking the camber measurements of PPCBs made at three precast plants for six bridge sites provided insight into possible discrepancies in the instantaneous camber due to the method of taking measurements at the precast plant. When evaluating data obtained from PPCBs at the transfer of the prestress, it is possible to determine a range over which bed deflections, friction, and inconsistent top flange surfaces contribute to the camber. While each of these factors individually may play minor roles in the camber discrepancies, the combined effect can introduce a significant error in the measured camber. Additionally, comparing the standard measurement practices of precasters and contractors and the method outlined in Section 4.1.6.1 has shown discrepancies resulting from the equipment used for

measurements, time-dependent effects, and the location chosen by each group to measure the camber.

To compare the measurement discrepancies among the methods used by contractors and precasters, data taken at the time of the transfer of the prestress was evaluated. The benefit of comparing measurement techniques at the transfer of the prestress is that the long-term effects of creep and shrinkage are not introduced yet and cannot further complicate the instantaneous camber measurement and prediction. Using a tape measure at the midspan, the camber was measured at the transfer of the prestress. This was based on the current method precasters use to measure the instantaneous camber. The method that represents the contractors' camber measurement procedure, in which the PPCBs were released and set on the bridge abutments or piers immediately, was also calculated. Additionally, the method that accounts for the bed deflections, friction, and inconsistent surface finishes (Section 4.1.6.1) was also compared to the precasters' and contractors' methods of taking the camber measurements. Table 4.2 summarizes the differences between the measurement methods used on 50 PPCBs that were cast at three different precast plants.

Table 4.2. Percent difference between measurement methods

	Percent Difference Between		
	Researcher and Precaster	**Contractor and Precaster**	**Researcher and Contractor**
Average	18.75	26.17	-7.56
Standard Deviation	16.6	18.32	8.11
Maximum	88.91	95.31	-43.11

Figure 4.31 illustrates in graphical form the differences between the measurement methods used on the same 50 PPCBs whose results were summarized in Table 4.2.

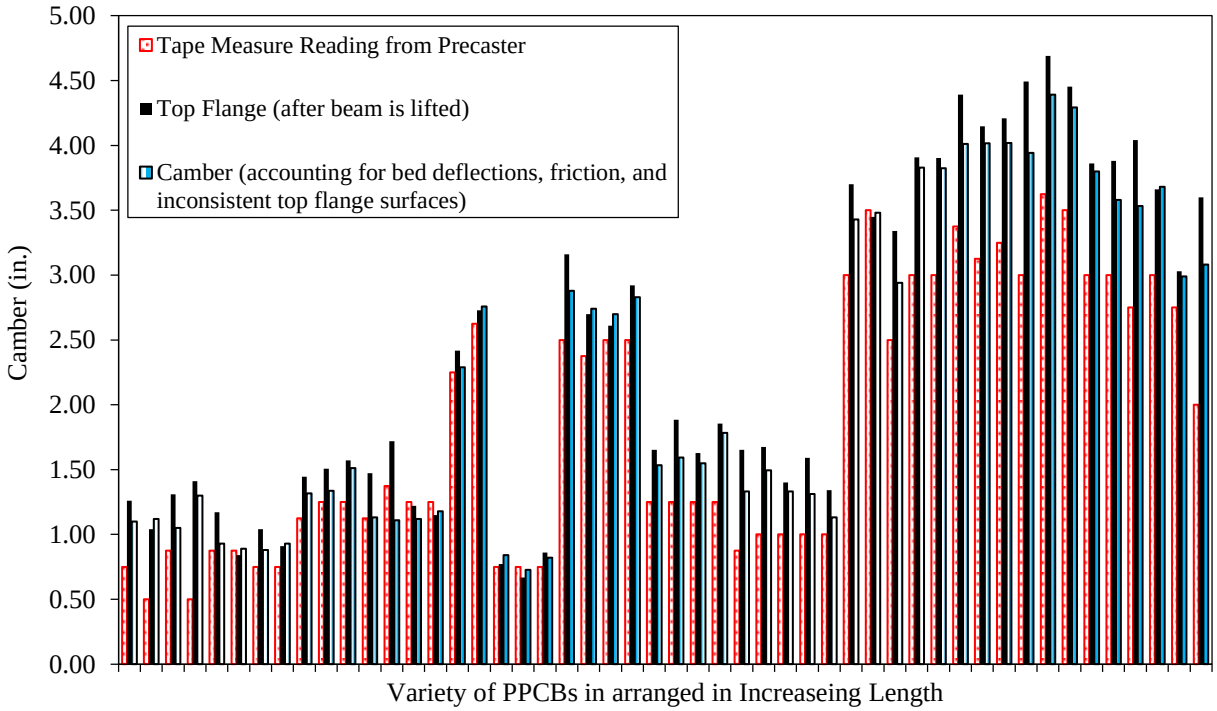

Figure 4.31. Comparison of the measurement techniques between precasters, contractors, and researchers

The results show that contractors' method measured the camber to be 7.6% greater than the researchers' accepted method. The precasters' measured camber showed a 26.2% difference from the contractors' method. When comparing the researchers' to the precasters' method of measurement, there is an 18.7% difference. The results from Figure 4.31 show that there are discrepancies in the accuracy of the precasters' and contractors' measurement methods. The precasters' method fails to account for the friction between the precasting bed and the PPCB, bed deflections, and surface conditions on the top flange. The contractor's method fails to account for the inconsistent top flange surface along the length of the PPCB and local inconsistencies in the top flange. There is an error associated with both methods due to their not accurately accounting for all the factors that influence the camber. Using the measurement method proposed in Section 4.1.6.1 will eliminate the magnitude of discrepancies between the methods used by the precasters and contractors.

Figure 4.32 shows a comparison of the three different measurement techniques that were adjusted to account for bed deflections and the friction that was present in the PPCBs.

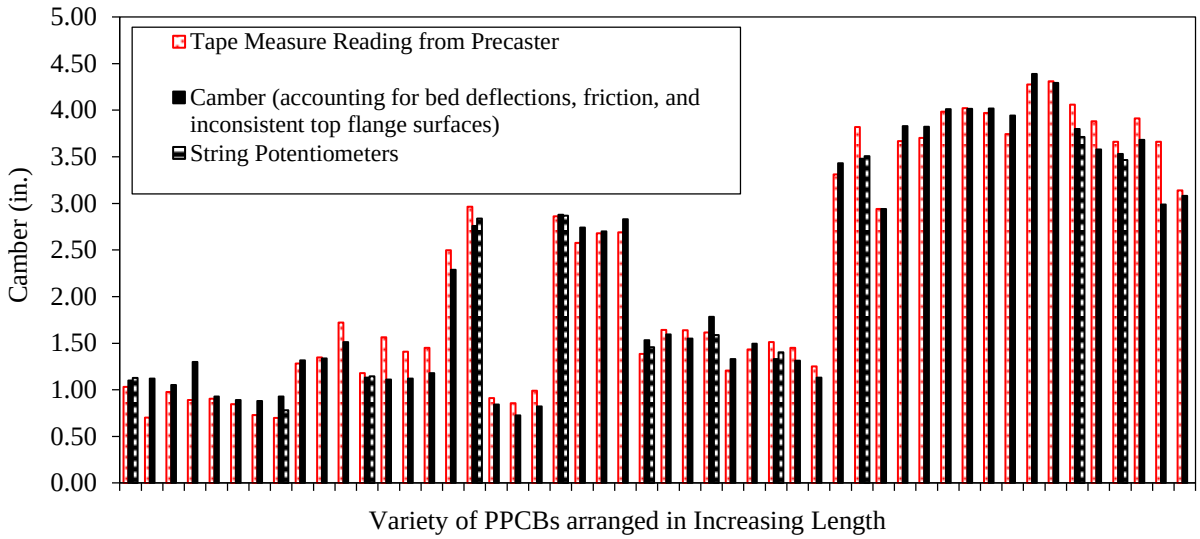

Figure 4.32. Differences between measurement techniques after accounting for the bed deflections, friction, and inconsistent top flange surfaces

The results show a close agreement with the rotary laser level camber measurements, which accounted for the measurement errors when the procedure outlined in Section 4.1.6.1 was followed. Discrepancies among the measurement techniques can be attributed to the time at which the measurements were taken and the precision of the tape measure readings. Laser level readings and string potentiometer readings were recorded immediately after the transfer of the prestress. Tape measure readings were typically taken immediately after the transfer but fluctuated by two hours depending on the precasters' schedule. The camber readings that were taken with a tape measure rounding to the nearest 1/8 inch lacked precision in comparison to the readings obtained with a laser level or string potentiometer. Due to the agreement among the three methods of camber measurement, as shown in Figure 4.32, it is appropriate to state that, regardless of the method used, adjusting for the possible errors will result in accurate camber measurements.

Table 4.3 quantifies the errors associated with measuring the camber at the transfer of prestress. Although these values were obtained using a rotary laser level, factors such as bed deflections, friction, and inconsistent top flange surfaces were verified with string potentiometer readings.

Table 4.3. Average and standard deviations associated with camber measurements at the transfer of prestress

Possible Errors	Maximum Value (in.)	Minimum Value (in.)	Average Value (in.)	Standard Deviation (in.)
Bed Deflections	-0.313	0.000	-0.030	0.062
Friction	1.080	0.040	0.392	0.294
Inconsistent Top Flange Depth along the Length of the PPCB	0.788	0.000	0.099	0.142
Inconsistent Top Flange due to Local Inconsistencies	0.900	0.000	0.113	0.119

4.1.8 Summary and Conclusions

4.1.8.1 Industry Practice Camber

Industry practice camber measurements recorded at precast plants for PPCBs that were previously cast were compiled to determine the following preliminary conclusions:

- The camber was overpredicted 75% of the time.
- The magnitude of the overprediction of the camber increased as the PPCB length increased.
- As PPCBs increased in length, there was a greater scatter in overprediction and underprediction.
- Specific groups of PPCBs have tendencies to be overpredicted or underpredicted.

The current camber measurement technique was investigated by the researchers, who found that the current measurement technique, which was used to evaluate the industry practice camber data, failed to account for various factors that misrepresent the camber. Therefore, the above conclusions have a limited value. Complications in accurately measuring the camber and the fact that several past mix designs are no longer used to construct PPCBs led researchers to independently measure the camber on 105 PPCBs.

4.1.8.2 Camber Measurement Technique

As part of the research reported herein, different measurement techniques were explored to determine a consistent, accurate way to measure the instantaneous camber. The measurement techniques include what the precast industry is currently using, methods that were used in past research studies, and a measurement method that accounts for previous errors that have been neglected.

While most state DOTs have guidelines on how to measure the camber, it was determined that there is not a consistent industry standard. Common methods of camber measurement for the precast industry include using different instruments, such as a stretched wire along the length of

the PPCB, a tape measure, and occasionally survey equipment. There is also variability in measuring the camber from the top flange, bottom flange, or web. The time after release when the camber measurement is taken has been observed to vary from before the transfer of the prestress is complete to three hours after the transfer of the prestress.

The camber research that was previously conducted involved taking independent camber measurements at precast plants. Methods employed to take independent camber measurements included the stretched-wire method, using survey equipment to take measurements at the top and bottom flange, and photogrammetry. The different methods used in past research to determine the camber often fail to account for variables such as precast bed deflections, inconsistent top flange surfaces, and the friction that inhibits the PPCB from reaching its full instantaneous camber.

Because some of the camber measurement methods used by precasters and in past research neglect bed deflections, inconsistent PPCB depths, and the friction between the PPCB and the precasting bed, a new method to measure the camber was used that accounts for each of these issues accurately and quantifies their impact on the instantaneous camber measurement. Additionally, the industry standard method for taking instantaneous camber measurements, along with instrumenting the PPCBs with string potentiometers, was used to compare results. Using newly collected data from 105 PPCBs made at three precast plants, the causes of error associated with the instantaneous camber were investigated, which led to the following conclusions:

- Factors such as bed deflections, friction, and inconsistent top flange surfaces misrepresent the camber that is recorded at the precast plants.
- The values obtained from field measurements show that the camber is, on average, affected by bed deflections by 0.030 in. ± 0.062 in., friction by 0.392 in. ± 0.294 in., the inconsistent top flange surfaces along the PPCB length by 0.099 in. ± 0.142 in., and inconsistent top flange surfaces due to local effects by 0.113 in. ± 0.119 in.
- Through the measurement technique used in this study, bed deflections were found to contribute to the error in the camber up to 16.1%, the friction between the PPCB ends and the precasting bed up to 38.4%, the inconsistent top flange surface along the length of the PPCB up to 29.1%, and the inconsistent top flange surface due to local effects up to 66.0%.
- The data obtained from the PPCBs at the transfer of the prestress using a tape measure, rotary laser level, and string potentiometers show good agreement when adjusting for the possible camber measurement errors. Despite good agreement between the tape measure and rotary level, the data based on the tape measure is easily affected by the precision of the person taking the measurement.
- The reverse friction is small in magnitude and can be ignored. This is verified by the string potentiometer graph shown in Figure 4.21 and the additional string potentiometer data in Appendix B. The contribution of vertical displacement due to the friction can be obtained by lifting/setting the PPCB and then taking the camber measurement.

Although the errors associated with measuring the instantaneous camber due to bed deflections, friction, and inconsistent top flange surfaces may be small individually, failing to account for each can result in an error of up to 150% between the measured and the designed camber. Using

the proposed camber measurement procedure described in Section 4.1.6.1 will account for errors that are currently not being accounted for, which in turn will improve the camber prediction and reduce unforeseen construction issues related to the camber in PPCBs.

4.2 Long-Term Camber Measurements

4.2.1 Introduction

At-erection camber for prestressed concrete PPCBs has been observed by the Iowa DOT to be typically lower than the design camber. This discrepancy changes the haunch design and leads to the unplanned placement of reinforcing concrete. The extra concrete in the field increases the dead load of the bridge, which results in additional costs; complicates the quality control of the finished bridge; and affects the composite action between the PPCB and the bridge deck.

Although the sources of the difference between the designed and measured camber at erection are not thoroughly recognized, a number of different factors contribute to this discrepancy. Some of the most significant parameters are the PPCB material properties, the precision of the instantaneous camber prediction, the fabrication process, the concrete creep and shrinkage, the support location, and the thermal effects.

To further investigate the time-dependent camber, PPCBs fabricated for five different bridges in Iowa were monitored for camber measurements from the precasting yard to the bridge site. Different types of Iowa DOT PPCBs with various lengths were selected for long-term camber measurement. The camber was measured from the top flange when the PPCBs were erected on the piers before and after the deck was cast. A rotary laser lever was used for all the long-term camber measurements. Also, the effects of the bunking condition and the thermal effects on camber variability were inspected. The measured data were subsequently used to validate the simplified model, and the finite element model was developed using midas Civil software.

4.2.2 Challenges Resulting from Inaccurate Prediction of Long-Term Camber

Predicting the camber of PPCBs has been a problem that precasters, contractors, and DOTs across the country have faced for many years. Overpredicting or underpredicting the camber typically causes difficulty with field assembly, delays in construction schedules, and serviceability problems with structures, which can increase the construction costs. The intensity of this challenge appears to have been exacerbated in recent years due to the use of more advanced high-strength concrete mix designs. For this reason, it was found that a significant discrepancy existed between the designed and actual values of the instantaneous and long-term cambers. While construction challenges tend to have drawn more attention to the long-term camber, it should be realized that an error associated with the instantaneous camber will significantly affect the long-term camber, as outlined in Section 4.1.

The majority of the problems associated with inaccurate camber are related to placing the bridge deck at the job site. A minimum deck thickness requirement needs to be fulfilled throughout the

entire length of the bridge. Inconsistent elevations along the length of the PPCB are typically present due to the camber in the PPCBs. For example, the elevation of a prestressed PPCB at the midspan is typically higher than the elevation at the ends of the PPCBs (see Figure 4.33). Due to the effect of different elevations along the length of the PPCBs, haunches are required to be built. A haunch is defined by the AASHTO Standing Committee on Highways and Subcommittee on Bridges and Structures (2005) as the space between the bottom of the slab and the top of the top flanges of the PPCBs (see Figure 4.34). The purpose of a haunch is to maintain a uniform deck thickness along the length of the PPCBs and to meet the desired bridge profile. It should be recognized that haunches vary over the length of the PPCB in order to account for the change in elevation over the length of the PPCB. Adding and adjusting haunches has been proven to be labor intensive, can add construction delays, and will increase the dead load without the addition of strength. Adding and adjusting haunches can increase costs through added labor that is unaccounted for in the plans, can increase the possibility of liquidated damages if the project runs over the allotted time that was budgeted, and can result in serviceability issues due to the larger dead load from additional concrete that was originally unaccounted for.

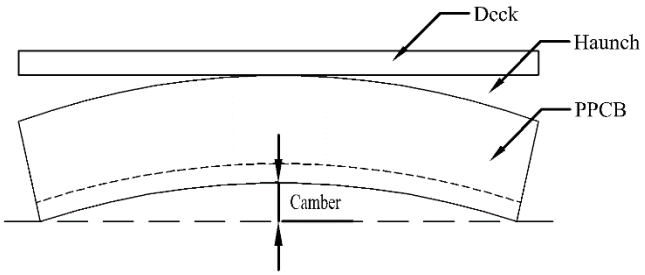

Figure 4.33. Schematic view of a PPCB showing the formation of the haunch

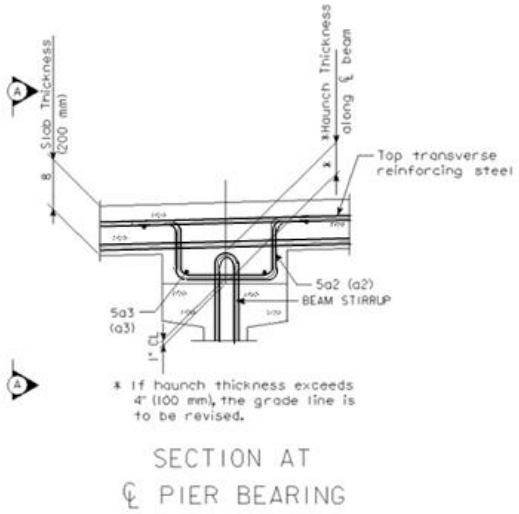

Figure 4.34. Cross-section of a PPCB, haunch, and slab (Iowa DOT 2011a)

An underpredicted camber (i.e., when the designed camber is smaller than the measured camber) will result in an excessive upward deflection greater than the designed camber (see Figure 4.35). Conversely, an overpredicted camber (i.e., when the designed camber is greater than the

measured camber) will result in an upward deflection that is less than the designed camber (see Figure 4.35). The area of concern with the overprediction and underprediction of the camber is typically at the midspan. Erecting PPCBs at a bridge site typically requires haunches/embedments, grade adjustments, or a combination of both to be utilized to account for either the overprediction or underprediction of the camber.

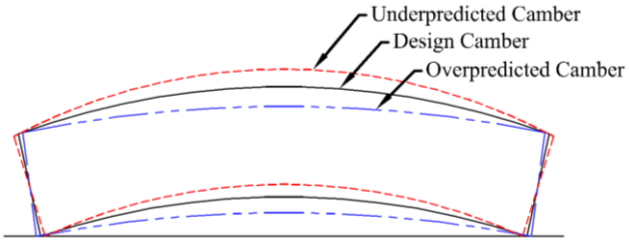

Figure 4.35. Underpredicted, designed, and overpredicted camber

A camber that is greater than the designed camber (i.e., underprediction) will require haunches to be built. In extreme cases where the maximum haunch exceeds four inches from the top flange of the PPCB, a grade adjustment will need to be considered (Iowa DOT 2011a). Lowering the grade of the top slab may decrease the height of the haunch below the four-inch maximum value. If this option is unavailable, the rebar may be bent so that clearances can be met at the midspan of the PPCB. Additional bending of these bars will increase the required labor and costs.

An underpredicted camber causes the PPCB to be susceptible to flexural cracking in the top flange due to tensile stresses from the prestressing. While storing PPCBs before the deck is cast, the top flange is exposed. If cracking is present, contaminants can reach the reinforcement. After the deck is placed, additional dead load is added to the PPCBs, causing less tensile stress to be present in the top flange and reducing the crack widths. The reduction of tensile stresses will reduce the risk that contaminants will penetrate into the PPCB unless the camber significantly increases further due to creep. In cases of large creep, the deck will be susceptible to cracking and present possible serviceability problems.

An overpredicted camber will result in a camber value that is smaller than the designed camber. The first option for mitigating problems with overpredicted camber is to build haunches along the entire length of the PPCB. If the haunches exceed the specified upper limit of four inches, lowering the grade of the slab is considered. When this option is unavailable, additional nonprestressed reinforcement may need to be added to the haunches exceeding four inches. An example of additional reinforcement is shown in Figure 4.34. There will be additional effort with bending and placing the extra nonprestressed reinforcement in the bridge deck to accommodate the large haunches, which will increase the required labor and ultimately affect the cost. Additionally, the extra concrete will add a larger dead load without increasing the strength of the bridge.

Having differential cambers on adjacent PPCBs has been observed to cause problems at the erection of the superstructure and during the construction of the haunches. To solve the problem of differential cambers, designers use an appropriate size for the haunches or embedment along

the length of the PPCBs to allow for the proper elevation required for the construction of the top surface of the deck. If the haunches exceed the maximum or minimum specified tolerances, grade adjustments or additional reinforcement is considered. Some cases require a combination of these solutions to solve the problem. Problems resulting from having differential cambers of adjacent PPCBs include the increase in time for adjusting the haunches or grades and for adding the nonprestressed reinforcement and concrete materials. In extreme cases, the PPCBs may be rejected or the PPCB seats may be adjusted.

The overprediction and underprediction of camber causes problems with assembling the PPCBs at the bridge site. The problems come from determining haunch heights, adjusting slab grade elevations, adding or bending additional nonprestressed reinforcement, and having differential cambers on adjacent PPCBs. Although the problems with inaccurate camber prediction are often overlooked, they are significant if they lead to serviceability issues, increased costs due to extra materials, and liquidated damages for the project.

4.2.3 Data Collection

Based on instantaneous cambers predicted using the Iowa DOT PPCB standards (Iowa DOT 2011), the PPCBs selected for measurements were divided into two groups. The first group included small-camber PPCBs, with estimated instantaneous cambers smaller than 1.5 in., and the second group included large-camber PPCBs, with the estimated instantaneous camber greater than 1.5 in., as presented in Table 4.4.

Table 4.4. Details of the collected camber measurements

PPCB	Number of PPCBs	Periodic Camber Measurements during Storage	Camber Measurements on the Piers before/after Deck Pour	Bridge Project Location	Precasting Plant
Small-camber PPCBs					
D 55	12	Yes	Yes	Sac 110 County	Plant C
D 60	12	Yes	Yes	Sac 110 County	Plant C
SBTD 75	3	No	Yes	Woodbury County	Plant C
Large-camber PPCBs					
C 80	4	Yes	No	Polk County	Plant C
D 105	12	Yes	Yes	Sac 110 County	Plant C
D 110	8	Yes	Yes	Sac 410 County	Plant A
BTE 110	9	Yes	Yes	Mills County	Plant B
BTC 120	3	Yes	No	NA	Plant A
SBTD 125	3	No	Yes	Woodbury County	Plant C
BTD 135	8	Yes	Yes	Dallas County	Plant C
BTE 145	6	Yes	No	Mills County	Plant B

The measurements were taken during storage when the PPCBs were sitting in the precasting yard before they were shipped to the job site. Most of the data were collected around noon and in the afternoon during storage. The camber was measured again after erecting the PPCBs on the piers at the job site and before the deck was cast. To obtain the camber measurements after the cast-in-place deck pour, pipes were attached to the PPCB's top flanges and were used after the deck was cast to measure the camber. The collected data for the long-term camber of the various PPCBs examined in this study are presented in Appendix C.

4.2.4 Support Location

After the strands were released on the precasting bed, the PPCBs were transported to the storage yard until they were to be shipped to the job site. During storage, the PPCBs were sitting on temporary supports with an overhang length varying from less than a foot to as high as eight feet for different precasting plants. The Iowa DOT does not require any specific support or overhang length for precasting plants. Hence, both the concrete blocks and timber were used as a means of temporary support at different plants. The overhang length was measured for all the PPCBs to quantify the amount of camber growth due to support locations using analytical models. Then, all the data points were analytically adjusted to eliminate the effect of the overhang length by shifting the supports to the ends of the PPCBs.

Figure 4.36 shows all the measured overhang lengths for different types of PPCBs.

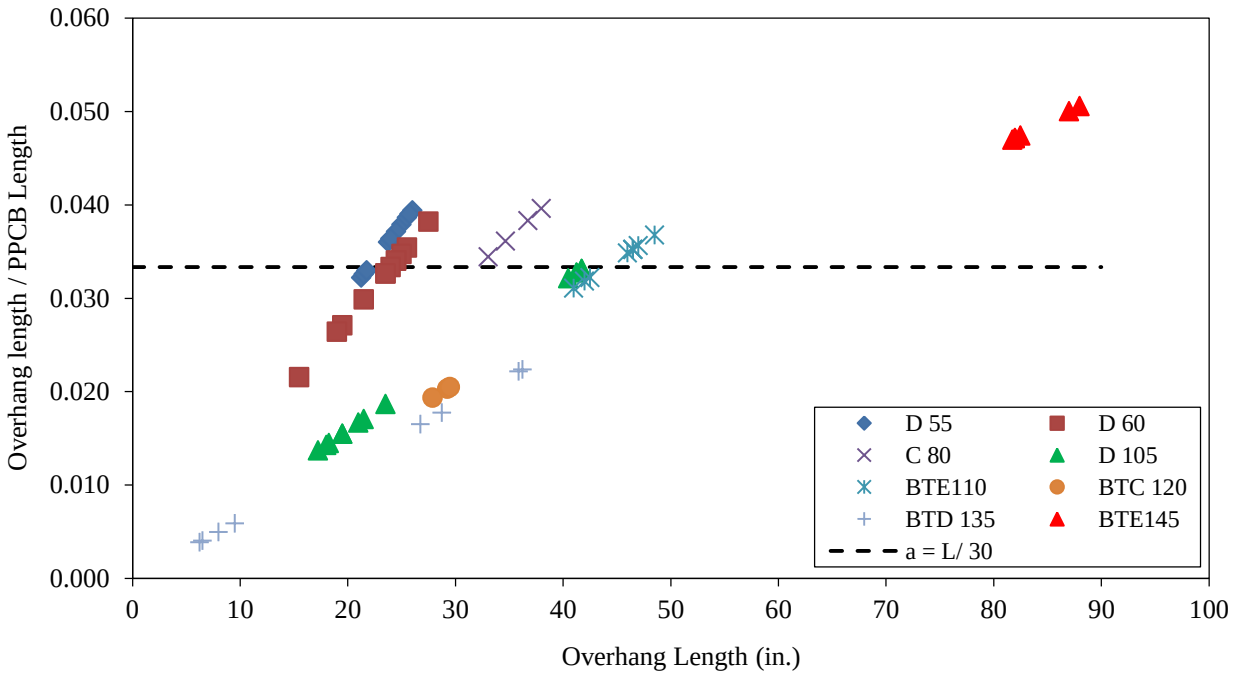

Figure 4.36. Measured overhang length

It can be seen that the ratio of the overhang length to the PPCB length varies among PPCBs. However, the calculated average ratio suggests that the overhang length of different PPCBs can

be estimated by $\frac{\text{PPCB Length(L)}}{30}$, as presented by the dashed line in Figure 4.36. This ratio is used in Chapter 7 to calculate multipliers that account for the effect of the overhang.

4.2.5 Investigation of the Thermal Effects

To further investigate the thermal effects on the long-term camber, 22 different PPCBs were instrumented with string potentiometers and thermocouples to measure the thermal deflection as a function of temperature over short durations. All PPCBs were instrumented at the midspan with one thermocouple on the top flange, one thermocouple on the underside of the bottom flange, and one string potentiometer attached to the side of the top flange (see Figure 4.37 and Figure 4.38).

Figure 4.37. Thermocouple attached to the bottom flange

Figure 4.38. Overall view of the instrumented PPCBs

The PPCBs' surface temperatures and vertical deflections were monitored for a cycle of 24 hours for each PPCB, except for 6 BTE 145 PPCBs that were only monitored for 6 hours. The measurements were taken at the Cretex Concrete Products precast plant in Iowa Falls, Iowa, at different times of the year to examine the impact of seasonal weather conditions on the thermal deflection as a function of time. Twelve PPCBs, including six BTE 145 PPCBs, three BTC 115 PPCBs, and three BTD 115 PPCBs, were instrumented in the summer when the solar radiation was expected to be the highest. Instrumentation was performed for six BTE 155 PPCBs in the winter when the temperature was below 0°F. Two BTE 155 and BTE 145 PPCBs were instrumented in the spring when moderate temperatures were observed.

Figure 4.39 shows a sample result for the measured BTE 145 PPCBs.

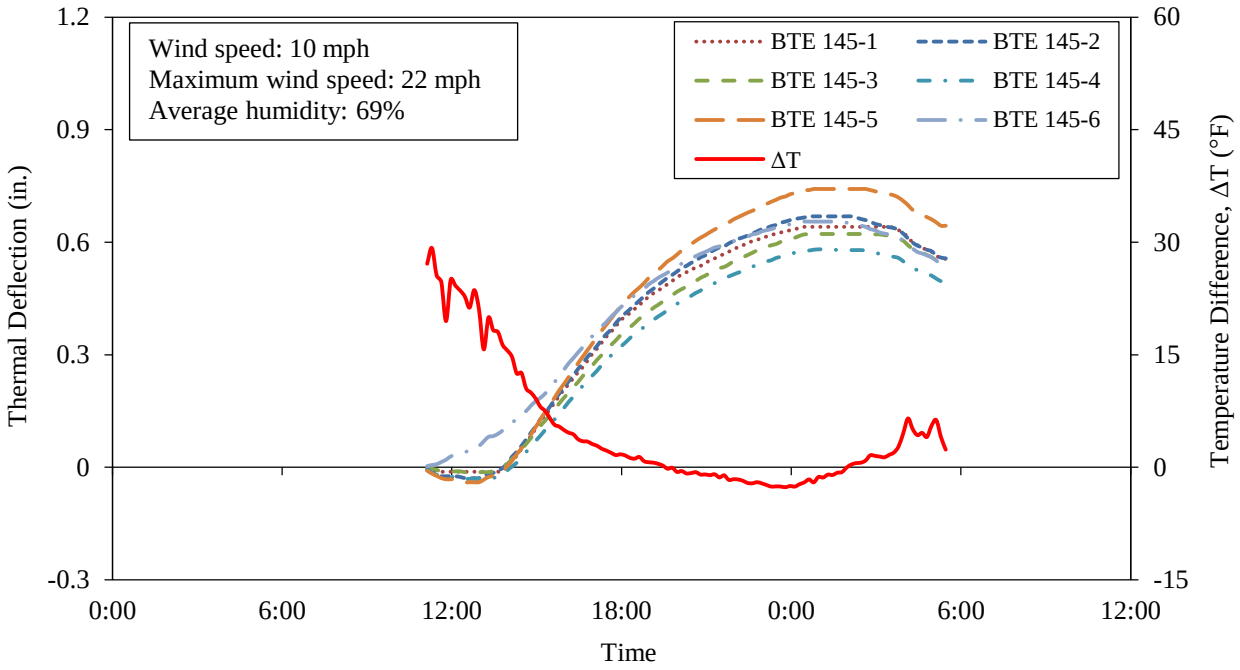

Figure 4.39. Thermal deflections and temperature difference versus time for BTE 145 in the summer (June)

It can be observed that the temperature difference of around 30°F at the PPCB midspan induced a thermal deflection as high as almost 0.75 inches. The remaining results for the measurements taken in different seasons can be found in Appendix D.

4.2.6 Measurements after Deck Pour

Further measurements were taken to confirm that the change in camber was inconsequential after the PPCBs were erected and the bridge deck slab was placed. The camber was measured from the top flange to be consistent with previous measurements. Before the deck pour, hollow steel pipes were attached to the top flange of the PPCBs at midspan and at the two ends. A plastic cap with a string on the inside was attached to the top of the steel pipe to prevent the concrete from infiltrating inside the pipe and to help find the pipe after the deck pour. After completing the deck pour, the strings sticking out of the finished surface of the concrete were used to find the pipes, and then the concrete was drilled to reach the bottom elevation of the pipes. Subsequently, a rod was inserted inside the pipe, and the measurements were taken from the top of the rod using a rotary laser level. Figure 4.40 demonstrates how the hollow steel pipe is attached to the top flange of the PPCB. Figure 4.41 shows a view of a pipe attached to the PPCB at the job site before pouring the deck.

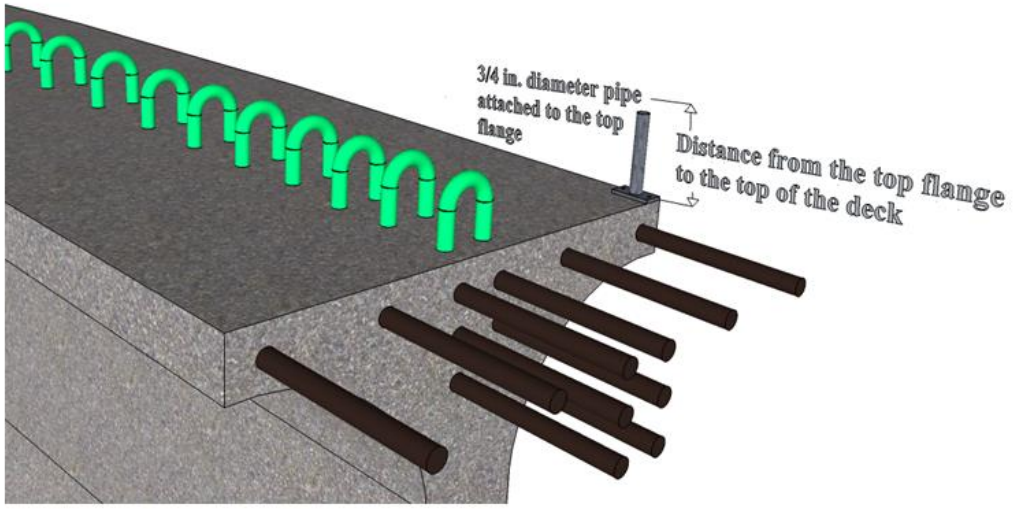

Figure 4.40. Details showing hollow steel pipes attached to the top flange of the PPCB

Figure 4.41. Hollow steel pipe attached to the PPCB at the bridge job site

4.3 Recommendations for Instantaneous and Long-Term Camber Measurements

Throughout the study of improving PPCB camber predictions, the production and design procedures were observed to significantly affect the accuracy of the predicted and measured camber. Evaluating and improving the design and production procedures will result in a closer agreement between the designed and measured cambers. The following sections constitute a list of recommendations that are suggested for precasters, contractors, and designers.

4.3.1 Measuring the Instantaneous and Long-Term Camber

The currently adopted camber measurement method is not consistent. The measurement technique and the location on the PPCBs where the measurements are taken vary. By observing and taking independent camber measurements, this study concluded that the average error in camber arising from the measurement techniques used by the precastrers and contractors was about 26%. To eliminate the difference in the camber due to the measurement technique, the researchers developed a simplified procedure that both precasters and contractors can use to accurately measure the camber and minimize any error associated with the measurement technique. The following are recommendations for the new camber measurement procedure:

1. Place a 2x4 on the top flange at the ends and at the midspan of the PPCB (Figures 4.42 and 4.43) before casting the PPCB.

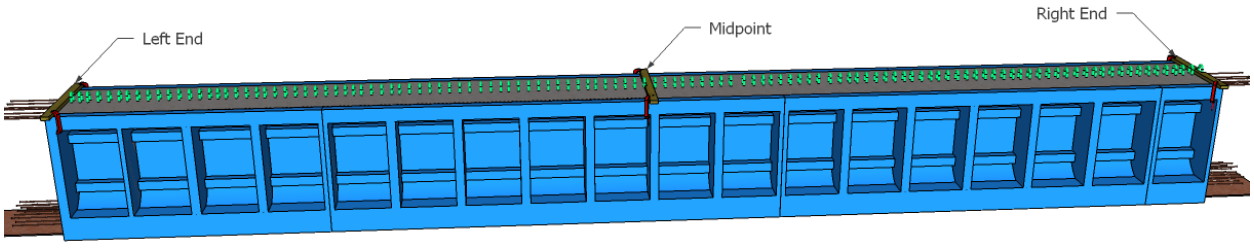

Figure 4.42. Casting of PPCB with 2x4s to establish flat surfaces

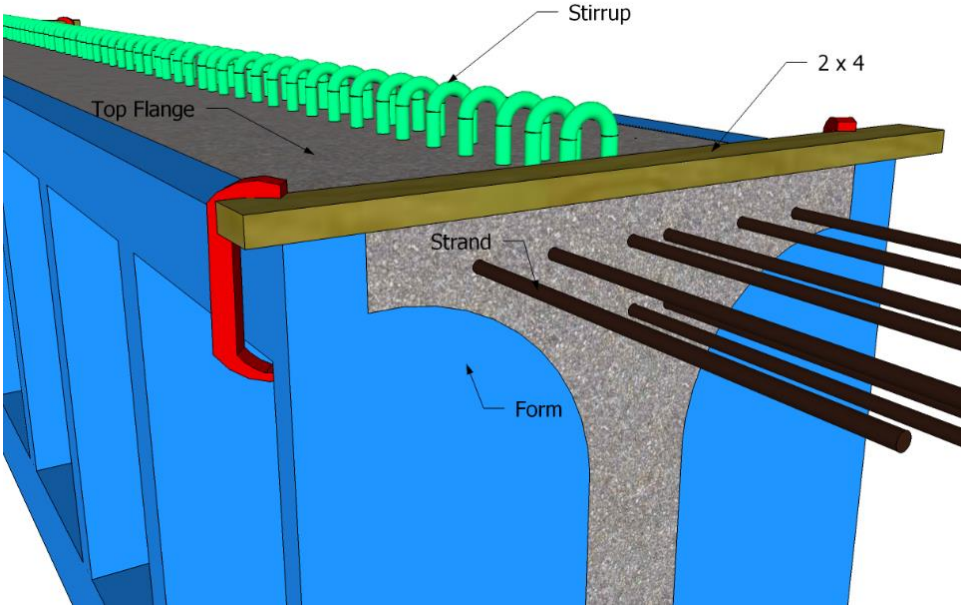

Figure 4.43. Close-up of a 2x4 positioned on a PPCB

2. Cast the concrete to the bottom elevation of the 2x4 to ensure that flat surfaces will be produced (underneath the 2x4s).
3. Cure the PPCB using the standard practice.
4. Remove all 2x4s from the top flange and the framework.
5. After the PPCB has been released, precasters have one of the following two options:
    a) Lift/set the PPCB on the precasting bed or
    b) Lift the PPCB and move it to the storage yard, placing it on temporary wooden supports at the PPCB ends.
6. Measure the elevation of the PPCB with a rotary laser level, a total station, or any other suitable survey equipment at the midspan and at the ends of the PPCB using the top flat surfaces created by the 2x4s. At each location, take measurements closer to each side and in the middle of the top flange, as shown in Figure 4.44. Although the use of a tape measure has been shown to provide accurate camber measurements, the equipment suggested for this step has been found to minimize the expected error.

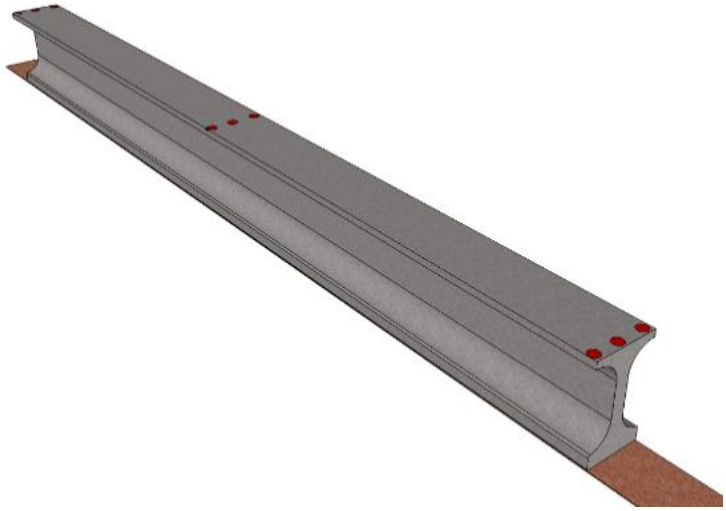

Figure 4.44. Location of the camber measurements after the transfer of the prestress

7. If option 5.b. is used, determine the contribution to the camber due to the reduced clear span and the overhang caused by the temporary supports.
8. Take the average of the end elevation readings and subtract it from the midspan elevation reading to obtain the camber.
9. If option 5.b. is used, subtract the contribution to the camber due to the temporary support placement from the camber value calculated in step 8.

The recommended procedure for measuring the camber improves accuracy and minimizes error for precasters. Measuring the camber with this method eliminates the inaccurate representation of the camber due to friction, inconsistent top flange surfaces, and bed deflection. The 2x4s cast at the top flange will ensure that the same reference points are being used to measure the camber in the field. Although the time to measure the camber will be greater than for the existing method, this method will minimize the role of inaccurate camber if haunch reinforcement is required.

4.3.2 Additional Recommendations to the Precasters

Observing and taking independent camber measurements at three separate precast plants led the researchers to make the following recommendations to improve camber predction for PPCBs:

- The prestress force is highly sensitive to the camber. Therefore, monitor and apply the designed prestress force as accurately as possible.
- Aim for reaching and not exceeding the design strength at the transfer of the prestress.
- Ensure consistency of concrete mixes and base materials (e.g., aggregates) regardless of the time and day of casting.
- Ensure consistent curing conditions and match the PPCBs' curing conditions to those of the sample cylinders used for obtaining the release strength.
- When the material or curing process changes, engineering properties, including the creep and shrinkage behavior of the concrete, should be appropriately revised.
- Minimize the error in the instantaneous camber measurements of identical PPCBs cast on different beds or at different times or days.
- Use the proposed camber measurement procedure to take the instantaneous camber measurements.
- Store the PPCBs with zero overhang or L/30 during storage.

Performing the above recommendations will help precasters produce PPCBs whose measured camber is in agreement with the designed camber. Despite the above recommendations, some variations in the materials and fabrication procedures may still exist, but their impact on camber measurements will be minimized.

CHAPTER 5: PREDICTING INSTANTANEOUS CAMBER

5.1 Introduction

The long-term camber can be estimated more accurately if the instantaneous camber is predicted more exactly. As discussed in Section 2.2.5, the prediction of the camber at the release of the prestress seems to be a relatively straightforward task because the theory of elasticity is applicable. Currently, the Iowa DOT uses the CON/SPAN software to estimate the instantaneous camber.

The challenges faced in predicting the instantaneous camber during design are related to the designer's ability to accurately estimate the material properties and to model the applied forces exerted on the PPCB after accounting for the effect of the prestress losses (see Section 2.2.2). The non-homogeneous properties of the concrete, such as the modulus of elasticity, strength, creep, shrinkage, and the maturity of the concrete, can lead to a large scatter in variables. Additionally, outside effects such as the curing conditions further impede the ability for designers to accurately predict the behavior of the concrete. Correctly representing both the material properties and the prestressing force when an active combination of prestressing steel and concrete is present is important for accurately determining the camber of a PPCB. This chapter focuses on the equations and methods that can be used to predict the instantaneous camber accurately.

5.2 Methodology

Calculating the camber using simplified methods is a straightforward procedure that involves calculating the upward deflection due to the prestress and the downward deflection due to the self-weight of the PPCB. The net deflection between the two components will result in the instantaneous camber. Due to its ability to represent the material properties and the behavior of the PPCB accurately, the moment area method was chosen to calculate the instantaneous camber, and it is discussed in the subsequent sections.

The first step in calculating the camber using the moment area method was gathering accurate variables for the PPCB of interest. The types of PPCBs that are produced have specified variables in the Iowa DOT PPCB standards (Iowa DOT 2011b). The specifications give the design properties of the materials used and the fabrication variables that are required to produce a PPCB. Included in the specifications are the nonprestressed and prestressed reinforcement layout, the material properties of the reinforcing steel, the cross-section dimensions, the area, the moment of inertia, the target release strength, the target instantaneous camber, and other geometric variables that may be necessary for producing a PPCB. To closely replicate the behavior of the PPCB, variables obtained from the design documents along with variables that are in agreement with the material properties of the specimen were used. Using a combination of specified variables and variables that are in agreement with the properties for each PPCB results in accuracy in the predicted and the measured camber values.

Secondly, the effects of the variation in the concrete material properties, such as the compressive strength, the modulus of elasticity, the maturity, and the uniformity, on the instantaneous camber were investigated. Subsequently, the best prediction method for the modulus of elasticity was found by comparing different methods (see Section 2.1.4.2). The equation proposed by AASHTO LRFD (2010) for estimating E_c was chosen to predict the instantaneous camber using the moment area method. Ultimately, a parametric study was performed on the different analytical parameters influencing the prediction of the camber, such as the moment of inertia, the prestress force, the prestress losses, the sacrificial prestressing reinforcement, and transfer length.

5.3 Variability of the Compressive Strength

The minimum f'_{ci} values for each type of PPCB (Equation 2-10) are specified in the Iowa PPCB standard used for the design of Iowa precast, prestressed concrete PPCBs. The purpose of the minimum f'_{ci} values is to ensure that the concrete will safely handle the stress applied to the concrete from the tensioned prestressing strands. To ensure that the proper compressive strengths are met, testing is conducted by the precast plant by taking the average strength from three cylinders. The average of the three compressive strength values has to be higher than the designed release strength in order for the precasters to transfer the prestress to the PPCB. Because the schedule is a crucial part of the productivity of the precast industry, the urgency for a PPCB to reach the release strength and for the workers to release and move the PPCB off the prestressing bed is emphasized. The urgency of obtaining the release compressive strengths quickly has resulted in the concrete compressive strengths being greater than the designed value (see Appendix E.1). Higher compressive strengths result in a higher modulus of elasticity when using the AASHTO LRFD (2010) method (Equation 2-3), causing the measured camber to be lower than the design camber.

Figure 5.1 shows a comparison of the measured release strength versus the designed release strength of 104 PPCBs that were included in this camber study.

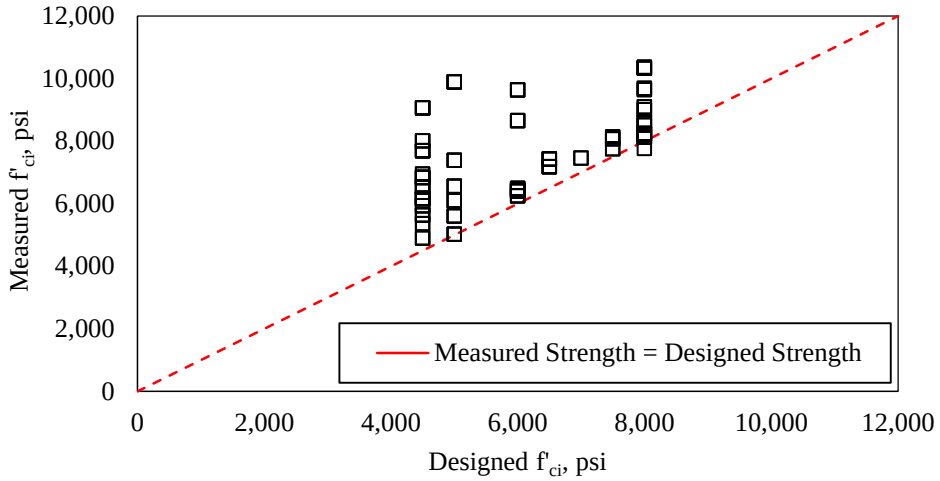

Figure 5.1. Measured release strength versus designed release strength

The line that extends from the vertex at a 45 degree angle signifies the point where the design strength meets the measured strength. It is expected that the measured release strength be higher than the design strength in order to safely transfer the prestress to the PPCB. The further the points are away from this line, the higher the measured compressive strength. In addition, the comparison between the designed released strength and the measured released strength at the three precast plants is tabulated in Table 5.1.

Table 5.1. Designed and measured release strengths

	Design Release Strength (psi)							
	4,500	**5,000**	**5,500**	**6,000**	**6,500**	**7,000**	**7,500**	**8,000**
Plant A								
Average	6,936.7	7,373.3			7,292.2	7,450		8,915.9
Standard Dev.	-	-			129.9	-		951.5
Plant B								
Average		5,812.8					7,978.7	9,298.4
Standard Dev.		596.64					179.1	873.0
Plant C								
Average	6,269.5	9,885		6,905.9				8,750. 7
Standard Dev.	874.2	-		942.3				674.9
Total								
Average	**6,315.5**	**6,916.5**		**6,905.8**	**7,292.2**	**7,450**	**7,978.7**	**8,875**
Standard Dev.	**859.81**	**1,738.6**		**942.3**	**129.9**	**-**	**179.1**	**804.6**

One trend in the measured versus the design strength results reveals that, as the release strength increases, the agreement with the 45 degree line improves. For PPCBs with designed release strengths of 4,500–5,500 psi, the measured f'_{ci} was 39.5% higher than the designed value. For designed release strengths of 6,000–8,000 psi, the measured f'_{ci} was 11.5% higher than the measured value. High release strength concrete mixes are often used for normal design strength values to ensure that specified strengths are met within one day and prefabrication schedules remain on time. As the release strengths increase, the capacity of the release strengths remains constant. This causes the higher design strengths to fall closer to the measured release strengths.

As discussed in Section 2.2.2.2, the impact of the high-strength concrete release strengths will affect the camber. The decrease in the release camber due to an increase in the concrete strength was replicated by using the AASHTO LRFD (2010) method of determining the modulus of elasticity. Additionally, the modulus of elasticity using ACI 363R-92 (1992) was also determined and plotted in Figure 5.2.

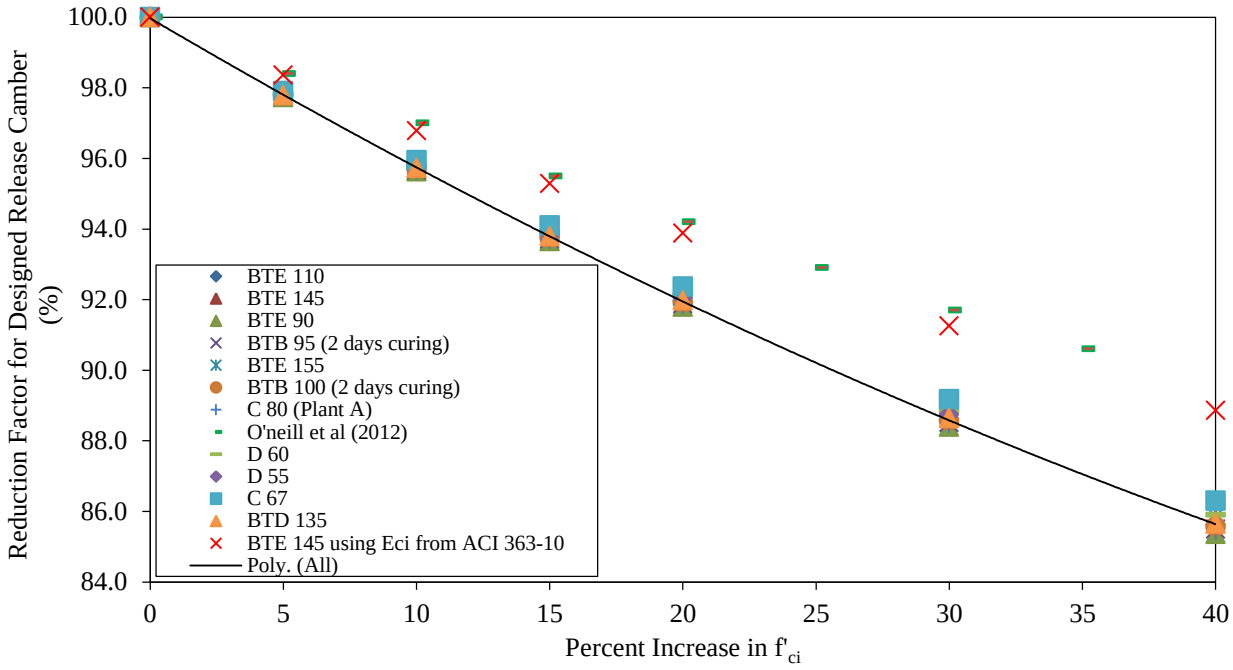

Figure 5.2. Impact of concrete release strengths on the camber

The results show that, as the concrete strength increased, the modulus of elasticity increased as well, which reduced the camber. The reduction of the camber was greater when using the AASHTO LRFD (2010) modulus of elasticity compared to the ACI 363R-92 (1992) method. The results in Figure 5.2 show that failing to account for the increase in concrete strengths by up to 40% will misrepresent the initial camber by decreasing the predicted value by 14%. Additionally, the effect of the variability of the compressive strength on the modulus of elasticity, and subsequently on the camber, is presented in Appendix E.2.

5.4 Modulus of Elasticity

The modulus of elasticity plays a significant role in the camber at the transfer of the prestress. The common method used by the Iowa DOT to determine the designed modulus of elasticity is to use the AASHTO LRFD (2010) equation (Equation 2-3). Variations on this method and its results may exist because it is dependent on the unit weight of the concrete and the release strength. In this study, comparing the calculated camber values to the measured camber values using different moduli of elasticity resulted in an overprediction or an underprediction of the camber and made it possible to determine which modulus of elasticity method produced the best agreement.

Figure 5.3 through Figure 5.7 show the measured versus predicted camber using different values for the modulus of elasticity.

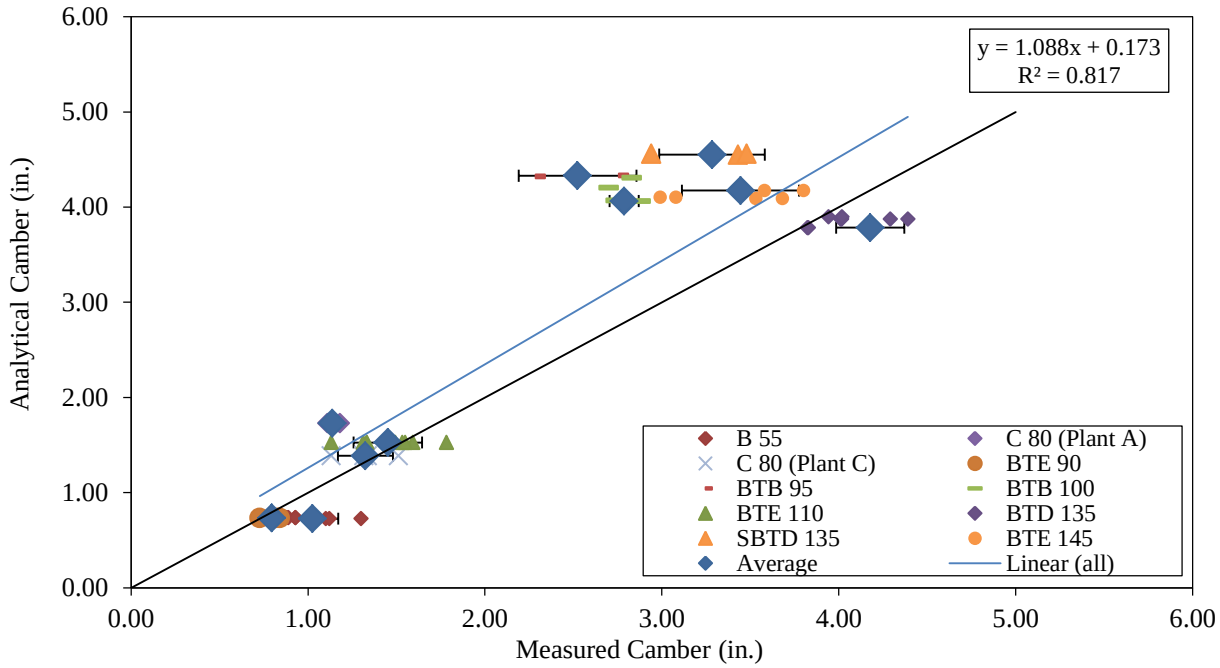

Figure 5.3. Measured camber versus analytical camber using E_{ci} obtained from the creep frames

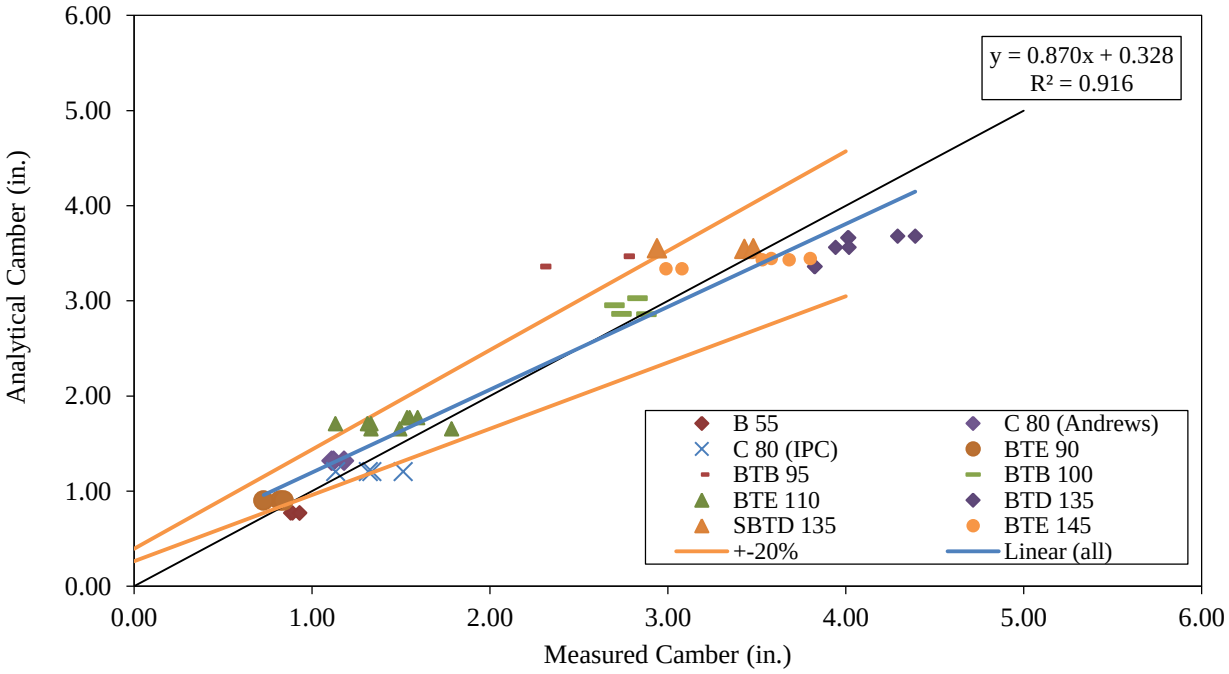

Figure 5.4. Measured versus analytical camber for PPCBs using AASHTO E_{ci} and specific f'_{ci} strengths that correspond to the measured PPCBs

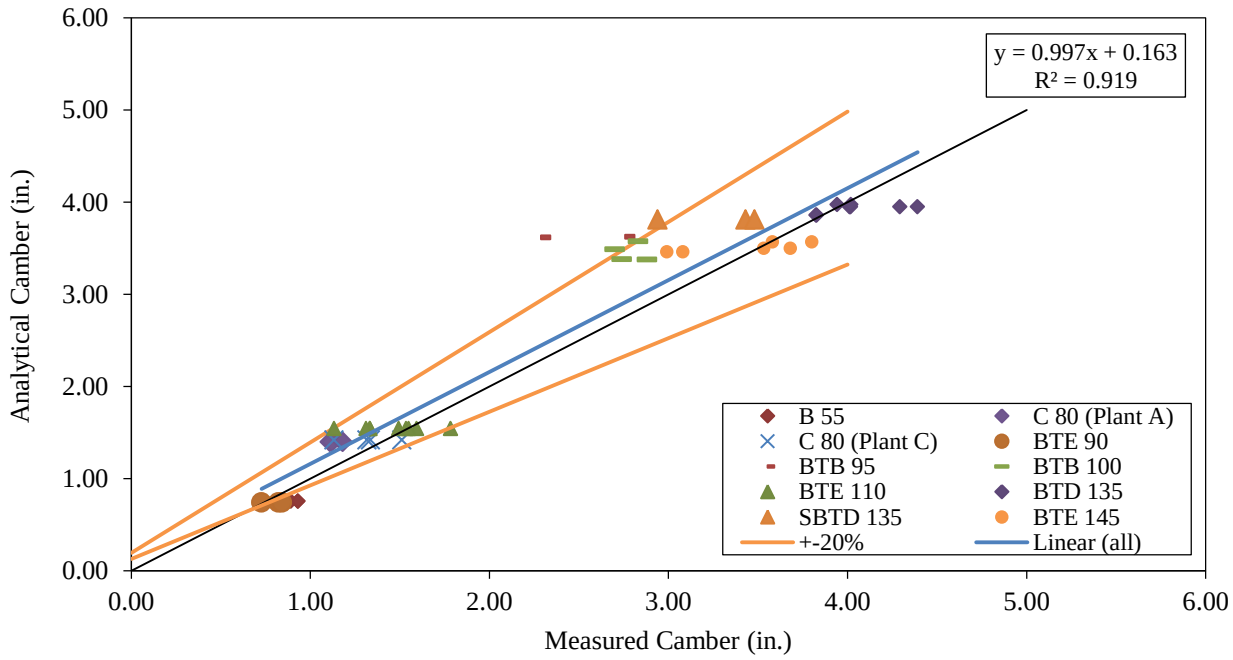

Figure 5.5. Measured versus analytical camber for PPCBs using AASHTO E_{ci} and the release strengths obtained from the samples

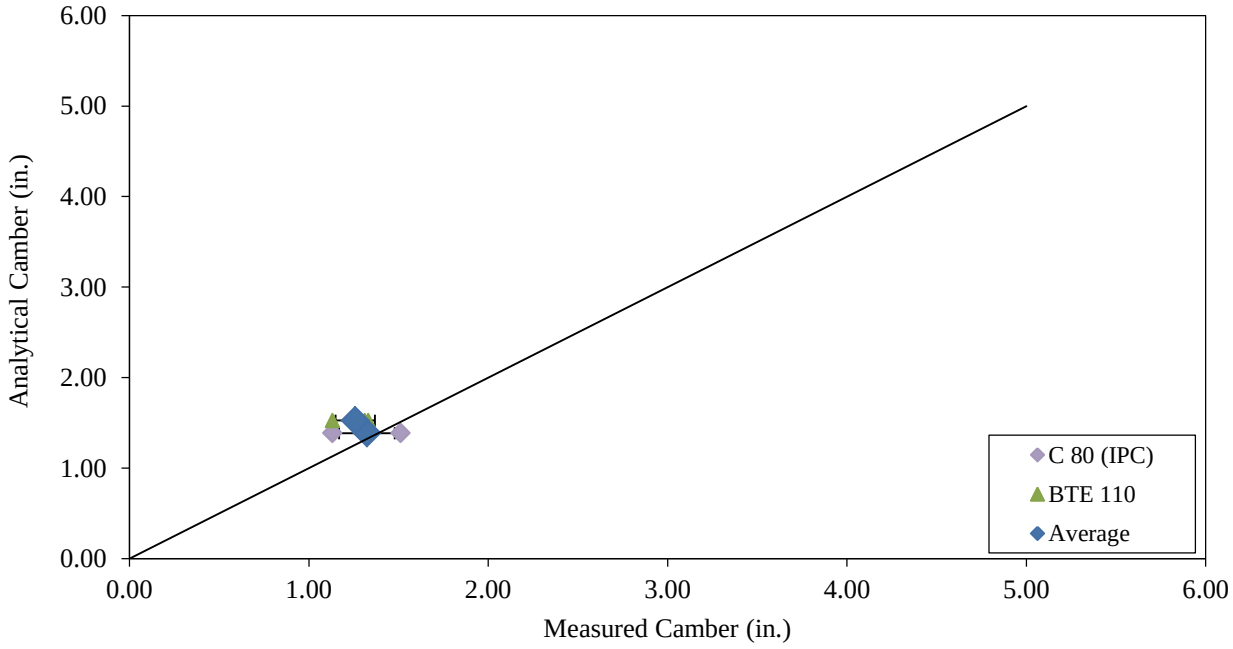

Figure 5.6. Measured camber versus analytical camber using E_{ci} obtained from the creep frames for the selected PPCBs

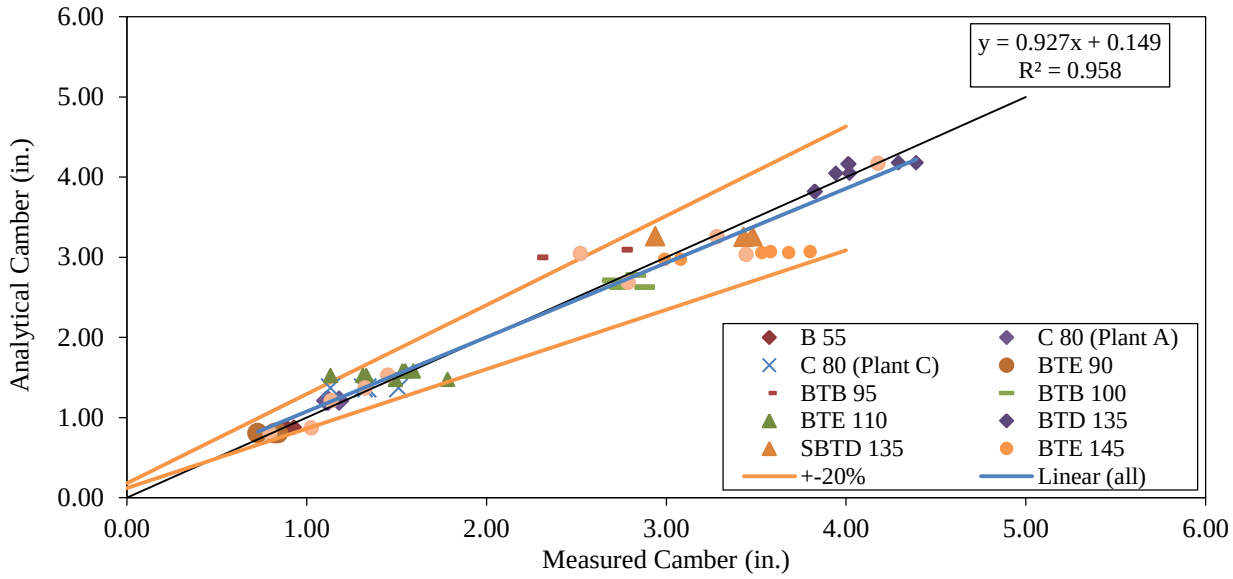

Figure 5.7. Measured camber versus analytical camber when adjusting the camber values based on the averages using AASHTO E_{ci} from the specific PPCB release strengths

In these figures, multiple lines project outward from the vertex. The line that extends at a 45 degree angle from the vertex shows where the measured and predicted cambers should be if the predicted and measured values match exactly with each other. In NCHRP Report 496 (Tadros et al. 2003), it was reported that material properties can cause the AASHTO LRFD (2010) modulus of elasticity to vary by approximately ±20%. The two lines that bound the data are a representation of the range of the AASHTO LRFD (2010) modulus of elasticity if adjusted by ±20%.

The different modulus of elasticity methods that were evaluated include the modulus of elasticity obtained from the creep frames using material samples from the three precast plants (Figure 5.3), the AASHTO LRFD (2010) method with the release strengths that correspond to the specific PPCBs that were measured (Figure 5.4), and the AASHTO LRFD (2010) method using the release strengths obtained from the Iowa State University compressive tests for specific mix designs obtained from the precasting plants (Figure 5.5). The measured and calculated instantaneous camber values resulting from the modulus of elasticity obtained from the creep frames that correspond to specific mix designs used at the three observed precast plants had an agreement of 91.2% ± 19.5% (Figure 5.3). The measured and calculated camber values resulting from the AASHTO LRFD (2010) method with the release strengths specific to the measured PPCBs had an agreement of 98.2% ± 14.9% (Figure 5.4). The AASHTO LRFD (2010) modulus of elasticity method using the release strengths obtained from the researchers after a sample of three cylinders was broken gave an agreement between the measured and calculated camber values of 95.6% ± 14.1% (Figure 5.5).

For the three methods that were compared, the AASHTO LRFD (2010) method using the release strengths that correspond to the measured PPCBs gave the best results. Calculating the E_{ci} value obtained from the creep frames of the concrete mixes obtained from the three precast plants

produced the least accurate results relative to the other two methods. Applying the material properties obtained from the creep frames for the specific mixes to a large range of PPCBs that use a wide variety of mixes may contribute to the discrepancy between the designed and the measured camber. When eliminating PPCBs that were not composed of the specific mix design that was used to obtain the modulus of elasticity using the creep frames, the agreement was 87.8% ± 10.7% (Figure 5.6). Although the agreement was lower than that found when using the calculated camber from the AASHTO LRFD (2010) method with the release strengths specific to the measured PPCBs, the standard deviation was also lower. This suggests that if plant personnel were to use a multiplier to adjust for the modulus, the scatter in the data could be significantly reduced. A conclusion from these results is that using material properties from specific samples that correspond to the measured values will result in close agreement between the measured and the predicted cambers.

Adjusting the average of the data so that it agrees with the 45 degree line made it possible to evaluate the scatter in the data. By taking the most accurate method for determining the modulus of elasticity to predict the camber, it was possible to adjust the average value of each precast plant by a single multiplier. The results of adjusting the average value by multipliers can be seen in Figure 5.7. When using the multipliers, the agreement between the predicted and the measured camber went from 98.2% to 100%. The standard deviation decreased from 14.9% to 10.4%. When adjusting each plant's data by a single multiplier, it was possible to reduce the scatter and to obtain a closer agreement between the predicted and the measured camber.

5.5 Discrepancies in the Concrete

The factors that affect the behavior of concrete are consistency and maturity. Maturity is dependent on the time and temperature of the specimen during curing. The consistency and maturity are also affected by the precaster's method of producing PPCBs and the uniformity of the materials used. These variables are difficult to predict due to the inconsistencies of concrete. Additionally, the curing conditions of PPCBs and of the cylinders during curing and storage can produce discrepancies between the predicted and actual concrete properties.

5.5.1 The Maturity of the Concrete

Problems resulting from the prediction of material properties from the maturity of the concrete are due to different curing methods, curing temperatures, and curing durations between the test cylinders and the PPCBs to which they correspond. The use of steam or natural curing is dependent on the precaster's preference and the weather conditions at the time of the casting. It has been observed that steam curing is used most of the time. When producing PPCBs, the temperatures are similar for multiple PPCBs cast on the same day on the same precasting bed. Differences in the temperature occur due to the uniformity of the insulating covers used and the placement of the PPCBs. If steam curing is used, the steam is applied to the PPCB underneath the insulated cover. PPCBs that are better insulated will have a higher temperature and reach a greater maturity. The placement of the PPCB will also affect its ability to cure under the same temperatures as other PPCBs. The interior PPCBs may reach greater temperatures due to the heat

from the adjacent PPCBs. The PPCBs cast at the ends of the line may be subject to wind and other thermal effects if not properly insulated, which will affect the maturity of the concrete.

Discrepancies between the properties of the sample cylinders and the concrete PPCBs may also be present. The differences between the sample cylinders and the concrete PPCBs are dependent on the uniformity of the concrete and the maturity of the concrete. The following is the procedure for obtaining sample cylinders and is in accordance with Iowa DOT Materials IM 570 (Iowa DOT 2013a), which states the following:

> For each release and shipping strength a set of three (3) cylinders representing three different portions of the line cast (each end and the center) shall be cast. The average of three (3) cylinders shall be used to determine the minimum strength requirements for either release or shipping.
>
> For either release or shipping strengths the set of cylinders tested shall meet the following requirements.
>
> a. The average strength of the specimens tested shall be equal to or greater than the minimum strength required.
> b. No individual cylinder of the set tested shall have a compressive strength less than 95% of the specified strength.
> c. If both conditions a. & b. are not met after the appropriate curing period, another set of specimens representing the line shall be tested.

The text goes on to mention the curing of concrete test cylinders:

> Concrete strength specimens shall receive the same curing as the cast units. Curing can be accomplished by either steam-cure or sure-cure systems.

The three plants that were included in this study cure 4 in. by 8 in. cylinders with a sure-cure system (see Figure 5.8).

Figure 5.8. Plastic-molded and sure-cured cylinders

The sure-cure system uses temperature sensors placed in the interior of the precast PPCB to regulate the temperature of the cylinders. The advantages of this system are that the precasters can keep track of the internal temperature of the PPCB and adjust the steam based on the desired temperature during the curing. This allows the PPCBs to mature more quickly and reach higher strengths within a shorter amount of time, which prevents the precaster's schedule from being hindered.

A disadvantage of the sure-cure system is that the cylinders may have a higher maturity than the PPCBs to which they correspond. One reason the discrepancies occur between the maturities of the PPCB and the sample cylinder is the placement of the sure-cure sensor in the PPCB. If the sensor is placed closer to the steam on the precast bed, the temperature at the sensor will be higher than in the rest of the PPCB. The cylinder will then be heated to the same temperature as the sensor, and the maturity of the concrete cylinder will be greater than that of the PPCB. Another reason the maturity between the sample cylinders and the PPCBs may be different is the different volume-to-surface ratios. A 4 in. by 8 in. cylinder has a smaller volume-to-surface ratio than a PPCB. When a sure-cured cylinder is heated, the temperature is regulated by a mold that heats the outside of the cylinder. The smaller amount of concrete volume in the cylinder will reach a greater maturity than the PPCB and ultimately misrepresent the strength of the concrete in the PPCB. Relying on the compressive strengths of the cylinders that have a greater maturity than the PPCB can produce inconsistencies in the release strength and, ultimately, the modulus of elasticity.

Naturally cured cylinders are also used to determine the compressive strengths of the concrete. The accuracy of the compressive strength of a naturally cured cylinder can also be misrepresented. Naturally cured concrete cylinders are cured with the concrete PPCBs under the tarps or insulated covers. Because the quality control personnel need to determine the

compressive strength before uncovering the PPCB and removing the molds, cylinders are typically placed in areas where they are easily accessible. Potential problems arise when the cylinders are placed in areas that are not as insulated as the rest of the PPCB. Cylinders that are not heated to the same temperatures as the PPCB will misrepresent the PPCB because the cylinders have a lower concrete maturity than the PPCB.

The duration of curing may also differ between the sample cylinders and the PPCBs. Sample cylinders are broken prior to the workers releasing the PPCBs. The additional time it takes workers to release the PPCBs when the release strengths are met can range from zero to four hours. The additional time the PPCB has to cure will increase the maturity of the PPCB and misrepresent the correlation between the sample cylinder and PPCB.

5.5.2 Uniformity of the Concrete

The consistency of a mix design is dependent on the materials and the ability of the quality control personnel to regulate each batch of concrete. The materials may be unique for each batch depending on the uniformity of the properties of the materials or the consistency of the quantity of the materials in each batch. The properties of the materials include the moisture content of the aggregate, the shape of the coarse and fine aggregate, and the hardness of the aggregate. The quantities of each material and the special additives can differ slightly from each batch. Both the consistency and quantity of the materials can influence the strength, the amount of creep and shrinkage that will be present, and other factors that affect the camber of a PPCB.

Errors that occur when relating the cylinder's concrete properties to the PPCB's concrete properties are due to the consistency of the concrete between different batches in the same and adjacent PPCBs. When placing the concrete, some PPCBs require multiple batches to complete the PPCB. Although the quality control personnel monitor the consistency of the batches, there is the possibility that the batches may be inconsistent. Different consistencies between batches will affect the behavior of the PPCB, and, depending on when the sample cylinders are obtained and from what batch, they may detract from the ability to predict the camber.

Another area of concern is the disturbance to the concrete samples relative to the PPCBs that were left to cure without any duisturbances. The concrete samples that are cured near the PPCBs are typically handled before they are taken to the laboratory to be tested. Although the simple task of transporting the cylinders to the quality control room seems insignificant, handling the cylinders may cause them to break earlier than expected.

Modeling the material properties of the PPCBs based on the test cylinders is a challenging task due to the numerous variables that differ between the two. Although small changes in the curing, the concrete batches, and the testing seem insignificant, they can influence the analytical variables used to predict the camber. It is important to recognize the sources of error in sample cylinders and realize that the behavior of cylinders, as well as PPCBs, may differ from one to the other.

5.6 Discrepancies in PPCBs Cast and Released on the Same Day

The measured camber will often vary between identical PPCBs. Multiple variables can contribute to the inconsistencies between the measured values. It is believed that the measured cambers for the PPCBs cast on the same bed on the same day vary less than those of PPCBs cast on different days on different precasting beds. Variables that affect the consistency of the camber for the PPCBs cast on the same day include the prestress force, the prestress losses, and the maturity of the concrete. The following examples explain why discrepancies between the precast PPCBs cast together may have different camber values.

Six BTE 145s were cast at one plant. All of the PPCBs were installed on the same bridge and were designed to have the same camber. The bed dimensions allowed the precaster to produce two PPCBs at a time. Information related to the six PPCBs is listed in Table 5.2.

Table 5.2. PPCBs' measured instantaneous camber and dates of casting and release

PPCB	Casting Date	Released Date	Instantaneous Camber (in.)
BTE 145	6/26/2012	6/27/2012	3.80
BTE 145	6/26/2012	6/27/2012	3.58
BTE 145	6/28/2012	6/29/2012	3.53
BTE 145	6/28/2012	6/29/2012	3.68
BTE 145	7/24/2012	7/25/2012	2.99
BTE 145	7/24/2012	7/25/2012	3.08

The results indicate that the PPCBs cast on the same day had closer camber values, but there were differences in the measured values between two PPCBs cast and released on the same date. Additionally, comparing the PPCBs cast on separate dates tends to show a larger range in the camber. The differences in the camber in this case can be attributed to a variation of prestress forces, including the losses; the mix consistency; and the curing conditions.

The mix consistency may also be contributing to the discrepancy among the PPCBs cast on the same day. The bulb-tee 145 PPCBs require 30.4 cubic yards of concrete. The limitations of the precasting plant require that multiple trips be taken to the batch plant to fill each PPCB. Among the multiple batches of concrete that are used, it is possible to have slightly varying material properties, which could affect the camber.

The curing conditions of the PPCBs are certainly different on separate days. The sure-cure system helps regulate the temperature at the desired temperature to accelerate the curing. Depending on the time when the PPCB was cast, the temperature to cure the PPCB can be pushed to the maximum or be maintained at normal conditions to meet the strength requirements before the next day.

A combination of all these factors can exist in the PPCBs cast on the same day and certainly between the PPCBs cast on separate days. The discrepancies in materials and fabrication procedures will cause different measured cambers at the transfer of the prestress.

5.7 Analytical Prediction Variables for PPCBs

The effects of the variation in the material properties on the instantaneous camber predictions were discussed above. In this section, different variables that analytically affect the moment area method are investigated. The contribution of each variable to the estimated instantaneous camber was determined (see Appendices E.1 through E.6). Finally, the analytical camber was calculated for the various PPCBs based on the material properties and the prestress force (see Appendix E.7).

5.7.1 Moment of Inertia

The moment of inertia influences the ability of a PPCB to resist bending. For a PPCB, determining the correct value for the moment of inertia will influence the accuracy of the camber predictions. Because this study is primarily concerned with the prediction of the instantaneous camber, the gross or transformed moment of inertia was appropriate to use because the cross-section was not cracked. The gross moment of inertia was calculated based on the assumption that the entire section was composed of concrete. This assumption can cause a small error because the PPCBs use prestressed and nonprestressed steel. Steel has a higher modulus of elasticity and, therefore, has the ability to undergo greater stresses and strains than concrete. This was accounted for in the transformed moment of inertia because the reinforcement is converted, by the modular ratio, to an equivalent unit that represents the property of the bending in terms of the concrete.

The transformed moment of inertia varies due to the cross-section and to the amount of reinforcement that is present. In the Iowa PPCB standards (Iowa Department of Transportation 2011b), the PPCBs are grouped according to type and arranged according to length. With varying lengths, the amount of prestressed and non prestressed reinforcement will change. The increase in the reinforcement is to account for the additional forces due to the increased span and the amount of loading that a PPCB can withstand. As the amount of reinforcement changes, the transformed moment of inertia will also change. Naaman (2004) states that using the transformed moment of inertia is acceptable on members with bonded tendons, although the additional calculations do not result in increased accuracy.

Complications when determining the transformed moment of inertia can occur due to the use of harped prestressing strands. Harped strands are prestressing reinforcements that start at one elevation and change throughout the length of the PPCB. The Iowa DOT uses PPCBs that are doubly harped or have two bends in the reinforcement over the length of the PPCB. Due to the varying height of the harped reinforcement over the length of the PPCB, the transformed moment of inertia will change over the length of the PPCB. Taking a weighted average of the transformed moment of inertia along the length of the PPCB gives an accurate representation of the moment of inertia.

A parametric study investigating the effects of the moment of inertia on the camber was conducted (see Appendix E.3). In this study, the camber was determined based on the gross moment of inertia, the transformed moment of inertia at the ends of the PPCB, the transformed moment of inertia at the midspan of the PPCB, and the transformed moment of inertia over the whole length of the PPCB. Holding all other variables fixed, the effects of the moment of inertia can be seen in Figure 5.9. Additionally, the calculated camber using the different moment of inertia values is presented in Table 5.3.

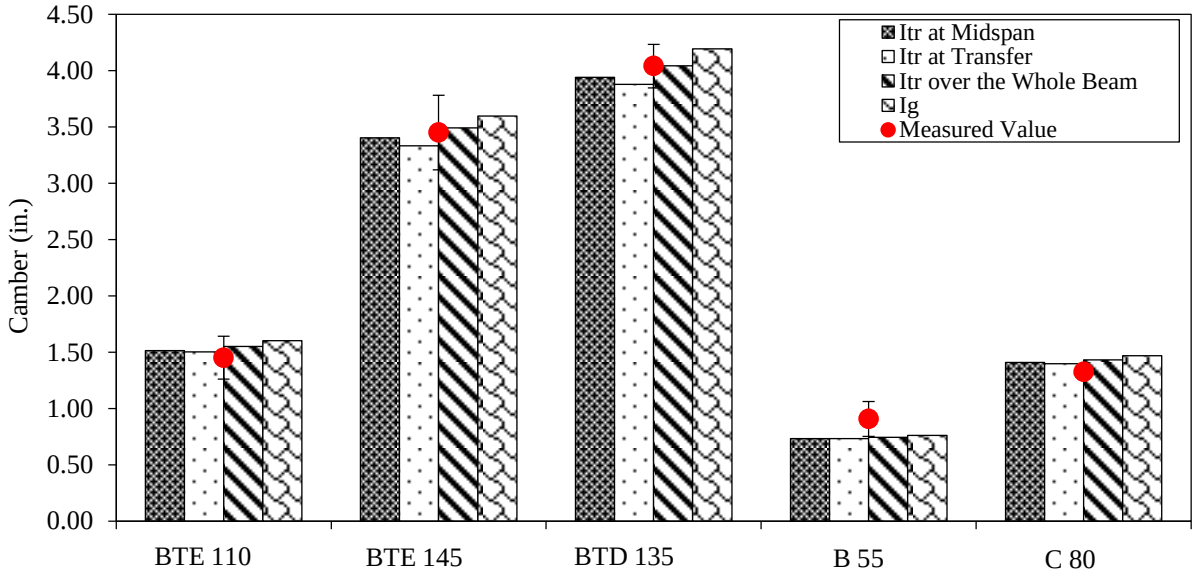

Figure 5.9. Comparison of camber using different moment of inertia values

Table 5.3. Camber of five PPCBs with different moment of inertia values

PPCB	Camber (in.)			
	I_{tr} along the length of the PPCB	I_{tr} at Midspan	I_{tr} at End	I_g
B55	0.74	0.73	0.73	0.76
C80	1.43	1.41	1.40	1.47
BTE 110	1.55	1.52	1.50	1.60
BTD 135	4.04	3.94	3.88	4.19
BTE 145	3.49	3.40	3.33	3.60

The most accurate variable in Figure 5.9 is the transformed moment of inertia (I_{tr}) along the length of the section. Comparing the I_g, I_{tr} at the PPCB ends, I_{tr} at the midspan, and I_{tr} along the length of the PPCB gives the camber comparisons for the five PPCBs. It should be noted that different PPCBs have different quantities of the harped and straight reinforcement. The variation of the prestressed reinforcement can change the difference that is observed between the transformed moment of inertia across the whole section and other moment of inertia values.

The results show that I_g has a 2.9% difference when compared to I_{tr} along the length of the PPCB. This is because I_{tr} is a larger value due to the rigidity of the reinforcement. Accounting

for the rigidity of the reinforcement will produce less bending, which will result in a lower camber than when using I_g. Another trend is the transformed moment of inertia along the length of the PPCB, which agrees closely with the measured camber value. Taking the moment of inertia along the length of the PPCB compared to the gross moment of inertia is believed to accurately represent the reinforcement that is present. Additionally, the close agreement among the measured values led the researchers to calculate the instantaneous camber on multiple PPCBs using the corresponding transformed moment of inertia along the length of the PPCB.

5.7.2 Prestress Force

The force of the prestress that is applied to the PPCB is an important variable in predicting the camber. The amount of the prestress force per strand, the total amount of the prestress force per PPCB, and the prestress material properties are dictated by the Iowa DOT. The specified prestressing strands are ASTM A416 grade 270, 0.6 in., low-relaxation prestressing strands. Equations 5-1 and 5-2 show the steps in calculating the designed prestress force per strand and per PPCB.

$$72.6\% \times f_{pu} = 72.6 \times 270 \text{ ksi} = 196.02 \text{ ksi} \quad \textbf{(5-1)}$$

$$\text{Stress} \times \text{Area} = 196.02 \text{ ksi} \times 0.217 \text{ in}^2 = 42.53 \text{ kips/strand} \quad \textbf{(5-2)}$$

The prestress force that is specified in the Iowa PPCB standard represents the force of the prestress before the transfer of the prestress. Therefore, the seating losses along with the relaxation losses from the time of the jacking to immediately after the release would be included. Tolerances set by the Iowa DOT restrict precasters to fabricating the PPCBs within ± 5% of the designed prestress force. A comparison of the designed prestress force and the as-built tensioning force recorded by the precasters for the specific PPCBs is summarized in Table 5.4 and in Appendix E.4.

Table 5.4. Summary of the designed versus the tensioned prestress from 41 PPCBs

	Difference of Designed and Tensioned Prestress (kip)	Ratio (Tensioned Prestress/ Designed Prestress)
Average	-11.036	1.009
Standard Deviation	33.909	0.025
Minimum	40.370	1.089
Maximum	-87.845	0.962
Plant A	-19.567	1.007
Plant B	-10.619	1.006
Plant C	-0.975	1.011

The results show that the averages of 41 PPCBs that were investigated have an agreement of 100.9% ± 2.5% and fall within the ± 5% tolerance that is accepted. However, when looking at individual PPCBs, the maximum and minimum values are +8.9% and -3.8%, respectively. The maximum applied ratio of the applied-to-designed prestress force of 8.9% lies outside of the allowable tolerance of ± 5% for the Iowa PPCBs.

5.7.2.1 Tensioning Procedure

In the tensioning process, the top sacrificial prestressing strands are completed first. The number of top sacrificial prestressing strands is determined by the PPCB specifications but can range from two to six strands tensioned with a single jack to the pressure of 3 to 5 kips in each strand. Once the top sacrificial strands are tensioned, the harped strands, if any, are laid out along the length of the bed. Initially, the harped strands are positioned to the elevation of the final height near the end of the PPCB line. An example of this can be seen in Figure 5.10.

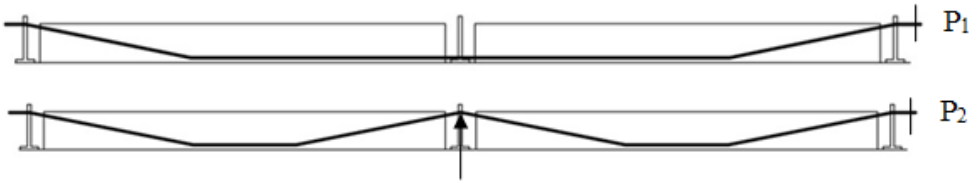

Figure 5.10. Initial and final positions of the harped prestressing strands when tensioning

While in this position, the strands are tensioned to an initial value, which is less than the final prestress force (P_1 in Figure 5.10). Mechanical means of raising the interior harped strands at the end of every PPCB are then used.

As a result of raising the interior harped supports to the final location where the prestressing strand was positioned in Figure 5.10, additional prestress force is added. The total amount of the prestress force present in the harped strands is determined by adding the prestress force before the interior supports were raised with the additional prestress force caused by the elongation from raising the harped supports to their final location.

The method of tensioning the straight bottom strands is unique to each precaster. It has been observed that some precasters use a multi-pull jack that has the ability to tension multiple prestressing strands to the desired tension. Other precasters use a single prestressing jack to tension all of the bottom strands. The Iowa DOT requires strands to be pulled to an elongation and then checked with a gauge reading to verify the correct prestress force. It has been observed that precasters pull the prestressing strands to a minimal force of approximately 3 kips as a reference point for the start of the elongation. After the initial pull to 3 kips, the precasters are able to mark the initial distance and tension the prestressing strands until the designed elongation is reached.

5.7.3 Prestress Losses

The instantaneous prestress losses result from elastic shortening and seating. At the time of the instantaneous losses, some relaxation has occurred from the time between the initial stressing of the prestressing strands to the transfer of the prestress. A combination of the instantaneous losses and the relaxation that is present can be calculated and subtracted from the initial prestress force obtained from the tensioning sheets to determine the effective prestress force. When calculating the instantaneous camber for the PPCBs in this section, prestress losses caused by the creep and shrinkage of the concrete were not considered. During the time when the PPCB was fabricated until the time when it was released, there was no load applied. After the transfer of the prestress, the PPCB was axially loaded through the prestressing stands and was subjected to self-weight and prestress moments. The instantaneous camber measurements occurred immediately after the transfer of the prestress, which allowed the researchers to neglect the effects of the creep of the concrete during this time period. The curing duration for a PPCB is typically 18 to 24 hours. During this time, the concrete is usually steam-cured in a moist environment. Due to the curing conditions, it is assumed that minimal shrinkage of the concrete occurs and can be ignored in calculating the camber at the transfer of the prestress.

A parametric study was conducted to determine the effect of prestress losses on the camber. When determining the prestress force, tensioning sheets from the precasters were used to get the initial jacking force of the prestressing strands on specific PPCBs. Using the initial jacking force and the methods that coincide with Section 2.2.4, the magnitude of the prestress that was lost due to the elastic shortening, seating, and relaxation was calculated. Losses to elastic shortening were calculated based on the equation presented in Section 2.2.4.1.1. Seating losses were calculated in accordance with Section 2.2.4.2. Also, for the distance of seating (Δ), which is typically between the values of 0.125 in. and 0.375 in., depending on the type of the anchorage, a value of 0.23 was used, which corresponded to the distance of the seating for the wedge commonly used by precasters. Eventually, losses due to the strand relaxation between the time of tensioning and release were calculated according to Section 2.2.4.3. Then, the prestress force before and after the prestress losses was used to compare the effect of the prestress losses on the camber. The results in Table 5.5 show the prestress and the camber values before and after the prestress losses. Additionally, the ratio of the prestress and the camber before and after the prestress losses is shown.

Table 5.5. Comparison of the prestress and the camber with and without the prestress losses

PPCBs	Prestress Force Before Losses (kip)	Prestress Force After Losses (kip)	Difference in Prestress without and with losses (kip)	((Prestress with Losses/Prestress without Losses)-1)*100	Camber with Losses (in.)	Camber without Losses (in.)	((Camber with Losses/Camber without Losses)-1)*100
BTE 145	2,211.57	2,040.32	171.25	8.39	3.43	4.00	-14.21
BTE 110	1,292.82	1,199.71	93.11	7.76	1.77	1.99	-11.25
BTD 135	2,332.50	2,154.74	177.76	8.25	3.56	4.16	-14.50
B 55	519.46	490.73	28.73	5.85	0.77	0.83	-7.20
C 80	950.58	902.42	48.16	5.34	1.32	1.44	-8.46
BTE 90	870.06	816.78	53.28	6.52	0.90	0.99	-8.90
BTB 95-3 Days Curing	1,867.66	1,721.75	145.91	8.47	3.36	3.83	-12.28
D 55	523.91	499.21	24.70	4.95	0.19	0.20	-7.88
D 60	620.62	585.95	34.67	5.92	0.30	0.33	-9.12
D 90	924.09	876.09	48.00	5.48	1.24	1.36	-8.96
D 105	1,405.79	1,307.76	98.03	7.50	2.20	2.48	-11.45
C 67	795.60	740.33	55.28	7.47	0.75	0.85	-11.02
BTD 130-2 Days Curing	2,337.81	2,161.67	176.14	8.15	3.75	4.33	-13.50
BTB 100-2 Days Curing	1,881.35	1,800.11	81.24	4.51	3.03	3.43	-11.67
D110-1 Day Curing	1,477.22	1,371.79	105.43	7.69	2.44	2.78	-12.22
BTE 135-3 Days Curing	2,031.72	1,875.80	155.92	8.31	2.86	3.32	-13.96
SBTD 135-3 Days Curing	2,327.60	2,158.19	169.41	7.85	3.55	4.13	-14.09
BTC 120-1 Day Curing	2,229.30	2,070.34	158.96	7.68	3.61	4.16	-13.38
Average				**7.00**			**-11.34**
Maximum				**8.47**			**-7.20**
Minimum				**4.51**			**-14.50**

The results in Table 5.5 indicate that the average ratio of the prestress losses is 7.3%. However, the 7.3% ratio of the losses affects the camber by 11.9%, on average. By evaluating 43 PPCBs, the researchers found that the PPCBs have the capability of having a reduced camber by as much as 15.0% if the prestress losses are not accounted for (see Appendix E.5).

5.7.4 Sacrificial Prestressing Reinforcement

The Iowa DOT specifications require reinforcement in the top flange of the PPCBs. Installing a nonprestressed reinforcement along the entire length of the PPCB to the correct height is time-consuming and requires a lap splice between two nonprestressed reinforcing bars. Instead of using nonprestressed reinforcement, precasters often used two to six strands of prestressed reinforcement tensioned from 3–5 kips along the top flange of the PPCB. The advantages of using the prestressed reinforcement along the top flange include the ease of the fabrication, the close tolerances that can be achieved, the reduced reinforcement with no lap splices, and the

ability to hang shear stirrups, lifting hooks, and other non prestressed reinforcements along the length of the PPCB.

When determining the analytical camber, accounting for the sacrificial strands has been observed to contribute an additional 2.6% to the final camber value, on average. On specific PPCBs, the contribution to the camber can be as high as 6.7% or as low as 0.7%. The contribution of the sacrificial prestressing strands to the camber is affected by the amount of sacrificial prestressing strands present, the sacrificial prestressing strand force, and the eccentricity of the sacrificial prestressing strands to the center of gravity of the cross-section. Table 5.6 shows 20 PPCBs with the camber calculated with and without the sacrificial prestressing strands. The difference, the percent difference, and the ratio between including and excluding the effect of the sacrificial strands are also given.

Table 5.6. Percent difference and the contribution to the camber with and without sacrificial prestressing strands

PPCB	Camber with Sacrificial Strands (in.)	Camber without Sacrificial Strands (in.)	Difference in Camber Between No Sacrificial Strands and Sacrificial Strands (in.)	Percent Difference	(Camber without Sacrificial Prestressing Strands/Camber with Sacrificial Prestressing Strands)*100
BTE 145	3.33	3.49	0.154	4.50	104.61
BTE 145	3.44	3.47	0.026	0.75	100.75
BTE 145	3.43	3.54	0.111	3.18	103.23
BTE 110	1.77	1.84	0.073	4.05	104.13
BTD 135	3.68	3.73	0.054	1.45	101.46
B 55	0.76	0.78	0.029	3.72	103.79
C 80	1.19	1.24	0.053	4.31	104.40
C 80	1.32	1.35	0.030	2.26	102.29
BTE 90	0.90	0.96	0.060	6.46	106.67
BTE 155-1 Day Curing	3.95	4.02	0.078	1.97	101.99
BTE 155-2 Day Curing	3.91	3.99	0.080	2.02	102.04
BTE 155-3 Day Curing	3.64	3.72	0.080	2.17	102.20
BTB 95	3.47	3.56	0.095	2.70	102.73
D 90	1.24	1.27	0.027	2.12	102.14
D 105	2.20	2.23	0.029	1.32	101.33
BTB 100	3.03	3.09	0.063	2.06	102.08
D110	2.37	2.40	0.031	1.32	101.33
BTE 135	2.86	2.91	0.053	1.84	101.86
SBTD 135	3.54	3.61	0.062	1.73	101.75
BTC 120	3.61	3.67	0.061	1.69	101.70
		Average		**2.58**	**102.62**
		Maximum		**6.46**	**106.67**
		Minimum		**0.75**	**100.75**
		Plant A		**1.82**	**101.83**
		Plant B		**3.09**	**103.15**
		Plant C		**2.58**	**102.63**

There are cases where multiple PPCBs of the same cross-section and length are listed multiple times. These are instances that apply to specific PPCBs that were cast and released on different days from each other. Note that the prestressing force, the prestress losses, and the material properties may differ between PPCBs of the same cross-section and length.

5.7.5 Transfer Length

The transfer length is the distance required for the prestressing strand to transfer the effective prestress force to the concrete. The force on the PPCB end is assumed to be zero and increases rapidly until it fully develops into the effective prestress force at the transfer length distance. The transfer length is affected by the ability of the concrete to bond to the tensioned prestressing strand. Factors that influence the ability for a prestressing strand to bond are the amount of prestress force applied to the prestressing steel, the maturity of the concrete, and the mechanical bond that is created from the geometry of the prestressing strand. Additionally, factors that affect the camber are the effective prestressing force per strand, the method used to predict the transfer length, the length of the PPCB, and the number of prestressing strands.

There are multiple methods to predict the transfer length. The researchers compared the cambers obtained using two methods to predict the transfer length on five different types of PPCBs (Table 5.7).

Table 5.7. Comparison of the AASHTO LRFD and ACI transfer length methods

PPCB	Method Used	Transfer Length (ft)	Camber (in.)	Difference (in.)	Percent Difference
BTE 110	AASHTO LRFD	3.00	1.58		
BTE 110	ACI	3.12	1.58	0.001	0.05
BTE 145	AASHTO LRFD	3.00	3.41		
BTE 145	ACI	3.04	3.41	0.001	0.02
BTD 135	AASHTO LRFD	3.00	4.19		
BTD 135	ACI	3.03	4.19	0.001	0.03
C 80	AASHTO LRFD	3.00	1.38		
C 80	ACI	3.10	1.38	0.001	0.10
B 55	AASHTO LRFD	3.00	0.67		
B 55	ACI	3.03	0.67	0.001	0.13

The methods that were compared were the AASHTO LRFD (2010) transfer length and the ACI 318-11 (2011) transfer length. Holding other variables the same, it was possible to determine the difference in the camber when using the two different transfer length prediction methods. The results show that the percent difference between the two methods is 0.6% ± 0.1%. Due to the small differences between the calculated camber using AASHTO LRFD (2010) and ACI 318-11 (2011), it was concluded that AASHTO LRFD (2010) be used for the remaining transfer length calculations. In addition to the small difference between the two methods, AASHTO LRFD (2010) is currently used by the Iowa DOT for camber calculations.

The researchers were able to analytically predict the camber with and without the transfer length for multiple PPCBs. Conducting a parametric study allowed the effects of the transfer length to be quantified and the percent difference to be calculated. The PPCBs analyzed consisted of bulb-tee and AASHTO PPCBs. The lengths ranged from 46.33 to 156.33 ft. The results of analytically determining the camber with and without the transfer length are shown in Table 5.8.

Table 5.8. Comparison of the camber with and without the transfer length

PPCBs	Calculated Camber with Transfer Length (in.)	Calculated Camber without Transfer Length (in.)	Camber with Transfer Length/ Camber without Transfer Length)*100	Difference (in.)	Percent Difference
BTE 145	3.33	3.37	98.82	-0.040	-1.19
BTE 145	3.44	3.48	98.84	-0.040	-1.16
BTE 145	3.43	3.47	98.83	-0.041	-1.18
BTE 110	1.77	1.79	98.95	-0.019	-1.05
BTD 135	3.36	3.41	98.55	-0.049	-1.46
BTD 135	3.68	3.73	98.54	-0.055	-1.47
BTD 135	3.66	3.72	98.54	-0.054	-1.47
BTD 135	3.56	3.61	98.56	-0.052	-1.45
B 55	0.76	0.78	96.95	-0.024	-3.10
B 55	0.77	0.80	96.96	-0.024	-3.08
C 80	1.19	1.22	97.63	-0.029	-2.40
C 80	1.32	1.35	97.68	-0.031	-2.34
BTE 90	0.90	0.91	98.92	-0.010	-1.09
BTE 155	3.95	4.00	98.73	-0.051	-1.28
BTB 95	3.47	3.52	98.47	-0.054	-1.54
D 55	0.19	0.19	99.34	-0.001	-0.66
D 60	0.30	0.30	99.45	-0.002	-0.55
D 90	1.24	1.27	97.79	-0.028	-2.23
D 90	1.25	1.28	97.77	-0.029	-2.25
D 105	2.20	2.23	98.57	-0.032	-1.44
D 106	2.50	2.53	98.54	-0.037	-1.47
C 67	0.75	0.76	99.58	-0.003	-0.42
BTC 45	0.20	0.20	99.22	-0.002	-0.78
BTD 130	3.75	3.80	98.71	-0.049	-1.30
BTB 100	3.03	3.08	98.36	-0.050	-1.65
D110	2.44	2.47	98.7	-0.032	-1.31
BTE 135	2.86	2.89	98.91	-0.032	-1.10
BTC 120	3.61	3.66	98.55	-0.053	-1.46
Average	**2.24**	**2.27**	**98.52**	**-0.033**	**-1.50**
Minimum	**0.19**	**0.19**	**96.95**	**-0.055**	**-3.10**
Maximum	**3.95**	**4.00**	**99.58**	**-0.001**	**-0.42**
Plant A	**2.46**	**2.49**	**98.59**	**-0.036**	**-1.42**
Plant B	**2.68**	**2.72**	**98.78**	**-0.035**	**-1.23**
Plant C	**1.76**	**1.79**	**98.33**	**-0.029**	**-1.69**

Multiple PPCBs of an identical design were analyzed using the AASHTO equation for the transfer length (Equation 4-12). The differences between the identical PPCBs are due to the applied prestress force, the modulus of elasticity for a specific PPCB, and the curing duration. The results for the other PPCBs can be found in Appendix E.6.

Evaluating the results from Table 5.8 revealed the effects of the transfer length on the camber calculations. The results include the following:

- As the PPCB length increases, the impact on the camber due to the transfer length decreases.
- The contribution of the camber due to the transfer length is dependent on the amount of prestress force in the PPCB.

Utilizing the full potential of the prestressing strands requires that designers tension each strand to its specified capacity regardless of the PPCB length to maximize efficiency. Because prestressing strands in shorter PPCBs have the same or a similar stress applied per prestressing strand as long PPCBs, the transfer length will be comparable between short and long PPCBs. However, the length of the PPCB will influence how much the final camber is affected by the transfer length. When calculating the camber, ignoring the prestress force over a short PPCB will be more significant than ignoring the same length over a long PPCB. For example, ignoring three ft of the transfer length on a PPCB that is 56 ft long will have more impact on the camber than ignoring the same transfer length over a PPCB that is 156 ft long.

Another result was that some shorter PPCBs experienced a smaller impact on the camber due to the transfer length than longer PPCBs. This can be related to the amount of prestress force that was present in the PPCBs. A BTE 110 has fewer prestressing strands, which will result in lower compressive forces acting along the length of the PPCB than a BTE 145 or a BTD 135. It is assumed that the same distance is required to reach the effective prestressing in each of these PPCBs. Because the total force that is reached in the BTE 110 is significantly less than that in the BTE 145 and the BTD 135, the effect of the transfer length is also less significant. These results from Table 5.8 prove that the effect the transfer length has on the camber can be related to the length of the PPCB and the effective prestressing force.

5.8 Impact of the Assumptions during the Design of the Instantaneous Camber

The variables that affect the instantaneous camber design include material properties and design procedures. The material properties include the modulus of elasticity, while the design procedures include the prestress force, the prestress losses, the transfer length, the sacrificial prestressing strands, and the moment of inertia. Correctly modeling the material properties and the design procedures will result in an agreement with the measured instantaneous camber when measured correctly. The percent difference among various designed camber values was calculated by conducting a parametric study, which determined the effect of each variable and how it affects the camber. Calculating the camber based on using the designed camber variables and the variables that are representative of the PPCB are summarized in Table 5.9.

Table 5.9. Extent of variation in the instantaneous camber due to the design variables and material properties

Analytical Variable	Average Percent Difference	Maximum Percent Difference	Minimum Percent Difference
Modulus of Elasticity based on the designed f'_{ci} versus measured f'_{ci}	-14.7	-0.1	-28.9
Applied Prestress Force versus Designed Prestress Force	11.5	16.2	7.2
Prestress Losses versus No Prestress Losses	13.7	17.6	2.6
AASHTO LRFD (2010) Transfer Length versus No Transfer Length	-1.5	-0.4	-3.4
Sacrificial Prestressing Strands versus No Sacrificial Prestressing Strands	-2.6	-0.8	-6.5
I_{tr} versus I_g	2.9	3.7	2.2

5.9 Conclusions and Recommendations

Predicting the camber has presented challenges due to the need to accurately model the concrete and prestressing steel properties. Relating the calculated camber to the measured camber is dependent on the ability to model the material properties and the actual conditions of the PPCB. The instantaneous camber was predicted based on the minimum specified variables. This calculation included the minimum design release strengths to predict the modulus of elasticity, the designed prestress forces and estimated prestress losses, and the transfer length based on AASHTO LRFD (2010) for the contribution of the sacrificial prestressing strands that was neglected. The instantaneous camber was also predicted for previously constructed PPCBs using variables that were accurate for the material properties of the PPCBs. Comparisons between the analytical predictions of the camber using the properties used in the design and the properties based on the previously cast PPCBs resulted in different instantaneous camber values. The analytical camber predictions were also compared to the camber that was measured on over 105 PPCBs. Additionally, a parametric study was conducted that compared the effects of neglecting different variables. Based on the analytical camber predictions and the parametric study, the following conclusions can be made about the analytical camber prediction and the accuracy of the material properties that are used:

- The modulus of elasticity using the equation in AASHTO LRFD (2010) provides 98.2% ± 14.9% agreement with the measured camber values when using the specific unit weight and release strengths corresponding to the specific PPCBs.
- A multiplier was used to adjust the analytical camber to the measured camber. This resulted in a 100% agreement with a standard deviation of 10.4%. The standard deviation of 10.4% can be attributed to the inconsistent material properties and the fabrication procedures.
- The AASHTO LRFD (2010) modulus of elasticity is dependent on the designed release strength. The release strength is higher than the design strength by 39.5% and 11.5% for PPCBs with a designed release strength of 4500–5500 psi and 6000–8500 psi, respectively.

Conducting a parametric study on the variables that affect the instantaneous camber resulted in the following conclusions:

- The designed prestress force has an agreement with the precasters' applied prestress force value of 100.9% ± 2.5%, as shown in an evaluation of 41 PPCBs.
- It was found that 34% of PPCBs fell outside the ± 5% tolerance set by the Iowa DOT for the applied prestress versus the designed prestress force. The maximum and minimum ratios of the applied to the designed prestress force were 108.9% and 96.2%, respectively.
- The sacrificial prestressing strands are affected by the prestress force and the eccentricity from the strands to the center of gravity of the section. On average, this affects the camber by 2.6%. Ignoring the sacrificial prestressing strands can contribute to an error of up to 6.7%.
- The prestress losses at the transfer of the prestress include the elastic shortening, the seating losses, and the relaxation. A combination of prestress losses contributes to a reduction in the prestress by 7.0% on average, which reduces the camber on average by 11.3%.
- The moment of inertia can be represented by the transformed section along the length of the PPCB. The transformed moment of inertia along the length of the PPCB compared to the gross moment of inertia will produce instantaneous cambers that have a +2.9% difference from each other.
- Measuring the transfer length using the ACI 318-11 (2011) method and the AASHTO LRFD (2010) method produced an average difference of 0.6% ± 0.1%.
- An average percent difference of -1.50% is present when ignoring the transfer length and using the AASHTO LRFD (2010) method. Ignoring transfer length can contribute to an error of up to 3.1%.

Determining the potential errors and the magnitude of each error allows designers to adjust the design procedures to more accurately predict the instantaneous camber. Improving the instantaneous camber predictions will also improve the at-erection and long-term camber predictions, as described in Chapter 7.

5.9.1 Recommendations for Designers

Methods for predicting the instantaneous camber were studied by the researchers using the moment area method. The following recommendations for designers are made for predicting the instantaneous camber:

- The decrease in the camber due to the transfer length is dependent on the number of prestressing strands and the length of the PPCB. Due to the convenience of its design and accuracy, the AASHTO LRFD (2010) equation for the transfer length should be used.
- The modulus of elasticity is a sensitive variable and can impact the accuracy of the camber. Using the AASHTO LRFD (2010) modulus of elasticity with an accurate release strength and unit weight will improve the camber predictions.
- When calculating the design release camber, designers should increase the design release strength by 40% and 10% for PPCBs with a designed release strength of 4500–5500 psi and 6000–8500 psi, respectively.

- The moment of inertia of the section changes along the length of the PPCB if harped sections are used. Due to the convenience of its design, the gross moment of inertia should be used for the design equations.
- The prestress force is an important variable to which the camber is highly sensitive. A close agreement between the designed and actual prestress force will give a good agreement between the designed and the measured camber.
- Prestress losses have been observed to reduce the initial prestress force by 7.0%. The camber will be affected by 11.3%, on average. Therefore, the prestress losses should be accounted for in the design.
- The sacrificial prestressing strands will reduce the camber by as much as 6.5% and should be taken into account in the instantaneous camber prediction.

It is recognized that all variables may not be accurately adjusted due to the uncertainty of the fabrication and the materials used for constructing the PPCBs. Using the above recommendations will reduce the current error between the designed and measured camber.

CHAPTER 6: LONG-TERM CAMBER PREDICTION USING SIMPLIFIED METHODS

6.1 Introduction

The goal of the research described in this chapter was to find the most accurate simplified method for long-term camber prediction by comparing the results of different simplified methods with the measured camber data. The effects of the errors associated with different parameters, such as the modulus of elasticity, creep and shrinkage, and the prestress force on the camber, are investigated. To evaluate the current camber prediction method, predicted long-term cambers were compared to values obtained by the current Iowa DOT method using Martin's multipliers (1977).

The long-term camber is estimated using simplified methods of analysis such as Tadros' method (2011), Naaman's method (2004), and the incremental method, all of which were discussed in Section 2.3.3. The average sealed creep coefficient and the average sealed shrinkage values, which were proposed in Chapter 3, were used in this process. The transformed section properties were used to conduct related calculations. In addition, the AASHTO LRFD (2010) refined method was used to estimate the long-term prestress losses. Twenty-six PPCBs were analyzed, including three BTC 120 PPCBs produced by plant A, nine BTE 110 PPCBs and six BTE 145 PPCBs produced by plant B, and eight BTD 135 PPCBs produced by plant C. More details about these PPCBs can be found in Appendix F. The analyzed results of the camber calculations were compared with the measured values. It was observed that Naaman's method and the incremental method best predict the camber of PPCBs, and the results of these two methods are similar.

A more robust analytical assessment using a finite element analyses is presented in Chapter 7.

6.2 Tadros' Method

Tadros' method is highly dependent on the release camber, creep coefficient of HPC, and prestress losses. Figure 6.1 and Figure 6.2 show a comparison of the predicted camber and measured camber with and without overhang, respectively.

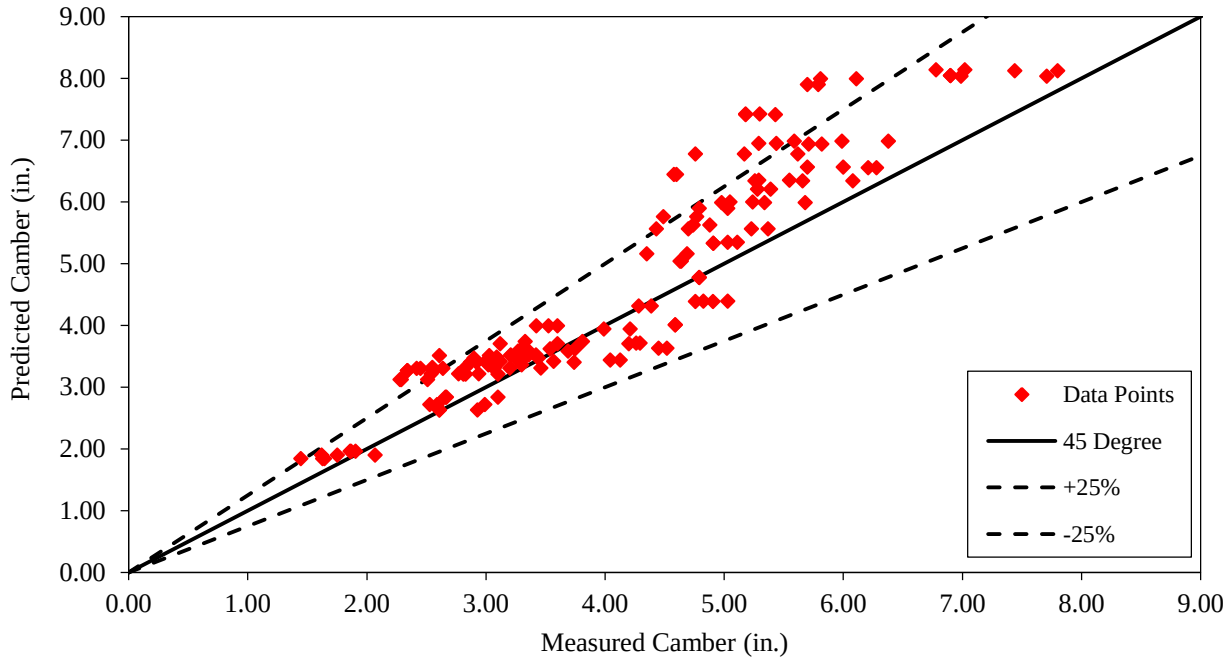

Figure 6.1. Comparison of the predicted camber and the measured camber with overhang using Tadros' method

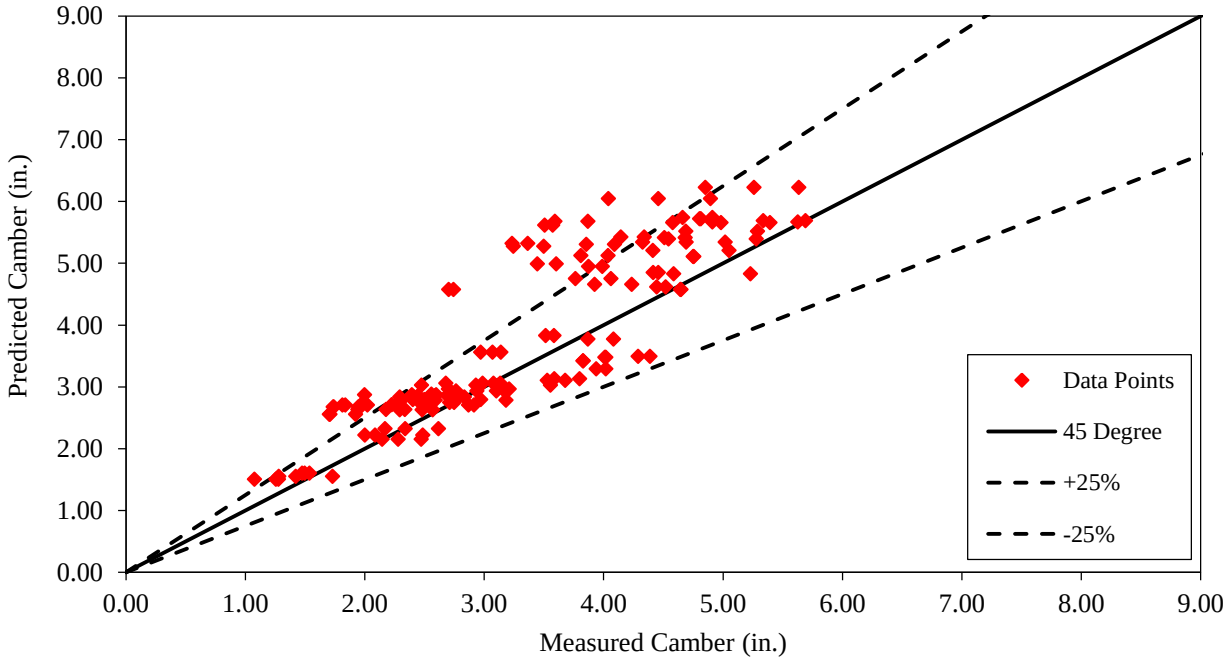

Figure 6.2. Comparison of the predicted camber and the measured camber without overhang using Tadros' method

The release camber calculated using the incremental method is used to predict the long-term camber of PPCBs. It can be seen that the average difference between the camber predicted using

Tadros' method and the measured value was 12% for PPCBs with overhang and 15% for PPCBs without overhang, which means that Tadros' method typically overestimates the long-term camber.

6.3 Naaman's Method

Naaman's method is dependent on the time-dependent prestress forces, the time-dependent modulus of elasticity, and the creep. Figure 6.3 and Figure 6.4 show a comparison of the predicted camber and the measured camber with and without overhang, respectively.

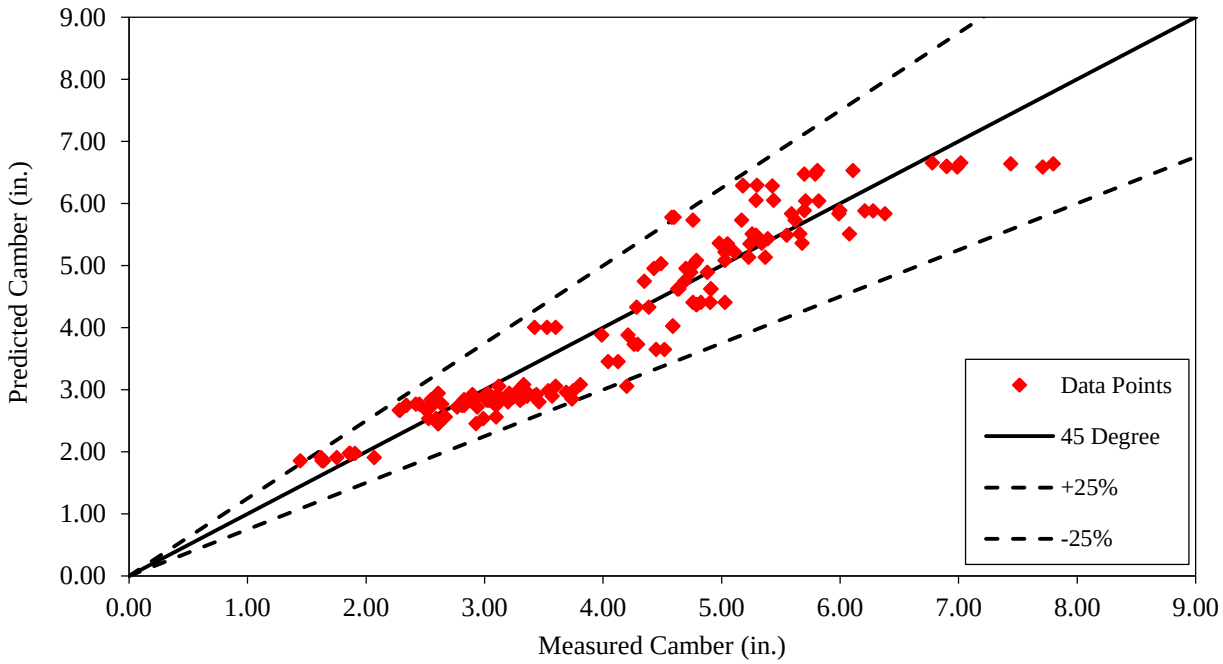

Figure 6.3. Comparison of the predicted camber and the measured camber with overhang using Naaman's method

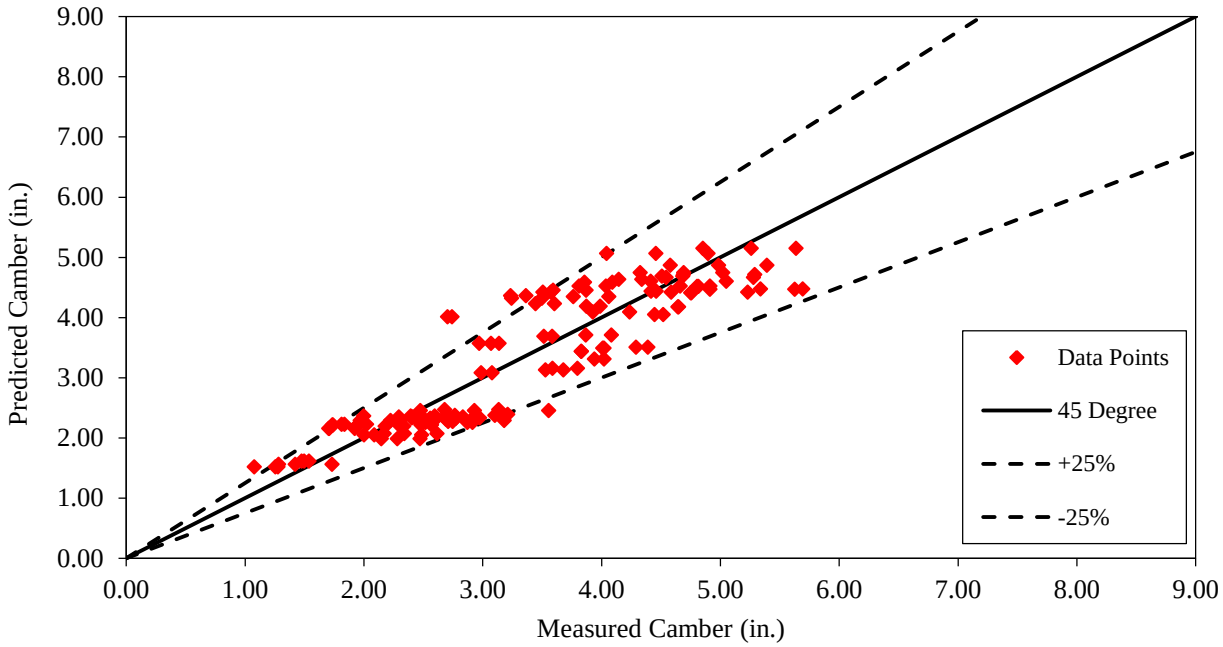

Figure 6.4. Comparison of the predicted camber and the measured camber without overhang using Naaman's method

It can be observed that almost all data points are located within the ±25% lines. It can also observed that the average difference between the camber predicted using Naaman's method and the measured value is -1% for the PPCBs with overhang and 0% for the PPCBs without overhang. Naaman's method is a good method to predict the long-term camber.

6.4 Incremental Method

The incremental method is affected by the same factors as Naaman's method. Figure 6.5 and Figure 6.6 show a comparison of the predicted camber and the measured camber with and without overhang, respectively.

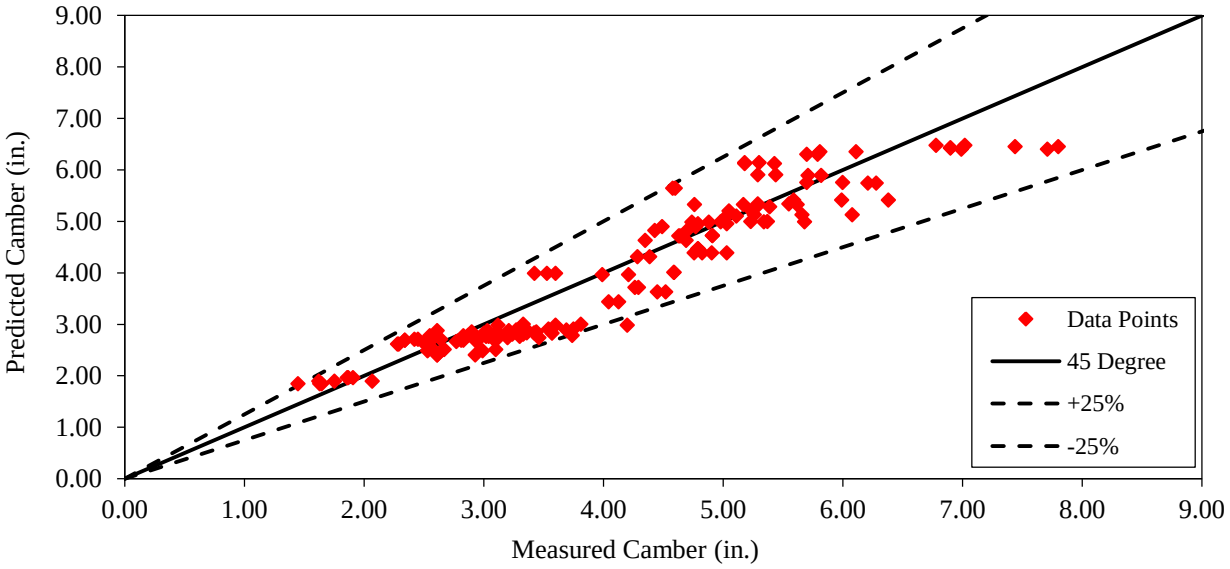

Figure 6.5. Comparison of the predicted camber and the measured camber with overhang using the incremental method

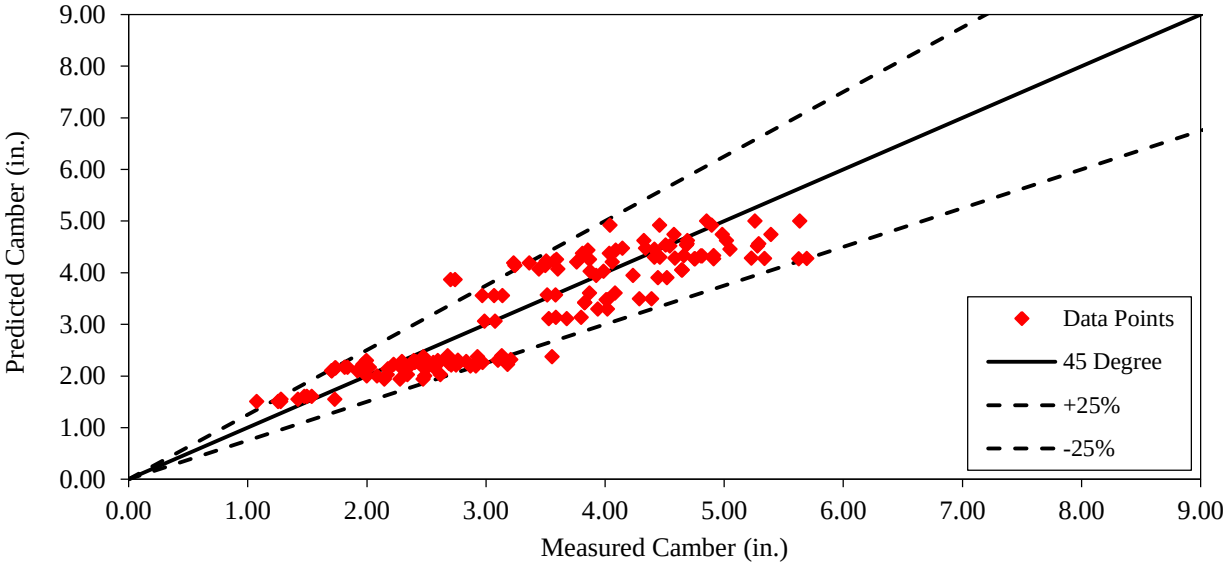

Figure 6.6. Comparison of the predicted camber and the measured camber without overhang using the incremental method

It can be observed that almost all data points are located within the ±25% lines. It can also be observed that the average difference between the camber predicted using the incremental method and the measured value is -1% for the PPCBs with overhang and 0% for the PPCBs without overhang. The incremental method is also a good method to predict long-term camber.

6.5 Comparison of the Effects of the Gross Section and the Transformed Section on the Estimation of the Camber

A comparison of the predicted cambers of PPCBs obtained using the three methods for the gross section and the transformed section is shown in Appendix G and Appendix H. It can be observed that the predicted cambers of the PPCBs using the gross section properties are always larger than those using the transformed section properties. The average difference obtained for all 26 PPCBs is 13%.

6.6 Comparison of the Effects of the Average Creep and Shrinkage and the Specified Creep and Shrinkage on the Estimation of the Camber

For the analysis conducted in Section 6.5, the results of the average sealed creep coefficient and the average sealed shrinkage were used to predict the long-term camber of the PPCBs for both gorss and transformed section properties. The predicted cambers of the PPCBs obtained using the average sealed creep and shrinkage data from the four HPC mixes are summarized in Appendix G. The predicted cambers of the PPCBs obtained using the measured specified sealed creep and shrinkage data are shown in Appendix H, where, due to the absence of measurements from the specified mix used for BTE 110 at Plant B, the average values of the sealed creep coefficient and the sealed shrinkage of HPC 2 and HPC 4 of plant B were applied. It can be observed that the average difference in the cambers of the PPCBs based on the two creep and shrinkage data sets (i.e., average versus specified) differed on average by ±2%. Therefore, it was concluded that it would be acceptable to use the average values of the sealed creep coefficient and the sealed shrinkage obtained for the four HPC mixes to predict the long-term camber of the PPCBs.

6.7 Comparison of the Effects of the AASHTO LRFD Creep and Shrinkage Model and the Measured Creep and Shrinkage on the Estimation of Camber

The AASHTO LRFD unsealed creep and shrinkage values and the gross section properties are typically used to calculate the long-term camber of prestressed bridge PPCBs. When the average AASHTO LRFD unsealed creep and shrinkage values and the gross section properties were used to calculate the long-term camber of the PPCBs for the duration of the first year, over which time the creep and shrinkage measurements were taken, it was found that the camber based on the AASHTO LRFD values was on average 22% higher than the camber calculated by using the measured sealed creep and shrinkage values and the transformed section properties. This is one reason why the predicted camber at erection is typically higher than actual value for long-span bulb-tee PPCBs.

6.8 Estimated Prestress Losses and Camber Growth

Table 6.1 and 6.2 how the short-term and long-term prestress losses in percent and the camber growth in percent at the age of three months and one year, respectively.

Table 6.1. Summary of the estimated prestress losses and the camber growth at three months

PPCB Type	Plant	PPCB ID	Prestress losses due to anchorage set, relaxation, and elastic shortening	Prestress losses due to creep, shrinkage and relaxation at three months	Camber growth at three months
BTC 120	A	103-09, 103-10, 103-11	6%	10%	44%
BTE 110	B	144-270, 144-272, 144-268	6%	10%	45%
		144-274, 144-275, 144-278	6%	10%	44%
		144-284, 144-283, 144-280	6%	10%	45%
BTE 145	B	144-311, 144-334	7%	10%	40%
		144-316, 144-317	7%	11%	40%
		144-366, 144-367	7%	10%	40%
BTD 135	C	13501, 13502	7%	10%	42%
		13503, 13504	7%	10%	42%
		13507, 13508	7%	10%	42%
		13511, 13512	7%	10%	42%
		Average	**7%**	**10%**	**42%**

Table 6.2. Summary of the estimated prestress losses and the camber growth at one year

PPCB Type	Plant	PPCB ID	Prestress losses due to anchorage set, relaxation, and elastic shortening	Prestress losses due to creep, shrinkage and relaxation after one year	Camber growth at one year
BTC 120	A	103-09, 103-10, 103-11	6%	12%	52%
BTE 110	B	144-270, 144-272, 144-268	6%	12%	53%
		144-274, 144-275, 144-278	6%	12%	53%
		144-284, 144-283, 144-280	6%	12%	53%
BTE 145	B	144-311, 144-334	7%	12%	44%
		144-316, 144-317	7%	12%	43%
		144-366, 144-367	7%	12%	47%
BTD 135	C	13501, 13502	7%	12%	49%
		13503, 13504	7%	12%	50%
		13507, 13508	7%	12%	50%
		13511, 13512	7%	12%	49%
		Average	**7%**	**12%**	**50%**

The transformed section properties were used to calculate the short-term and long-term losses. The long-term prestress losses were estimated using the AASHTO LRFD (2010) refined method as outlined in Section 2.3.2.1 The camber calculated by using Naaman's method was used to compute the camber growth in percent using Equation 6-1.

$$\text{Camber growth in percent} = \frac{\Delta_{\text{long-term}} - \Delta_{\text{release}}}{\Delta_{\text{release}}} \times 100 \qquad \textbf{(6-1)}$$

It can be observed from Table 6.1 and

Table 6.2 that the short-term prestress losses due to anchorage set, relaxation, and elastic shortening for the 26 PPCBs on average was 7%, and the average long-term prestress losses due to creep, shrinkage, and relaxation was 10% at three months and 12% at one year. It was also found that an average camber growth for the 26 PPCBs was 42% at three months and 50% at one year.

6.9 Effect of Errors in Three Factors on the Prediction of the Camber

The errors associated with the following three variables were examined independently: (1) the modulus of elasticity, (2) the creep and shrinkage strains, and (3) the prestress forces. Table 6.3 shows the percentage of error in the camber of the prestressed bridge PPCBs at the age of one year due to the observed error associated with each of these variables.

Table 6.3. Average effect of the errors of three variables on the camber of the PPCBs at the age of one year

Source of Errors	Error	BTC 120	BTE 110	BTE 145	BTD 135	Average
Modulus of Elasticity of Concrete	±20%	±13%	±13%	±12%	±12%	±13%
Creep and Shrinkage	±20%	±7%	±8%	±8%	±8%	±8%
Prestress Forces	±5%	±10%	±10%	±11%	±11%	±11%

It was found that a ± 20% error in the modulus of elasticity caused a ± 13% error in the camber of the PPCBs, a ± 20% error in the creep and shrinkage values caused a ± 8% error in the camber, and a ± 5% error in the prestress forces resulted in a ± 11% error in the camber. Note that the chosen ± 20% error in the elastic modulus of concrete was as discussed in Section 5.3, ± 20% is the typical error of the creep and shrinkage tests observed from the current and previous research projects, and ± 5% is the tolerance of the error in the prestress force permitted by the Iowa DOT.

Based on these results, it is evident that the camber of a PPCB is sensitive to changes in the prestress forces, implying that any inaccuracy between the required and applied prestress force at the precast plants can markedly affect the camber of the PPCBs. The error in the modulus of elasticity of the concrete has a moderate effect on the camber of the PPCBs, while the error in the creep and shrinkage of the concrete has the smallest influence on the camber of a PPCB.

6.10 Comparison of the Camber Values at Erection Obtained from CON/SPAN and Naaman's Method

Table 6.4 and Table 6.5 summarize a comparison of the camber values at erection as obtained from CON/SPAN and Naaman's method for 26 prestressed bridge PPCBs. The release camber was calculated using Naaman's method, and the transformed and gross section properties are presented in Table 6.4 and Table 6.5, respectively.

Table 6.4. Comparison of the camber values at erection as obtained from CON/SPAN (with I_{tr}) and Naaman's method

Plant	PPCB Type	PPCB ID	Release Camber I_{tr} (in.)	Camber at Erection by CON/SPAN I_{tr} (in.)	Camber at erection by the Naaman's method (in.)	Ratio of the Naaman's method to CONSAPN (%)
A	BTC 120	103-09, 103-10, 103-11	3.57	6.27	5.15	82.15
B	BTE 110	144-270,144-272, 144-268	1.56	2.74	2.26	82.43
B	BTE 110	144-274,144-275, 144-278	1.61	2.83	2.33	82.36
B	BTE 110	144-284,144-283, 144-280	1.52	2.66	2.19	82.44
B	BTE 145	144-311, 144-334	3.15	5.49	4.42	80.51
B	BTE 145	144-316, 144-317	3.13	5.44	4.38	80.39
B	BTE 145	144-366, 144-367	3.02	5.25	4.23	80.48
C	BTD 135	13501, 13502	3.44	6.00	4.88	81.31
C	BTD 135	13503, 13504	3.51	6.13	4.99	81.42
C	BTD 135	13507, 13508	3.49	6.10	4.97	81.44
C	BTD 135	13511, 13512	3.31	5.78	4.69	81.25

Table 6.5. Comparison of the camber values at erection between CON/SPAN (with I_g) and Naaman's method

Plant	PPCB Type	PPCB ID	Release Camber I_{tr} (in.)	Camber at Erection by CON/SPAN I_{tr} (in.)	Camber at erection by the Naaman's method (in.)	Ratio of the Naaman's method to CONSAPN (%)
A	BTC 120	103-09, 103-10, 103-11	4.15	7.30	5.15	70.51
B	BTE 110	144-270,144-272, 144-268	1.76	3.09	2.26	72.99
B	BTE 110	144-274,144-275, 144-278	1.83	3.21	2.33	72.46
B	BTE 110	144-284,144-283, 144-280	1.7	2.99	2.19	73.44
B	BTE 145	144-311, 144-334	3.76	6.57	4.42	67.31
B	BTE 145	144-316, 144-317	3.75	6.55	4.38	66.83
B	BTE 145	144-366, 144-367	3.58	6.25	4.23	67.62
C	BTD 135	13501, 13502	4.11	7.20	4.88	67.80
C	BTD 135	13503, 13504	4.19	7.34	4.99	67.94
C	BTD 135	13507, 13508	4.16	7.29	4.97	68.16
C	BTD 135	13511, 13512	3.91	6.85	4.69	68.55

The prestressed bridge PPCBs are typically erected at the construction site three months after the time of the transfer. CON/SPAN uses multipliers to obtain the camber at erection, including 1.80 for the camber due to prestress forces and 1.85 for the deflection due to the self-weight of the PPCB. The camber at erection obtained using Naaman's method utilizes the transformed or gross section properties, along with the average creep and shrinkage values obtained at three months after the transfer. In this section, the overhang effect was not taken into account, and all reported cambers were calculated based on zero overhang. The camber at erection obtained using Naaman's method on average was 81% of the camber calculated from CON/SPAN when the transformed section properties were used and 69% of the camber obtained from CON/SPAN when the gross section properties were used. It was also found that the difference between the camber values at erection obtained using Naaman's method and CON/SPAN with the transformed section properties was 81.5% ± 0.8%, on average. Additionally, the difference between the camber at erection obtained using Naaman's method and CON/SPAN with the gross section properties was 69.4% ± 2.5%, on average.

Figure 6.7 and Figure 6.8 show a comparison of the adjusted measured camber without an overhang for a period of 75 to 100 days after the transfer and the camber at erection obtained using CON/SPAN for 12 PPCBs with the transformed and gross section properties, respectively.

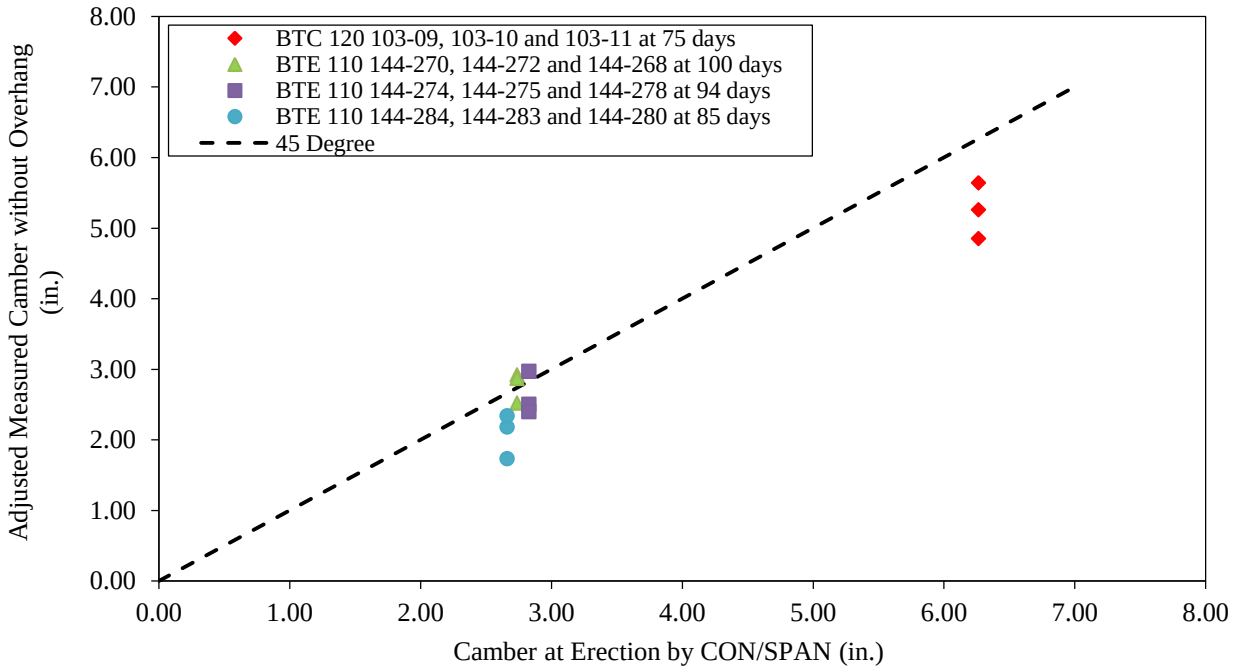

Figure 6.7. Comparison of the measured camber adjusted for a zero overhang at erection with that obtained at the same time from CON/SPAN with I_{tr}

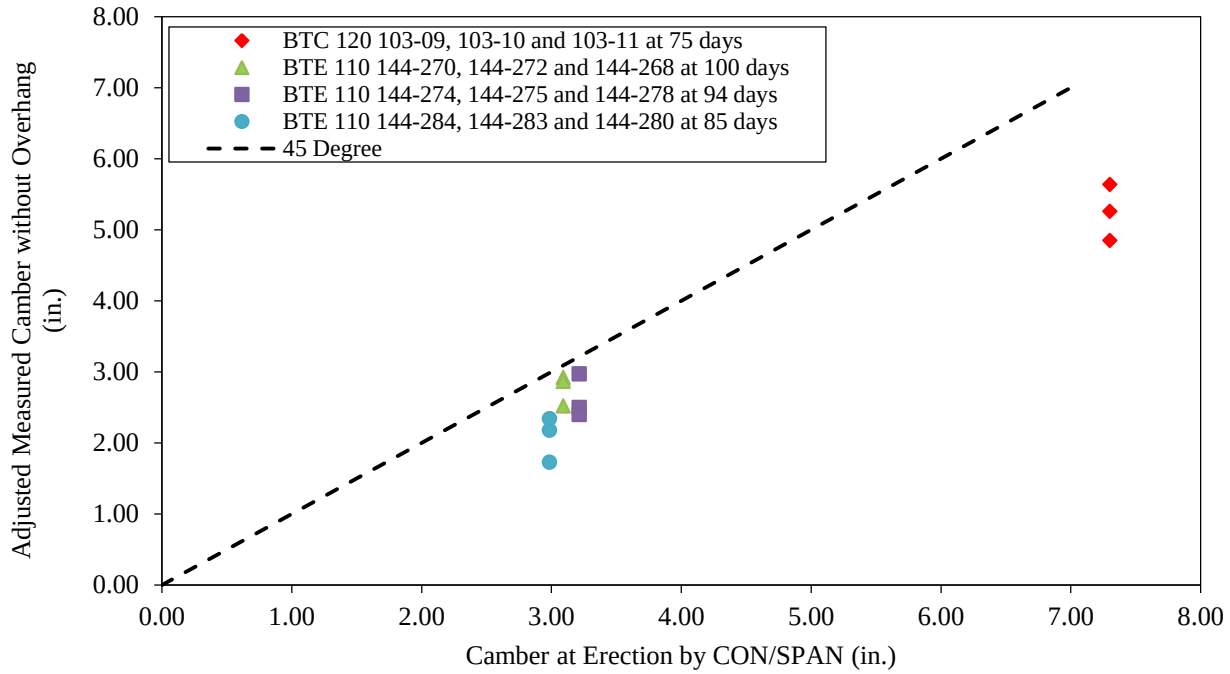

Figure 6.8. Comparison of the measured camber adjusted for a zero overhang at erection with that obtained at the same time from CON/SPAN with I_g

The camber obtained from CON/SPAN with the transformed section properties was found to be 14% higher than the measured camber adjusted for an overhang at the age of three months, on average. The camber obtained from CON/SPAN with the gross section properties was 30% higher than the adjusted measured camber at erection, on average. This indicates why the camber prediction at erection is typically higher than the actual value for the long-span bulb-tee PPCBs.

6.11 Comparison of the Current Study with the Three Previous Studies

It was observed that the refined method of prestress losses from AASHTO LRFD (2010) specifications provided good estimates, according to four different studies. These included the current study as well as the Washington study (Rosa et al. 2007), the North Carolina study (Rizkalla et al. 2011), and the Minnesota study (O'Neill and French 2012) discussed in Section 2.3.1. The current study has, however, offered more information, particularly with regards to the material properties and more accurate and detailed camber measurements. In the current study, the creep and shrinkage measurements were taken for four HPC mixes and three NC mixes during a period of one year. These mixes represented concrete mixes used at three different precast plants. It was found that the HPC mixes exhibited higher creep and shrinkage strains than the NC mixes due to the use of the slag and fly ash in the HPC mixes. The creep and shrinkage behavior of the laboratory specimens was also correlated to full-scale PPCBs in the field, and it was found that the sealed laboratory specimens better represented the creep and shrinkage behavior of full-scale PPCBs in the field than the unsealed laboratory specimens. Additionally, a simplified time-dependent method (known as Naaman's method) was found to predict the long-term camber of the PPCBs more accurately than the use of simple multipliers.

6.12 Conclusions

As indicated in Chapter 3, the measured creep and shrinkage behavior generally exhibited large discrepancies compared with the creep and shrinkage values obtained from five different predictive models. Hence, calculating the camber by relying on these models may cause a large error in the long-term camber prediction. Sealed specimens were found to represent the behavior of full-scale PPCBs more effectively than unsealed specimens. The Iowa DOT's current camber prediction method using Martin's multipliers results in large differences with the actual camber expected at erection, due to the uncertainty of the time of the erection after production and a neglect of the time-dependent material properties and the thermal effects. Additionally, the use of gross rather than transformed section properties contributes to the discrepancies between the designed and measured at-erection camber. Using the current method, the camber of long-span bulb-tee PPCBs is often overpredicted by more than 30%.

The following conclusions can be drawn from this chapter:

- The camber of 26 PPCBs obtained based on gross section properties on average was 13% higher than the camber computed using transformed section properties during one year.
- Using the average creep coefficients and shrinkage strains for the first year instead of using the values corresponding to the specific concrete mix caused an average error of 2% in the camber estimation of PPCBs.
- For the prediction of the long-term camber of PPCBs, Naaman's method was found to be most suitable. Both Naaman's method and the incremental method had comparable results, and the errors between the predicted and measured values were within ± 25%. In comparison, Naaman's method is easier to use than the incremental method, and both of them yielded better camber predictions than Tadros' method.
- The estimated average short-term prestress loss for 26 PPCBs was 7%, and the average long-term prestress loss was 10% at three months and 12% at one year. The average camber growth for these 26 PPCBs was 42% at three months and 50% at one year.
- The long-term camber of the PPCBs was more sensitive to errors in the prestress forces than to the modulus of elasticity and the creep and shrinkage.
- The CON/SPAN software used by the Iowa DOT typically overestimated the camber at erection compared with the results obtained by Naaman's method. The difference between the camber at erection obtained using Naaman's method and 70% of the camber estimated using the CON/SPAN-based gross section properties was within ± 5%.

6.13 Recommendations

An inaccurate prediction of the creep and shrinkage, as routinely occurs, contributes to 31% of the errors in the camber estimation at erection. This overestimation of the camber of PPCBs could lead to an increase in construction costs due to the need to add concrete haunches between the PPCB and the deck. In order to improve the accuracy of the prediction of the long-term camber of PPCBs, the following recommendations are provided:

- It is acceptable to use the AASHTO LRFD (2010) model to predict the modulus of elasticity based on the compressive strength and unit weight of the concrete.
- In order to obtain more accurate results, the creep and shrinkage tests results for concrete produced using local Iowa materials should be used.
- Sealed specimens should be used to obtain creep and shrinkage behavior similar to that of full-scale PPCBs.
- It is acceptable to use the average sealed creep coefficient and the average sealed shrinkage of four HPC mixes to predict the long-term camber of PPCBs within one year, and the proposed equations for the sealed creep coefficient and sealed shrinkage may be applied to predict the long-term camber beyond one year.
- For the prediction of the long-term camber of 26 PPCBs, Naaman's method is recommended over Tadros' method and the incremental method.
- The transformed section properties should be utilized for the calculation of the camber of PPCBs at the transfer as well as at erection.
- The measurement of prestress forces should be improved by precast plants due to the sensitivity of the camber of the PPCB to the actual prestress forces. The elongation of each strand should be recorded carefully before and after jacking.
- If CON/SPAN is to be used for estimating the at-erection camber, which typically takes place around three months after the transfer, a good estimate can be found by obtaining the at-erection camber using the gross section properties and a correction factor of 0.7. This value is suggested based on a comparison of the measured data from 26 PPCBs with the camber values calculated using CON/SPAN.

CHAPTER 7: FINITE ELEMENT ANALYSIS

7.1 Introduction

Currently, the Iowa DOT uses an elastic analysis (as adopted in CON/SPAN) and Martin's multipliers (1977) to estimate the camber at release and erection, respectively, as outlined in Section 0. The instantaneous camber prediction is straightforward once the design variables are chosen (see Section 2.2.5). Unlike for the instantaneous camber, the complexities associated with the time-dependent behavior of the concrete have led to inaccurate at-erection camber estimations using the current Iowa DOT approach. Moreover, the current approach used in Iowa and several other states does not provide any guidelines for including the thermal effects in the long-term camber prediction, while these effects can significantly increase the camber temporarily during the time of the measurements (see Section 4.2.5). Consequently, it was realized that the current Martin's multipliers (1977) need to be replaced by a new single multiplier or a set of multipliers that accounts for the variability of the time as well as the temperature gradients resulting from the fact that the PPCB top generally experiences warmer temperatures than the bottom flange.

A sophisticated finite element analysis approach using the midas Civil software was primarily used in this chapter. Various parameters discussed in Chapter 2 that could potentially affect the camber were incorporated into the finite element models. These analyses were conducted to study the change in the camber of the PPCBs from the release to the time of the erection with and without a PPCB overhang during storage. Subsequently, the long-term camber was compared to the instantaneous camber prediction to create a power function that can provide suitable multipliers, as well as a set of average multipliers to account for the time-dependent effects on the camber. Furthermore, the effect of the temperature gradient was investigated, and a modification to the multipliers is recommended.

7.2 Methodology

To utilize the measured long-term camber in this investigation, the PPCBs cast for five different bridges in Iowa were grouped based on the Iowa DOT standard PPCB (Iowa DOT 2011b) predicted values for the instantaneous camber as follows: (1) small-camber PPCBs with an instantaneous camber less than 1.5 in. and (2) large-camber PPCBs with an instantaneous camber greater than 1.5 in. Figure 7.1 shows the classification of the PPCBs based on the instantaneous camber for the different Iowa DOT PPCBs.

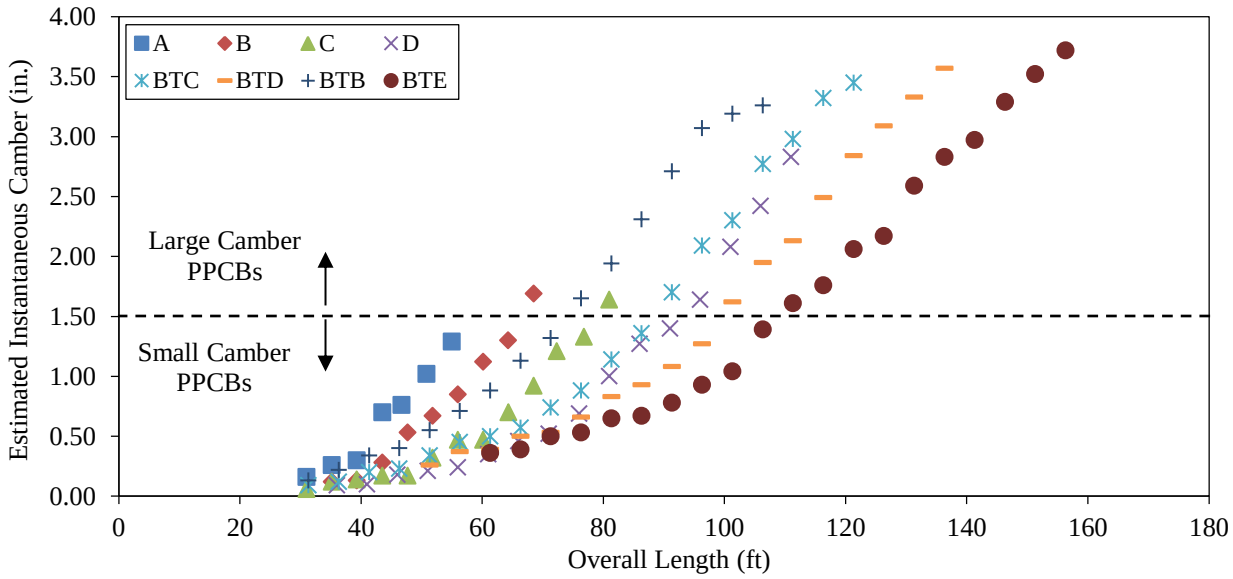

Figure 7.1. Expected release camber versus the PPCBs' overall lengths for different types of PPCBs

Each group consisted of different types of PPCBs with varying depths and lengths. A group of PPCBs that were produced on the same precasting bed with the same casting date, curing time, initial compressive strength, prestress force, and overhang length during storage was called a set of PPCBs. Thus, the PPCBs in each set were theoretically expected to have an identical camber. For instance, Table 7.1 presents the different sets defined for 12 measured D 55 PPCBs (the small-camber PPCB group), where Sets 1 and 2 each contain 5 PPCBs and Set 3 includes 2 PPCBs.

Table 7.1. Details of the measured D 55 PPCBs

PPCB Type	Group	Set Number	PPCB Number	Cast Date	Release Date	Plant	Bridge Project
D 55	Small Camber PPCBs	Set 1	BD05501E BD05502 BD05503 BD05504 BD05505	12/20/2011	12/21/2011	Plant C	Sac County
		Set 2	BD05506E BD05519E BD05520 BD05521 BD05522	12/27/2011	12/28/2011		
		Set 3	BD05523 BD05524E	12/29//2011	12/30/2011		

The details of different sets defined for the measured PPCBs can be found in Appendix F. Using the average creep and shrinkage values proposed for the HPCs used in this project (see Section 3.8.4.6), the long-term camber versus time for each set of PPCBs was predicted using a FEM with and without overhang, which helped separate the sets based on the amount of camber growth due to overhang. Subsequently, the measured long-term camber data during storage was

adjusted to eliminate the contribution of overhang to the camber (see Section 2.3.2.4). As a result, the adjusted measured camber at different times can be compared consistently to the analytical values without any overhang effect. These data are presented in Section 7.5.2.

Using the theoretically calculated camber values, a multiplier, as a function of time, was established for each set of PPCBs assuming zero overhang length. Then, an average multiplier was determined for each group by finding a best-fit power function curve. Although this function can be used to determine the long-term camber, the accuracy of the camber value depends on the time, which is usually an unknown design parameter. Hence, this power function was further examined over three different time intervals to find a suitable average time for each interval. This led to an average multiplier for each time interval that could be used in the design, although a designer can still use the power function to determine a more accurate multiplier. Similarly, the procedure was repeated to calculate the multipliers with the average overhang length calculated in Section 4.2.4.

Finally, to understand the influence of the ambient temperature gradients presented in Section 4.2.5, the measured data were used to calibrate the analytical models and quantify the additional thermal deflection induced by the temperature gradients. As a result, a temperature multiplier, $\lambda_{T,}$ was used to account for the increase in the camber due to the influence of the temperature gradients. Though this may be used as an optional multiplier, it is shown that using this multiplier together with that suggested for the long-term time-dependent effects will lead to more realistic camber predictions.

7.3 midas Civil Features

midas Civil is commercial software that utilizes FEA in combination with the time-step method to model a time-dependent response for bridges. The developed model consisted of nodes, elements, and boundary conditions. Each PPCB was modelled with several hundred PPCB elements that were connected by nodes. The status of the connections between the structure and the adjacent structure is represented by the boundary conditions.

midas Civil can model all the significant parameters affecting the camber, including concrete material properties, section properties, creep and shrinkage, instantaneous and long-term prestress losses, storage conditions, and thermal effects. Furthermore, construction stages that introduce changes to the boundary conditions can be incorporated in the analysis. This enabled an understanding of the change in the camber of the PPCBs from fabrication to the time of erection to the time after the deck is poured when the composite action between the PPCBs and the deck is initiated. Additionally, the variation in the location of the PPCB supports was taken into account by defining different construction stages.

7.4 Analytical Model Details

As previously mentioned, the PPCBs fabricated for five different bridges in Iowa were monitored for their long-term camber measurements (see Section 4.2.3). For each selected bridge project, an analytical model was developed. The model geometry included all PPCBs that were monitored for that specific bridge as well as the other PPCBs in the span adjacent to the monitored PPCBs. The PPCBs in the adjacent span were chosen to investigate the possible effect on the camber of continuity over the piers after the deck was cast. Figure 7.2 through Figure 7.4 show an example of the bridge geometry according to the bridge plan. In this prototype bridge, the following PPCBs were monitored by the research team for their long-term camber measurements: BTD 135-01, BTD 135-02, BTD 135-03, BTD 135-04, BTD 135-07, BTD 135-08, BTD 135-11, and BTD 135-12.

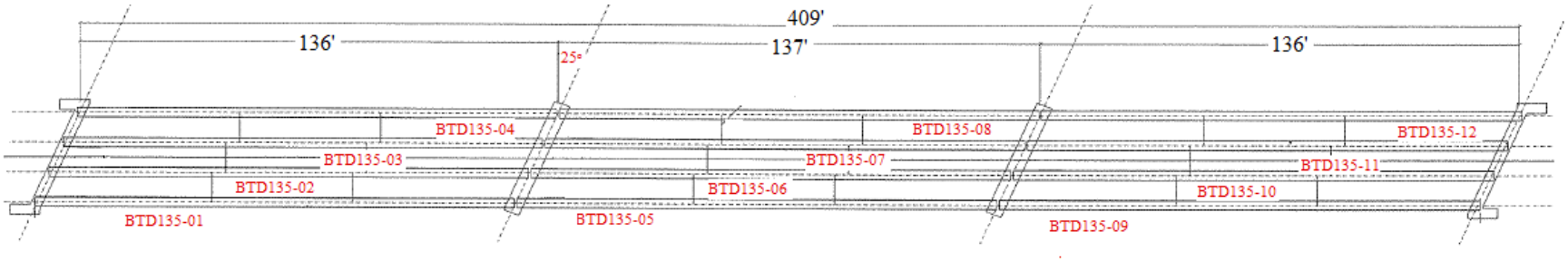

Figure 7.2. Plan view of the Dallas County Bridge

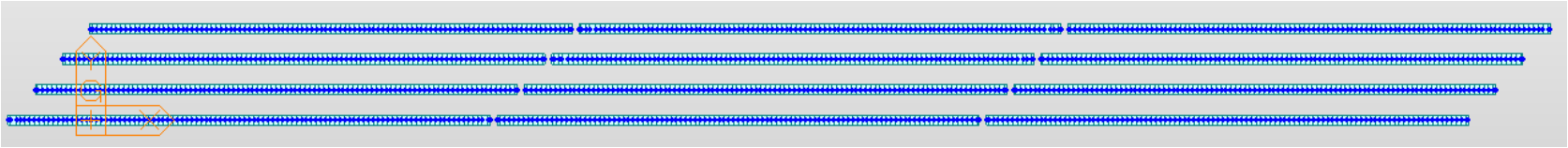

Figure 7.3. midas Civil model of the Dallas County Bridge before allowing for the composite action

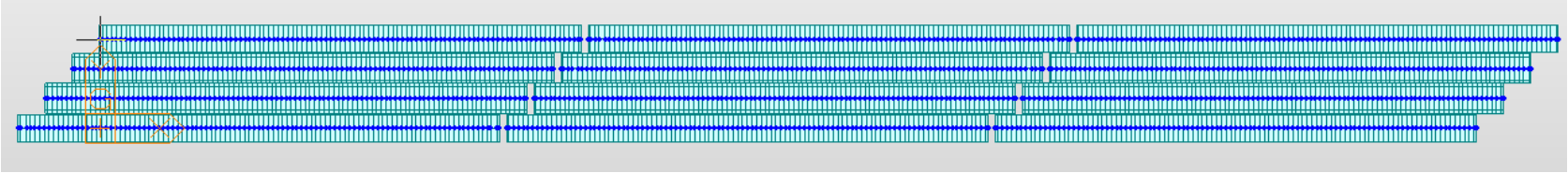

Figure 7.4. midas Civil model of the Dallas County Bridge after allowing for the composite action

7.4.1 Cross-Section Details

The cross-section of various PPCBs was modeled following the details presented in the Iowa DOT PPCB standards (Iowa DOT 2011b). Accordingly, straight strand, harped strand, and sacrificial strand profiles were all included for each PPCB. The strands were modeled as prestressed pretensioned strands with perfect bonding to the concrete. Hence, the section properties used in the analyses reflect the transformed areas. Also, the transfer length was modeled for each PPCB according to the AASHTO LRFD (2010) equation (see Section 2.2.5.1). The modeled cross-section and tendon profile for a BTD 135 PPCB are illustrated in Figures 7.5 and 7.6, respectively.

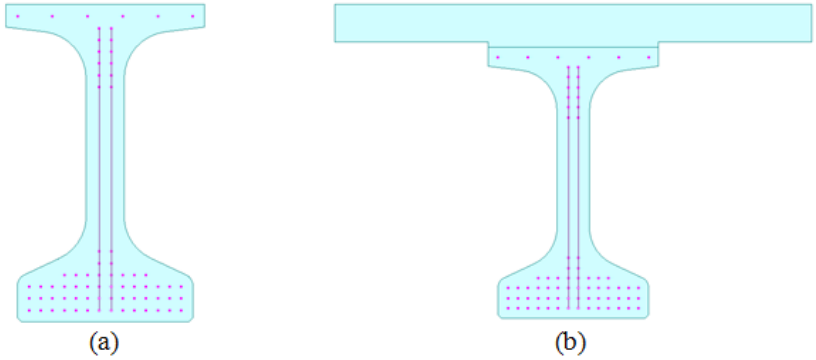

Figure 7.5. BTD 135 PPCB cross-section with tendon locations: (a) before the composite action, (b) after the composite action

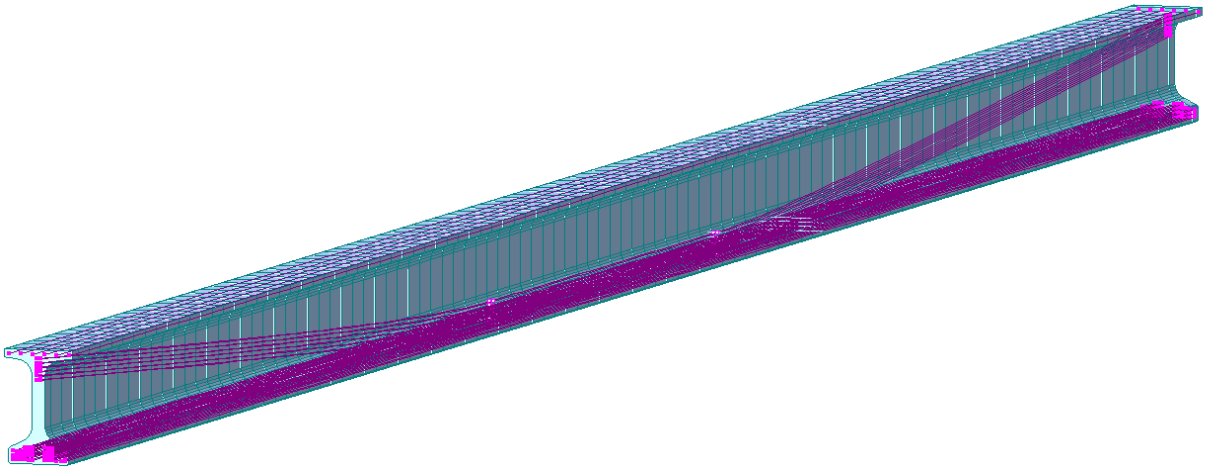

Figure 7.6. Tendons profiles along the length of a BTD 135 PPCB

7.4.2 Material Properties

Concrete and steel properties were defined for each PPCB model as follows:

- Concrete modulus of elasticity: E_c was estimated using the AASHTO LRFD (2010) equation based on the measured compressive strength of each PPCB at release (see Section 2.1.4.2.1).
- Steel modulus of elasticity: E_s was assumed to be 28,500 ksi.
- Concrete creep and shrinkage: The average creep and shrinkage curves recommended in Section 3.8.4.6, established using data from all HPC mixes, were used.

7.4.3 Construction Stages

Four different construction stages were defined for the PPCBs used in the bridges. These stages accounted for changes in the PPCB boundary conditions and/or the applied loads at different times in the PPCBs' lives. The first stage simulated the transfer of the prestress and accounted for all instantaneous losses such as the elastic shortening and the relaxation losses. The second stage was defined to model the condition of the PPCBs during storage in the precasting yard. For each PPCB, the measured overhang length was used in the model. The next stage reflected the PPCBs immediately after they were placed on the bridge piers before casting the concrete deck, at which stage the PPCBs had no overhang. The final stage investigated the composite action between the PPCBs and the deck after the deck was cast.

7.4.3.1 Composite Section for Construction Stage 4

A composite section was defined in Stage 4 to account for the composite action between the PPCBs and the bridge deck. It was assumed that the composite action began seven days after casting the deck. For each PPCB, the effective deck width was calculated based on the AASHTO LRFD (2010) recommendation, which is to use the spacing between two adjacent PPCBs for interior PPCBs and half of the spacing between two adjacent PPCBs plus the overhang width for exterior PPCBs. The member stiffness of the composite section was computed using the transformed section, for which the modulus of elasticity of the deck concrete was estimated using the AASHTO LRFD (2010) recommendation (see Section 2.1.4.2.1).

7.4.4 Loading

The loads acting on the PPCBs in the first stage were the prestress force and the self-weight. In Stage 2, the thermal load was modeled by applying a linear temperature gradient for the PPCB cross-section along the entire PPCB length. In Stage 4, the new dead loads, which included the weight of the deck and the weight of the bridge barrier, were added to the model.

7.4.5 Prestress Losses

All possible prestress losses were accounted for in the analyses. For the elastic shortening loss calculation, the PPCB gross section properties and the initial prestress force were used (see Section 2.2.4.1.1). The relaxation of the steel strands and the corresponding loss between the tensioning and the transfer was estimated in accordance with the ACI Committee 343R-95 (1995) method, as discussed in Section 2.2.2.1.3. (AASHTO has no recommendation for strand relaxation over such a short period of time.) Then, the time-dependent losses, including those due to the creep and shrinkage of the concrete and the relaxation of the prestressed tendons after the transfer, were included. The strands' relaxation after the transfer was estimated based on AASHTO LRFD (2010), as described in Section 2.3.2.1.1. Losses due to the concrete creep and shrinkage were estimated using a time-step method as adopted by the midas Civil software.

The time-step method was deployed by dividing the time into intervals to account for the continuous interaction between the creep and shrinkage of the concrete and the relaxation of the strands with time. The duration of each time interval was adjusted to be successively larger as the concrete aged. The stress in the strands at the end of each time interval was determined by subtracting the calculated prestress losses during the interval from the initial condition at the beginning of that time interval. The strand stress and the deformation at the beginning of each time interval corresponded to those at the end of the preceding interval. Using this method, the prestress level was approximated at any critical time during the life of the prestressed member. More information about this method can be found in the studies carried out by Nilson (1987), Abdel-Karim and Tadros (1993), and Hinkle (2006) and in the PCI Bridge Design Manual (PCI 1997).

7.4.6 Support Locations

As discussed in Section 4.2.4, the PPCBs were seated on temporary supports during storage in the precasting yard. Depending on how far the supports were located relative to the PPCB ends, the length of overhang increased the camber. The overhang length was measured with respect to the ends of the PPCBs. The overhang effect had two components: an elastic component caused by the dead load of the cantilever portions beyond the supports and a time-dependent component due to the creep of the concrete in the overhangs over time.

In order to compare the measured camber values at different construction stages consistently without any effect from the support locations, the data were adjusted to eliminate the camber growth due to the overhang. Therefore, the amount of the camber growth due to the overhang was determined in the analytical model, and it was subsequently subtracted from the measured camber to obtain the adjusted measured camber values. This step was necessary instead of adjusting the theoretical camber with consideration to the overhang because (1) the length of overhang varied between the PPCBs and (2) when the PPCBs were placed on piers and abutments, the corresponding overhang length is taken to be zero. For example, Figure 7.7 depicts the camber growth of a BTE 110 PPCB with and without an overhang length of 42 in.

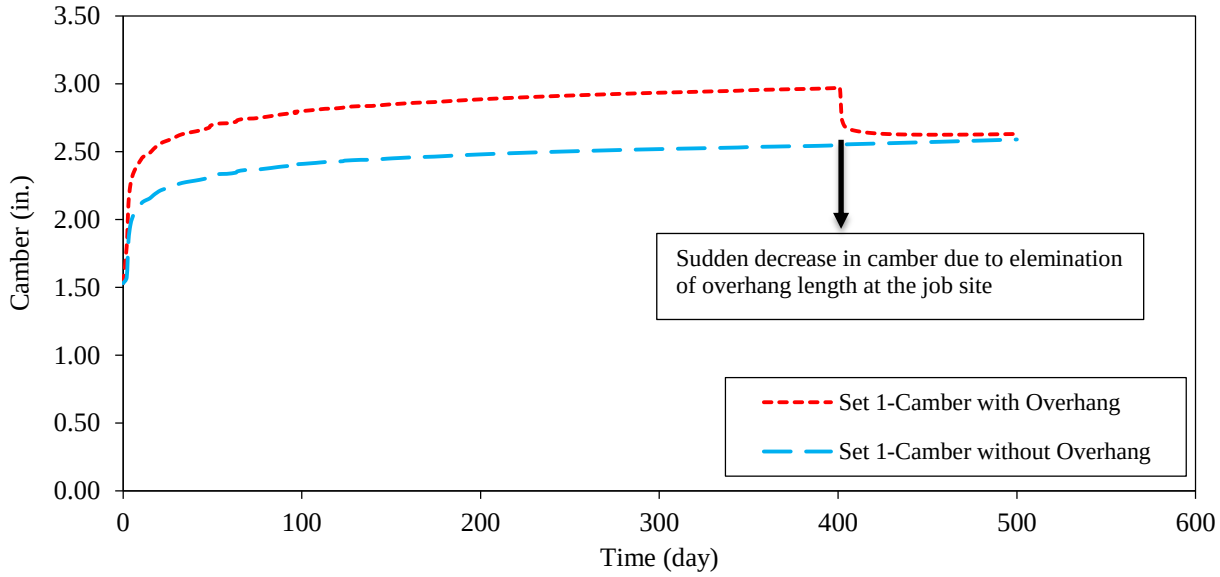

Figure 7.7. Analytical camber curves for a BTE 110 PPCB

The effect of the overhang in this case was included from the time of the transfer of the prestress until the PPCB was placed on the bridge piers. It is evident from the figure that the elimination of the overhang during construction decreases the camber, as shown by a sudden drop in the long-term camber in Figure 7.7. Figure 7.8 compares the measured and adjusted camber data for a BTE 110 PPCB.

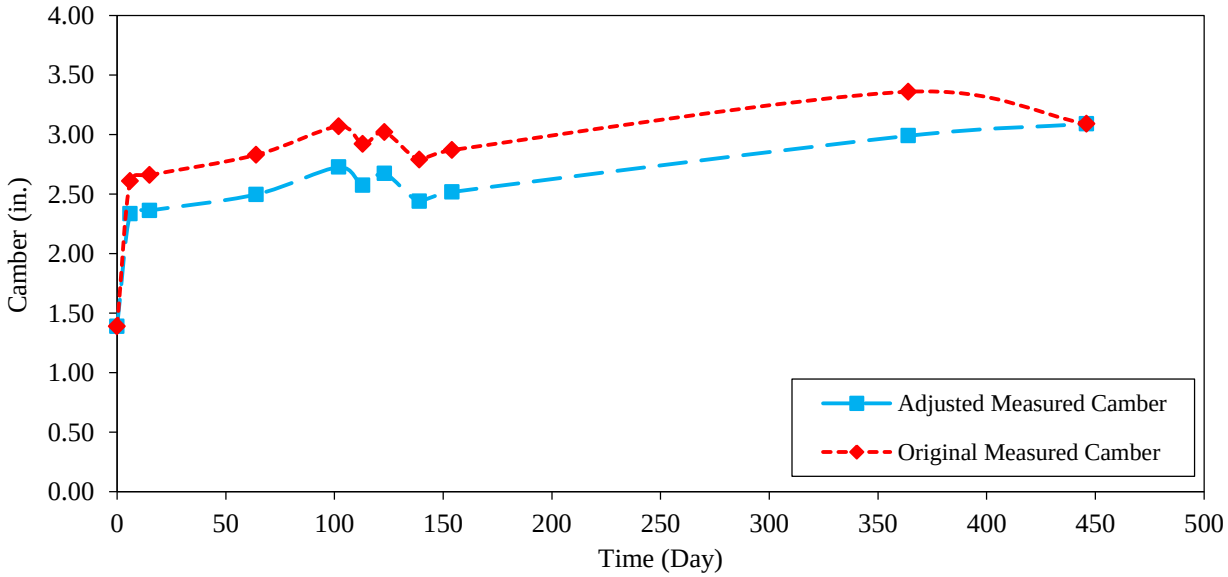

Figure 7.8. Measured and adjusted data for a BTE 110 PPCB

It is noted that the adjusted and original measured camber values are the same at release and at erection when the overhang is zero. Similar results for the remaining PPCBs can be found in Appendix I.

7.4.7 Thermal Effects

An investigation of the measured long-term camber of 66 PPCBs during storage revealed noticeable inconsistent trends in the data, which included identical PPCBs cast at the same precast plant at the same time. The contradictions between the data and theory included a significantly high camber at early ages and a reduction and/or no significant increase in the camber over time. The temperature gradients that develop down the PPCB depth due to solar radiation were suspected to be contributing to these observations. If significant, the effects of the temperature gradients, which are normally ignored, can cause construction difficulties when the PPCBs are erected and the deck elevations are set. Hence, the following analysis was undertaken to understand and quantify this effect and possibly integrate it into a design practice.

To include the maximum effect of the ambient temperature on the camber, a linear temperature gradient down the member depth was assumed, with the highest temperature at the top surface and the same temperature gradient maintained along the entire length of the PPCB. This temperature gradient induced an elastic moment at the midspan, causing a thermal deflection, which can be computed using Equation 7-1 for a beam element.

$$M = \alpha E_c I \frac{\Delta T}{h} \quad \textbf{(7-1)}$$

where α is the linear thermal expansion coefficient for the concrete, E_c is the concrete modulus of elasticity, I is the section moment of inertia, ΔT is the temperature difference between the two extremities (outermost faces) of the beam element, and h is the distance between the two extremities of the PPCB section.

All variables in Equation 7-1 are either known or can be estimated, except the temperature difference between the PPCB top and bottom flange, ΔT, at the time of the camber measurement. Hence, for each PPCB, the analysis was performed with different temperature differences to obtain the relationship between the thermal deflection and the temperature difference. Figure 7.9 shows an example of the results for a BTE 110 PPCB.

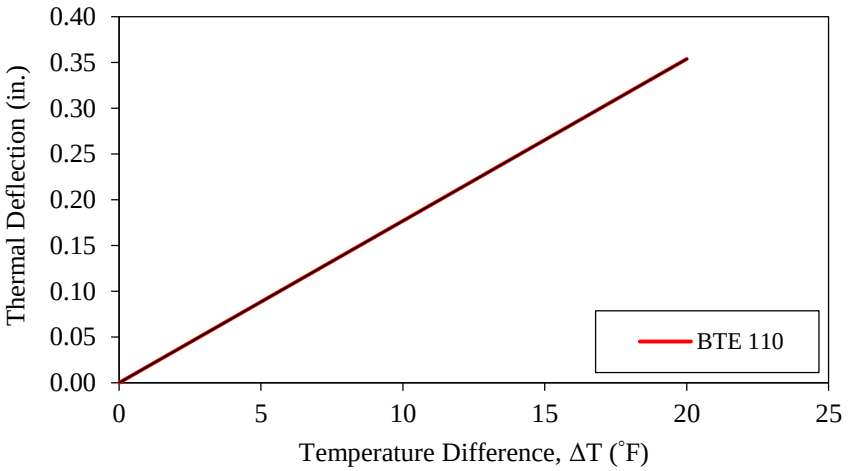

Figure 7.9. Thermal deflection versus temperature difference for a BTE 110 PPCB

As expected, the thermal deflection increases linearly as the temperature difference increases. It should be noted that, hereafter, the temperature difference is simply used to refer to the temperature difference between the PPCB top and bottom flange when the vertical temperature gradient is linear.

Subsequently, a sensitivity analysis of the temperature difference was conducted to determine the value of the temperature difference that captures the scatter in the data the most accurately. The results indicated that if the additional thermal deflection induced by a temperature difference of 15°F were included in the camber prediction, the error would be minimized, as shown in Figure 7.10. Therefore, this temperature difference was used to perform the analysis in the following sections.

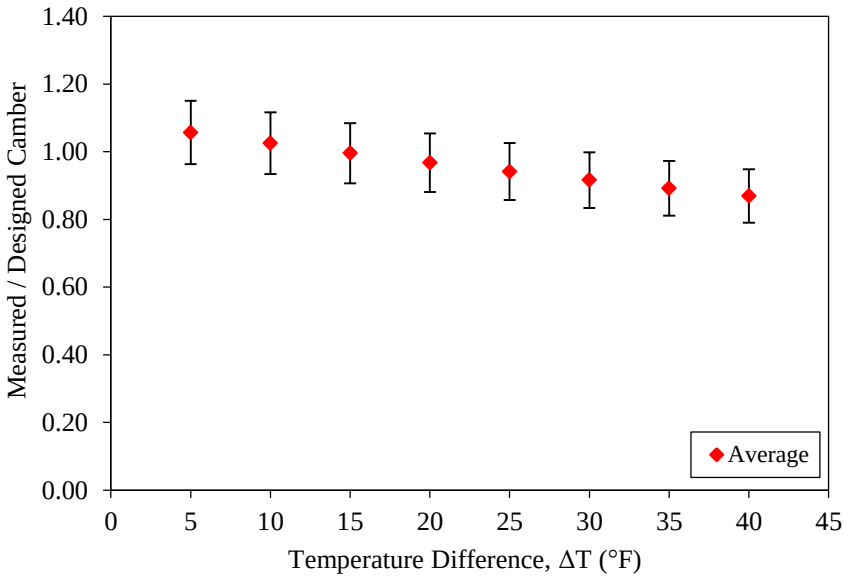

Figure 7.10. Ratio of the measured to designed camber versus the temperature difference

7.5 Analytical Model Results and Discussion

In this section, the analytical results for the instantaneous and long-term camber predictions are presented. New multipliers are calculated to estimate the at-erection camber with and without overhang. To account for the additional long-term camber resulting from the thermal effects, another multiplier, λ_T, is also introduced at the time of the measurement. It should be noted that, throughout this chapter, the error is positive when the measured camber is larger than the predicted camber.

7.5.1 Instantaneous Camber Prediction

Based on the recommendations for the material properties and analytical design variables presented in Chapter 5, the instantaneous camber was predicted and compared to the measured data for the large- and small-camber PPCBs using FEA, as shown in Figure 7.11. A good correlation was found between the measured and designed instantaneous camber, with an average error of -1.5% ± 8.3%.

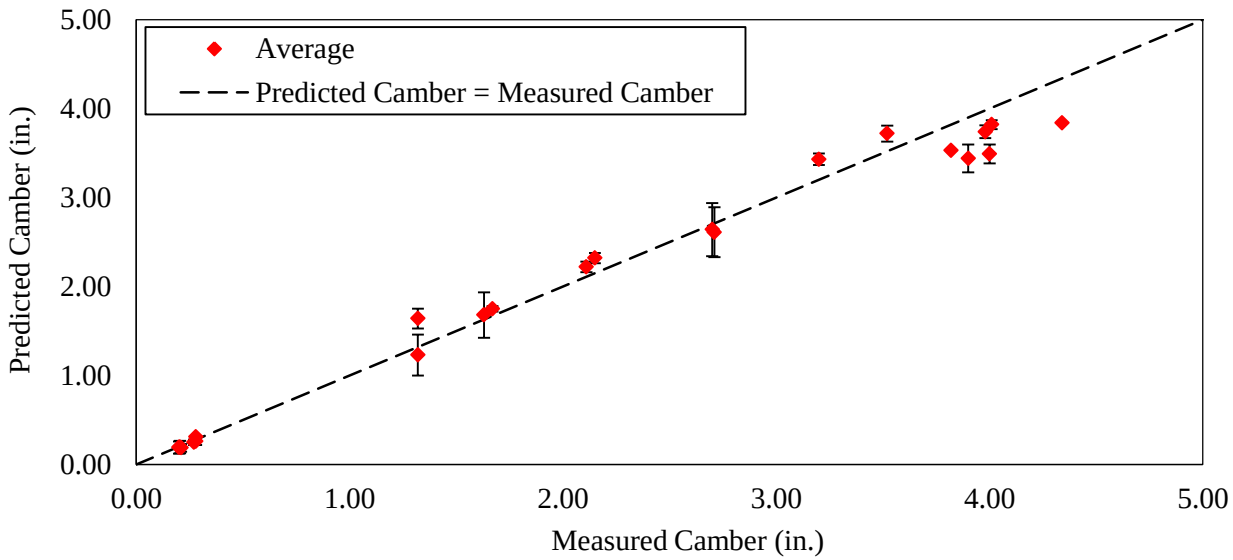

Figure 7.11. Predicted instantaneous camber by FEA versus the measured instantaneous

7.5.2 Long-term Camber Prediction

Representative modeling results for a few selected PPCB sets modeled in this study are shown in Figure 7.12 through Figure 7.15. The remaining FEA results for the other sets in graphic form are presented in Appendix J.

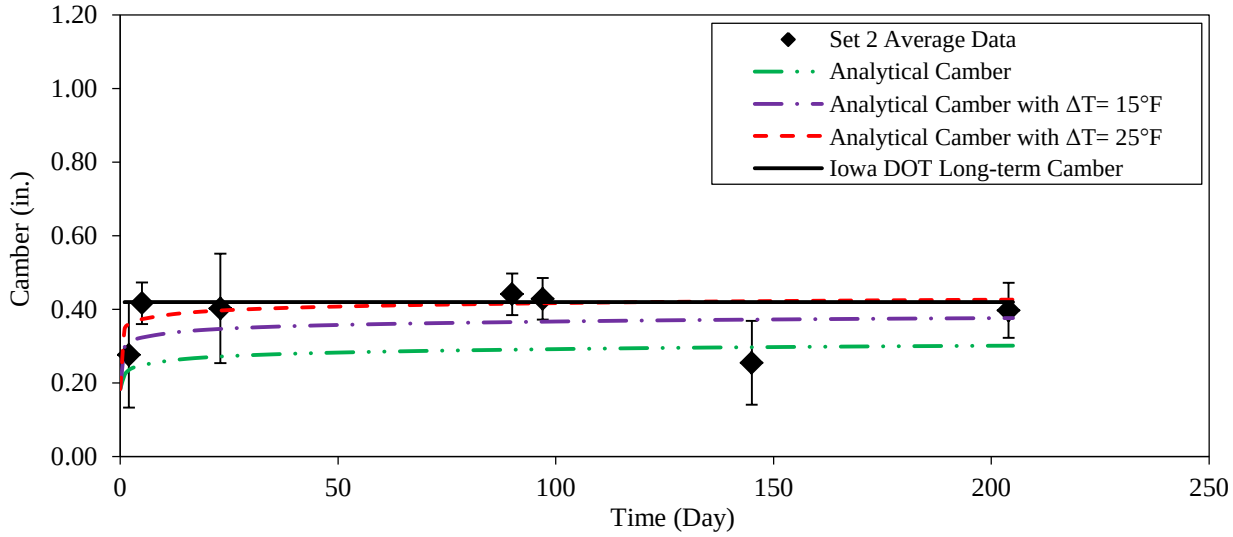

Figure 7.12. Prediction of the long-term camber for the D 55 Set 2 PPCBs

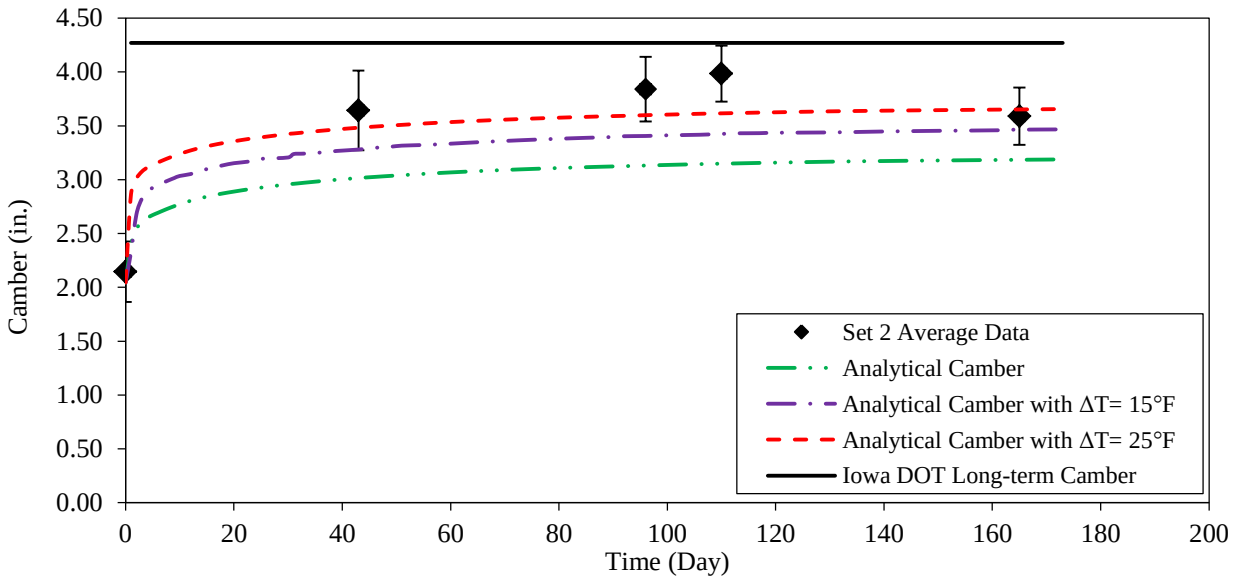

Figure 7.13. Prediction of the long-term camber for D 105 Set 2 PPCBs

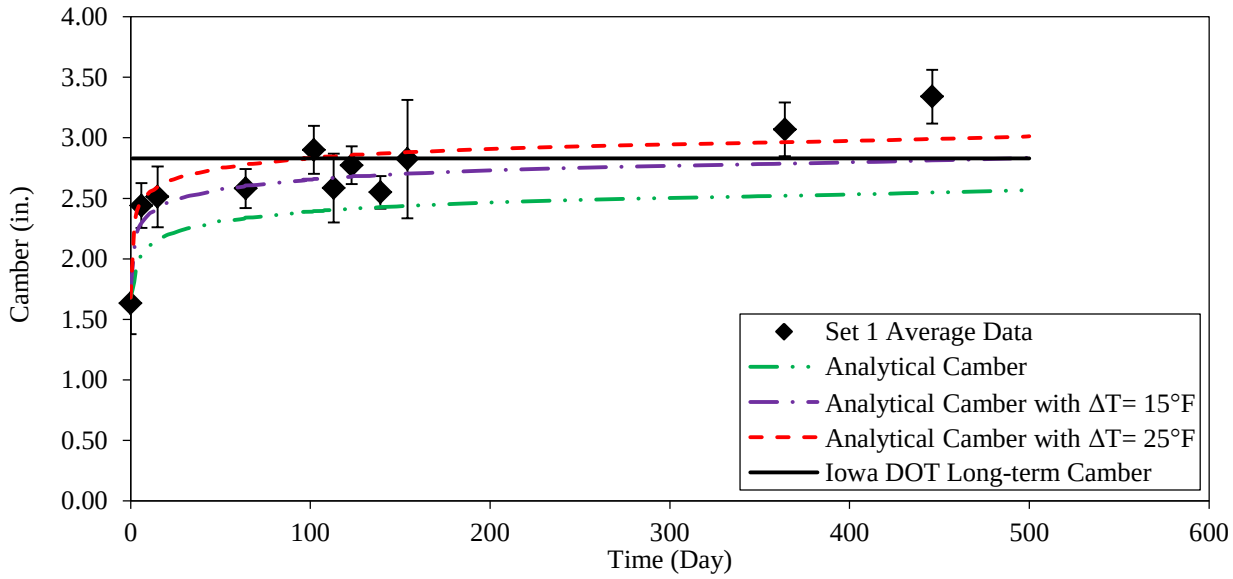

Figure 7.14. Prediction of long-term camber for BTE 110 Set 1 PPCBs

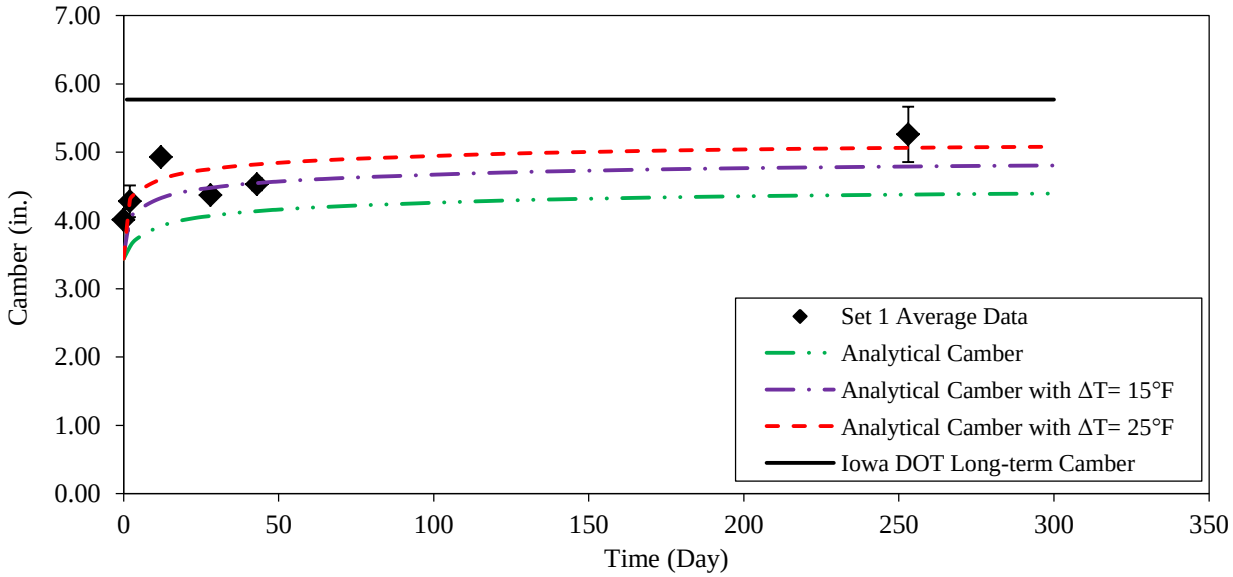

Figure 7.15. Prediction of the long-term camber for BTE 145 Set 1 PPCBs

In each of these figures, an analytical camber curve with no overhang, the same analytical curve with 15°F and 25°F temperature differences, the current Iowa DOT long-term design camber, and the adjusted measured camber data without overhang are presented. The adjusted measured camber data without overhang includes the average of the measured long-term camber data combined with an error bar to indicate the variation in the measured data within each set of PPCBs.

The analysis results presented above indicate that the current Iowa DOT method, which uses Martin's multipliers (1977), is appropriate for predicting the long-term camber within the

anticipated effects of the temperature gradient at an age beyond 200 days. However, this method can lead to significant errors when predicting the camber at an age of PPCB erection less than 200 days.

The FEA results also revealed that the scatter seen in the measured camber could have been largely due to the effects of the temperature gradients because the camber measurements were conducted at different times during the course of the day. This scatter was well captured by the analytical model using an assumed temperature difference of 15°F. The current Iowa DOT method of prediction is unable to account for the thermal effects in the analysis. Therefore, the current Iowa DOT method for predicting the camber should be replaced with a more accurate approach with due consideration given to the time of the erection and the possible effects of the temperature gradients.

Additionally, Figure 7.16 and Figure 7.17 show the FEA-predicted camber versus the measured camber for the large-camber PPCBs with temperature differences of zero and 15°F, respectively.

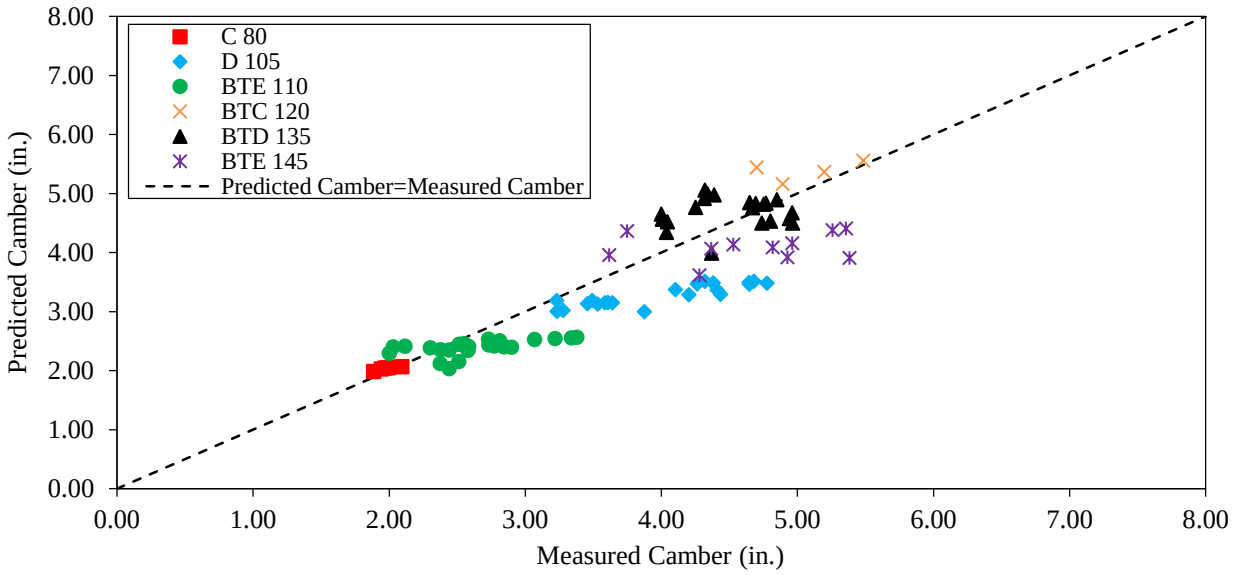

Figure 7.16. Predicted camber versus measured camber using the continuous power function with a zero temperature difference for the large-camber PPCBs

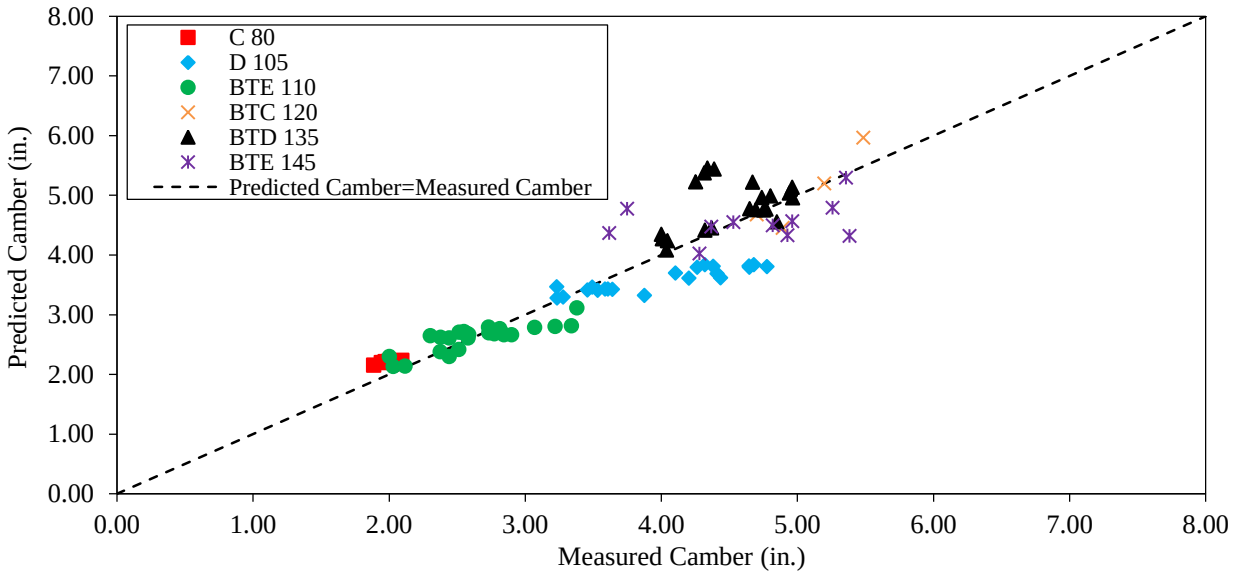

Figure 7.17. Predicted camber versus measured camber using the continuous power function with a 15°F temperature difference for the large-camber PPCBs

The FEA-predicted camber versus the measured camber for the small-camber PPCBs with zero and 15°F temperature differences are shown in Figure 7.18 and Figure 7.19, respectively.

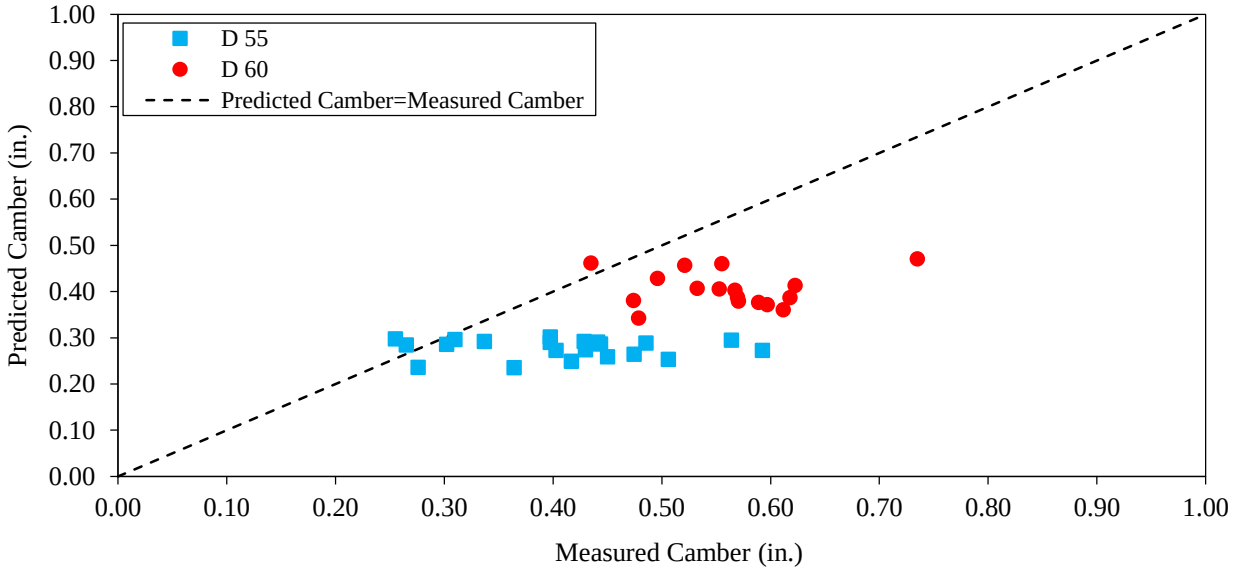

Figure 7.18. Predicted camber versus measured camber using the continuous power function with a zero temperature difference for the small-camber PPCBs

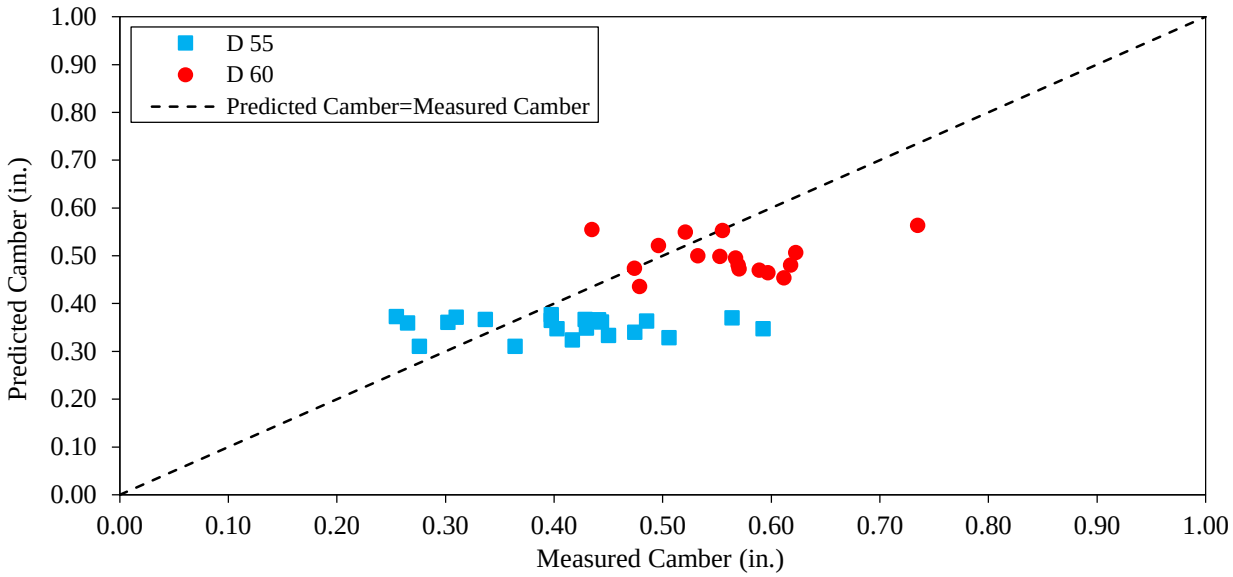

Figure 7.19. Predicted camber versus measured camber using the continuous power function with a 15°F temperature difference for the small-camber PPCBs

In summary, the average error between the measured camber and the FEA results was -8.6% ± 14.5% and 24.1% ± 29.5% for the large- and small-camber PPCBs, respectively, without accounting for the thermal effects. The low values of the camber (i.e., less than 0.6 in.) obtained for the small-camber PPCBs caused a relatively greater error than for the large-camber PPCBs with high camber values. Moreover, introducing a temperature difference of 25°F captured high-camber values due to the thermal effects. However, as the previous sensitivity analysis in Section 7.4.7 indicated, the error between the measured and analytical camber was minimized when the average temperature difference of 15°F was assumed for the analysis. So, using the temperature difference of 15°F changed the corresponding errors to -1.2% ± 10.7% and -14.7% ± 22.5% for the large- and small-camber PPCBs, respectively. The total average error for the group, including both small- and large-camber PPCBs, was -19.3% ± 25.9% and -5.2% ± 16.5% for the temperature differences of zero and 15°F, respectively. These observations suggest that the incorporation of a temperature difference of 15°F likely leads to a closer correlation between the measured and predicted long-term camber.

Furthermore, the predicted FEA camber was compared to the measured data in the same fashion as it was carried out in Section 6.6 with zero overhang. The results presented in Figure 7.20 indicate that the data points are generally bound within ± 15% lines, while the results in Section 6.6 were within ± 25% lines, which leads to the conclusion that the camber prediction accuracy of the FEA is superior to that of the simplified method.

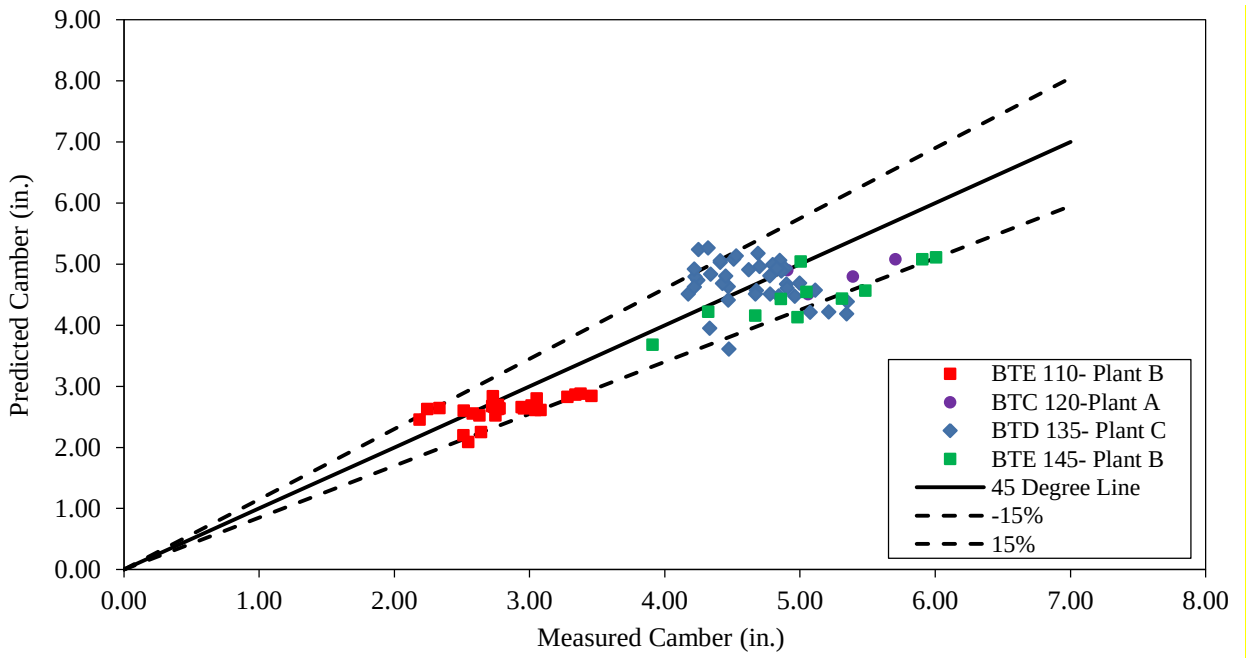

Figure 7.20. Comparison of the predicted camber using the FEA and the adjusted measured camber for the Iowa bub-tee PPCBs without overhangs

7.5.3 Multipliers

Although continuous analytical curves have been generated to predict the long-term camber for different PPCB types, such an approach may not be easy to implement in design practice. Therefore, suitable multipliers for accurately estimating the long-term camber of the PPCBs are established in this section. This was achieved by comparing the estimated instantaneous camber with the estimated long-term camber for the different standard PPCB lengths of the same PPCB type. Three different forms for the multipliers were given consideration: (1) a continuous power function, (2) a set of average multipliers, and (3) a single multiplier. The first option allows a designer to determine a suitable multiplier at a distinct time of PPCB erection. However, the exact time of erection for a PPCB during construction is commonly unknown, which could cause additional inaccuracies in the camber estimation. Hence, in the second approach, multipliers are presented for different durations within which the PPCBs may be erected, because it was realized that a single multiplier would not adequately account for the effect of the time variation on the at-erection camber. Based on the measured camber growth with time, three separate time intervals were found to be reasonable for establishing these multipliers: 0 to 60 days, 60 to 180 days, and 180 to 480 days. The change in the camber after 480 days is relatively small, and precasters are not expected to store the PPCB for a period beyond 480 days. The third option further facilitates the design process by eliminating the unknown variable of the at-erection age by using a single multiplier to predict the long-term camber at any time during a PPCB's life.

7.5.3.1 Multipliers for PPCBs without Overhang

The effects of overhang are excluded in this section because the current Iowa DOT practice does not provide any guidelines on the required overhang length for storage purposes (see Section 4.2.4). Figure 7.21 and Figure 7.22 show the multipliers calculated for different types of PPCBs in each group versus time, together with the average multipliers as a function of time, which in each case was found as the curve that best fit the average multipliers. The equations corresponding to the average multiplier and the R^2 value are included within each figure.

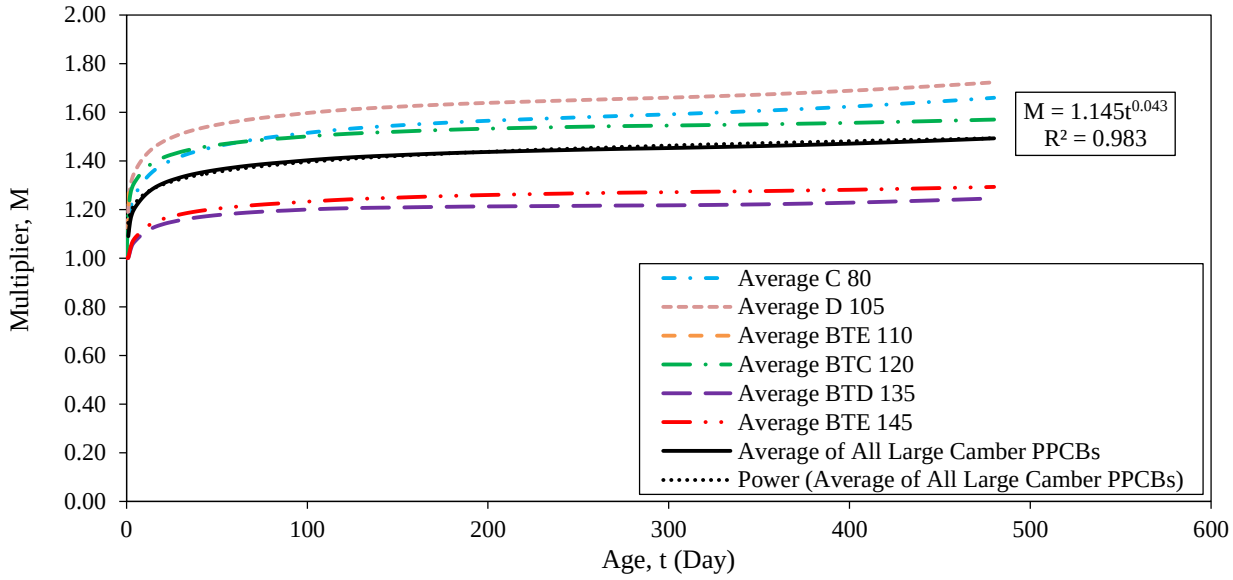

Figure 7.21. Long-term camber multipliers as a function of time for the large-camber PPCBs

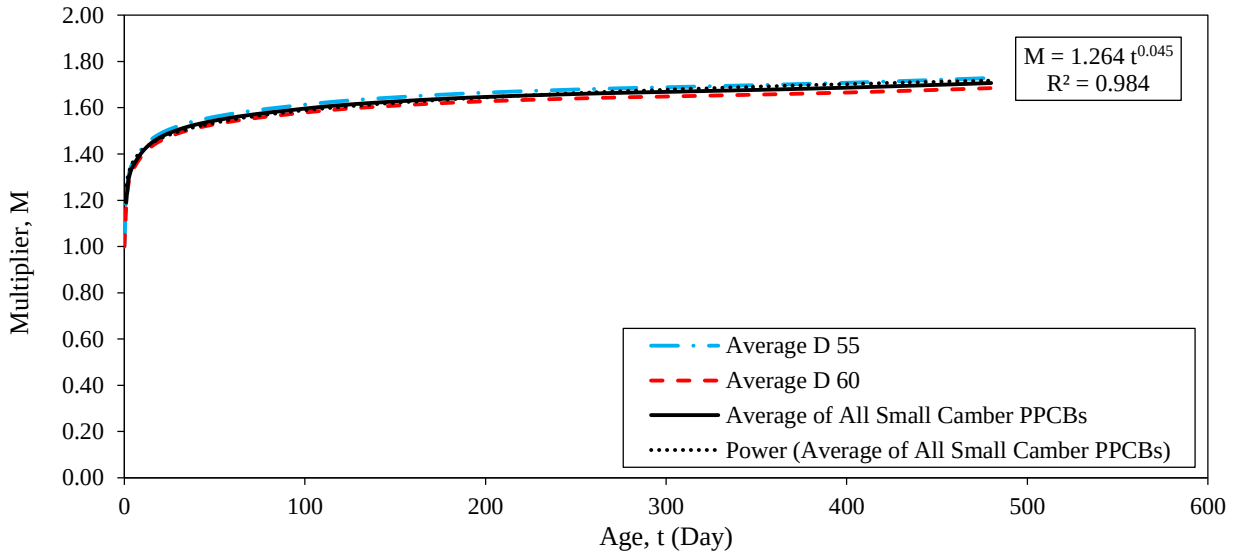

Figure 7.22. Long-term camber multipliers as a function of time for the small-camber PPCBs

Next, the proposed average continuous power function for each group was evaluated for three different time intervals, as introduced above. For each time interval, a power function that best fit the average multipliers curve was found. This power function was subsequently used to calculate the average multiplier and the corresponding average time for the three intervals, as shown in Table 7.2.

Table 7.2. Set of multipliers recommended for at-erection camber prediction with zero overhang during storage

Erection Period (days)	PPCB Type	Average Time Used (days)	Multiplier
0–60	Small Camber PPCBs	40	1.53 ± 0.02
	Large Camber PPCBs	40	1.35 ± 0.01
60–180	Small Camber PPCBs	120	1.61 ± 0.02
	Large Camber PPCBs	120	1.41 ± 0.02
180–480	Small Camber PPCBs	300	1.67 ± 0.02
	Large Camber PPCBs	310	1.46 ± 0.02

7.5.3.1.1 Accounting for the Temperature Gradients

To account for the influence of the temperature gradients on the long-term camber, an additional multiplier is suggested. This temperature multiplier, λ_T, is used in addition to those presented above to estimate the at-erection camber in such as way as to include the effects of the temperature gradients. λ_T was determined as the ratio of the summation of the long-term camber and the thermal deflection to the long-term camber. Figure 7.23 shows λ_T versus the temperature difference for the various types of large-camber PPCBs. λ_T is linearly proportional to the temperature difference and is almost the same for different types of PPCBs for lower values of ΔT in each group. Hence, an average linear function in Figure 7.23 is proposed to calculate λ_T for all the large-camber PPCBs. The same procedure was repeated for the small-camber PPCBs, and the results are shown in Figure 7.24.

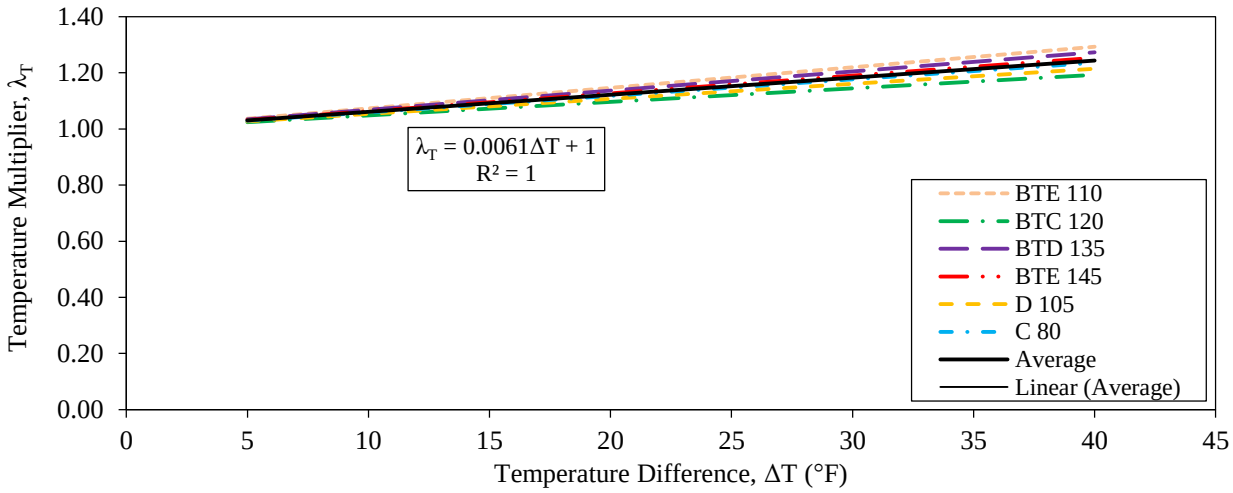

Figure 7.23. Temperature multiplier versus temperature difference for the large-camber PPCBs

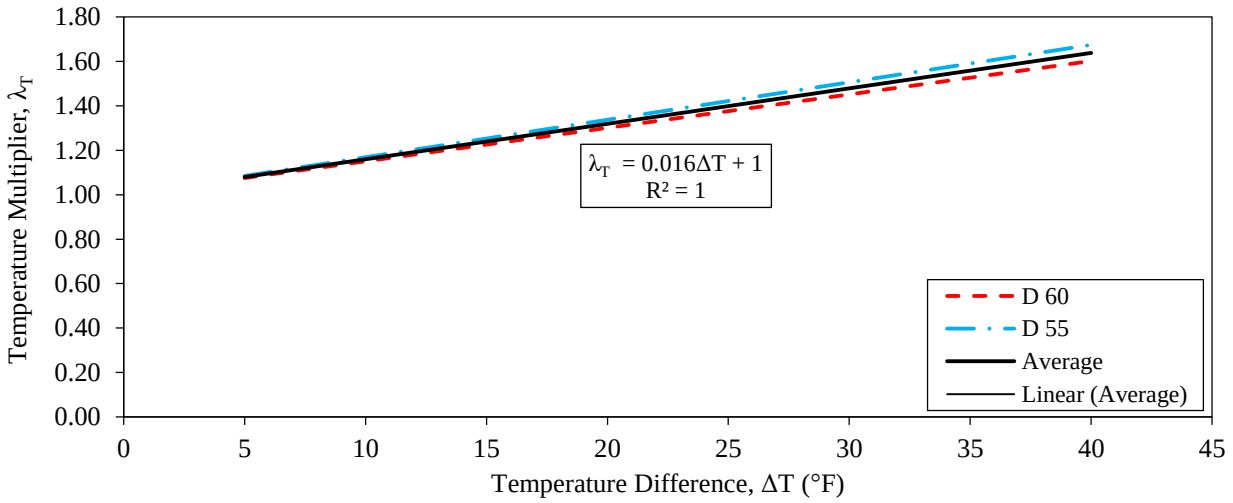

Figure 7.24. Temperature multiplier versus temperature difference for the small-camber PPCBs

Using the multipliers suggested in Table 7.2 and the temperature multiplier equation in Figure 7.23 and Figure 7.24, a few examples illustrating how well the cambers estimated from the proposed approach compared to the measured data are shown in Figure 7.25 through Figure 7.28. Similar comparisons for the other PPCBs can be found in Appendix K.

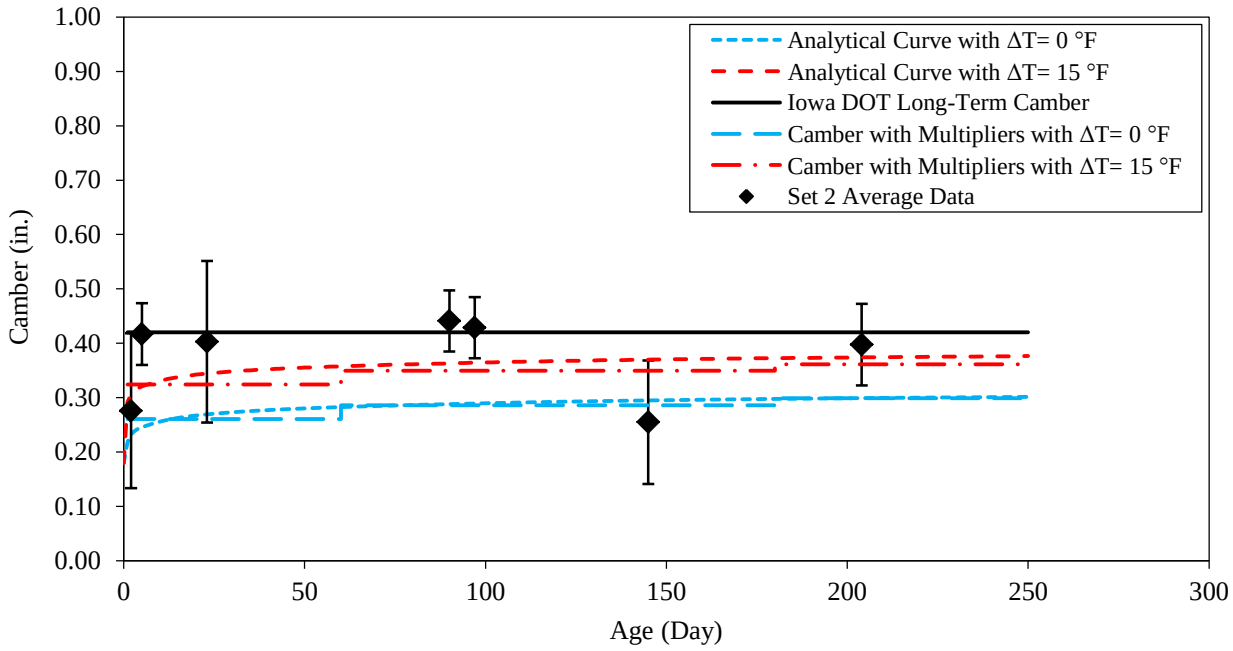

Figure 7.25. Measured and estimated long-term cambers for D 55 Set 2 PPCBs

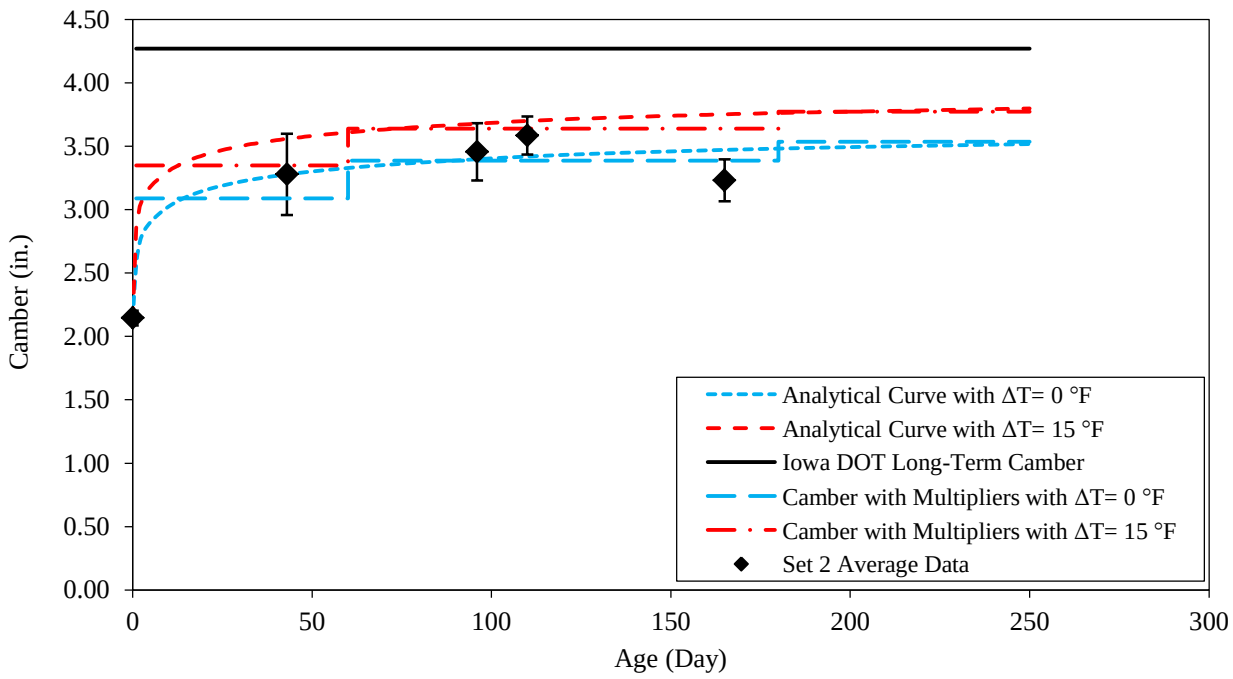

Figure 7.26. Measured and estimated long-term cambers for D 105 Set 2PPCBs

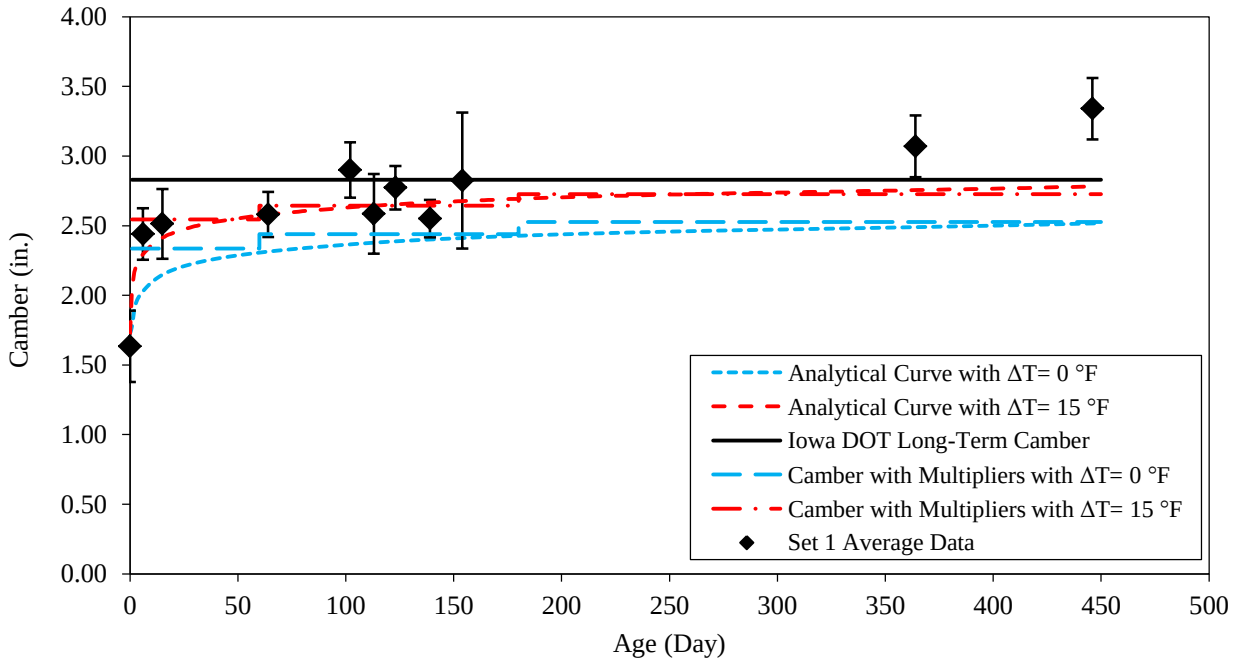

Figure 7.27. Measured and estimated long-term cambers for BTE 110 Set 1 PPCBs

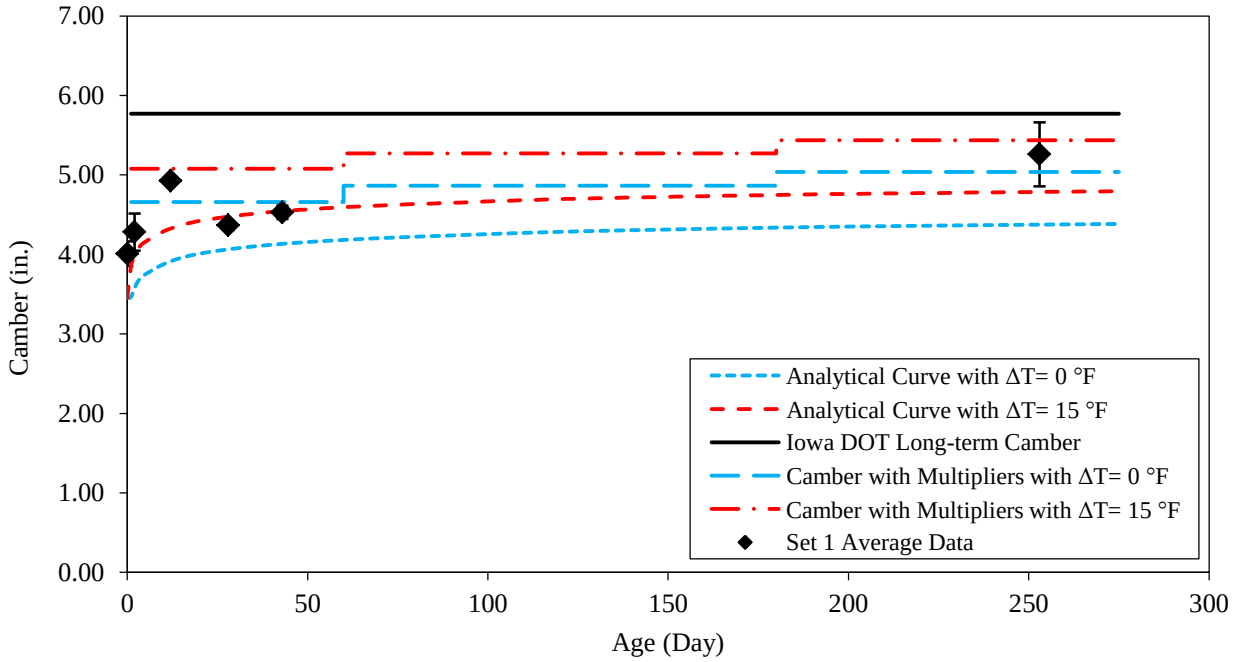

Figure 7.28. Measured and estimated long-term cambers for BTE 145 Set 1 PPCBs

A good agreement was also found between the measured data and the predicted camber when the set of multipliers was used instead of the continuous power function. In addition, it is noteworthy that the set of multipliers used in the figures above represents the average multipliers used for the entire set of small- and large-camber PPCBs, while the analytical continuous curves were

generated specifically for each PPCB set. This use of the average multipliers contributes to the difference observed between the analytical curve and the step-wise function, which represents the set of multipliers, as shown in Figure 7.28.

Furthermore, comparisons between the predicted camber and the measured camber using the set of multipliers for the small- and large-camber PPCBs with temperature differences of zero and 15°F are shown in Figure 7.29 throughFigure 7.32.

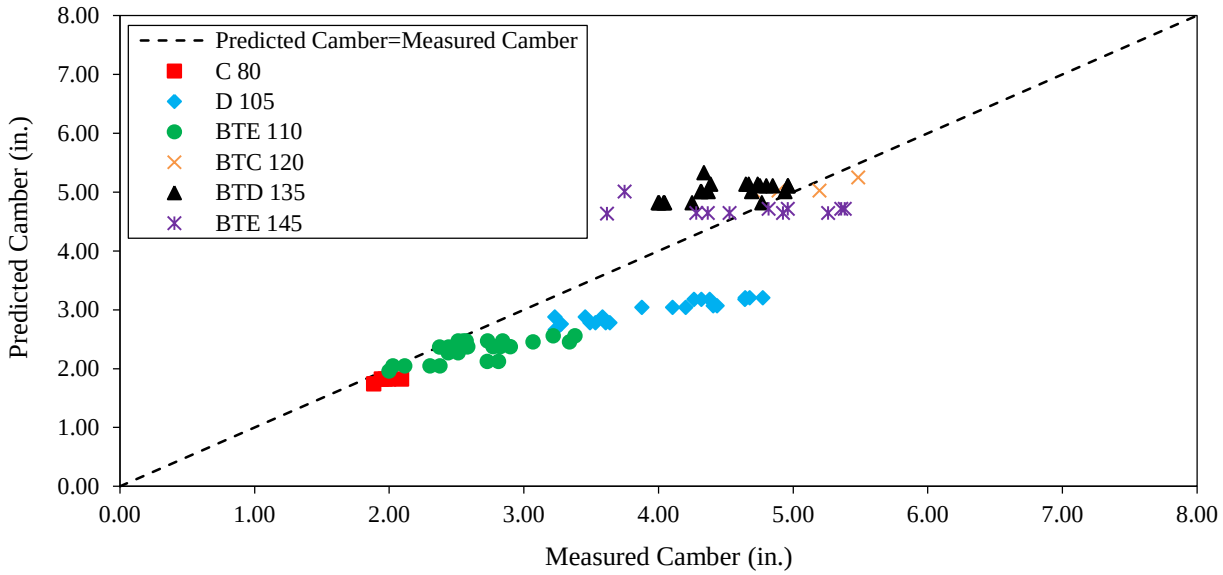

Figure 7.29. Predicted camber versus measured camber using the set of multipliers, excluding overhang, with a zero temperature difference for the large-camber PPCBs

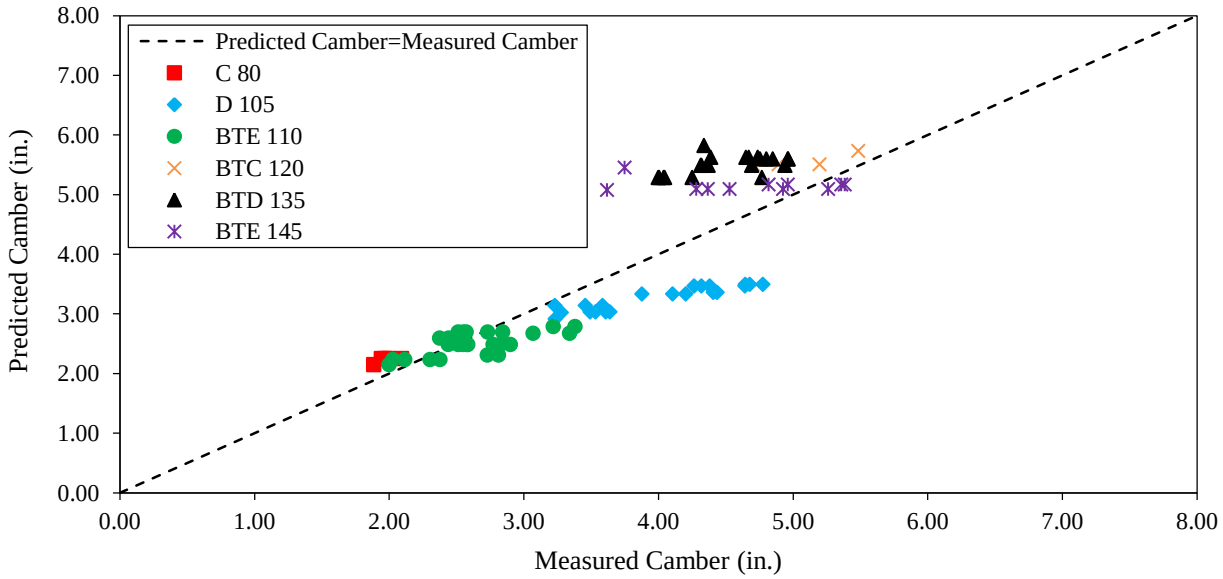

Figure 7.30. Predicted camber versus measured camber using the set of multipliers, excluding overhang, with a 15°F temperature difference for the large-camber PPCBs

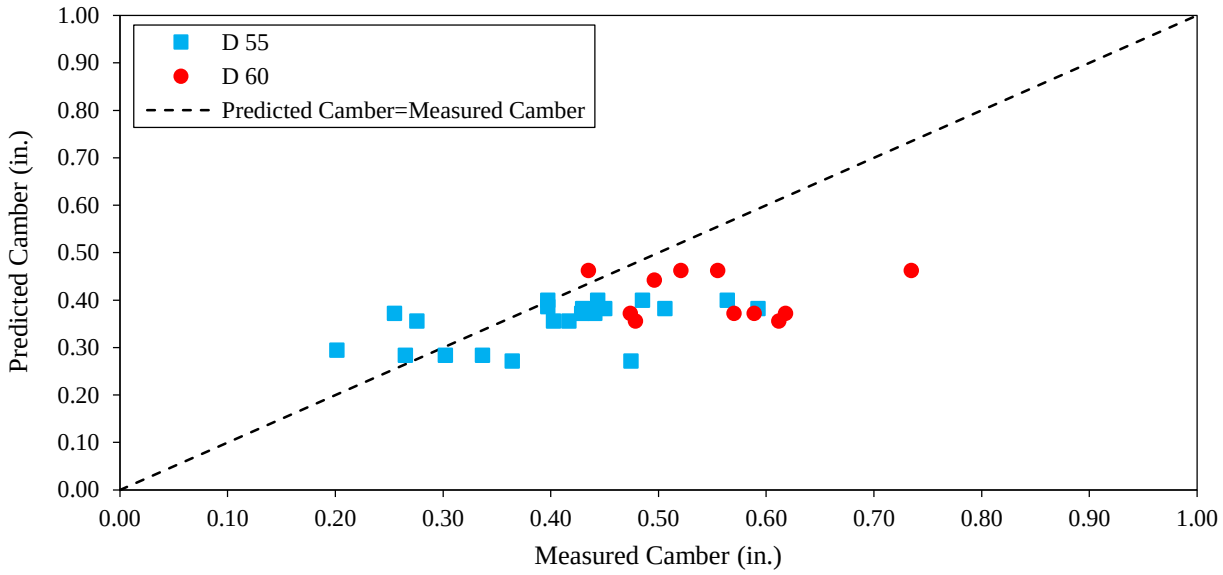

Figure 7.31. Predicted camber versus measured camber using the set of multipliers, excluding overhang, with a zero temperature difference for the small-camber PPCBs

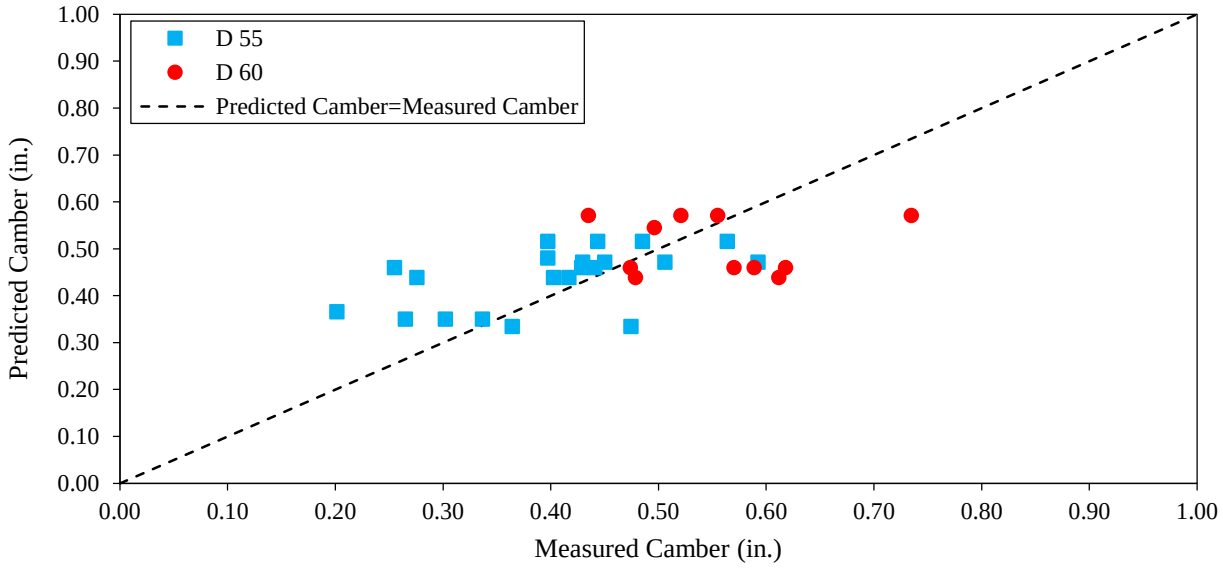

Figure 7.32. Predicted camber versus measured camber using the set of multipliers, excluding overhang, with a 15 °F temperature difference for the small-camber PPCBs

In summary, the average error between the measured camber and the predicted camber using the recommended multipliers was -10.1% ± 18.4% and -26.0% ± 27.0% for the large- and small-camber PPCBs, respectively, with zero temperature difference. When a 15°F temperature difference was included, the corresponding error was -0.2% ± 17.3% and -1.5% ± 22.1% for the large- and small-camber PPCBs, respectively. The total average error for the group, including both the small- and large-camber PPCBs, was -14.9% ± 22.5% and -0.6% ± 18.8% for temperature differences of zero and 15°F, respectively.

7.5.3.2 Multipliers with Overhang

The average overhang length (L/30) estimated in Section 4.2.4 was used to recalculate the multipliers in the same fashion as outlined in the previous section. Figure 7.33 and Figure 7.34 show the results for the proposed multiplier function for each group.

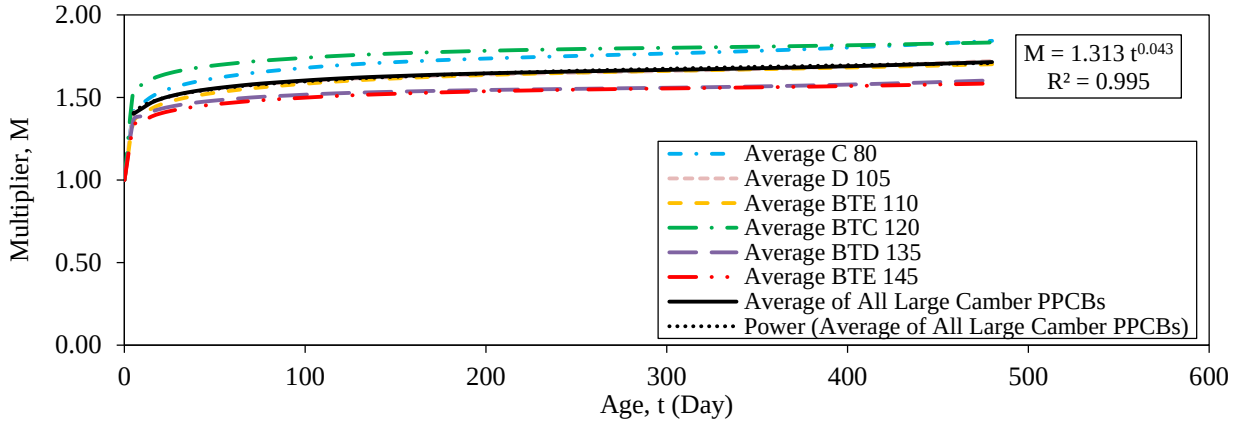

Figure 7.33. Multipliers versus time for the large-camber PPCBs with an overhang length of L/30

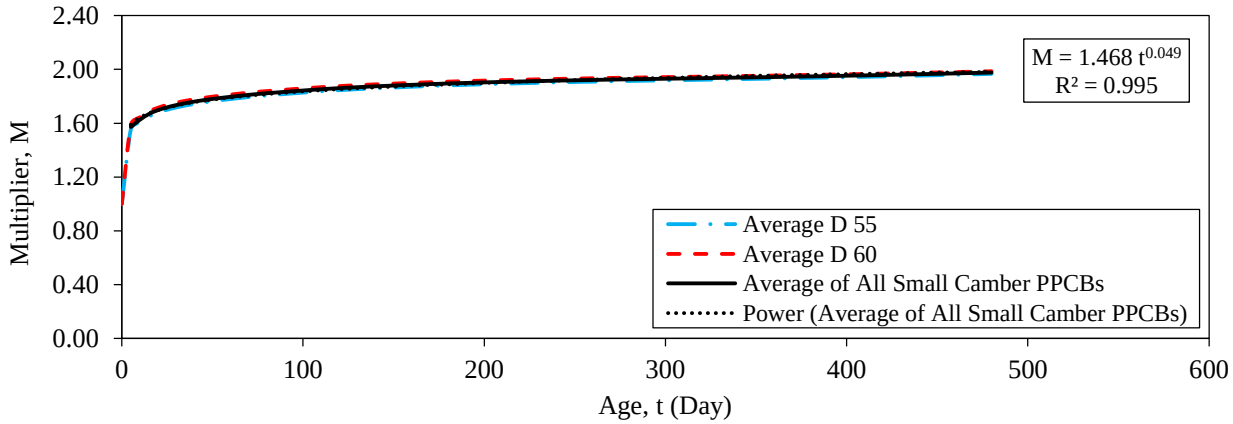

Figure 7.34. Multipliers versus time for the small-camber PPCBs with an overhang length of L/30

Table 7.3 presents the recommended set of multipliers for the long-term camber prediction of each group.

Table 7.3. Set of multipliers recommended for the at-erection camber prediction with an overhang length of L/30 during storage

Erection Period (days)	PPCB Type	Average Time Used (days)	Multiplier
0–60	Small-camber PPCBs	45	1.77 ± 0.02
	Large-camber PPCBs	45	1.55 ± 0.02
60–180	Small-camber PPCBs	120	1.86 ± 0.03
	Large-camber PPCBs	115	1.61 ± 0.02
180–480	Small-camber PPCBs	340	1.94 ± 0.02
	Large-camber PPCBs	320	1.68 ± 0.02

Using the multipliers in Table 7.3, the designed long-term camber was estimated for each group. The thermal effects were also included using the λ_T multiplier calculated in Section 0. Then, the predicted camber was compared to the measured camber for the small- and large-camber PPCBs with temperature differences of zero and 15°F, as shown in Figure 7.35 through Figure 7.38.

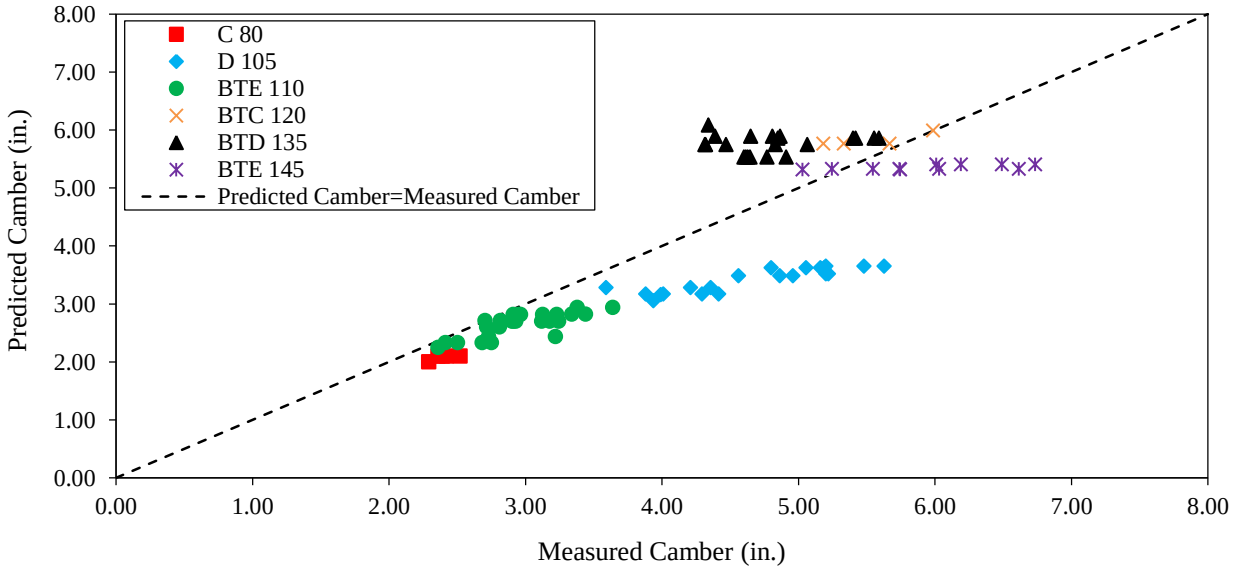

Figure 7.35. Predicted camber versus measured camber using the set of multipliers, including an average overhang length of L/30 with a zero temperature difference, for the large-camber PPCBs

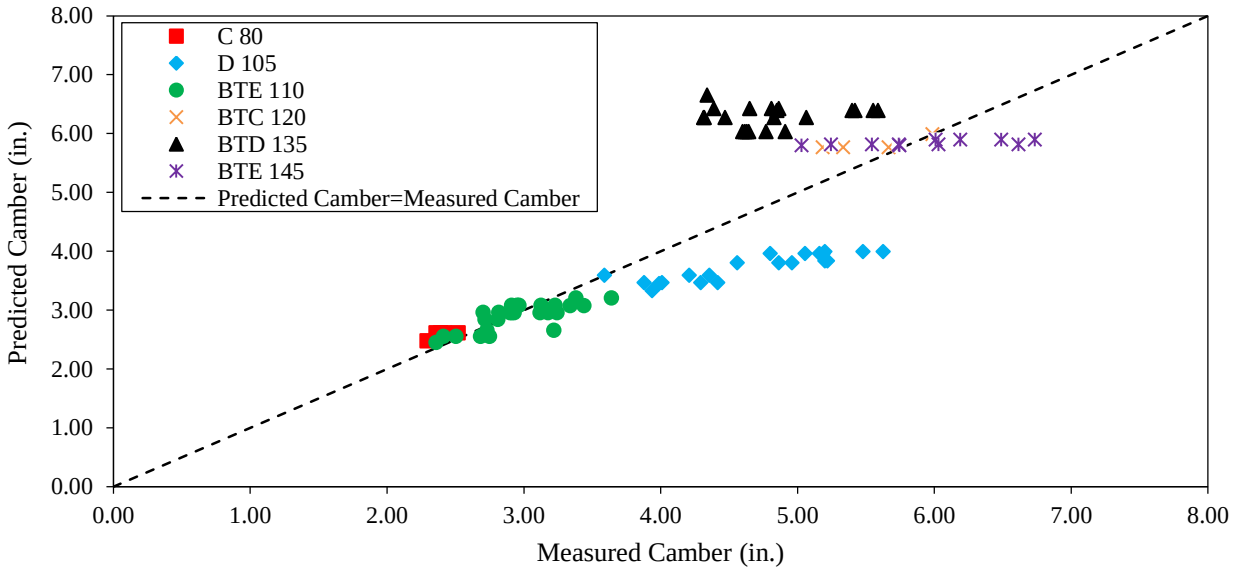

Figure 7.36. Predicted camber versus measured camber using the set of multipliers, including an average overhang length of L/30 with a 15°F temperature difference, for the large-camber PPCBs

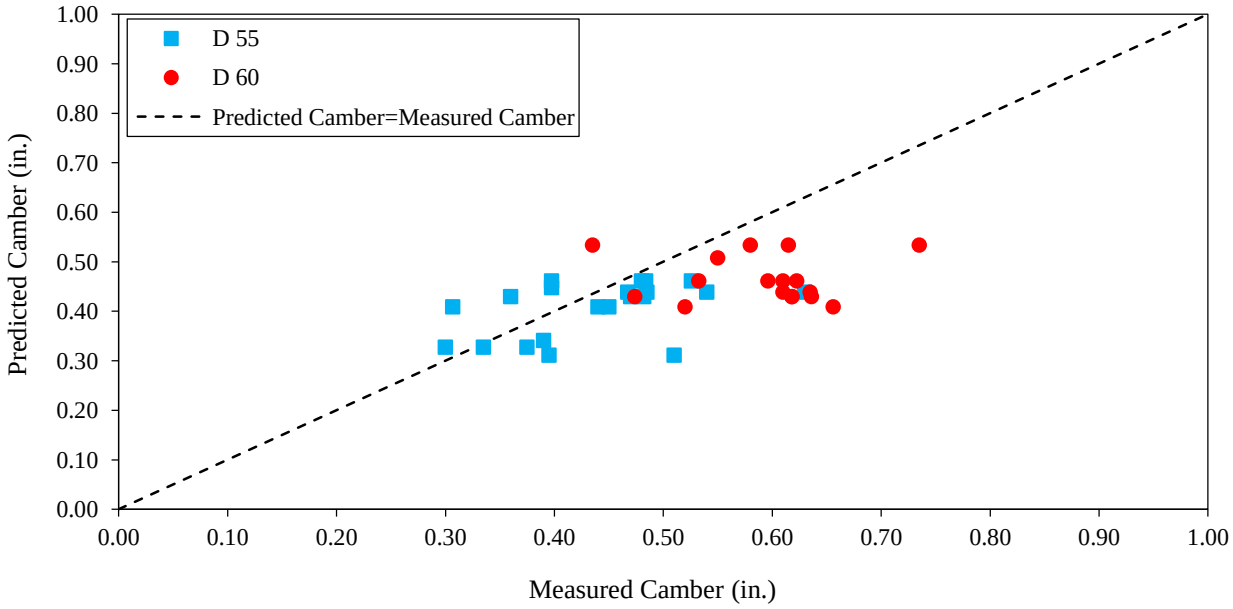

Figure 7.37. Predicted camber versus measured camber using the set of multipliers, including an average overhang length of L/30 with a zero temperature difference, for the small-camber PPCBs

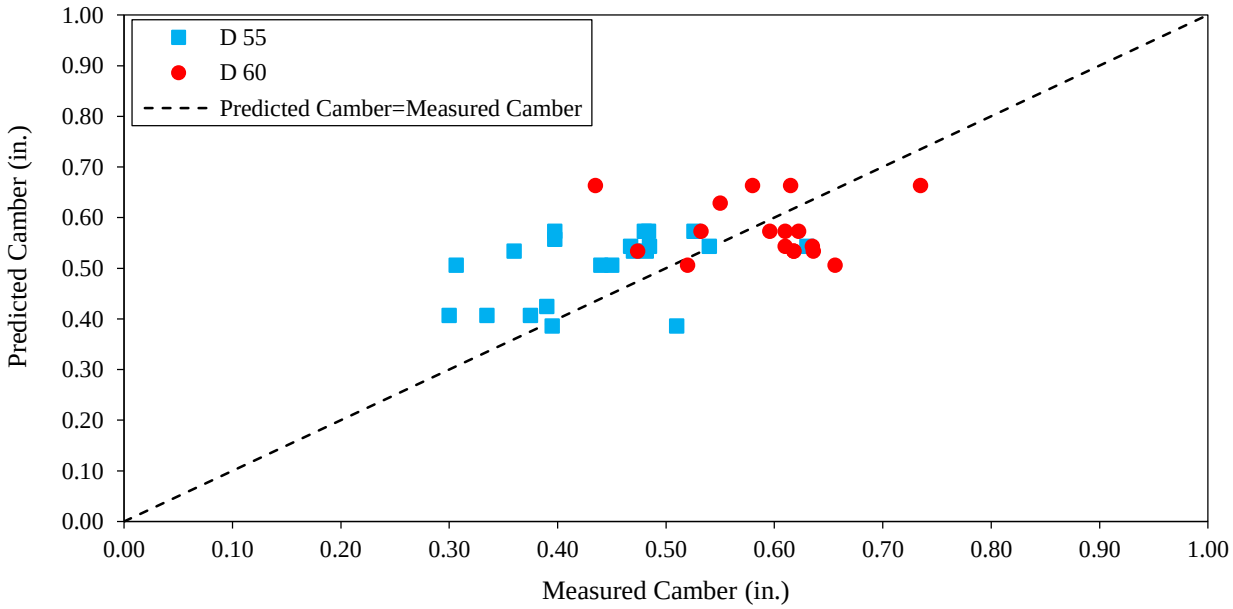

Figure 7.38. Predicted camber versus measured camber using the set of multipliers, including an average overhang length of L/30 with a 15°F temperature difference, for the small-camber PPCBs

It can be inferred from the results that the measured camber is typically higher than the designed camber if the thermal effects are excluded, while the measured camber is typically lower than the designed camber when the thermal effects are included. On average, the error between the measured and predicted camber was -10.2% ± 20.3% and -17.7% ± 21.7% for the large- and small-camber PPCBs, respectively, with a zero temperature difference. Also, on average, the error between the measured and predicted camber was -0.2% ± 18.6% and 5.1% ± 17.5% for the large- and small-camber PPCBs, respectively, with a 15°F temperature difference. The total average error between the measured and predicted camber, including both the large- and small-camber PPCBs, was -12.4% ± 20.9% and 1.4% ± 18.4% for the temperature differences of zero and 15°F, respectively. The thermal effects are one of the likely reasons that the camber is sometimes overpredicted and other times underpredicted. Underpredicting the camber can cause the PPCB to protrude into the deck profile in the midspan region, while overpredicting the camber leads to the placement of additional reinforcements.

7.5.3.3 Single Multiplier

A set of multipliers was proposed above to predict the long-term camber of PPCBs for three different time intervals. However, a single multiplier is introduced in this section to further simplify the camber prediction method; this may be preferred in design practice. This single multiplier is calculated for the average PPCB at erection separately for the large- and small-camber PPCBs with both a zero overhang length and an average overhang length of L/30. Table 7.4 shows the average PPCB age at the time of erection for different projects.

Table 7.4. Average ages of the PPCBs at the time of erection before the deck pour for different projects

Project Name	Average (Days)	Standard Deviation (Days)
Sac County Project (36 PPCBs)	168	20
Dallas County Project (8 PPCBs)	56	9
Polk County Project (4 PPCBs)	117	0
Mills County Project (15 PPCBs)	361	100
Other Projects (17 PPCBs)	128	32
Total Average of All Projects	166	116
Total Average of All Projects without Mills County Project	117	46

Among all the projects, Mills County Bridge showed some anomalies for the PPCB age at erection, which led to an unrealistic average age. Hence, the PPCB average age at erection was estimated by averaging the age of the PPCBs from all listed projects except the Mills County project. The results indicate that the average age of the PPCBs at the time of erection before the deck pour was 117 days, which was rounded to 120 days for the subsequent analysis. Figure 7.39 shows a histogram of the PPCB age at the time of erection before the deck pour.

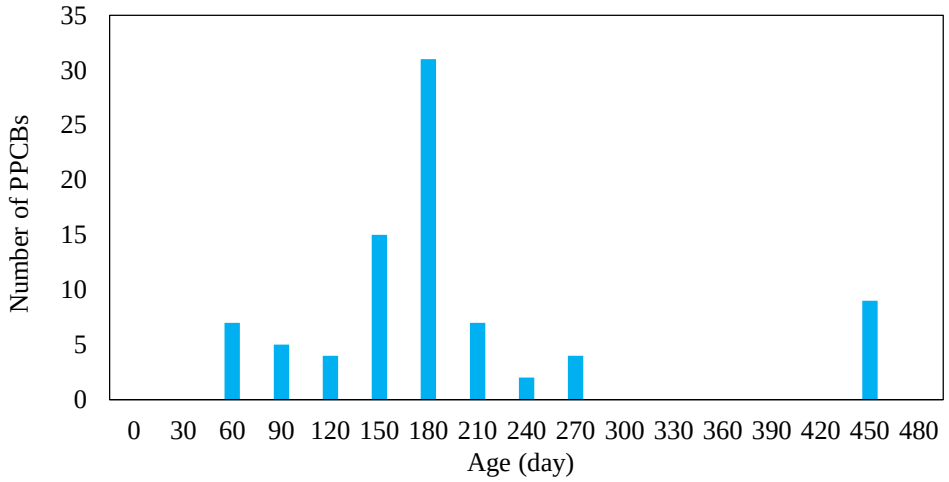

Figure 7.39. Histogram of the PPCB ages at the time of erection before the deck pour

Using the multiplier functions developed in Section 0 and the temperature multiplier developed in Section 0 for a temperature difference of 15°F, a single multiplier was calculated for an average time of 120 days for the large- and small-camber PPCBs. The recommended multipliers for the conditions of zero overhang length and an average overhang length of L/30 are shown in Table 7.5 and Table 7.6, respectively.

Table 7.5. Single multiplier recommendation for at-erection camber prediction with zero overhang during storage

Group	Average Time	Single Multiplier
Large Camber PPCBs	120	1.41
Small Camber PPCBs	120	1.57

Table 7.6. Single multiplier recommendation for at-erection camber prediction with an overhang length of L/30 during storage

Group	Average Time	Single Multiplier
Large Camber PPCBs	120	1.61
Small Camber PPCBs	120	1.86

Using the recommended multipliers, the long-term camber was recalculated and then compared to the measured data for both groups of PPCBs, as presented in Figure 7.40 through Figure 7.43.

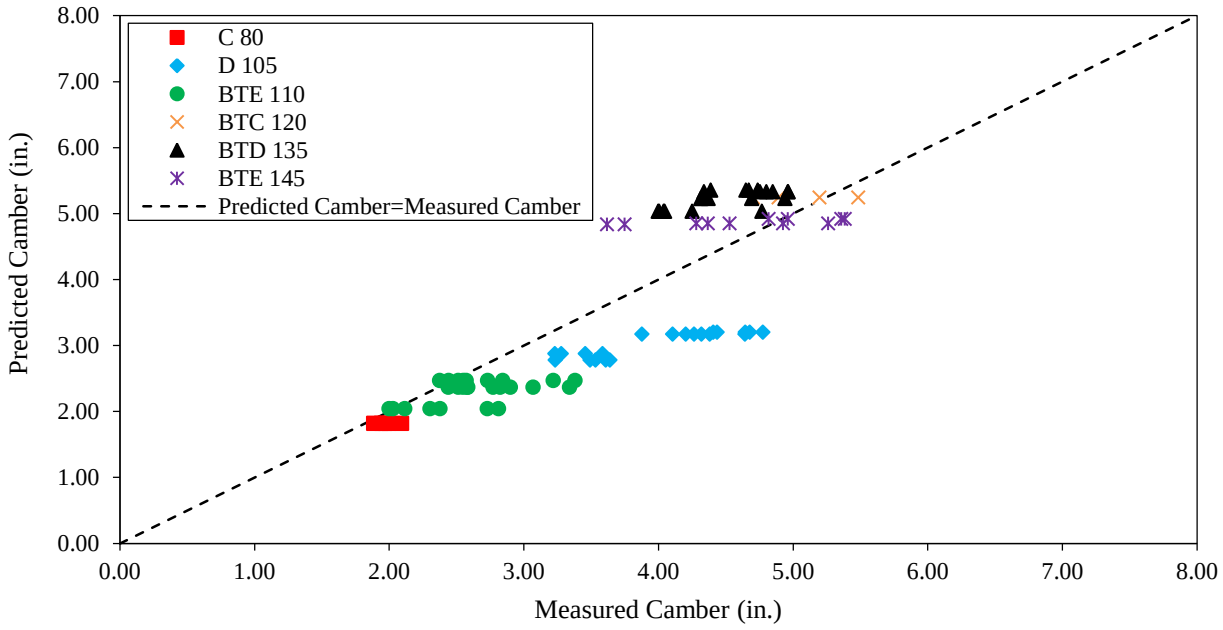

Figure 7.40. Predicted camber versus measured camber using the single multiplier, excluding overhang, for the large-camber PPCBs

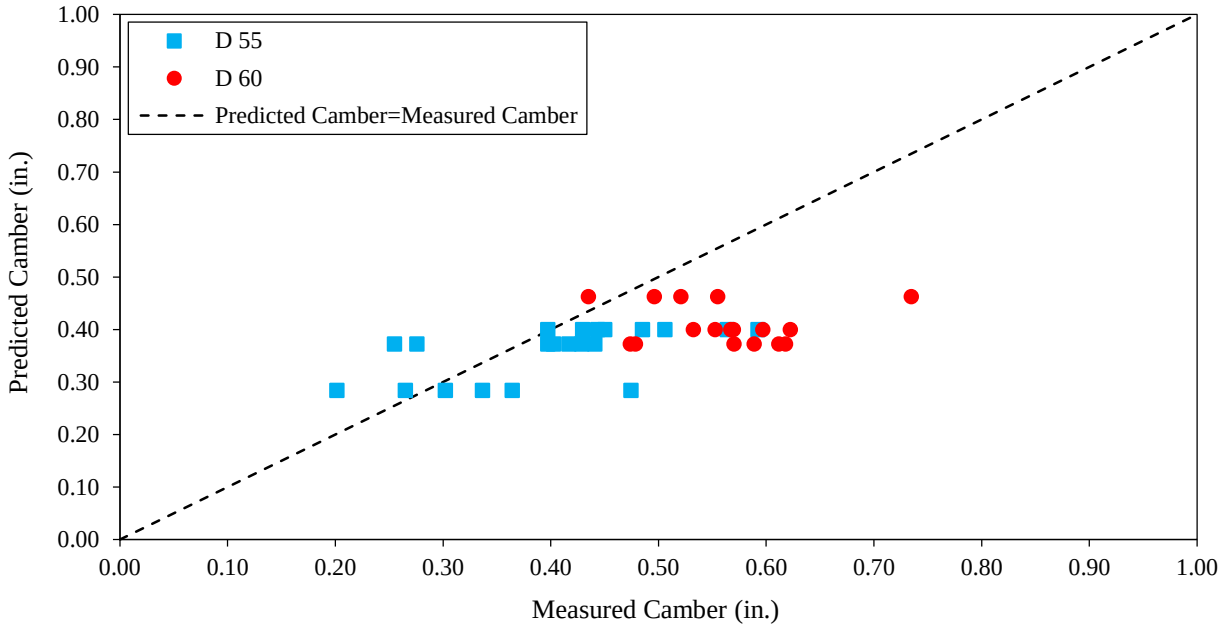

Figure 7.41. Predicted camber versus measured camber using the single multiplier, excluding overhang, for the small-camber PPCBs

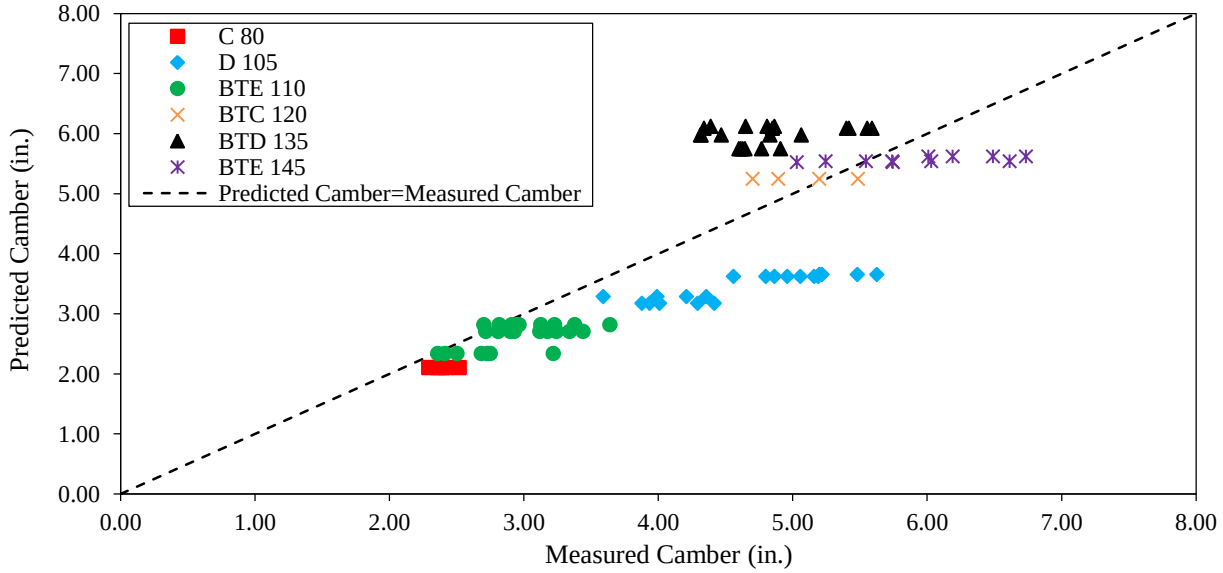

Figure 7.42. Predicted camber versus measured camber using the single multiplier, including the average overhang length of L/30, for the large-camber PPCBs

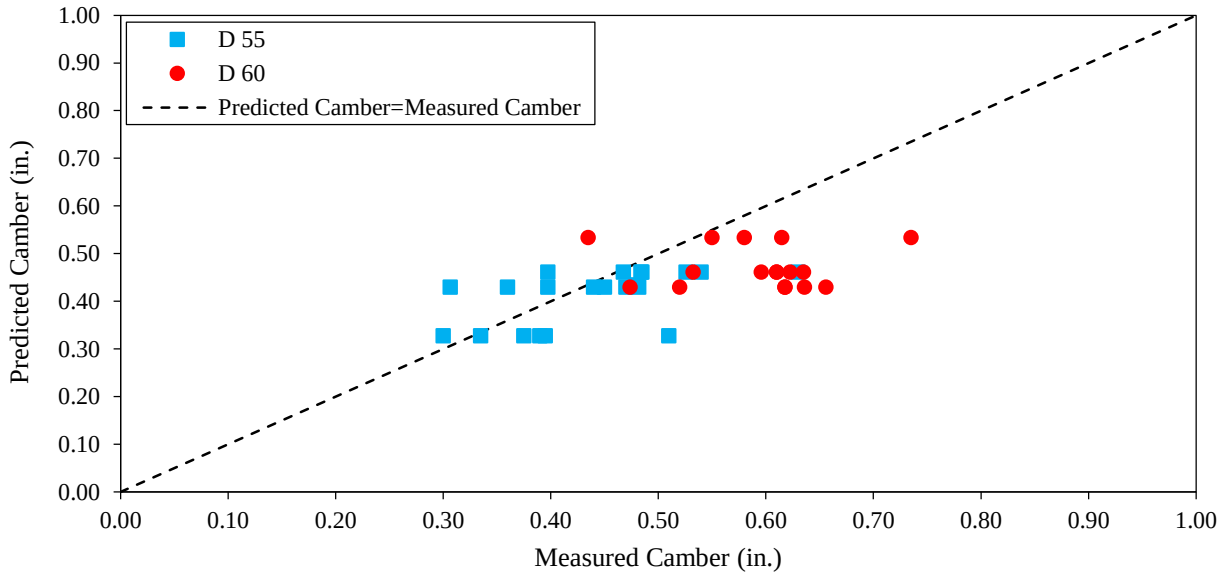

Figure 7.43. Predicted camber versus measured camber using the single multiplier, including an average overhang length of L/30, for the small-camber PPCBs

The average error between the predicted and the measured long-term camber was 4.5% ± 17.2% and 15.3% ± 20.9% for the large- and small-camber PPCBs, respectively, when the single multiplier method with the adjusted data for the zero overhang length was used. When the single multiplier method with an average overhang length of L/30 was used, the corresponding error was -8.5% ± 21.1% and 15.9% ± 20.5% for the large- and small-camber PPCBs, respectively.

7.6 Comparison of Different Proposed Long-term Camber Prediction Methods

Different long-term camber prediction methods were evaluated according to the criterion that if the difference between the measured and designed camber is less than ± 1.0 in., no construction difficulties would be expected in the field. Thus, a histogram of the difference between the measured and designed camber for each prediction method was created. The histogram was used to determine the percentage of the data that adhere to the aforementioned criterion. For instance, the histogram of the difference between the measured and designed camber for the entire set of PPCBs (i.e., the large- and small-camber PPCBs together) using the multiplier function with a zero overhang length and a temperature difference of 15°F is depicted in Figure 7.44. It can be seen that 93% of the data points fall within ±1.0 in.

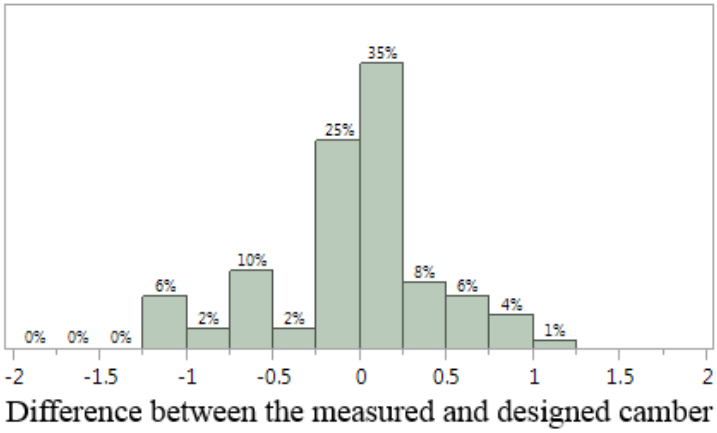

Figure 7.44. Histogram of the difference between the measured and the designed camber of all the PPCBs using the multiplier function

The same procedure was repeated to produce a histogram for each prediction method. Table 7.7 shows the average and standard deviation for the difference between the measured and designed camber as well as the percentage of the data for the difference between the measured and designed camber that falls within ±1.0 in. for the different prediction methods.

Table 7.7. Difference between the measured and the designed cambers for the different prediction methods

Prediction Method	Temperature Difference (°F)	Average (in.)	Standard Deviation (in.)	-1 in. ≤ Difference (%) ≤ 1 in.
Multiplier Function with Adjusted Data for Overhang	0	0.22	0.44	93
	15	-0.04	0.46	93
Set of Multipliers with Adjusted Data for Overhang	0	0.18	0.54	89
	15	-0.08	0.6	85
Set of Multipliers with Overhang Length of L/30	0	0.19	0.72	80
	15	-0.11	0.78	80
Single Multiplier with Adjusted Data for Overhang	15	0.12	0.58	89
Single Multiplier with Average Overhang Length of L/30	15	0.13	0.77	79
Iowa DOT	0	-0.17	0.71	75

Using the multiplier function with the data adjusted for overhang produced the best agreement between the measured and the designed camber, while using the current Iowa DOT prediction method produced the poorest agreement, as shown in Table 7.7. Additionally, it can be seen that using a single multiplier calculated for the condition of an average overhang length of L/30 produced results similar to that of the single multiplier method used by the Iowa DOT. However, by using a single multiplier, which eliminated the contribution of the overhang to the long-term camber, a better correlation was found between the measured and the designed camber than that produced by the Iowa DOT method.

7.7 Summary and Conclusions

Analytical models, including different parameters affecting the long-term camber estimation, as outlined in Section 2.3.2, were developed using the FEM. The analyses were carried out to predict the camber history from the release to the time of erection for Iowa DOT PPCBs of varying lengths and depths as used in five different bridge projects. The average error between the measured data and the FEA results was computed to be 8.6% ± 14.5% and 24.1% ± 29.5% for the large- and small-camber PPCBs, respectively, when the temperature gradients were ignored. Also, inconsistencies in the measured camber due to the thermal effects necessitated an investigation of this issue, in which different temperature gradients were considered. The results showed that a linear temperature gradient with an average temperature difference of 15°F can most accurately capture the scatter in the data with an average error of -1.2% ± 10.7% and -14.7% ± 22.5% the for the large- and small-camber PPCBs, respectively. Moreover, by comparing the estimated long-term camber with the estimated instantaneous camber, a multiplier as a function of time, a set of average multipliers, and a single multiplier were proposed for the large- and small-camber PPCBs without an overhang. Also, the additional deflection due to the thermal effects was superimposed upon the long-term camber by employing the temperature multiplier, λ_T.

Using the recommended average set of multipliers and the temperature multiplier in combination with the adjusted data for the overhangs greatly improved the long-term camber estimation compared to the current Iowa DOT method. Also, it was seen that the scatter in the data due to the thermal effects can be satisfactorily captured using the proposed λ_T. In summary, the average error between the measured camber and the predicted camber was -10.1% ± 18.4% and -26.0% ± 27.0% for the large- and small-camber PPCBs, respectively, for a zero temperature difference. When a 15°F temperature difference was used, the corresponding errors were -0.2% ± 17.3% and -1.5% ± 22.1% for the large- and small-camber PPCBs, respectively.

A multiplier as a function of time and subsequently a set of average multipliers were also calculated for an average overhang length of L/30. Using the average set of multipliers, the long-term camber was recomputed and compared to the measured data with an overhang. The average error between the measured and predicted camber indicated that the camber was underpredicted when the thermal effects were not included, while the camber was overpredicted when the thermal effects were taken into account. When a zero temperature difference was used, the error between the predicted and measured camber was -10.2% ± 20.3% and -17.7% ± 21.7% for the large- and small-camber PPCBs, respectively. Using a 15°F temperature difference changed the corresponding errors to -0.2% ± 18.6% and 5.1% ± 17.5 for the large- and small-camber PPCBs, respectively.

Additionally, in light of the design practice, a single multiplier based on the average at-erection age of the monitored PPCBs was determined to further facilitate the long-term camber prediction procedure. In determining this single multiplier, the thermal effects as well as a zero overhang length or an average measured overhang length of L/30 were given consideration. The long-term camber was reevaluated using the single multiplier with a zero overhang length and an average overhang length of L/30 and compared to the measured data. The error between the predicted

and the measured long-term camber was -8.5% ± 21.1% and 15.9% ± 20.5% for the large- and small-camber PPCBs, respectively, when an average overhang length of L/30 was used. By using the single multiplier, which eliminated the contribution of the overhang to the long-term camber, the long-term camber accuracy was improved, with the corresponding errors of 4.5% ± 17.2% and 15.3% ± 20.9% for the large- and small-camber PPCBs, respectively.

In summary, the accuracy of the long-term camber was greatly improved by using FEA in conjunction with the time-step method, while the thermal effects were also included. However, due to the complicacy of such an analysis for design practice, a set of multipliers as well as a single multiplier were produced to facilitate the long-term camber prediction. Recognizing the contribution of overhang length to the long-term camber, these multipliers were computed for the conditions of zero overhang length and an average measured overhang length of L/30. It was verified that the multipliers or a single multiplier can yield more accurate results when the camber growth due to the overhang is eliminated.

CHAPTER 8: SUMMARY, CONCLUSIONS, AND RECOMMENDATIONS

8.1 Summary

The Iowa DOT has observed that the at-erection camber of PPCBs is often underestimated for longer PPCBs while it is overestimated for shorter PPCBs. This inaccurate design camber prediction has led to construction delays and an increase in costs. This study was undertaken to systematically identify the potential sources of the discrepancies between the designed and measured camber in order to improve the accuracy of the at-erection camber estimation. As part of this study, concrete material properties were characterized through laboratory testing at the Iowa State University structural engineering laboratories. PPCBs with varying lengths and depths were monitored for periodic camber measurements from release to time of erection. In addition, analytical models were developed using a simplified analysis as well as FEA (midas Civil) to predict the instantaneous and long-term camber.

To reduce the uncertainties in the long-term camber predictions, a total of seven different concrete mix designs, representative of three precast plants, were studied for their material properties, such as the modulus of elasticity and the creep and shrinkage strains as a function of time. Four of the seven mixes were HPC and are currently used for casting prestressed bridge PPCBs. The rest were NC mix designs used in PPCBs in the recent past. The measured creep and shrinkage behavior generally indicated large discrepancies between the measured values and the values obtained from five different predictive models. However, the AASHTO LRFD (2010) creep and shrinkage models were found to give the best estimates when compared to the measurements taken from the four HPC and three NC mixes over one year. Other models investigated were the ACI 209R-92 model, the ACI 209R model modified by Huo et al. (2001), the CEB-FIP 90 model, and the B3 model proposed by Bazant (2000). Although the AASHTO LRFD (2010) models were found to be better than the other four models, large errors still existed between the measured and predicted values even when using the AASHTO models, which underpredicted both the creep coefficient and the shrinkage strains. Furthermore, sealed specimens were found to represent the behavior of full-scale PPCBs more effectively than unsealed specimens. Consequently, to avoid the errors in the long-term camber produced by the creep and shrinkage prediction models, two equations were proposed to calculate the average creep coefficient and the average shrinkage strain for the four current HPC mixes used by three precasting plants for producing PPCBs for the Iowa DOT. These average curves were subsequently used to obtain long-term camber estimations.

As part of the research reported herein, a combination of the measurement techniques used by precasters and researchers, along with new methods, were explored to determine a consistent, accurate way to measure the instantaneous camber. While some previous measuring methods neglected bed deflections, inconsistent PPCB depths, and friction between the PPCB and the bed, the proposed method accounts for each of these issues as accurately as possible and quantifies their impacts on the instantaneous camber measurement. Additionally, it was observed that reverse friction, if any, is small in magnitude and can be ignored. The contribution of the vertical displacement due to friction can be eliminated by lifting and placing back the PPCB and then taking a camber measurement.

Although instantaneous camber prediction is a straightforward task, the discrepancy between the measured and designed camber is caused by the difficulties in accurately modeling the concrete and prestressing steel properties and the procedures used to construct the PPCBs. Hence, using the moment area method, different parameters affecting instantaneous camber prediction were investigated analytically. The influence of the modulus of elasticity, prestress force, prestress losses, transfer length, sacrificial strands, and section properties on instantaneous camber prediction was quantified. The modulus of elasticity that was estimated using the AASHTO LRFD (2010) method provided 98.2% ± 14.9% agreement between the measured and predicted instantaneous camber when the specific unit weight and release strengths corresponding to specific PPCBs were used. Ignoring sacrificial strands and transfer length in the camber prediction produced an average error of 2.6% and 1.5%, respectively. The designed prestress force was observed to have an agreement with the precasters' applied prestress force value of 100.9% ± 2.5% when evaluating 41 PPCBs. A combination of instantaneous prestress losses contributed to a reduction in the prestress by 7.0%, on average, which reduced the camber by 11.3%. The transformed moment of inertia along the length of the PPCB compared to the gross moment of inertia produced a 2.9% reduction in the instantaneous camber.

A total of 66 Iowa DOT PPCBs were monitored for periodic long-term camber measurements during storage and at the time of erection at the site. The effects of support locations during storage and the ambient temperature gradients on the long-term camber measurements were investigated. An average overhang length of L/30 was derived by measuring the overhang length of different PPCBs while they were stored at the precast plants. Moreover, an additional 22 Iowa DOT PPCBs were instrumented with thermocouples and string potentiometers to measure the temperature and the deflections, respectively, as a function of time over short durations. The recorded data indicated that the camber varied significantly by as much as 0.7 in. due to variations in temperature down the PPCB depth. Furthermore, measurements were taken to confirm that the change in camber was negligible after the PPCBs were erected and the bridge deck slab was cast.

A combination of simplified analysis and FEA was utilized to study the changes in the camber from time of release to erection and beyond. The predicted instantaneous camber using the FEA correlated well with the measured data, which were corrected for measurement errors. An investigation of different simplified methods for long-term camber prediction indicated that Naaman's method was the best method, which had an error of ±25%. In addition, sophisticated analytical models that considered the different parameters affecting the long-term camber estimation, as outlined in Section 2.3.2, were developed using the midas Civil software. The FEA results showed that the long-term camber can be predicted with an average error of 8.6% ± 14.5% and 24.1% ± 29.5% for the large- and small-camber PPCBs, respectively, when the thermal effects are ignored. A sensitivity analysis of the temperature difference indicated that a temperature difference of 15°F can most accurately capture the scatter in the measured data due to the thermal effects. By incorporating this temperature difference in the long-term camber predictions, the corresponding errors were reduced to -1.2% ± 10.7% and -14.7% ± 22.5% for the large- and small-camber PPCBs, respectively.

For design practice, a multiplier as a function of time, a set of average multipliers, and a single multiplier with and without an overhang were proposed to calculate the long-term camber. In

addition to these multipliers, a temperature multiplier, λ_T, was introduced to account for the additional short-term deflection that occurs due to the thermal effects. In general, using the proposed multipliers improved the accuracy of the long-term camber prediction compared to the current Iowa DOT approach. The improvement was more pronounced when the contribution of the overhang to the long-term camber was eliminated.

8.2 Conclusions

The primary goals of this study were to improve both the short-term and long-term camber predictions and to reduce the discrepancy between the measured and the designed at-erection camber observed by the Iowa DOT. The project goals were achieved through systematically characterizing concrete engineering properties, examining and modifying the camber measurement techniques, and improving the short-term and long-term predictions. The following conclusions can be drawn from this study:

- The AASHTO LRFD (2010) creep and shrinkage models were found to give the best estimates when compared to the measurements taken from four HPC and three NC mixes over one year.
- The sources of errors caused by the current instantaneous camber measurement techniques were identified and subsequently eliminated by the proposed measurement technique.
- By isolating the measurement errors from the errors caused by the prediction methods, the accuracy of the instantaneous camber prediction was improved using a combination of appropriate material properties and design procedures.
- The modulus of elasticity estimated using the AASHTO LRFD (2010) and based on the specific unit weight and release strengths corresponding to the specific PPCBs provided the best agreement between the measured and designed instantaneous camber.
- By reducing the errors in the instantaneous camber prediction, the accuracy of the long-term camber prediction was also improved when the multipliers were used.
- The uncertainties in the long-term camber predictions associated with the time-dependent material properties were mitigated using the proposed average measured creep coefficient and shrinkage strain.
- For the prediction of the long-term camber using a simplified analysis, the long-term camber predicted by Naaman's method correlated better with the measured long-term camber compared to Tadros' method and the incremental method.
- Using the sophisticated analytical models developed with due consideration given to creep and shrinkage, accounting for the thermal effects and changes in the prestress and support locations significantly improved the accuracy of the long-term camber predations.
- The produced multipliers improved the long-term camber predictions compared to the current Iowa DOT method, particularly when the multipliers were adjusted to account for the overhang length and the thermal effects.

More detailed conclusions for various aspects of the project can be found at the ends of Chapters 3 through 7.

8.3 Recommendations

Based on the findings of this study, a set of recommendations is presented in this section for the concrete time-dependent properties, camber measurements, and camber predictions. Implementation of these recommendations is expected to significantly improve the accuracy of the camber measurements and predictions.

8.3.1 Concrete Time-Dependent Properties

Inaccurate estimation of the creep and shrinkage values by the current approach results in an average error of 31% for the camber at erection. In order to improve the predictive accuracy of the long-term camber of PPCBs, the following recommendations are provided:

- The creep and shrinkage values established for concrete mixes used by local precasters should be used; these values account for the influence of the quality of aggregates used in these mixes.
- It is appropriate to use the average sealed creep coefficient and the average sealed shrinkage values established in this research using the four HPC mixes from Iowa to predict the long-term camber of PPCBs for up to one year. The proposed equations for the sealed creep coefficient and the sealed shrinkage may be used to predict the long-term camber beyond one year (see Section 3.8.4.6).
- If independent creep and shrinkage values are to be taken, sealed specimens should be used for the purpose of creep and shrinkage because these samples' behavior corresponds well with the behavior of full-scale PPCBs.

8.3.2 Camber Measurements

Throughout this research, production and design procedures have been observed to significantly affect the accuracy of the predicted and measured camber. Evaluating and improving design and production procedures will result in a closer agreement between the designed and measured camber. Presented below are recommendations that are made for precasters and contractors to minimize the error between the designed and measured camber.

8.3.2.1 Camber Measurement Procedure

The currently adopted camber measurement method is not consistent. The measurement technique and the location on the PPCBs from which the measurements are taken vary. By observing and taking independent camber measurements, this study concluded that the error in camber arising from the measurement technique used by the precasters and contractors was about 26%, on average. To eliminate the difference in camber values due to the measurement technique, the researchers developed a simplified procedure that both precasters and contractors can use to accurately measure the camber and minimize any error associated with the measurement technique. The following are recommendations for the new camber measurement procedure:

1. Place a 2x4 on the top flange at the ends and at the midspan of the PPCB before casting the PPCB (Figures 8.1 and 8.2).

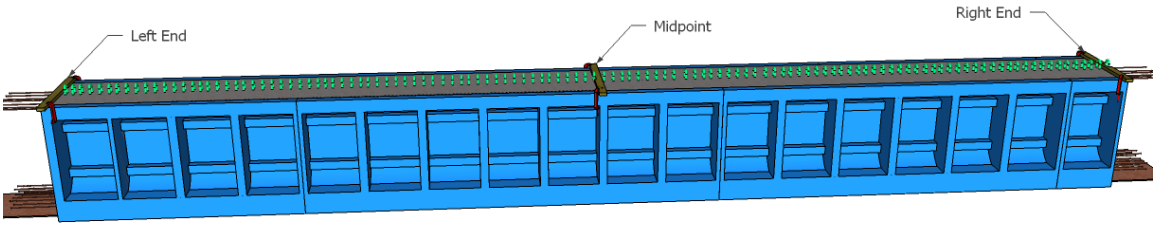

Figure 8.1. Casting of PPCB with 2x4s to establish flat surfaces

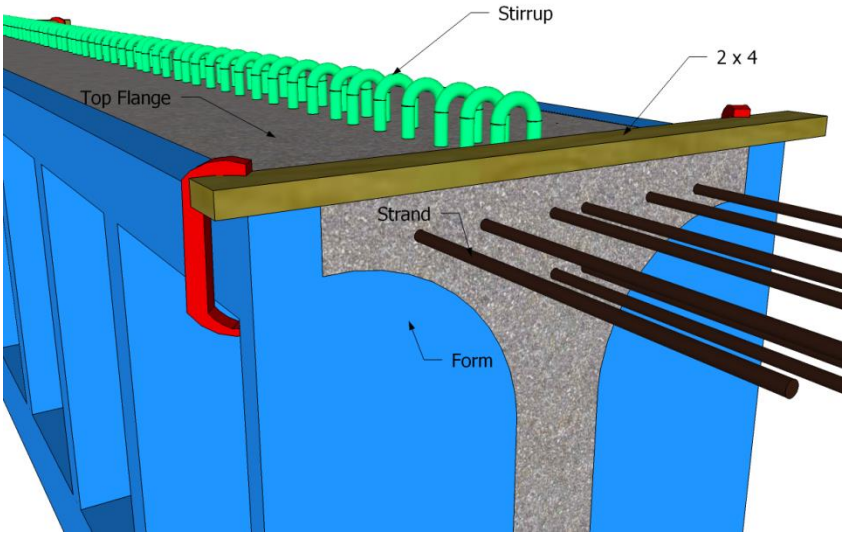

Figure 8.2. Close-up of a 2x4 positioned on a PPCB

2. Cast the concrete to the bottom elevation of the 2x4s to ensure that flat surfaces will be produced (underneath the 2x4s).
3. Cure the PPCB using the standard practice.
4. Remove all these 2x4s from the top flange and the framework.
5. After the PPCB has been released, precasters have one of the following two options:
   a. Lift/set the PPCB on the precasting bed, or
   b. Lift the PPCB and move it to the storage yard, placing it on temporary wooden supports at the PPCB ends.
6. Measure the elevation of the PPCB with a rotary laser level, a total station, or any other suitable survey equipment at the midspan and at the ends of the PPCB using the top flat surfaces created by the 2x4s. At each location, take measurements closer to each side and in the middle of the top flange, as shown in Figure 8.3. Although the use of a tape measure has been shown to provide accurate camber measurements, the recommended approach has been found to minimize the operator error.

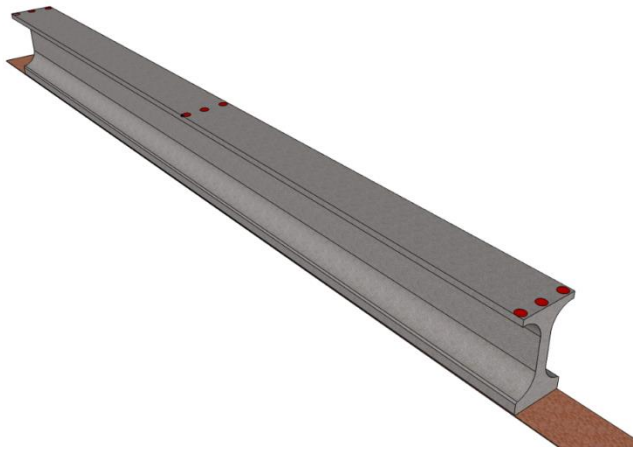

Figure 8.3. Location of camber measurements after the transfer of prestress

7. If option 5.b is used, determine the contribution to the camber of the reduced clear span and the overhang caused by the temporary supports.
8. Take the average of the end elevation readings and subtract it from the midspan elevation reading to obtain the camber.
9. If option 5.b is used, subtract the contribution to the camber of the temporary support placement from the camber value calculated in step 8.

The recommended procedure for measuring the camber has benefits in terms of improving accuracy and minimizing the error for precasters. Measuring the camber with this method eliminates the inaccurate representation of the camber due to friction, inconsistent top flange surfaces, and bed deflection. The 2x4s cast at the top flange will ensure that the same reference points are being used for measuring the camber in the field. Although the time to measure the camber will be greater than the time required for the existing method for precasters, this method will minimize the precasters' role if haunch reinforcement requirement becomes an issue.

8.3.2.2 Precasters' Practices

Observing and taking independent camber measurements at three separate precast plants led the researchers to make the following recommendations to improve the ability to predict the camber of PPCBs:

- The prestress force is highly sensitive to the camber; therefore, monitor and apply the designed prestress force as accurately as possible.
- Aim for reaching and not exceeding the design strength at the transfer of the prestress of the PPCBs.
- Ensure consistency of concrete mixes and base materials (e.g., aggregates) regardless of the time and day of casting.
- Ensure consistent curing conditions and ensure that the PPCBs' curing conditions replicate those of the sample cylinders used for obtaining the release strength.

- When there is a change in the material or curing process, engineering properties, including creep and shrinkage behavior of concrete, should be appropriately revised.
- Minimize the error in the instantaneous camber of identical PPCBs cast on different beds or at different times or days.
- Use the proposed camber measurement procedure to take the instantaneous camber measurements.
- Store the PPCBs with zero overhang or L/30 during storage (see Section 8.3.2.3).

Implementing the recommendations above will help the precasters produce PPCBs for which the camber is in agreement with the designed camber. Despite the above recommendations, some variations in the material and fabrication procedure may still exist, but their impact on camber will be minimized.

8.3.2.3 Support Locations

The overhang lengths were measured for 66 different Iowa DOT PPCBs during storage. The data showed that the average overhang length is approximately L/30 (see Section 4.2.4). Thus, it is recommended that different PPCBs be stored with the same overhang length of L/30 during storage. A consistent overhang length during storage will lead to a more accurate estimation of the at-erection camber.

8.3.2.4 Thermal Effects

The inconsistencies in the measured data during storage indicated that the camber can vary significantly during the course of the day due to the thermal effects. It was observed that the thermal effects were exacerbated in the afternoon on hot, sunny summer days when the solar radiation is the most intense. Hence, in order to obtain more consistent data, it is recommended that the secondary measurements be conducted at dawn, or early morning, when the solar radiation is less intense.

8.3.3 Camber Predictions

8.3.3.1 Instantaneous Camber

A method for predicting the instantaneous camber was studied by the researchers using the moment area method. The following recommendations are made for the prediction of the instantaneous camber:

- The decrease in the camber due to the transfer length is dependent on the number of prestressing strands and the length of the PPCB. Due to the convenience of its design and accuracy, the AASHTO LRFD (2010) equation for the transfer length should be used.

- The modulus of elasticity is a sensitive variable and can impact the accuracy of the camber. Using the AASHTO LRFD (2010) recommended modulus of elasticity with an expected release strength and unit weight will improve the camber predictions.
- Assume that the release strength is equal to 40% and 10% higher than the specified concrete strength for PPCBs when the design value is in the 4500–5500 psi and 6000–8500 psi range, respectively.
- The transformed moment of inertia of a section changes along the length of the PPCB if harped sections are used. For simplification in design, the gross moment of inertia may be used for estimating the instantaneous camber.
- The prestress force is an important variable that greatly influences the camber. A close agreement with the designed and actual prestress force will give a good agreement between the designed and measured camber.
- Prestress losses have been observed to reduce the initial prestress force by 7.0% upon prestress transfer. Consequently, the camber will be affected by 11.3%, on average. Therefore, prestress losses should be accounted for when estimating the instantaneous camber.
- Sacrificial prestressing strands will reduce the camber and should be accounted for when estimating the instantaneous camber.

8.3.3.2 At-Erection Camber

Currently, the Iowa DOT uses Martin's multipliers (1977) to determine the at-erection camber of PPCBs. In this study, various camber prediction methods were investigated and their accuracies evaluated. First, the best simplified method is recommended to calculate the at-erection camber. Then, different recommendations based on the sophisticated analytical models are presented for calculating the at-erection camber more accurately. Accordingly, the following three different multipliers for calculating the at-erection camber have been established: (1) a multiplier as a function of time, (2) a set of average multipliers for three different time intervals, and (3) a single multiplier. The first option allows the designer to decide the time of the PPCB erection and subsequently calculate the multiplier. In the second option, the multiplier is already calculated for the designer according to three different time intervals (see Section 7.5.3). The third option further simplifies the prediction method by eliminating the at-erection age and finding a single multiplier. Additionally, to account for the additional deflection caused by the thermal effects, a temperature multiplier, λ_T, is proposed, which can be applied to the long-term camber multipliers. All of the recommendations are presented below:

- For the prediction of the long-term camber using a simplified analysis, Naaman's method should be used.
- Equations 8-1 and 8-2, as a function of time, can be used for each group of PPCBs to calculate the at-erection camber with zero overhang.

$M=1.145\ t^{0.043}$ (large-camber PPCBs; i.e., estimated instantaneous camber > 1.5 in.) **(8-1)**

$M=1.264\ t^{0.045}$ (small-camber PPCBs; i.e., estimated instantaneous camber ≤ 1.5 in.) **(8-2)**

where M is the multiplier, and t is the time (day).

- Multipliers from Equations 8-3 and 8-4, as a function of time, can be used for each category of PPCBs to calculate the at-erection camber with an assumed overhang length of L/30 during storage.

$M=1.313\ t^{0.043}$ (large-camber PPCBs; i.e., estimated instantaneous camber > 1.5 in.) **(8-3)**

$M=1.468\ t^{0.049}$ (small-camber PPCBs; i.e., estimated instantaneous camber ≤ 1.5 in.) **(8-4)**

where M is the multiplier, and t is the time (day).

- A set of proposed average multipliers is presented in Table 8.1 to calculate the at-erection camber for three different time intervals, assuming zero overhang during storage.

Table 8.1. Multipliers recommended for at-erection camber prediction with zero overhang during storage

Erection Period (days)	PPCB Type	Average Time Used (days)	Multiplier
0–60	Small-camber PPCBs	40	1.53 ± 0.02
	Large-camber PPCBs	40	1.35 ± 0.01
60–180	Small-camber PPCBs	120	1.61 ± 0.02
	Large-camber PPCBs	120	1.41 ± 0.02
180–480	Small-camber PPCBs	300	1.67 ± 0.02
	Large-camber PPCBs	310	1.46 ± 0.02

- A set of proposed average multipliers is presented in Table 8.2 to calculate the at-erection camber for three different time intervals with an assumed average overhang length of L/30 during storage.

Table 8.2. Multipliers recommended for at-erection camber prediction with an overhang length of L/30 during storage

Erection Period (days)	PPCB Type	Average Time Used (days)	Multiplier
0–60	Small-camber PPCBs	45	1.77 ± 0.02
	Large-camber PPCBs	45	1.55 ± 0.02
60–180	Small-camber PPCBs	120	1.86 ± 0.03
	Large-camber PPCBs	115	1.61 ± 0.02
180–480	Small-camber PPCBs	340	1.94 ± 0.02
	Large-camber PPCBs	320	1.68 ± 0.02

- The multipliers in Table 8.3 may be used to predict the at-erection camber with zero overhang during storage. These multipliers account for the additional thermal deflection induced by an assumed temperature difference of 15°F.

Table 8.3. Multipliers recommended for at-erection camber prediction with a temperature difference of 15°F and zero overhang during storage

Erection Period (days)	PPCB Type	Average Time Used (days)	Multiplier
0–60	Small-camber PPCBs	45	1.90
	Large-camber PPCBs	40	1.47
60–180	Small-camber PPCBs	120	2.00
	Large-camber PPCBs	120	1.54
180–480	Small-camber PPCBs	300	2.07
	Large-camber PPCBs	310	1.59

- The multipliers in Table 8.4 may be used to predict the at-erection camber with an assumed overhang length of L/30 during storage, and account for the additional thermal deflection induced by an assumed temperature difference of 15 °F.

Table 8.4. Multipliers recommended for at-erection camber prediction with a temperature difference of 15°F and an overhang length of L/30 during storage

Erection Period (days)	PPCB Type	Average Time Used (days)	Multiplier
0–60	Small-camber PPCBs	40	2.19
	Large-camber PPCBs	40	1.69
60–180	Small-camber PPCBs	120	2.31
	Large-camber PPCBs	120	1.75
180–480	Small-camber PPCBs	300	2.41
	Large-camber PPCBs	310	1.83

- The single multipliers in Table 8.5 may be used to predict the at-erection camber with zero overhang during storage.

Table 8.5. Single multiplier recommended for at-erection camber prediction with zero overhang during storage

Group	Average Time	Single Multiplier
Large-camber PPCBs	120	1.41
Small-camber PPCBs	120	1.57

- The single multipliers in Table 8.6 may be used to predict the at-erection camber with an assumed overhang length of L/30 during storage.

Table 8.6. Single multiplier recommended for at-erection camber prediction with an overhang length of L/30 during storage

Group	Average Time	Single Multiplier
Large-camber PPCBs	120	1.61
Small-camber PPCBs	120	1.86

REFERENCES

Abdel-Karim, A., and M. K. Tadros. 1993. Computer analysis of spliced girder bridges. *ACI Structural Journal*, 90(1), 21–31.

Ahlborn, T. M., C. K. Shield, and C. W. French. 2000. *High-Performance Concrete Prestressed Bridge Girders: Long Term and Felxural Behavior*. Minnesota DOT, St. Paul, MN.

Alexander, M. G. 1996. Aggregates and the deformation properties of concrete. *ACI Materials Journal*, 93(6): 569–577.

Alfes, C. 1992. Modulus of elasticity and drying shrinkage of high-strength concete containing silica fume. ACI Proceedings Fourth International Conference: Fly Ash, Silica Fume, Slag, and Natural Pozzolans in Concrete, Istanbul, Turkey, 1651–1671.

American Association of State Highway and Transportation Officials (AASHTO). 2006. *AASHTO LRFD Bridge Design Specifications*. 3rd Edition, 2006 Interim Revisions. American Association of State Highway and Transportation Officials, Washington, D.C.

American Association of State Highway and Transportation Officials (AASHTO). 2010. *AASHTO LRFD Bridge Design Specifications*. 5th Edition. American Association of State Highway and Transportation Officials, Washington, D.C.

American Association of State Highway and Transportation Officials (AASHTO), Standing Committee on Highways and Subcommittee on Bridges and Structures. 2005. *Haunched Girder*. American Association of State Highway and Transportation Officials, Washington D.C. http://www.iowadot.gov/subcommittee/bridgeterms.aspx.

American Concrete Institute (ACI) 209R-92. 1992. Prediction of Creep, Shrinkage and Temperature Effects in Concrete Structures. American Concrete Institute, Farmington Hills, MI.

American Concrete Institute (ACI) 209.2R-08. 2008. Guide for Modeling and Calculating Shrinkage and Creep in Hardened Concrete. American Concrete Institute, Farmington Hills, MI.

American Concrete Institute (ACI) 232.2R. 1996. Use of Fly Ash in Concrete. American Concrete Institute, Farmington Hills, MI.

American Concrete Institute (ACI) 233R. 2003. Slag Cement in Concrete and Mortar. American Concrete Institute, Farmington Hills, MI.

American Concrete Institute (ACI) 234R. 2006. Guide for the Use of Silica Fume in Concrete. American Concrete Institute, Farmington Hills, MI.

American Concrete Institute (ACI) 318-11. 2011. Building Code Requirements for Structural Concrete. American Concrete Institute, Farmington Hills, MI.

American Concrete Institute (ACI) 343R-95. 1995. Analysis and Design of Reinforced Concrete Bridge Structures. American Concrete Institute, Farmington Hills, MI.

American Concrete Institute (ACI) 363R-92. 1992. State-of-the-Art Report on High-Strength Concrete. American Concrete Institute, Farmington Hills, MI.

American Concrete Institute (ACI) 517. 1963. Low pressure steam curing. *ACI Journal Proc.*, 60: 953–986.

American Society for Testing and Materials (ASTM) C39. 2004. Standard test method for compressive strength of cylindrical concrete specimens. American Society for Testing and Materials, West Conshohocken, PA.

American Society for Testing and Materials (ASTM) C512. 2002. Standard test method for creep of concrete in compression. American Society for Testing and Materials, West Conshohocken, PA.

American Society for Testing and Materials (ASTM) C617. 2009. Standard practice for capping cylindrical concrete specimens. American Society for Testing and Materials, West Conshohocken, PA.

Baalbaki, M., S. L. Sarker, P. C. Isabelle, and H. Aitcin. 1992. Properties and microstructure of high-performance concretes containing silica fume, slag and fly ash. ACI Proceedings Fourth International Conference: Fly Ash, Silica Fume, Slag, and Natural Pozzolans in Concrete, Istanbul, Turkey, 921–942.

Barr, P., E. Fekete, M. Eberhard, J. Stanton, B. Khaleghi, and J. Hsieh. 2000. High Performance Concrete in Washington State SR 18/SR 516 Overcrossing: Interim Report on Girder Monitoring. FHWA-RD-00-070. Federal Highway Adminitration, Washington, D.C.

Bazant, Z. P. 2000. Creep and shrinkage prediction model for analysis and design of concrete structures: Model B3. ACI SP-194. Adam Neville Symposium: Creep and Shrinkage - Structural Design Effects, Farmington Hills, MI, 1–83.

Bennett, E. W., and D. R. Loat. 1970. Shrinkage and creep of concrete as affected by the fineness of Portland cement. *Magazine of Concrete Research*, 22(71): 69–78.

Bissonnette, B., P. Pierre, and M. Pigeon. 1999. Influence of key parameters on drying shrinkage of cementitious materials. *Cement and Concrete Research*, 29(10): 1655–1662.

Brooks, J. J. 1989. Influence of mix proportions, plasticizers and superplasticizerson creep and drying shrinkage of concrete. *Magazine of Concrete Research*, 41(148): 14–153.

Brooks, J. J., P. J. Wainwright, and A. F. Al-Kaisi. 1991. Compressive and tensile creep of heat-cured ordinary Portland and slag cement concretes. *Magazine of Concrete Research*, 43(154): 1–12.

Brooks, J. J., P. J.Wainwright, and M. Boukendakji. 1992. Influence of slag type and replacement level on strength, elasticity, shrinkage, and creep of concrete. ACI Proceedings Fourth International Conference: Fly Ash, Silica Fume, Slag, and Natural Pozzolans in Concrete, Istanbul, Turkey, 1325–1341.

Bryant, A. H., and C. Vadhanavikkit. 1987. Creep, shrinkage-size, and age at loading effects. *ACI Materials Journal*, 84(2): 117–123.

Buil, M., and P. Acker. 1985. Creep of silica fume concrete. *Cement and Concrete Research*, 15(3): 463–466.

Carlson, R. W. 1937. Drying shrinkage of large concrete members. *ACI Journal Proc.*, 33(3): 327–336.

CEB-FIP Model Code. 1990. Evaluation of the Time Dependent Behavior of Concrete. Comite Euro-International du Beton, Bulletin d'information, No. 199, Paris.

Chern, J. C., and Y. W. Chan. 1989. Deformations of concretes made with blast furnace slag cement and ordinary Portland cement. *ACI Materials Journal*, 86(4): 372–382.

Davis, R. E., and H. E. Davis. 1931. Flow of concrete under the action of sustained loads. *ACI Journal Proc.*, 27: 410–417.

Davis, R. E., H. E. Davis, and J. S. Hamilton. 1934. Plastic flow of concrete under sustained stress. *ASTM Proc*., 34(Part 2): 354–386.

Ghosh, R. S., and J. Timusk. 1981. Creep of Fly Ash Concrete. *ACI Journal Proc*., 78(5): 351–357.

Gilbertson, C. G., and T. M. Ahlborn. 2004. A Probabilistic comparison of prestress loss methods in prestressed concrete beams. *PCI Journal*, 49(5): 27–31.
Glanville, W. H. 1933. Creep of concrete under load. *The Structural Engineer*, 11(2): 54–73.
Glanville, W. H., and F. G. Thomas. 1939. Studies in reinforced concrete-IV: Further investigations on creep or flow of concrete under load. Building Research Technical Paper No. 21. Dept. of Scientific and Industrial Research, London, UK.
Glucklich, J. 1968. The effect of microcracking on time-dependent deformations and the long-term strength of concrete. Intern. Conf. on the Structure of Concrete: Cement and Concrete Association, London, UK, 176–189.
Gvozdev, A. A. 1966. Creep of Concrete. Mekhanika Tverdogo Tela, Proc. of the 2nd Nat. Conf. on Theor. and App./Mech., Moscow, Russia, 137–152.
Hannant, D. J. 1967. Strain behavior of cocnrete up to 95°C under compressive stresses. Conf. on Prestressed Concrete Pressure Vessels, Institution of Civil Engineers, London, UK, 57–71.
Hansen, T. C., and A. H. Mattock. 1966. Influence of size and shape of member on the shrinkage and creep of concrete. *ACI Materials Journal*, 63(2): 267–290.
Hansen, T. C., and K. E. C. Nielsen. 1965. Influence of aggregate properties on concrete shrinkage. *ACI Journal Proc*., 62: 783–794.
Hanson, J. A. 1964. Prestress loss as affected by type of curing. *PCI Journal*, 9(2): 69–93.
Haranki, B. 2009. Strength, modulus of elasticity, creep and shrinkage of concrete used in Florida. MS thesis, Universiy of Florida.
Hinkle, S. D. 2006. Investigation of time-dependent deflection in long span, high strength, prestressed concrete bridge beams. MS thesis, Virginia Polytechnic Insitute and State Uniersity.
Hirsch, T. J. 1962. Modulus of elasticity of concrete affected by elastic moduli of cement paste matrix and aggregate. *ACI Journal Proc*., 59: 427–451.
Hobbs, D. W. 1974. Influence of aggregate restraint on the shrinkage of concrete. *ACI Journal Proc*., 71(9): 445–450.
Hummel, A. 1959. Des wasserzementverhaltnisses und des belastungsalters auf das kriechen von beton. *Zement-Kalk-Gips*, 12: 181–187.
Huo, X. S., N. Al-Omaishi, and M. K. Tadros. 2001. Creep, shrinkage, and modulus of elasticity of high-performance concrete. *ACI Materials Journal*, 98(6): 440–449.
Iowa Department of Transportation (DOT). 2011a. *Iowa LRFD Bridge Design Manual*. Iowa Department of Transportation, Ames, IA. www.iowadot.gov/bridge/manuallrfd.htm/.
Iowa Department of Transportation (DOT). 2011b. Index of Beam Standards. Iowa Department of Transportation, Ames, IA. www.iowadot.gov/bridge/standards/english/EnglishBeams.pdf.
Iowa Department of Transportation (DOT). 2013a. Iowa Department of Transportation Office of Materials IM 570. Precast Prestressed Concrete Bridge Units. Iowa Department of Transportation, Ames, IA. www.iowadot.gov/erl/current/IM/content/570.pdf.
Iowa Department of Transportation (DOT). 2013b. Iowa Department of Transportation Prestress Manual. Prestress Inspection. Iowa Department of Transportation, Ames, IA. www.iowadot.gov/training/ttcp/training_manuals/PrestressManual.pdf.
Jáuregui, D. V., K. R. White, C. B. Woodward, and K. R. Leitch. 2003. Noncontact Photogrammetric Measurement of Vertical Bridge Deflection. *Journal of Bridge Engineering*, 8(4): 212–222.

Jayaseelan, H., and B. W. Russell. 2007. *Prestress Losses and the Estimation of Long-Term Deflections and Camber for Prestressed Concrete Bridges*. Final Report. Oklahoma State University, Stillwater, OK.

Johnson, B. R. 2012. Time-Dependent Deformations in Precast, Prestressed Bridge Girders. M.S. thesis, Auburn University.

Jones, R. S., and F. E. Richart. 1936. The effect of testing speed on strength and elastic properties of concrete. *ASTM Proc*., 36(Part 2): 380–391.

Keene, P. W. 1960. *The Effect of Air-Entrainment on the Shrinkage of Concrete Stored in Laboratory Air*. Technical Report TRA/331. Cement and Concrete Association, London, UK.

Keeton, J. R. 1960. Time-dependent deformations of plain concrete. *Highway Research Board Proc*., 39: 310–335.

Kelly, D. J., T. E. Bradberry, and J. E. Breen. 1987. *Time Dependent Deflections of Pretensioned Beams*. Research Report CTR 381-1. Center for Transportation Research, University of Texas, Austin.

Khan, A. A., W. D. Mitchell, and D. Cook. 1997. Creep, shrinkage, and thermal strains in normal, medium and high-strength concretes during hydration. *ACI Materials Journal*, 94(2): 156–163.

Khatri, K. P., V. Sirivivatnanon, and W. Gross. 1995. Effect of different supplementary cementitious materials on mechanical properties of high performance concrete. *Cement and Concrete Research*, 25(1): 209–220.

Khayat, K. H., and D. Mitchell. 2009. *Self-consolidating concrete for precast, prestressed concrete bridge elements*. NCHRP Report 628. Transportation Research Board of the National Academies, Washington, D.C.

Kordina, K. 1960. Experiments on the influence of the mineralogical character of aggregates on the creep of concrete. *RILEM Bulletin*, 6: 7–22.

Kosmatka, S. H. 2008. *Design and control of concrete mixtures*. Portland Cement Association, Skokie, Illinois.

L' Hermite, R. G., and M. Mamillan. 1968. Further results of shrinkage and creep tests. Intern. Conf. on the Structure of Concrete, London, UK, 423-433.

Lane, R. O., and J. F. Best. 1982. Properties and use of fly ash in portland cement concrete. *Concrete International: Design & Construction*, 4(7): 81–92.

Lim, S. N., and T. H. Wee. 2000. Autogenous shrinkage of ground-granulated blast furnace slag concrete. *ACI Materials Journal*, 97(5): 587–593.

Lin, T. Y., and N. H. Burns. 1981. *Design of Prestressed Concrete Structures*. Wiley, New York, NY.

Lorman, W. R. 1940. The theory of of concrete creep. *ASTM Proc*., 40: 1082–1102.

Malhotra, V. M., M. H. Zhang, P. H. Ryell, and J. Read. 2000. Long-term mechanical properties and durability characteristics of high-strength/high-performance cocnrete incorporating supplementary cementing materials under ourdoor exposure conditions. *ACI Materials Journal*, 97(5): 518–525.

Martin, L. D. 1977. A rational method for estimating camber and deflection of precast prestressed members. *PCI Journal*, 22(1): 100–108.

Martinez, S., A. H. Nilson, and F. O. Slate. 1982. Spirally Reinforced High-strength Concrete Columns. Research Report No. 82-10. Department of Structural Engineering, Cornell University, Ithaca, NY.

Mazloom, M., A. A. Ramezanianpour, and J. J. Brooks. 2004. Effect of silica fume on mechanical properties of high-strength concrete. *Cement and Concrete Composites*, 26: 347–357.

Muller, H. S., and M. Pristl. 1993. Creep and shrinkage of concrete at variable ambient conditions. In *Creep and Shrinkage of Concrete, Proceedings of the Fifth International RILEM Symposium*. Z. P. Bazant and I. Carol, Eds. E&FN Spon, London, UK.

Naaman, A. E. 2004. *Prestressed Concrete Analysis and Design: Fundamentals*. Techno Press 3000, Ann Arbor, MI.

Nagataki, S., and A. Yonekura. 1978. Studies of the volume of changes of high strength concretes with superplasticizer. *Journal of Japan Prestressed Concrete Engineering Association*, 20: 26–33.

Naik, T. R., Y. Chun, and R. N. Kraus. 2007. Shrinkage of cocnrete with and without fly ash. ACI International Conference on Fly Ash, Silica Fume, Slag, and Natural Pozzolans in Concrete, Poland.

Nasser, K. W., and A. M. Neville. 1965. Creep of concrete at elevated temperatures. *ACI Journal Proc.*, 62: 1567–1579.

Neville, A. M. 1975. Time-dependent behavior of Cemsave concrete. *Concrete*, 9(3): 36–39.

Neville, A. M. 1963. A study of deterioration of structural concrete made with high-alumina cement. *ICE Proceedings*, 25: 287–324.

Neville, A. M. 1997. Aggregate bond and modulus of elasticity of concrete. *ACI Materials Journal*, 94(1): 71–74.

Neville, A. M. 1970. *Creep of Concrete: Plain, Reinforced, and Prestressed*. North-Holland Publishing Company-Amsterdam American Elsevier Publishing Company, New York, NY.

Neville, A. M. 1981. *Properties of Concrete*. Pitman Publishing Limited, London, UK.

Neville, A. M. 1958. The effect of warm storage conditions on the strength of concrete made with high-alumina cement. *ICE Proceedings*, 10: 185–192.

Nilson, A. H. 1987. *Design of Prestressed Concrete*. 2nd Ed. John Wiley and Sons Inc., New York, NY.

Nishiyama, M. 2009. Mechanical properties of concrete and reinforcement – State-of-the-art Report on HSC and HSS in Japan. *Journal of Advanced Concrete Technology*, 7(2): 152–182.

Odman, S. T. A. 1968. Effects of variations in volume, surface area exposed to drying, and composition of concrete on shrinkage. RILEM/CEMBUREAU Intern. Colloquium on the Shrinkage of Hydraulic Concretes, Madrid, Spain.

O'Neill, C. R., and C. E. French. 2012. *Validation of Prestressed Concrete I-Beam Deflection and Camber Estimates*. Final Report. Minnesota DOT, Saint Paul, MN.

Precast/Prestressed Concrete Institute (PCI) Committee on Prestress Losses. 1975. Recommendations for Estimating Prestress Losses. *PCI Journal*, 20(4): 43–75.

Precast/Prestressed Concrete Institute (PCI). 1997. *Bridge Design Manual*. Precast/Prestressed Concrete Institute, Chicago, IL.

Precast/Prestressed Concrete Institute (PCI). 2010. *PCI Design Handbook: Precast and Prestressed Concrete*. 7th Ed. Precast/Prestressed Concrete Institute, Chicago, IL:

Persson, B. 1998. Experimental studies on shrinkage of high-performance concrete. *Cement and Concrete Research*, 28(7): 1023–1036.

Pickett, G. 1956. Effect of aggregate on shrinkage of concrete and hypothesis concerning shirnkage. *ACI Journal Proc*., 52: 581–90.

Polivka, M., D. Pirtz, and R. F. Adams. 1964. Studies of creep in mass concrete. Paper 12. ACI Special Publication. Symp. on Mass Concrete.

Rizkalla, S., P. Zia, and T. Storm. 2011. *Predicting Camber, Deflection, and Prestress Losses in Prestressed Concrete Members*. Final Report. North Carolina State University, Raleigh, NC.

Rosa, M., J. Stanton, and M. Eberhard. 2007. *Improving Predictions for Camber in Precast, Prestressed Concrete Bridge Girders*. Washington State Transportation Center (TRAC), University of Washington, Seattle, WA.

Roy, R., and F. Larrard. 1993. Creep and shrinkage of high-strength concrete. In *Creep and Shrinkage of Concrete, Proceedings of the Fifth International RILEM Symposium*. Z. P. Bazant and I. Carol, Eds. E&FN Spon, London, UK, 500–508.

Saric-Coric, M., and P. C. Aitcin. 2003. Influence of curing conditions on shrinkage of blended cements containing various amounts of slag. *ACI Materials Journal*, 100(6): 477–484.

Sakai, K., H. Watanabe, M. Suzuki, and K. Hamazaki. 1992. Properties of granulated blast-furnace slag cement concrete. ACI Proceedings Fourth International Conference: Fly Ash, Silica Fume, Slag, and Natural Pozzolans in Concrete, Istanbul, Turkey, 1367–1383.

Saucier, K. 1984. High-strength Concrete for Peacekeeper Facilities. Miscellaneous Paper SL-84-3. U.S. Army Engineer Waterways Experiment Station, Vicksburg, MS.

Schindler, A. K., R. W. Barnes, J. B. Roberts, and S. Rodriguez. 2007. Properties of self-consolidating concrete for prestressed members. *ACI Materials Journal*, 104(1): 53–61.

Soroka, I. 1979. *Portland Cement Paste and Concrete*. Macmillan Press Ltd.

Swamy, R. N. 1986. *Cement Replacement Materials*. Surrey University Press, London.

Swartz, B. D., A. Scanlon, and A. J. Schokker. 2012. AASHTO LRFD Bridge Design Specifications provisions for loss of prestress. *PCI Journal*, 57(4): 108–132.

Swayze, M. A. 1960. Discussion on: Volume changes of concrete. Proc. 4th Int. Symp. on the Chemistry of Cement, Washington, D.C., 700–702.

Tadros, M. K., N. Al-Omaishi, S. J. Seguirant, and J. G. Gallt. 2003. *Prestressed Losses in Pretensioned High-Strength Concrete Bridge Girders*. NCHRP Report No. 496. Transportation Research Board, National Academy of Sciences, Washington, D.C.

Tadros, M. K., F. Fawzy, and K. E. Hanna. 2011. Precast, prestressed girder camber variability. *PCI Journal*, 30(1): 135–154.

Tazawa, E. A., A. Yonekura, and S. Tanaka. 1989. Drying shrinkage and creep of concrete containing granulated blast furnace slag. Proceedings of the Third International Conference: Fly Ash, Silica Fume, Slag, and Natural Pozzolans in Concrete, Trondheim, Norway, 1325–1343.

Tazawa, E., and S. Miyazawa. 1993. Autogenous shrinkage of concrete and its importance in concrete technology. In *Creep and Shrinkage of Concrete, Proceedings of the Fifth International RILEM Symposium*. Z. P. Bazant and I. Carol, Eds. E&FN Spon, London, UK, 159–168.

Tazawa, E., and S. Miyazawa. 1997. Study on the prediciton of autogenous shrinkage. *Proceedings of JSCE*, 571/V-36: 211–219.

Townsend, B. D. 2003. Creep and shrinkage of a high strength concrete mixture. MS thesis, Virginia Polytechnic Institute and State University.

Troxell, G. E., J. M. Raphael, and R. E. Davis. 1958. Long-time creep and shrinkage tests of plain and reinforced concrete. *ASTM Proc.*, 58: 1101–1120.

U.S. Army Engineer Waterways Experiment Station. 1958. Investigation of creep in concrete. Report 3, creep of mass concrete. Miscellaneous Paper 6-132. U.S. Army Engineer Waterways Experiment Station, Vicksburg, MS.

Wainwright, P. J., and N. Rey. 2000. The influence of ground granulated blast furnace slag (GGBS) additions and time delay on the bleeding of concrete. *Cement and Concrete Composites*, 22(4): 253–257.

Wang, K. J., S. M. Schlorholtz, S. Sritharan, H. Seneviratne, X. Wang, and Q. Z. Hou. 2013. *Investigation into Shrinkage of High Performance Concrete Used for Iowa Bridge Decks and Overlays*. IHRB Project TR-633. Iowa DOT, Ames. IA.

Woolf, D., and C. E. French. 1998. *A Camber Study of MnDOT Prestressed Concrete I-Girders*. MnDOT Final Report 1998-08. Minnesota DOT, St. Paul, MN.

Yashin, A. V. 1959. Creep of young concrete. Investigation of properties of concrete and reinforced concrete construction. Gosudarstviennoye Izdatielstvo Literaturi po Stroitielstvu, Moscow, Russia, 18–73.

Yildirim, H., and O. Sengul. 2011. Modulus of elasticity of substandard and normal concretes. *Construction and Building Materials*, 25(4): 1645–1652.

Yuan, R. L, and J. E. Cook. 1983. Study of class C fly ash concrete. Fly Ash, Silica Fume, Slag and Other Mineral By-Products in Concrete. ACI SP-79. 307–319.

Zia, P., H. K. Preston, N. L. Scott, and E. B. Workman. 1979. Estimating prestress losses. *ACI Concrete International*, 1(6): 32–38.